Stable Carbon Isotopic Composition of Methane from Ancient Ice Samples

by

Hinrich Schaefer
B.S. (Vordiplom), Kiel University, 1993
M.S. (Diplom), Kiel University, 1997

A Dissertation Submitted in Partial Fulfillment of the
Requirements for the Degree of

DOCTOR OF PHILOSOPHY

in the School of Earth and Ocean Sciences

Supervisor: Dr. Michael J. Whiticar

ABSTRACT

Stable Carbon Isotopic Composition of Methane from Ancient Ice Samples

This study developed a method to extract gas from ice samples and measure the concentration and stable carbon isotope ratio of evolved methane. Ice samples were analyzed from 3 sites: (i) Agassiz ice cap (Ellesmere Island, Canada), (ii) Greenland Ice Sheet Project 2 (GISP2), and extensively from (iii) the western margin of the Greenland ice shield in Pakitsoq. Agassiz and GISP2 provided accuracy and precision tests of the analytical method. Pakitsoq ice yielded a record to reconstruct the atmospheric $\delta^{13}C_{CH4}$ history of the methane cycle across the cold Younger Dryas – warm Pre-Boreal transition (YD-PB) with a temporal resolution of decades.

$\delta^{13}C_{CH4}$ values measured for YD-PB are relatively uniform from -46.0 ‰ to –45.8 ‰ (±0.4 ‰), i.e. that tropospheric methane in YD-PB is more enriched in ^{13}C than previously expected or measured today.

$\delta^{13}C_{CH4}$ measurements represent true atmospheric signals and are not affected by post-occlusion oxidation or production of methane in ice. Atmospheric mixing and isotope fractionation during diffusion of air in the unconsolidated snow/firn layer shift $\delta^{13}C_{CH4}$ preserved in ice, but models developed in this study compensate for these effects.

Model work shows that variations in anthropogenic, climatic, and C_3, C_4 vegetation changes affect $\delta^{13}C_{CH4}$ of emissions and sinks.

The $\delta^{13}C_{CH4}$ shift between the YD-PB and modern times may be explained by including emissions of thermogenic natural gas in the atmospheric methane budget and by revising $\delta^{13}C_{CH4}$ for specific source types, in particular that of tropical wetlands. The impact of rice farming, before the start of the industrial period, may also be detectable in the $\delta^{13}C_{CH4}$ record.

This YD-PB $\delta^{13}C_{CH4}$ record does not support a catastrophic burst of methane from marine gas hydrates. Furthermore, a gradual emission of marine hydrate methane would require the release of the entire gas hydrate reserves in a globally synchronized, 200-year event.

The rapid increase in atmospheric methane concentration at YD-PB is likely caused by additional emissions from C_4-dominated wetlands, having an isotope signature consistent with the YD-PB $\delta^{13}C_{CH4}$ record. During the PB, this new source configuration persists, supported by the uniform $\delta^{13}C_{CH4}$ values, despite the higher methane concentrations.

Supervisor: Dr. Michael J. Whiticar, (School of Earth and Ocean Sciences)

Table of Contents

List of Tables

Table of Figures

Acknowledgments

This thesis could not have been written without the support of many people. First of all I would like to thank Dr. Michael Whiticar for getting me involved with this project, and for providing supervision, feedback, assistance and invaluable advice. One of the formative experiences during my work was to feel his confidence no matter if progress was good or slow. I also thank my committee members Dr. Kevin Telmer, Dr. Andrew Weaver and Dr. Olaf Niemann.

The second pillar of support came from the team I was lucky to work with. Without exception, everyone working in the IRMS laboratory was pleasant to be around, practically minded when dealing with problems, as well as accommodating and helpful. Thanks to all of you. Paul Eby, our lab manager, deserves special mentioning for answering any question anytime (and then again), for discussions and valuable suggestions, for solving technical problems and straightening out my bloopers. At my arrival and during the first time of my work I especially appreciated the help of my fellow graduate students with scientific and everyday issues. Thanks to Scott Harris for endlessly assisting a digital dyslexic, Nick Grant for working hand in hand on technical problems and to Ruben Veefkind and Mike Kory for helping with details from broken glass to tax breaks. Most of all I am grateful to Magnus Eek, basically for solving problems that I had not even identified. It would be difficult to overstate the help that Magnus provided.

Too many other people at UVic assisted me one way or another, as that I could mention all. There is no way, however, to forget Hannah Hickey, Mike Roth, Ed Wiebe and Jan Dettmer for getting me started with computer modeling and getting me through tough parts of coding and mathematics. Katrin Meissner, besides being a good friend, helped me with various questions concerning paleo-data. Another dear memory is how Ina Bureau from the cafeteria management provided a makeshift cold lab in a walk-in freezer.

Thanks to Drs. David Fisher and Roy Koerner from the Geological Survey of Canada in Ottawa for their hospitality, introduction to the world of ice cores, and trusting me with precious sample material. Also, the National Ice Core Laboratory boosted this project by sending samples from their de-accession program. Dr. Mark Twickler was particularly helpful in organizing the most suitable ice.

The field campaigns in Greenland were a highlight of this project, to the biggest part due to the wonderful team. To work so closely together for weeks in all kinds of conditions without tensions says a lot about the personalities of everyone. I fondly remember the seasons with Ed Brook, Jeff Severinghaus, Vas Petrenko, Paul Rose, Niels Reeh, Katy Lanke, every member of the Danish teams and the folks from VECO Polar (Tricky, what's your last name?). I enjoyed sharing their stories, knowledge, humour and appreciation of the surrounding beauty.

I want to thank Julie for supporting me through hard times of the project and for her enthusiasm when things went well. My friends, roommates and family were dear and important to me during this time. I also want to thank the UVic scuba club, the UVic outdoors club and the Vancouver Island chapter of the Alpine Club of Canada, as well as many friends, for sharing with me aspects of rock, water, snow and ice beyond science.

Time is precious,

But truth is more precious than time.

(from a fortune cookie)

1. Introduction

Methane is an atmospheric trace gas with high radiative forcing and an important role in atmospheric chemistry. It is released to the atmosphere from different natural and anthropogenic sources, all of which involve the anaerobic breakdown of organic matter (Cicerone and Oremland, 1988). Due to its long residence time in the atmosphere (estimates range from 7.9 to 8.9 years; Lelieveld et al., 1998; Prather et al., 2001; Prinn et al., 1995) it is a well-mixed component. Minor concentration gradients result from source proximity and geographic variability in sink strength (Fung et al., 1991). The concentration of methane in the atmosphere in the year 2001 was 1.75 ppmV (parts per million by volume)(Prather et al., 2001); it has since increased to 1.8 ppmV (Dlugokencky et al., 2004).

Since the beginning of direct atmospheric measurements methane concentrations have been increasing, a trend that stopped in 2000, when concentrations started to stabilize (Simpson et al. 2002; Dlugokencky et al., 2003), although this may have been only temporary (Dlugokencky et al., 2004). The rise is of concern because methane is a strong greenhouse. A major portion of today's methane emissions is anthropogenic so that methane may contribute to man-made global warming. It is an important question how much elevated methane concentrations will affect global temperature. The issue becomes even more pressing because many methane sources are temperature sensitive, so that the currently observed warming (IPCC TAR 2001; Mann and Jones, 2003) could increase emissions and start a positive feedback loop. In order to assess the potential climatic impact of atmospheric methane we have to understand how methane affects climate. In addition, we have to evaluate how observed and projected increases in methane and temperature would influence the system.

Methane contributes to greenhouse warming through absorption in the 7.66 mm band (Cicerone and Oremland, 1988). Donner and Ramanathan (1980) calculated that an atmospheric methane concentration of 1.5 ppmV raises global temperature by 1.3 K; today's atmospheric levels would result in an even bigger warming. Compared to

pre-industrial times, Lelieveld et al. (1998) estimated the additional climate forcing since the year 1850 as 0.57 W/m2. This radiative forcing is referred to as the direct climate effect of methane. Indirect effects add to its impact on climate. These result from the chemical interactions of methane in the atmosphere. The dominant sink for methane is breakdown by the hydroxyl radical OH•. In turn, methane is a major sink for OH•. Therefore, it determines the oxidative capacity of the atmosphere for other trace gases (Cicerone and Oremland, 1988; Thompson, 1992). The interdependence between methane and hydroxyl also means that changes in methane concentrations are subject to a positive feedback, where enhanced methane levels decrease its own sink, leading to even higher concentrations (Prather, 1994; Prather et al., 2001). The methane breakdown involves a series of reactions, which produce other chemically or radiatively active compounds, such as ozone and carbon monoxide, which amplify the climatic impact of methane by around 30 % in so-called chemical feedbacks (Lelieveld et al., 1998). One of the oxidation products is water vapour. Especially in the stratosphere, methane oxidation is a significant source of this gas and leads to cloud formation and associated effects on climate through changes in albedo and greenhouse forcing. Taken together, the direct and indirect climate forcing of the man-made methane increase has a significant effect on climate.

The modern methane increase, however, may not be unique in rate of change and magnitude in Earth history. How climate adjusted to similar or even bigger natural perturbations could provide information on the importance of the current rise. Therefore, it is necessary to know the natural variations of the atmospheric methane budget. These can be studied using air archived in the pore space of unconsolidated snow (firn) and occluded bubbles of polar ice. The occlusions form several tens of meters below the glacier surface, where compaction seals off air bubbles and the gas can no longer communicate with the pore space of the firn and the atmosphere. There are certain differences between the occluded and the contemporaneous atmospheric air, due to diffusion and occlusion processes, which can be corrected for (Craig et al., 1988a; Trudinger et al., 1997). Notwithstanding these processes, several lines of evidence prove that the chemical signature of many gas species in the atmosphere, including methane, is

preserved permanently and truthfully (Raynaud et al., 1993). The resulting records extend the atmospheric measurements back into the pre-industrial Holocene (PIH) (Etheridge et al. 1998) and the Pleistocene, covering four full glacial cycles (Petit et al., 1999) and have recently expanded back to 620 000 yrs before present (BP) (Stocker et al., 2004). Data from various locations in both hemispheres are in excellent agreement. Together with the tie between paleo- and modern records this is the most important proof that ice cores are a reliable archive of atmospheric methane.

Methane data from ice cores show that concentration changed only very gradually throughout the Holocene, varying by a total of ±150 ppbV (Blunier et al., 1995); and that the current increase started with the industrial revolution (Etheridge et al., 1998). Anthropogenic methane emissions, like biomass burning, animal herding, agriculture, landfills and natural gas production intensified or started at this time, providing the sources for the increase in atmospheric concentration. This is strong evidence that the rise is man-made. But is this anthropogenic disturbance significant compared to the natural variations in the methane cycle? Ice core records are now both long enough and provide sufficient detail during specific time periods to answer this question.

Throughout the pre-modern record, methane shows cyclicity with oscillations between well-defined upper and lower concentration limits (Petit et al., 1999). These cycles are very closely associated with changes in global temperature, i.e. glaciations and interglacials. Methane also strikingly parallels even short-lived climatic events as they are recorded in Greenland ice cores (Brook et al., 1996). It displays the same pattern of slow decrease and rapid rise as temperature. The most fascinating examples are abrupt warming events during the glacial terminations, when temperatures increase from glacial to interglacial values and methane concentrations double, both within a few decades (Chappellaz et al., 1990 and 1993a; Brook et al., 1996). Even compared to these abrupt events, e.g. the end of the Younger Dryas (YD) cold period, the current methane increase is larger in total magnitude (increase by ca. 1000 ppbV vs. ca. 250 ppbV), relative change (plus 133 % vs. 50 %), and rate of change (0.9 % per year in 1984, Dlugokencky et al., 2003, vs. 0.33 % per year at the end of the YD). It also results in unprecedented

atmospheric concentrations, exceeding all previously recorded values by almost a factor of three. In addition, all comparable increases in the past occurred in cold periods, when climatic and environmental conditions were very different from now. The current situation clearly presents an anthropogenic perturbation of the natural system with unknown consequences. For the reasons given above, past methane changes cannot be used as a direct analogy of the present. They can, however, provide valuable insight into the causes of methane concentration changes, the mechanisms involved and the feedbacks with climate. Once these are known, one can assess whether or not those processes will come into play in the current situation and act as positive or negative feedback to the anthropogenic change.

All previous concentration increases were associated with rapid and strong warming events. This does not necessarily mean that the same will happen today, because the paleorecords show that the scenario is more complex than a simple control of temperature through the methane greenhouse effect. In fact, natural methane sources depend on environmental conditions, including climate as the most influential. Therefore, climatic changes can trigger higher methane emissions and in the past these reinforced, rather than caused, the warming. As discussed below, there are indeed several lines of evidence supporting this scenario. Consequently, a different concern arises for the modern situation. Global warming, as observed now (IPCC TAR, 2001; Mann and Jones, 2003), could cause more methane emissions and a positive feedback on temperature. How realistic such a scenario is depends on the process that increases methane concentrations and its potential under current climatic and environmental conditions.

Different theories have been put forward regarding the cause of rapid methane increases in the natural system, particularly during the glacial terminations when the dynamic is greatest. During these events either additional methane is emitted to the atmosphere or less methane is removed from it. In either case, there are four scientific findings that put constraints on the exact nature of the process and allow testing of different hypotheses.

First, the process must have the potential to cause the observed change. The methane content of the atmosphere almost doubles within decades. Such a fundamental re-organization must be caused by a major process of the methane cycle.

Second, some evidence indicates where the active processes take place. There is a concentration gradient between northern and southern polar regions, which results from the concentration of methane sources, most of which are terrestrial, in the northern hemisphere (Chappellaz et al., 1997; Brook et al., 2000; Dällenbach et al., 2000). The gradient is an expression of source proximity and changes with the latitudinal distribution of methane emissions. It is possible to estimate the emissions from three latitudinal belts using ice core data from Greenland and Antarctica, as well as an atmospheric transport model. In warm periods, methane production is higher in the tropics and the northern latitudes compared to cold intervals. Both increase by a similar percentage. Unfortunately, the resolution of the records allows us only to study times with stable atmospheric concentrations. It is not high enough to verify if the same pattern applies during the actual period of change. Nevertheless, the findings of the quoted studies may indicate the geographic origin of the additional methane.

Third, frequency analysis has shown that atmospheric methane concentration varies in unison with irregularities in the Earth's orbit, which are described by the Milankovitch theory (Petit et al. 1999). Whatever increases methane levels must be caused or triggered by environmental changes linked to the energy budget of the northern hemisphere. This excludes tectonic processes or those that operate on an independent cycle (unless this cycle is synchronized to the orbital changes). Instead, the synchronicity of orbital cycles and methane variations strongly suggests that methane is controlled by climate. More specifically, methane is strongly linked to precession, which affects the Asian monsoon cycle (Chappellaz et al., 1990) and temperatures in higher latitudes, e.g. Siberia (Crowley, 1991).

Fourth, the sequence of events at the abrupt warming events shows that methane- and temperature increase start almost simultaneously. Using $\delta^{15}N$ of N_2 as a temperature proxy in the gas phase, the exact relationship at the end of the Younger Dryas (YD) cold period was established as a lead of temperature over methane increase by 0 to 30 yrs (Severinghaus et al., 1998). Similar results have since been established for other abrupt warming events (Severinghaus and Brook, 1999; Severinghaus and Brook, 2000). For one, this indicates that the temperature rise and associated environmental changes cause or trigger the methane increase and not vice versa (although there will be a feedback through the radiative forcing of methane). For the other, the response of the methane system to the warming occurs extremely fast. The mechanism to increase methane levels must have a very short start-up time.

In conclusion, the process that controls variations of atmospheric methane concentration, or at least the rapid increases at glacial terminations, is a major methane source or sink. It is likely to be active in tropical and mid- to high latitudes affected by the monsoon cycle. The process responds quickly to warming or an associated environmental change.

Different hypotheses on the exact nature of the methane control can be tested against the above evidence. The scenario of decreased sink strength has not received much attention. Several studies investigated the abundance of hydroxyl radicals in the past, using ice core proxy measurements or atmospheric modeling (Crutzen and Brühl, 1993, Thompson et al., 1993; Osborn and Wigley, 1994; Martinerie et al., 1995; Lelieveld et al., 1998). The consensus is that hydroxyl was more abundant by approximately 30 %. This means that the sink was stronger in pre-industrial times, but the findings apply to the stable periods of PIH and the last glacial maximum (LGM) and not to times of rapid change. Only qualitative results are available for the latter. The warming associated with the events must result in faster reaction rates. Consequently, methane removal would increase, which is contrary to our premise. A new model of atmospheric chemistry includes a study of non-methane hydrocarbons (NMHC), which compete with methane for hydroxyl radicals (Kaplan et al., 2004). NMHC are emitted by plants and the

authors investigate if vegetation changes could have affected atmospheric chemistry and consequently methane concentrations. At this point, the study is still in progress. It is well established that increasing methane levels deplete hydroxyl and therefore sink activity (Prather, 1994), but this would be a reinforcing feedback rather than the initial cause for methane increase. Other sinks for atmospheric methane, i.e. soil uptake and reaction with chlorine in the stratosphere and the marine boundary layer, are too small to have played a significant role. In conclusion, decreasing sink strength is thought to have contributed to higher methane concentrations (Chappellaz et al., 1993b; Thompson et al., 1993), but it certainly did neither cause nor fully sustain the rapid methane increase of the YD-termination.

Most natural methane sources can be discounted as the driver for the increase during glacial terminations because they are not large enough. Emissions from wildfires, termites, ruminants, freshwater and marine systems are not large enough to double atmospheric concentrations in a short time. Geologic methane emissions, i.e. the outgassing of thermogenic methane in tectonically active zones, might have an emission potential of yet unresolved magnitude. The release to the atmosphere, however, is dependent on tectonic activity and cannot be linked to climatic cycles.

Wetlands are the dominant natural source for methane (Fung et al., 1991). They have not only the emission potential to increase atmospheric methane concentration but are also dependent on environmental conditions that control methane output in accordance with climatic cycles (Chappellaz et al., 1990 and 1993a; Crowley, 1991). The observed warming during terminations would increase anaerobic methane production. More importantly, however, is that tropical precipitation increased strongly at the critical time. This would have led to expansion of wetland areas and enhanced methane production (Petit-Maire et al., 1991; Street-Perrot 1993). The wetland hypothesis is the most widely accepted theory today. Wetlands theoretically satisfy all the preconditions for the driver of rapid atmospheric methane increase. Critique concerns their latitudinal distribution and whether this fits the geologic evidence. Research so far has focused on tropical wetlands, mostly because boreal wetland regions were ice covered at the time

(Chappellaz et al., 1993a). However, Brook et al. (1996) concluded in a study of the long record of methane concentration in GISP2 that tropical sources could not sustain the observed fluctuations alone and that correlation with insolation patterns of the Northern Hemisphere indicate a substantial contribution from temperate and boreal wetlands. This is supported by independent work (Crowley, 1991; Chappellaz et al., 1997, Dällenbach et al., 2000; Brook et al., 2000). The main controversy about wetland methane is whether the emissions could have increased suddenly enough to produce the rapid increase. The geologic record shows that extensive mature wetlands developed only after the climate transition, i.e. too late to have caused the methane rise (Nisbet, 1992; Kennett et al., 2003). The counter argument is that methane production in wetlands depends on primary productivity rather than above-ground biomass (Whiting and Chanton, 1993). Consequently, newly flooded areas could have emitted large amounts of methane without accumulating peat layers for the geological record. Notwithstanding this as yet unresolved debate, wetlands are a likely candidate to have increased atmospheric methane at the glacial terminations.

The only other methane reservoir that is large enough to account for the shifts between glacial and interglacial atmospheric concentrations are gas hydrates, also known as methane clathrates. Today hydrates are only a minor source of methane, but that was not necessarily the case under different, or rapidly changing, environmental conditions, especially when those were changing rapidly. Gas hydrates are ice like compounds and stable only within a narrow pressure and temperature range. They occur in permafrost regions and marine sediments (Kvenvolden and Lorenson, 2001). Both environments are particularly sensitive to the changes during glacial cycles. During deglaciations receding permafrost must have emitted large amounts of methane to the atmosphere, especially when exposed shelf areas got flooded. This process, however, would have taken place on longer time scales and after the initial warming event, i.e. the abrupt increase in methane concentrations. Therefore, terrestrial hydrates are not considered a source for this initial rise. Instead, marine hydrates are discussed as the critical methane reservoir.

An older theory assumed that the pressure drop from lower glacial sea levels destabilized the hydrates, so that free gas accumulated in the sediment and was released in catastrophic bursts. This would multiply the amount of atmospheric methane and end the ice age through greenhouse warming (MacDonald 1990; Nisbet 1990; Paull et al., 1991). With improving knowledge of the structure of marine hydrate deposits, this theory was considered unrealistic. A new theory postulates that temperature is the cause of hydrate destabilization. Changes in ocean circulation (their character or cause are not identified) bring warmer intermediate depth water masses in contact with the hydrate bearing sediment. As the heat pulse penetrates the sediment it dissociates the clathrate, releasing methane that escapes to the atmosphere and causes the climatic shift to terminate the ice age. The scenario is known as the "clathrate gun theory". It has been reviewed by Nisbet (2002) and Kennett et al. (2003). It offers convincing explanations for several features of the geologic record, such as the abruptness of the glacial terminations and variations in the ^{14}C record. Evidence of massive release of oceanic methane at the end of cold periods comes from stable isotope studies of benthic and planktonic foraminifera in the Santa Barbara basin (Kennett et al., 2000) and off East Greenland (Smith et al., 2001).

Other records, however, do not show the signals expected from a hydrate burst. The methane concentration increase measured in ice cores is not large enough to induce enough radiative forcing to cause the observed warming (Raynaud et al., 1993; Chappellaz et al., 1993a). A short-lived methane spike could have gone unnoticed due to lacking resolution of the record (Thorpe et al., 1996), but with a mounting number of ice cores and high-resolution analysis this is less and less plausible (Chappellaz et al., 1997; Brook et al., 2000). Also, the stable carbon isotope composition of the oceanic carbon reservoir does not show the depletion expected from the methane input (Maslin and Thomas, 2003). Massive submarine landslides have been found in potentially hydrate bearing areas, indicating where the release could have occurred. Dating of the sediments, however, reveals that they slightly post-date the glacial termination (Maslin et al., 2004). Another contradiction to the clathrate gun theory is that the temperature increase starts

shortly before the rise in methane concentrations (Severinghaus et al. 1998; Severinghaus and Brook, 1999).

The main attraction of the hydrate theory is the large potential of the clathrate reservoir, implying that the destabilization of only a small fraction could alter atmospheric methane levels drastically and lead to global warming. Estimates of the global clathrate reservoir depend on a multitude of parameters (for a review see Kvenvolden, 1999). The revision of any of these parameters through ground truthing can strongly affect the total number. Based on new in-situ measurements of the actual percentage of hydrate in potentially clathrate-bearing sediment, Milkov et al. (2003) estimate the marine hydrate reservoir as 2100 – 3600 Tg (Teragram = 10^{12} g). This is significantly lower than previous studies (Kvenvolden, 1999) and implies that a much larger portion of the hydrate reservoir must destabilize to supply the necessary amount of methane. All these counter arguments address the assumption of catastrophic hydrate outgassing as a trigger for warming. They do not rule out continuous and gradual emissions from clathrates, either marine or terrestrial. Gas hydrates are a possible source of methane during deglaciations and their large potential as a climate amplifier could give them a key role in glacial cycles. Together with wetlands, they are the main candidates to control the variability of atmospheric methane.

Tests of the wetland and the hydrate hypotheses have focused on geologic evidence, e.g. peat accumulation and pollen records or marine geochemistry and sedimentology. There is, however, a more direct approach to the problem. In the composition of stable carbon isotopes atmospheric methane preserves the signal of the sources it came from and the sink processes it was subject to. The stable isotopes ^{12}C and ^{13}C are fractionated through physical and biological processes during the formation of methane and its transport to the atmosphere. The result is that methane source types have specific and characteristic ranges for their isotopic composition. The latter is commonly, and in this work, defined as the ratio of ^{13}C over ^{12}C compared to the PDB standard and expressed in per mille (‰). This is known as the delta notation or $\delta^{13}C$. Atmospheric methane is a mixture of gas from different sources and its isotopic signature ($\delta^{13}C_{CH4}$)

depends on how much methane each source contributes and the isotopic composition of this source. In this mass balance large sources and those with extreme $\delta^{13}C$ will leave the biggest signal. The absolute value of the atmosphere, however, is also influenced by sink processes, which remove ^{12}C faster than ^{13}C and therefore enrich the atmospheric methane pool in the heavier isotope. This fractionation is reasonably well known, as are the $\delta^{13}C$ ranges of the different source types. As a consequence, it is possible to constrain methane budgets. An assumed composition of the global source is a possible scenario if the isotope numbers and emission volumes add up to the measured atmospheric value. It is now common to constrain the modern methane budget using the isotope mass balance (Stevens and Engelkemair, 1988; Fung et al., 1991; Whiticar, 1993; Gupta et al., 1996; Hein et al., 1997).

If the relative contributions from different source types with different isotope ratios changed over time, it would be detectable in a record of $\delta^{13}C_{CH4}$. Direct atmospheric isotope measurements do not reach back far enough to study variations of the natural methane cycle. To use the isotope mass balance approach for reconstructions of methane budgets in the past, the isotope analysis has to be done on old air samples that have been preserved unaltered. As for the paleorecords of atmospheric methane concentration, air occlusions in polar ice offer such a reservoir. In both cases, the recorded signal will not represent the global average because of latitudinal gradients in concentration and $\delta^{13}C_{CH4}$. In the case of isotopic composition, however, the difference between the hemispheres is around 0.5 ‰ today, a negligible offset (Quay et al., 1999). Unfortunately, stable isotope analysis requires larger amounts of gas than concentration measurements. The only published results to date (Craig et al., 1988b) are from the late pre-industrial Holocene (PIH). The isotopic composition at that time was –49.6 ‰, considerably more depleted in ^{13}C than today. This confirmed two results. For one, that the lower methane concentrations observed in ice cores are not the result of methane consumption after the bubbles closed off. That process would have enriched the remaining gas in ^{13}C instead of depleting it. This is additional proof of the suitability of ice cores for gas analysis. For the other, the low $\delta^{13}C$ is in accordance with the assumption that anthropogenic methane sources, which are predominantly enriched in

^{13}C, caused the increase in modern times. Craig et al. (1988b) used their findings as a baseline scenario without emissions from fossil fuel burning to calculate the modern magnitude of the latter. Unfortunately, analytical techniques at the time were not suitable to gain a record that would monitor changes over time in the pre-modern era. With advances in mass spectrometry it is becoming feasible to measure high-resolution records of $\delta^{13}C_{CH4}$ in ice samples and study the natural variability of this parameter. Preliminary results of a more recent study confirm the findings of Craig et al. (1988b) and reveal some of the natural variability in the late PIH (Etheridge et al., 2003). The major shifts of the methane system during glacial cycles, however, have not been studied.

The goal of this project is to develop an analytical technique for the measurement of stable carbon isotopes of methane in the air occlusions of ice. The method must be sensitive enough to resolve dynamic changes on the order of decades. The precision must enable us to detect variations on the order of one per mille. The basic principle of the technique is to liberate the gas from the ice by melting it under vacuum, which is known as a wet extraction (as opposed to a dry extraction, where the air is extracted mechanically through crushing or grating). From the melt water and the headspace a helium stream will purge the gas onto a cold trap in order to collect the methane, and then inject it into a gas chromatograph, where it is separated from other compounds. Finally, methane is combusted to carbon dioxide and enters the isotope ratio mass spectrometer (IRMS). Here the ratio of ^{13}C to ^{12}C is measured. The raw data then must be corrected for various processes that occur before occlusion of the air, while it is diffusing through the firn layer. To this end computer models have to be developed and applied.

The analytical technique will be used to measure samples that span the end of the last ice age. This will provide a record of how $\delta^{13}C_{CH4}$ varied while global temperatures and atmospheric methane concentrations underwent severe shifts. With the isotope mass balance approach, any observed variations can be interpreted as changes in the composition of methane source types. In this manner, the following questions can be addressed. How much variability is there in $\delta^{13}C_{CH4}$ during stable periods when neither temperature nor methane concentrations change? Are there differences in $\delta^{13}C_{CH4}$ between

different climatic periods? Does $\delta^{13}C_{CH4}$ indicate different source compositions in warm periods with high methane concentrations than in those with low temperatures and atmospheric methane? Does $\delta^{13}C_{CH4}$ change during the terminations while methane levels increase rapidly, indicating that new sources become active and drive the rise?

The answer to all these questions may bring us closer to understanding how the natural methane cycle works, how it is influenced by changes in global climate and how, in turn, it affects climate. In times when both global temperatures and atmospheric methane undergo significant, if not unprecedented changes; when man-made warming could potentially affect natural methane production while humanity emits large quantities of methane due to the production of food and energy, this knowledge is indispensable for the assessment of the potential impact on the natural system and an evaluation of our actions.

2. Methods

The analysis of paleorecords of atmospheric $\delta^{13}C_{CH4}$ requires measurements of the gas preserved in ice cores as well as reconstruction of the actual atmospheric history from these data. The former comprises an extraction technique to liberate the gas from the ice occlusions and analysis of stable isotope ratios by mass spectrometry. The latter consists of the correction for any alterations of the atmospheric signal that occur during the diffusion of air in the snow layer and the occlusion process by means of a diffusion model. This chapter describes the analytical procedure and the diffusion model used in this project.

2.1. Gas extraction and isotope ratio mass spectrometry

A major part of this project was the development of an on-line extraction method for methane from ice core samples.

2.1.1. Principle

The ice sample is placed in an evacuated extraction chamber. Melting liberates the entrapped air, which is flushed out with a Helium stream and trapped on a cold finger. The same Helium stream strips any dissolved gas from the melt water. From the cold trap the gas is injected into the GC-IRMS.

2.1.2. Extraction line

A schematic of the extraction line is shown in Figure 2.1.1. A Helium inlet (1/4" copper tubing) enters a stainless steel extraction chamber; it can be shut off by a Nupro™ bellows valve. The chamber seals with an O-ring both under vacuum and slight overpressure. The outlet line bifurcates to a roughing pump line and the trap line, both of which can be shut off by Nupro™ bellows valves. The trap line passes through a water trap of 1/4 " and 1/8 " copper tubing that is immersed in a dry ice/ethanol bath at –60 °C during operation. It is attached to a Valco six-way valve by a Cajon Ultratorr™ fitting, which is easily disconnected to vent the water trap. The six-way valve operates in either

trapping or injection mode. During trapping the sample stream runs through a loop of 1/8" stainless steel filled with the absorbent Hayesep™, which can be cooled with a cold block to –125 °C, before it goes to waste. In injection mode the carrier gas stream of the gas chromatograph passes through the Hayesep™ loop and introduces the sample into the GC-IRMS.

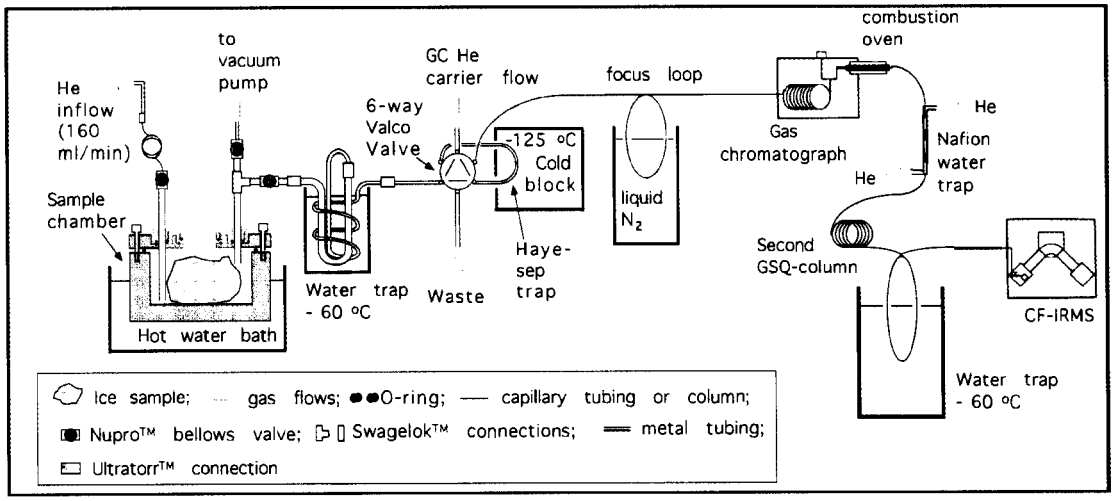

Fig. 2.1.1: Micro-extraction line and GC-CF-IRMS for extraction of gases from ice samples and stable isotope analysis

2.1.3. Gas extraction procedure

The outer surface of the ice sample is scraped off to avoid surface contamination. Then the sample is weighed and placed in the pre-cooled stainless steel extraction chamber. A Leybold Trivac™ rotary vane pump evacuates the chamber to the vapour pressure of ice. This eliminates contamination through atmospheric gases or lab air. Pumping time is 5 min while the pressure in the chamber is monitored. After closing the connection to the pump, the chamber is heated with a hot water bath to melt the ice. This takes between five and ten minutes, depending on sample size. Still under vacuum, the melt water is left to equilibrate with the headspace for at least one minute after melting is complete. Opening the inlet valve fills the chamber with Helium at a rate of 250 ml per minute. Just before the calculated time to fill the chamber is elapsed, the cold block is placed around the Hayesep™ trap. Then the outlet stream of the chamber is opened and the water trap is immersed in a cold bath at –60 °C. This sequence proved suitable to

prevent both contamination from air getting drawn in through the waste line while cooling the traps and sample loss due to a pressure pulse going through the Hayesep™ trap.

Helium passes through the melt water to strip any remaining methane from it and flushes the headspace out. Water vapour is removed from the outflowing gas in the water trap. Methane freezes out on the Hayesep™ trap at –125 °C while oxygen, nitrogen and nitrogen compounds are purged off. This step is important to remove gases that would otherwise interfere with the chromatography. A flushing time of fifteen minutes, equivalent to around ten headspace volumes of He flow, is suitable to ensure complete trapping of methane and prevention of breakthrough.

After trapping is complete, a loop of the GC capillary column is immersed in liquid nitrogen. The Valco six-way valve is switched from trapping to injection mode and the cold block is removed from the Hayesep™ trap. The carrier gas flushes the trapped methane onto the focus loop, which takes ten minutes. This step is necessary to create a sharp peak as opposed to the gradual release of methane from the Hayesep™. Then the valve is switched back to trapping mode and the focus loop removed from the liquid nitrogen to introduce the methane into the GC.

It is crucial to efficiently dry and purge the system between sample runs. The chamber is emptied, wiped dry and then evacuated together with the water trap for 3 min to remove remaining water. To this end the trap is disconnected from the six-way valve, the end sealed with a rubber stopper and the tubing heated with a heat gun. After closing the outlet valve the chamber is evacuated for another minute, then filled with Helium. The water trap is heated a second time while Helium flushes through it. In a next step the Hayesep™ trap is connected again, flushed with Helium and heated. This step purges off any remaining compounds from the absorbent. It was necessary to flush Helium through the extraction line for another 15 min to efficiently purge off residual water and other compounds.

All on/off-valves in the system are Nupro™ bellows valves. Like the Valco six-way valve they were tested and found to provide good seals without generating methane when operated. It proved unnecessary to purge impurities from the He carrier gas upstream of the extraction cycle. Certain steps of the extraction procedure required fine-tuning to ensure optimal results.

2.1.3.1. Pumping time

Compared to many methods reported in the literature a relatively short evacuation time is used after the ice is enclosed in the chamber. Pumping time is only 5 min as opposed to 30 - 60 min (Brook et al., 2000; Tohjima et al., 1991). Several tests showed that longer pumping times did not result in lower blanks or more consistent isotope numbers for test samples. Monitoring the pressure in the pump line proved that the roughing pump was not a limiting factor. Instead, the vacuum depends on the vapour pressure in the system. Over the course of a measuring day the vacuum changes from 0.03 torr to 0.07 torr, presumably as a result of residual water in the line. If the system was not well adjusted up to 0.2 torr were observed, but none of these changes affected blank height or isotope ratios.

2.1.3.2. Melting time

The time to melt an ice sample will depend on its size and shape. A range from three to ten minutes was observed in tests and measurements. Replacing the hot water bath of the chamber with new boiling water speeds up the process, but overheating the system results in higher blanks. I therefore used only a single water bath and monitored the melting through the window in the chamber lid. After melting is complete, an equilibration time between melt water and headspace of one minute is sufficient. In fact, an experiment showed no effect on either isotope number or amount of extracted gas when the Helium stream started before melting was complete. This suggests that all the extracted gas goes into the headspace immediately. In contrast, earlier experiments, where the ice melted in a Helium headspace and not under vacuum, showed that 60 % of the gas dissolved in the water first (see Fig. 2.1.11).

2.1.3.3. Flushing time

As a general rule, flushing an amount of gas equal to between five and ten volumes of headspace is necessary to efficiently transfer the initial head space gas to the cold trap. Incomplete flushing will result in sample loss and may be associated with an isotope effect. At the same time it must be ensured that there is no breakthrough of methane through the Hayesep™ trap during extended flushing times, which can be prevented by setting a lower trapping temperature. In this set-up this is easily done because the Hayesep™ trap is cooled by a stainless steel block, where an electric heater works against cooling by liquid nitrogen to reach a set temperature. A third point to consider is that Oxygen and Nitrogen compounds must be purged off efficiently during the trapping step so they will not interfere with the gas chromatography. Consequently, trapping time and temperature must be optimized with regards to the three problems outlined above. Various experiments tested this by injecting known volumes of gas upstream of the chamber and monitored the amount trapped on the Hayesep™ trap and its isotopic composition in dependence of flushing times or volumes of gas exchanged. An additional set of experiments used varying trapping times and temperatures for artificial ice samples, made of water that had equilibrated with outside air before freezing.

The results (Fig. 2.1.2) show that methane is transferred quantitatively from the chamber to the Hayesep™ trap after 16 min or eight exchanged volumes, using Helium flow rates of 160 ml/min. Breakthrough was not observed before 25 min at –125 °C. Also, purging of Oxygen and Nitrogen compounds is efficient when purging exceeds ten minutes at –125 °C.

Measurements of ice samples of different size show that additional factors influence the system. For large samples flushing of ten headspace volumes resulted in poor reproducibility of isotope numbers. This was not observed at longer flushing times. It is not clear whether the geometry of the chamber becomes an influence or if partitioning of methane into the melt water is a problem. Consequently, when measuring samples flushing time were set to 20 min or ten headspace volumes, whatever is longer.

Another test investigated the difference between a Helium inlet stream that bubbled through the melt water to strip dissolved gas and an inlet that introduced the Helium into the headspace. There was no difference, suggesting that partitioning of gas into the water is not a problem, at least not if flushing times are sufficiently long. Nevertheless, for measurements Helium strips the melt water, although the 1/4 " tubing does not produce suitably fine bubbles.

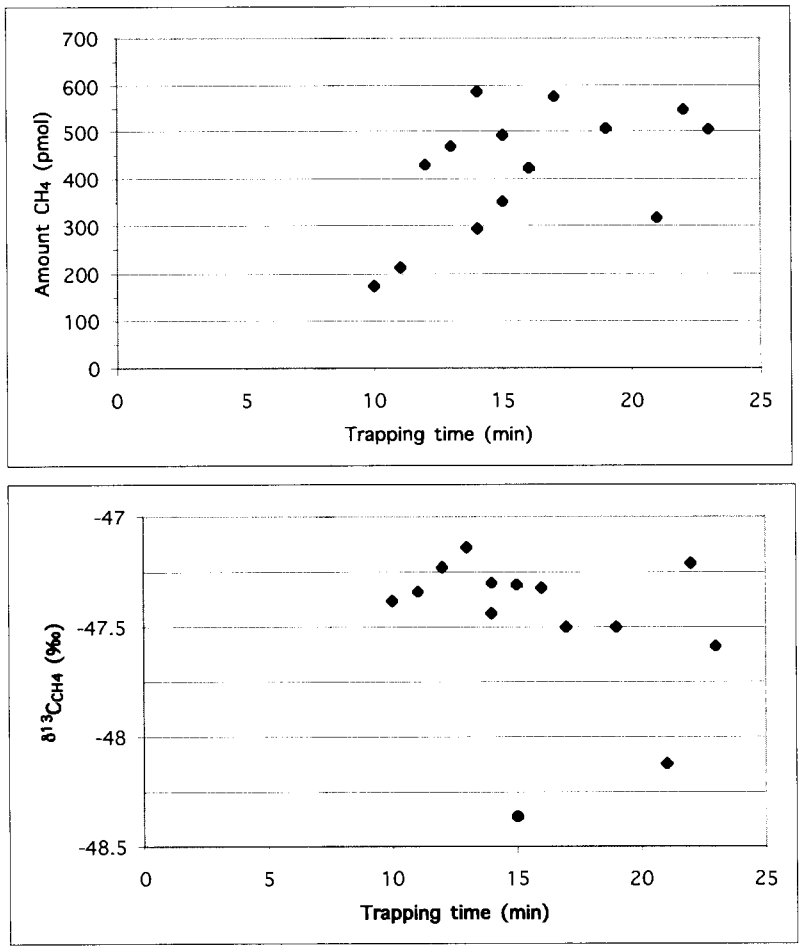

Fig. 2.1.2: Methane yield (top panel) and $\delta^{13}C$ (bottom panel) of ice standards in dependence of trapping times

2.1.3.4. Focusing time

Ten minutes are sufficient for the Hayesep™ trap to warm from -125°C and release the trapped methane onto the focus loop.

2.1.4. Gas chromatography

Measurements are performed with a SRI 8610 gas chromatograph equipped with a 30 m GSQ™ capillary column (ID 0.53 mm). The Helium carrier gas flow rate is 1 ml/min. The column is cooled to 0 °C, which results in good separation of methane and carbon dioxide. In a next step, the sample passes through a combustion oven at 1080 °C. Here methane combusts quantitatively to carbon dioxide using a nickel-platinum catalyst and Oxygen bleed. A Nafion™ trap then removes water from the gas stream. A second GSQ™ capillary column (30 m x 0.53 mm ID) separates the methane, now converted to carbon dioxide, efficiently from nitrous oxides and carbon monoxide (Fig. 2.1.3). An additional loop of the capillary immersed in a mixture of ethanol and dry ice at –60 °C forms a last water trap. It is purged off after every run while the source inlet of the mass spectrometer is closed.

2.1.5. Mass spectrometry

The measurements were made on a Finnigan MAT 252 isotope ratio mass spectrometer. The instrument is set up to detect molecules with mass 44 (e.g. $^{12}CH_4$, $^{12}CO_2$, N_2O) and mass 45 (e.g. $^{13}CH_4$, $^{13}CO_2$). Different gas compounds hit the detector at their specific elution time (Fig. 2.1.3). The isotope ratio of that gas species is calculated from the co-eluting mass 44 and 45 peaks. Peaks of gases with the same molecular mass have to be completely separated. For this study, nitrous oxides, which enter the IRMS as N_2O, and CO, as well as CO_2, have to be separated from CH_4. Note that the last three compounds all have been combusted to CO_2 before reaching the mass spectrometer. Complete peak separation between all species could be achieved through chromatography and especially through the use of a second column after the combustion step.

The online intake from the open split (a regulator between gas delivered from the extraction line and gas introduced to the IRMS) is set to 0.5 ml/min, resulting in a 50 % yield of the extracted methane. The isotope ratios are calculated relative to an internal

standard, which is a carbon dioxide tank that injects gas pulses at different times of the mass spectrometer run. This reference tank is in turn calibrated against samples of VPDB CO_2 gas provided by the National Institute of Standards and Technology (NIST). The mass spectrum is recorded and interpreted using Finnigan's software Isodat™ for Windows NT.

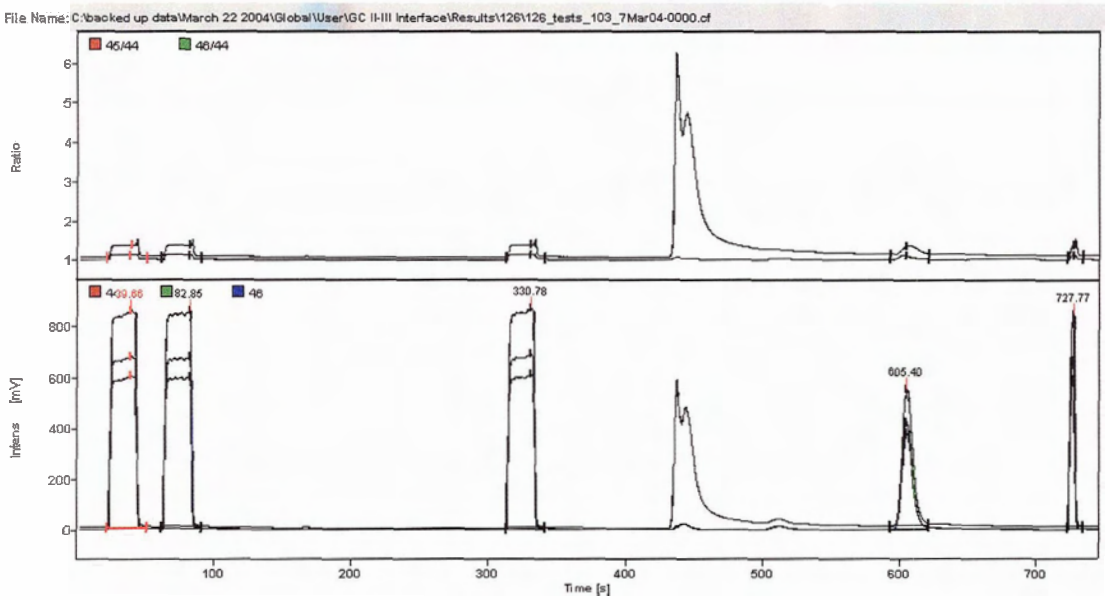

Peak nr.	Gas	Retention time (s)	Peak width (s)	Amplitude 44 (mV)	Amplitude 45 (mV)	Amplitude 46 (mV)	$\delta^{13}C$
1*	Ref.	39.7	29.3	602	681	853	-33.11
2	Ref.	82.8	29.1	599	677	848	-33.113
3	Ref.	330.8	28.6	609	688	862	-33.173
4	CH_4	605.4	28.3	381	425	536	-47.042
5	Ref.	727.8	11.5	589	666	832	-33.303

Fig. 2.1.3: Mass spectrogram of an artificial ice sample
The mass spectrogram shows the measured intensities of masses 44, 45, and 46 (lower panel) and the ratios of 45/44 and 46/44 (upper panel). The first three peaks and the last one are the reference CO_2 gas. The peaks at 450 s and 520 s are N_2O and CO, respectively, followed by methane at 605 s. Separation between all peaks is good, note that the elevated baseline after the elution of N_2O is mass 46 only and does not affect the $\delta^{13}C$ of CH_4.

2.1.5.1. Detection limit

The precision of a measurement depends on the signal to noise ratio and therefore on sample size. The lower threshold is the smallest peak height at which the measurements of the different masses are accurate enough to calculate a reliable isotope ratio. Peaks below this limit will yield isotope numbers of poor precision known as shot noise. An experiment determined a threshold for peak size and established the detection limit. Different volumes of a methane-gas mixture (1.8 ppbV in He; $\delta^{13}C = -41.8$ ‰) were injected via a port upstream of the chamber to find the smallest peak height with consistent results (Fig. 2.1.4). Isotope values become unstable for peaks smaller than 250 mV. An experiment with six artificial samples (expected $\delta^{13}C = -47.2$) showed a standard deviation of 0.34 ‰ at an average peak size of 237 mV (Fig. 2.1.4). These experiments define a lower limit for sample size. For a conservative approach peak heights should exceed 400 mV for ice measurements. This is equivalent to 430 pmol of methane or an ice sample volume between 130 and 260 cm^3 depending on the concentration in the bubbles.

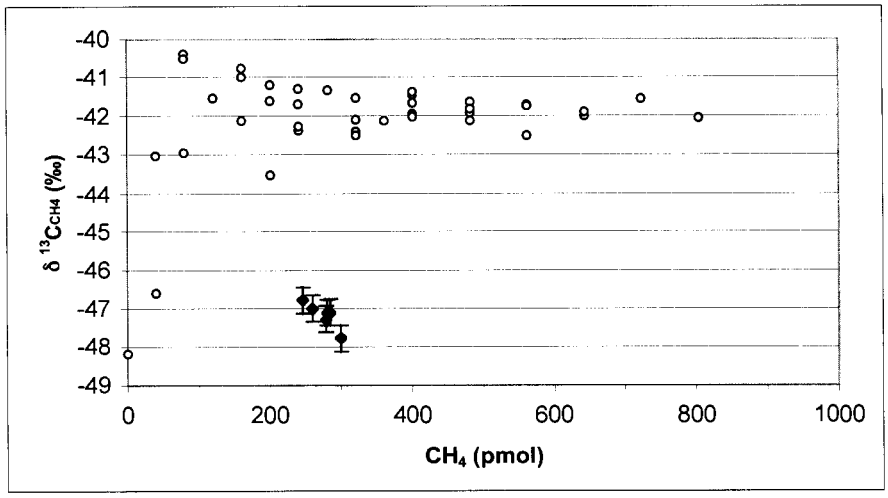

Fig. 2.1.4: $\delta^{13}C$ of gas and ice standards at the lower detection limit
Circles are measurements of standard gas (1.8 ppmV CH_4 in He), diamonds are ice standards (80 g) with error bars of ±1 standard deviation

2.1.5.2. Calibration and standards

All measured isotope ratios were calculated relative to a CO_2 tank, which in turn is calibrated against VPDB standard CO_2 gas by NIST. In addition, different working standards were used during the measurements to monitor the performance of the line and to calibrate the results. Known volumes of outside air, which has a methane concentration of 1.8 ppmV, was injected with a syringe into a port upstream of the extraction chamber and provided calibration curves for the amount of methane retrieved (an example is shown in Fig. 2.1.5). The fact that methane concentration in air and its isotopic composition is constant over time was also established with routine measurements using the gas analysis set-up of the laboratory, which uses the same gas chromatograph, combustion line and mass spectrometer. The air measurements with the ice extraction line also are very consistent for the amount of methane ($r^2 = 0.9963$ with $n = 51$) over at least the period of a measurement cycle (i.e. several weeks). In contrast, the isotope numbers usually vary by ± 0.9 ‰ (one standard deviation, Fig. 2.1.6). The most likely cause for this lack of precision is isotopic fractionation while the air (or a standard gas) is injected with a syringe. Such a step is not part of the ice measurements and the latter show good precision.

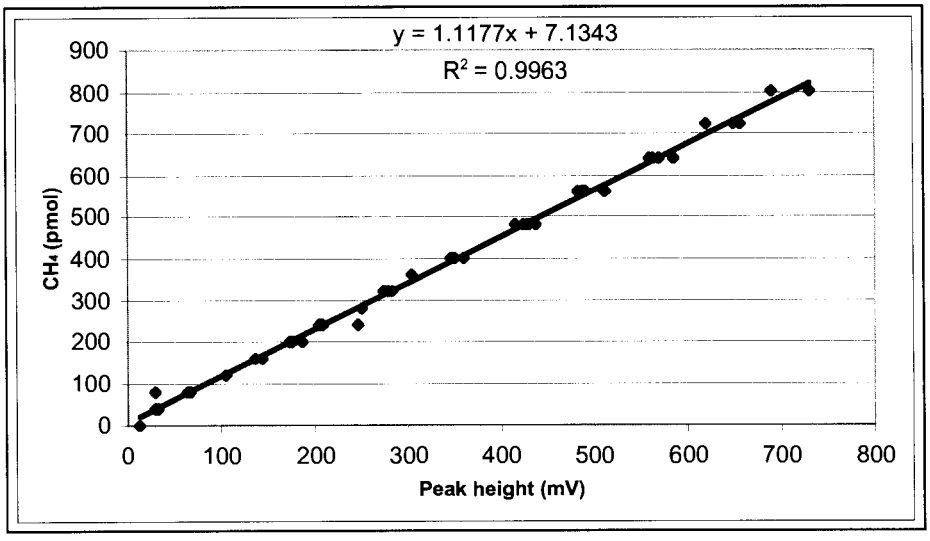

Fig. 2.1.5: Calibration curve of air standards to calculate the methane content of ice samples

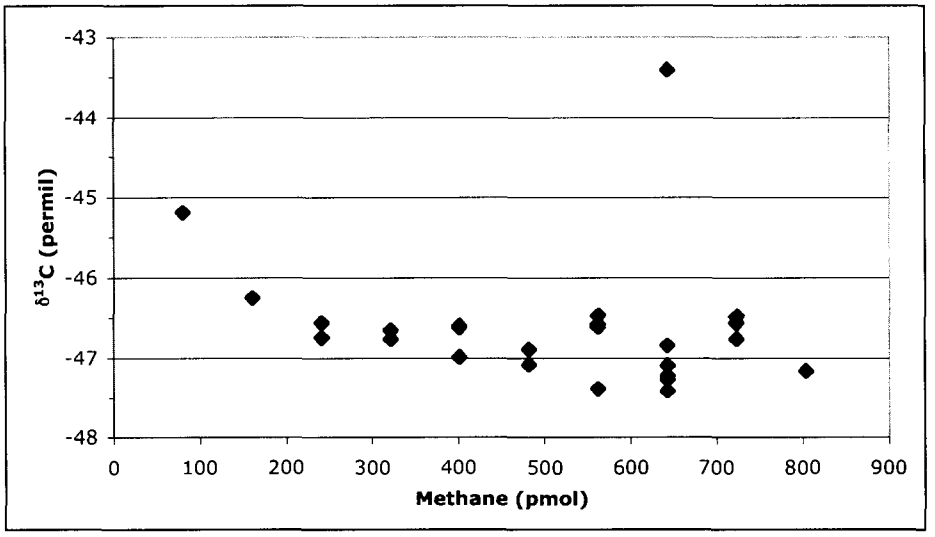

Fig. 2.1.6: $\delta^{13}C$ values of air measurements
The isotopic composition of outside air samples measured on the extraction line during analysis of the 2002 Pakitsoq data set. The average of this sample set is –46.8 ‰, slightly more ^{13}C rich than the results of Quay et al. (1999) and measurements with a set-up

It was also observed that for air measurements in between ice samples the shorter processing time (omission of certain extraction steps) seems to affect the capacity of the line to reset between runs. The same is true for other standard gases used to calibrate the system. The reason for this is unknown. Air standards were typically run at the start and the end of a measuring day.

Another type of standard used in this study is artificial ice. The ice is frozen from tap water. The latter has high concentrations of methane with low $\delta^{13}C$ when it is taken directly from the line. Therefore, the water must equilibrate with outside air for several hours while stirred. It is then frozen in known quantities using plastic containers in a commercial chest freezer. A major assumption is made when using this ice as a standard, namely that the dissolved methane has the same isotopic composition as outside air and that this value is retained throughout the freezing process. If this assumption does not hold true one would still expect the ice samples of one batch to have consistent isotopic composition because they were all treated in the same way.

Artificial samples consistently showed atmospheric isotope composition for the methane as seen in Figure 2.1.6. Ice standards shown in this plot were measured in between ice samples during a six day measurement period and illustrate the stability of the analytical system. The only exceptions occurred when the tap water had not completely equilibrated with air and was depleted in ^{13}C. This is easily recognized from higher levels of methane. Generally, the samples provided a reliable standard with standard deviations between 0.3 and 0.6 ‰, depending on sample size. Larger samples had higher reproducibility. Two ice standards of different size were analyzed routinely during a day of measurements. Additional ones were measured if the system seemed not to be working properly.

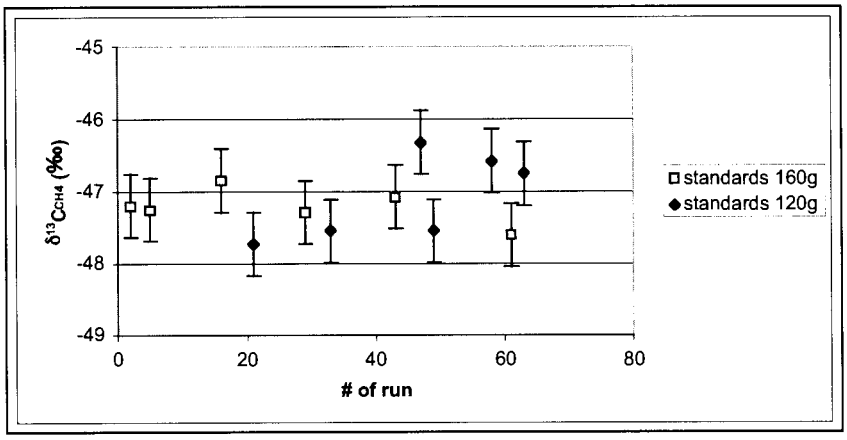

Fig. 2.1.7: $\delta^{13}C_{CH4}$ values measured in artificial ice samples during a measurement period The x-axis indicates when the individual standards were run, interspersed between samples, over six days.

As an additional experiment, artificial samples were created by freezing water that had been equilibrated with a gas mixture of 1.8 ppbV CH_4 in N_2. The methane has a $\delta^{13}C$ of –41.8 ± 0.5 ‰, which was measured with the gas analysis set-up, as well as the ice extraction line (Fig. 2.1.4). The ice samples that had equilibrated with this gas, however, measured –44.9 ± 0.5 ‰ (n= 12, one standard deviation). The discrepancy could be an error caused by the procedure, but the most likely cause for the offset is that the water had not completely equilibrated with the tank gas prior to freezing and retained partly an atmospheric signature. The precision of these measurements is comparable to normal ice

standards. The offset between ice extractions and direct gas measurements, however, shows that the equilibration probably was not complete. Consequently, these samples were not used as a standard, because they don't indicate problems with the procedure as clearly.

It is a drawback that standards used routinely have atmospheric isotope composition. Because the air in the laboratory will be close to that value it is difficult to detect contamination in the standard runs. However, there is no easy way to create an ice standard with known isotopic composition and the attempt to do so would introduce more uncertainty. In addition, one can argue that loss of methane or contamination during the extraction step can be detected through isotope effects, which are likely associated, or changes in the methane yield.

Air standards also provided the calibration curves (e.g. Fig. 2.1.5) for calculating methane concentration of the samples. Peak size of the IRMS mass 44 trace of sample methane peaks is proportional to volume of methane. Sample weight is converted to a volume of enclosed air using literature data for GISP2 (Raynaud et al., 1997), and was calculated for Agassiz samples (after Raynaud et al., 1997). Methane concentration is then the ratio of volume of extracted methane and the volume of air enclosed in the ice sample (Fig. 2.1.8).

2.1.5.3. Precision and accuracy

Measurements of ice from the GISP2 core section #139 from central Greenland established the precision of the technique. Six measurements using the established technique had a standard deviation of 0.32 ‰ (Fig. 2.1.8). The same data provide a test of accuracy. Atmospheric concentration as calculated from the yield of methane is 690 ± 19 ppbV for the sample age of 225 – 229 yr BP (rel. to AD 1950). This is in reasonable agreement with the value of 730 ppbV for the same core by Brook et al. (1996, 2000) (Fig. 2.1.8). A limiting factor in measuring concentration is that air content of the sample is not determined during the analysis and the use of literature values for the calculation introduces uncertainty. The absolute concentration values obtained with the technique presented here are not as good as those obtained with specific concentration

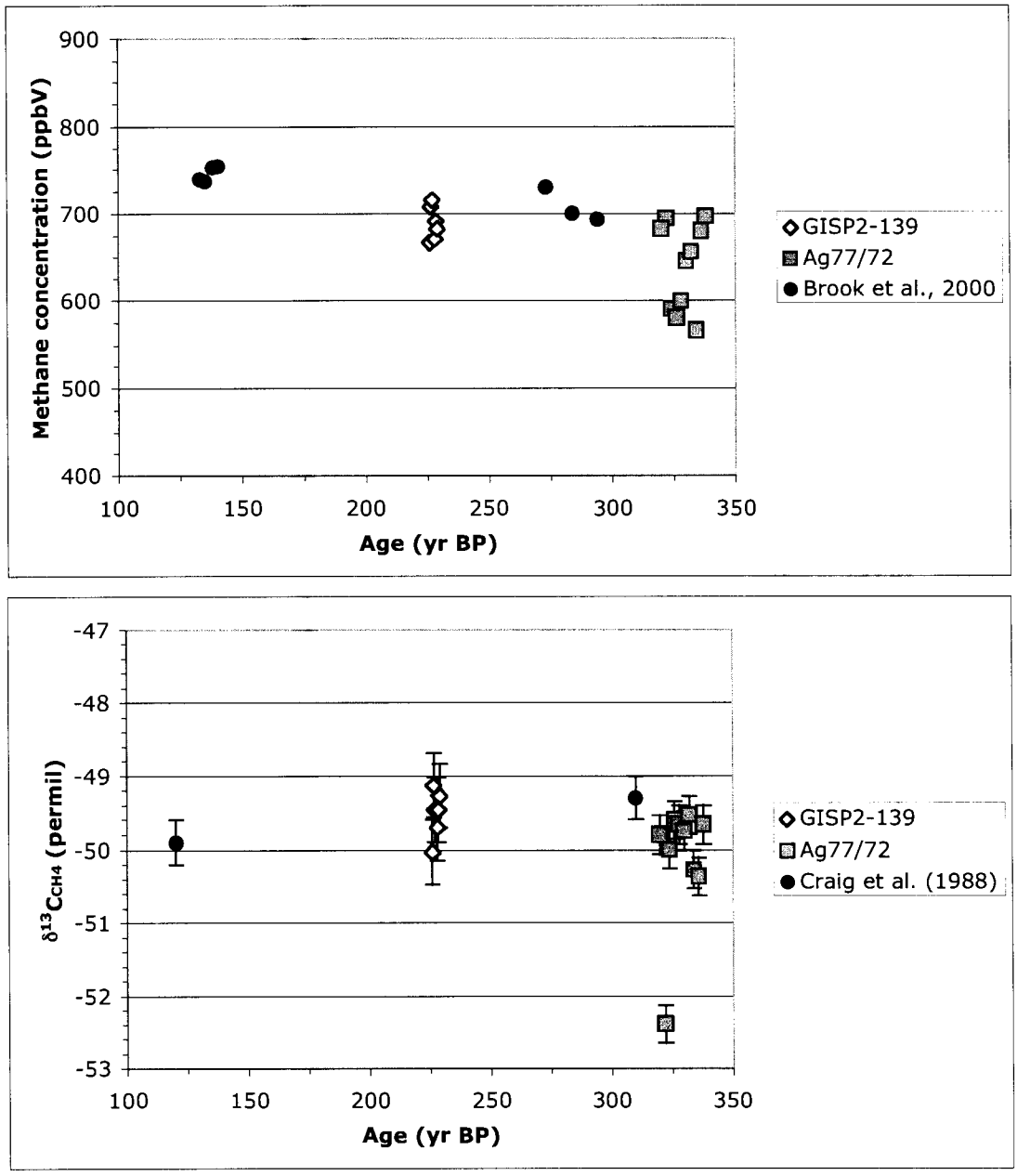

Fig. 2.1.8: Methane concentration and $\delta^{13}C_{CH4}$ from GISP2 and Agassiz 77/72
Top panel shows methane concentrations measured in samples from the GISP2 ice core in central Greenland and core Ag77/72 from Ellesmere Island. GISP2 data from Brook et al. (1996, 2000) plotted for comparison.
Bottom panel shows $\delta^{13}C_{CH4}$ values from GISP2 and Agassiz 77/72 ice core. Data from Craig et al. (1988b) plotted for comparison. A single outlier in the Ag 77/72 series ($\delta^{13}C$ = -52.1 ‰) is from the only sample with significant melt layers (>30 %).

measurements, but they are suitable to determine the contemporaneous atmospheric concentration and its relative changes, which provides a time scale for the samples.

The $\delta^{13}C_{CH4}$ of methane in the GISP2 samples of –49.5 ±0.3 ‰ is very close to the values measured in ice from the Agassiz 1977 core section #72 (Ellesmere Island, Canadian Arctic) of –49.8 ±0.3 ‰ for 330 yr BP (Fig. 2.1.8). Note that these data have been corrected for the gravitational fractionation in the firn layer according to Craig et al. (1988a). Both results are in excellent agreement with the findings of Craig et al. (1988b), who measured –49.6 ±0.2 ‰ for the time between 120 and 310 yr BP.

2.1.5.4. Blanks

Different tests show the degree of contamination introduced by certain steps of the procedure. To simply trap methane from the Helium flow through the system shows the purity of the Helium and will detect leaks. The amount of methane introduced by 15 min of flushing was detectable but no source of concern. It proved unnecessary to install a trap upstream of the extraction chamber to clean the Helium. The standard procedure to measure blanks was to follow the complete extraction procedure without inserting ice in the chamber. This was done routinely once every measuring day. The methane blanks were consistently lower than 40 mV and mostly below 30 mV, which is equal to, or less than, 10 % of the signal during measurements. This amount of contamination is considered acceptable and peak height of the samples was corrected accordingly. The isotope ratio of the blanks was usually more depleted in ^{13}C than the atmospheric value (between –49 ‰ and –54 ‰), but peaks this small do not give reliable isotope numbers. Therefore, no correction was applied to the measured isotope values.

Different influences affect the blanks. Overheating of the chamber during the melting step, when the hot water bath is replaced once or several times with fresh boiling water, strongly increases the blanks. Therefore only a single bath was used, resulting in longer melting time. Repeated blank runs show decreasing blanks. This points to the possibility that desorbtion from the chamber walls is the source of contamination. It was also noted that water building up in the extraction line over several runs causes higher

blanks. The extraction procedure as outlined above, including the drying and purging steps between runs, is a suitable compromise between low blanks and a workable technique.

The standard blank runs do not rule out that the presence of ice and melt water in the system may result in higher contamination. Measurements of methane free ice samples provide a test for this. The first problem with this experiment is that one cannot distinguish between methane introduced by the sample and contamination that results from the extraction procedure. The blank ice comes from re-freezing extracted melt water in the chamber by cooling the latter with liquid nitrogen. Consequently, these tests examine the extraction efficiency of the method as well as the contamination in the wet system. While it is impossible to quantitatively attribute any detected methane to either source, low enough yields will prove both to be satisfactory. Another set of samples was frozen from water, which had been degassed by boiling it. The ice blanks were somewhat higher than dry blanks (between 30 and 50 mV). Given the uncertainty of remaining methane in the sample itself, either due to incomplete extraction or degassing, these values are acceptable. The refrozen samples had high blanks if the sample was left in the original shape, fitting the chamber exactly. Any sample broken in half and then placed in the chamber resulted in acceptable blanks. It seems that the tight fit of sample and extraction chamber decreases pumping efficiency. This is not considered a problem for the more irregular shaped glacial samples.

2.1.5.5. Extraction efficiency

High extraction efficiency is desirable to optimize methane yield and indispensable to rule out isotopic fractionation during the extraction. Methane could be retained in either the chamber headspace due to inefficient flushing or it could be dissolved in the melt water. The first process should not be associated with an isotope effect, because methane is transported passively in the purge stream. In contrast, solution of methane in water does fractionate isotopes. A theoretical model explores the possible isotope effects of incomplete extractions.

A Rayleigh distillation model expresses the isotopic fractionation between melt water and headspace. The isotopic composition of the dissolved methane over the extraction process is:

$$\delta^{13}C_d = (\delta^{13}C_i + 1000) \times f^{(\alpha-1)} - 1000 \qquad (2.1)$$

where d denotes dissolved and $\delta^{13}C_i$ is the isotopic composition of the dissolved methane before extraction begins, f is the fraction of remaining dissolved methane and α is the kinetic fractionation coefficient. According to Knox et al. (1992) $\alpha = 1.0008$.
The isotopic composition of the extracted gas $\delta^{13}C_e$ follows from a mass balance calculation:

$$\delta^{13}C_e = (\delta^{13}C_i - \delta^{13}C_d \times f)/(1-f) \qquad (2.2)$$

Assume that a certain fraction F of methane is dissolved during the melting. The remainder goes directly from the bubbles into the headspace without fractionation. The isotopic composition of the headspace gas $\delta^{13}C_h$ at any given time during the extraction is then a mixture between initial headspace gas and extracted dissolved methane:

$$(1 - F \times f) \times \delta^{13}C_h = \delta^{13}C_i \times (1-F) + \delta^{13}C_e \times (F \times (1-F)) \qquad (2.3)$$

substituting (2.2) into (2.3) yields:

$$\delta^{13}C_h = (\delta^{13}C_i - \delta^{13}C_d \times F \times f)/(1 - F \times f) \qquad (2.4)$$

Equations (2.1) and (2.4) give $\delta^{13}C$ of the methane in the headspace depending on the efficiency of the extraction as well as the isotopic composition of dissolved and extracted methane (Fig. 2.1.9). The isotopic composition of the headspace methane starts at the true value. It then becomes depleted in ^{13}C when it starts to mix with the ^{13}C-depleted extracted methane. Finally, it approaches the true value again as extraction goes to completion. The worst effect on the headspace gas occurs when the extraction of gas from the melt water reaches the half-way point. The magnitude of the offset depends on how much methane was dissolved in the melt water. Fig. 2.1.10 shows the offset for

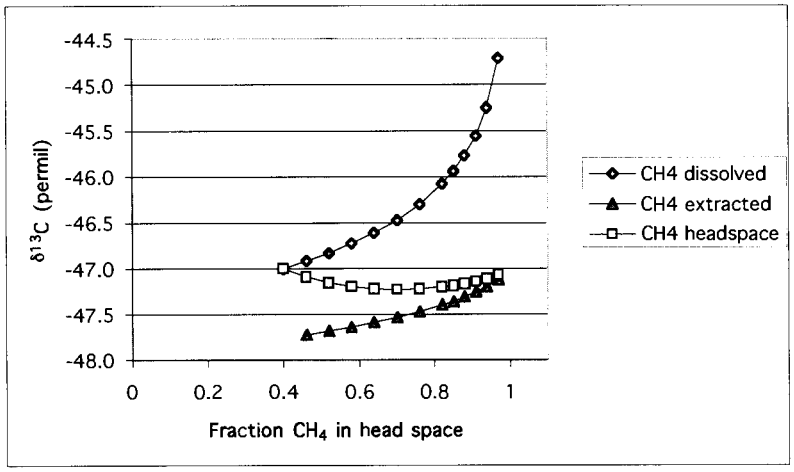

Fig. 2.1.9: Isotopic partitioning between melt water and headspace during methane extraction
Three curves illustrate the isotopic compositions of dissolved, extracted, and headspace methane for a fraction of initially dissolved methane of 0.6 and total $\delta^{13}C = -47$ ‰.

30 %, 60 % and 99 % of initially dissolved methane. The maximum error ranges from 0.1 ‰ to almost 0.7 ‰. An extraction model estimates how much methane is dissolved during the experiments. It combines gas exchange rates between dissolved and gaseous phase with transport calculations for the flushing. The result is a curve showing how much methane reaches the cold trap as a function of time. This curve is strongly dependent on the amount of initially dissolved methane. 60 % dissolution provides the best match with experimental data (Fig. 2.1.11). For this experiment, however, the ice melts in a Helium atmosphere and not under vacuum, as it does during sample analysis. Vacuum facilitates the transfer of methane into the headspace. The experiments on equilibration times after melting and on stripping the melt water with Helium indicate no sign of dissolved methane in the water. Using an initially dissolved fraction of 60 % as a conservative estimate, the isotopic deviation from the true value is 0.23 ‰. For extraction efficiencies higher than 90 % the offset would drop below 0.15 ‰. The extraction of refrozen samples (see above) show that extraction efficiency during sample analysis is at least 90 %, which proves that according to these theoretical arguments, isotope fractionation due to incomplete extraction is of minor concern.

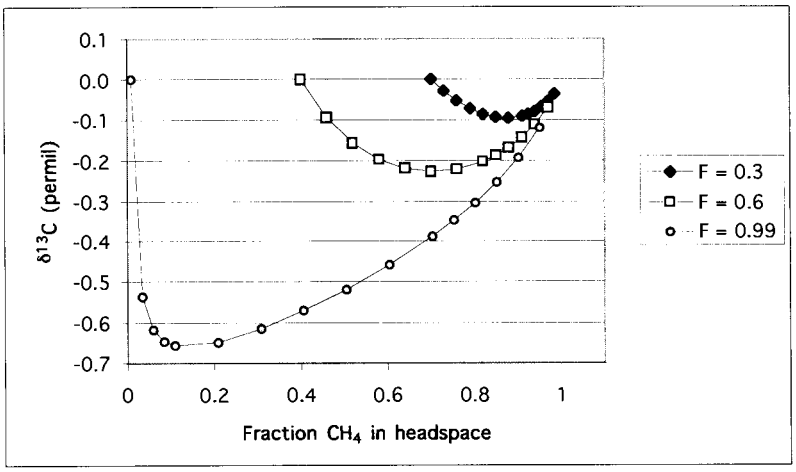

Fig. 2.1.10: Effect of Rayleigh distillation on $\delta^{13}C$ of trapped methane.
The curves show the isotopic composition of methane as it is trapped for analysis during extraction from melt water for fractions of 0.3, 0.6, and 0.99 initially dissolved gas.

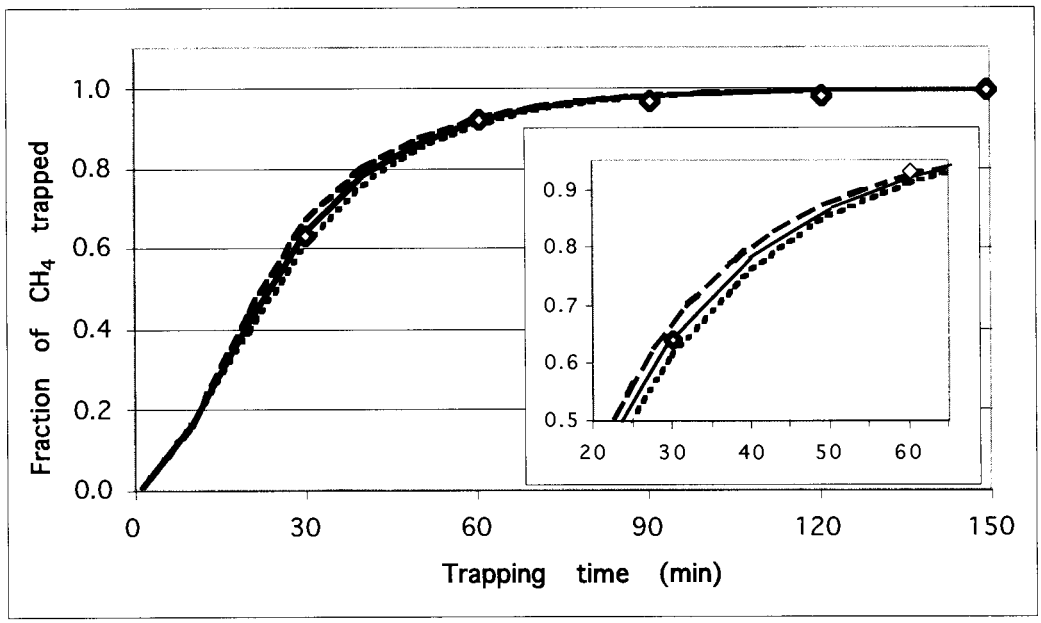

Fig. 2.1.11: Methane extraction in dependence of the initially dissolved fraction.
Amount of methane extracted from melt water over time in dependence of the initially dissolved fraction. (stippled curve: f = 0.4; solid curve: f = 0.6; dashed curve: f = 0.8). Experimental data (diamonds) fit the modeled curve for f = 0.6 initially dissolved methane, which is seen more clearly in the inset.

Two more experiments ruled out that incomplete extraction is a problem. One can quantify the amount of methane left in the extracted melt water by re-freezing it as was done for the ice blanks. This process drives gas into the headspace so it can be measured. Unfortunately, the system cannot be flushed out between the extraction run and the measurement of the residual. As a consequence, water vapour is not efficiently removed from the system before the repeated run and possibly there is leaking into the line without a He stream to prevent this. The result is a bad baseline of the mass 44 trace, which would potentially mask peaks up to 17 mV. Because no peak was recorded the residual methane must be less than 17 mV. At a peak size for the first extraction of 415 mV this is less than 6 % methane remaining after the extraction. In a second experiment, flushing time varied, which will increase extraction efficiency because any dissolved methane has more time to equilibrate with the headspace or to be stripped by the Helium stream. The consistent isotope numbers for flushing times between 13 and 25 min indicate that incomplete extraction is not a problem for the measurements.

2.1.6. Troubleshooting

A number of problems were encountered during the development of the extraction technique. This section summarizes the most important ones.

2.1.6.1. Water vapour

It proved very challenging to extract the methane without trapping too much water vapour and, even more so, to prevent vapour levels to build up over several runs. A number of problems indicate if water is interfering with the chromatography or mass spectrometry:

- higher blanks levels (above 50 mV) with ^{13}C-depletion.
- high background levels of water and CO_2 in the mass spectrometer
- shorter retention times combined with peak broadening and inconsistent isotope measurements
- sudden change to ^{13}C-rich isotope numbers after several runs
- contamination of smaller samples to produce consistently ^{13}C-depleted isotope ratios.

Some of these signs are quite obvious whereas others build up imperceptibly over several days. It is therefore necessary to perform tests for several days to ensure the system is working properly. It seems that water, depending on where and how much is present, can affect either the mass spectrometry or chromatography or retain methane and carbon dioxide and partition them isotopically.

Although some of the problems mentioned above seem contradictory in their effect on the isotope measurements, optimizing the removal of water from the system could solve them all. The length and diameter of the water trap tubing is crucial. If it is too short water will break through onto the Hayesep™ trap. If the water trap is too long it cannot dry completely between runs and residual water will be injected onto the GC column. A U-shaped piece (OD = 1/4 "; 15 cm), followed by two coils (OD = 1/8 "; 50 cm) of copper tubing provided a good solution using the drying and purging procedure as outlined above. The two water traps on the chromatographic line were not effective in solving the problems, but they are necessary to keep water levels in the mass spectrometer low. The background levels of water and carbon dioxide in the mass spectrometer were monitored before every run.

2.1.6.2. Carbon monoxide

Because the rotary vane pump that evacuates the sample headspace is also used to sublimate ice and dry out the system water vapour will accumulate in the pump line. If it contaminates the pump oil, pumping efficiency will drop. In severe cases the pump starts to produce carbon monoxide that contaminates the system and interferes with the mass spectrometry. Even the foreline trap with activated alumina would not protect the system. The carbon monoxide is clearly generated by the pump, because an oil change immediately solved the problem. Any interference can be prevented if clean oil is used at all times. As an additional measure to prevent the contamination of pump oil through water from the extraction line, a glass cold trap cooled by ethanol and dry ice traps water before it reaches the pump. At the same time this cold trap prevents gases generated by

the pump from flushing back to the extraction line where they would contaminate the system.

2.1.6.3. Valves and stirrers

Contamination by methane generated from moving parts has been reported before (e.g. Fuchs et al., 1993). Here, certain valves were found to generate enough methane to affect the blanks. Especially live-loaded valves (i.e. a spring or elastic material provides the seal), which had been chosen for their higher operational temperature range, were not suitable. Nupro™ bellows valves worked reliably and without contamination.

In early experiments a magnetic stirrer enhanced the equilibration between melt water and headspace. The amount of methane generated by the plastic coated stir bar is enormous, although the mechanism of methane formation is unknown. It turned out that gas transfer into the headspace was sufficiently fast and complete without the use of a stirrer (see extraction efficiency).

2.1.6.4. Brine

In an abandoned attempt, the liberated gas was displaced from the headspace into a sample bottle by filling the extraction chamber with oversaturated salt brine. Theoretically, no methane should dissolve in the brine. Evacuating the headspace for at least an hour before using it further degassed the brine. Despite the fact that blank values were acceptable, the isotopic composition of methane would change during the displacement. This suggests a partitioning of gas into the brine. Because there was no obvious solution for the problem and no way to quantify and correct for it the technique was abandoned.

2.1.6.5. Column cooling

In order to achieve good separation between peaks, the gas chromatograph runs at 0 °C. If both columns are placed in the GC the metal frames touch the capillary columns. During cooling pulses water vapour and maybe other compounds freeze at the contact points and subsequently either interfere with flow or they partition isotopes. This results in wavy baselines for the mass traces and consequently the isotope ratio. The easiest

solution is to place the second column outside the GC and cool only the first one, which results in good peak separation with undisturbed baselines.

2.1.6.6. Overloading

If too much gas is injected in the GC the absorbing coating of the capillary column becomes oversaturated. The results are shorter retention times, peak broadening and poor separation. This is known as overloading of the column. This problem occurred when the water trap failed (see above). This was apparent not so much in the water levels of the mass spectrometer but in huge carbon dioxide peaks with extensive tailing that affect background levels for hours. It is suspected that water pockets in the line provide a reservoir for CO_2 that depletes only as the line dries out.

Even during routine operation the method extracts large amounts of carbon dioxide from the ice and possibly the melt water. This peak is highly variable, it influences retention times in an unpredictable manner and makes it impossible to use a set method with reference peaks and run times for the spectrometry. Instead, a reference peak is set manually after the methane peak and the run is stopped before carbon dioxide elutes. Peak separation is not negatively affected although the last reference peak, which is used routinely for reintegration, must be timed carefully and may be shorter than other reference peaks.

2.1.7. Comparison with other techniques

Methane in ice is most commonly sampled using wet extraction techniques, i.e. melting of the ice to liberate the enclosed air. Other methods like mechanical crushing or sublimation may be necessary for other gas compounds but have specific disadvantages or challenges. In wet extractions the water is usually re-frozen to drive any dissolved gas into the headspace. The pressure increase in the headspace is measured to calculate the amount of extracted gas. Then latter is expanded onto a sample loop and injected into the GC. In contrast, the presented method strips the gas from the melt water with a Helium stream, which also transfers the headspace to a cold trap where the methane is frozen out.

The principle is based on a methane stripping line for seawater developed in our laboratory.

Whereas the conventional method requires precut samples that fit the extraction chamber tightly, the new approach allows for the measurement of samples in a variety of sizes and shapes. This is important for measurements of ice from different locations and with varying amounts of methane. The approach to expand the liberated gas onto the sample loop means that all the gas remaining in the headspace and the lines is lost for the measurement. This is not a problem for determination of methane concentrations, which requires far smaller quantities. For isotope measurements, however, this is a serious disadvantage. In this system, all the gas is flushed through the cold trap where the methane freezes out and is captured quantitatively.

A disadvantage of this technique is that it does not measure the amount of extracted gas. Therefore the gas content of the sample must be estimated from density and literature values, which introduces uncertainties for the calculated atmospheric methane concentrations. Theoretically, one could refreeze the sample and measure the headspace pressure, but the large ratio of headspace to sample volume would result in poor results for the pressure readings. Moreover, experiments showed that the refreezing step leads to a deterioration of the measured isotope data.

2.1.8. Field measurements of methane concentration

Field measurements of methane concentration were conducted with an adapted version of the laboratory set-up used at Washington State University (WSU). The latter is essentially described in Brook et al. (2000). Notable differences are that the sample containers are now glass cylinders, which seal to their stainless steel lids with a system of Viton O-rings and clamps. Teflon ferrules are replaced by stainless steel. The gas chromatograph is a Shimadzu GC14-A). For the refreezing step the same cold bath (ca. –30°C) is used as for the initial evacuation of the samples. No blank tests were performed in the field. A standard tank (1033 ppbV in compressed air) was used for calibration. For

the field season of 2003 overall precision of all calibration runs was ±2 ppbV (2 x standard error, n=129), while the daily precision ranged from ±2 ppbV (n=7) to ±7 ppbV (n=8) with one day of ±17 ppbV (n=9), which was caused by a single outlying measurement.

Ice samples ranged from 110 g to 150 g in weight. Typically pressure in the sample loop was between 40 and 50 mTorr, but this depends strongly on sample size and ranged from 26 to 74 mTorr. Samples were reanalyzed if gas yield was high enough and if there was doubt about the first value, these measurements usually gave a loop pressure of around 25 mTorr. No temperature correction was applied to standards or measurements, although temperature was recorded for every run. Differences over one day were typically less than 5°C, this margin was exceeded only three times with 6°C (twice) and 8°C.

2.2 Firn diffusion model

The isotopic composition of methane measured in ice samples is not exactly the same as that of the contemporaneous atmosphere. Processes associated with diffusion and occlusion of the gases in the firn layer cause natural artifacts that shift the $\delta^{13}C_{CH4}$ in ice occlusions relative to the atmosphere. These have to be quantified and corrected for in order to obtain the true atmospheric isotope signature. Some effects can be measured using other gas species. Other corrections must be calculated with firn models that simulate diffusion and quantify associated isotope effects. The following sections describe the model developed for this study, which is specific for calculation of effects associated with changing atmospheric methane concentration. Under such conditions the atmospheric signal for $^{13}CH_4$ reaches the close-off zone with a delay relative to $^{12}CH_4$, which is caused by different diffusivities. This leads to isotopic fractionation of methane in the ice.

2.2.1. Description of the diffusion model

The model calculates the diffusion of $^{12}CH_4$ and $^{13}CH_4$, as well as a theoretical tracer, through a density profile of firn. Driving factor is the atmospheric concentration of methane and its isotopic composition as measured in both the GISP2 ice core (Brook et al., 2000) and the Pakitsoq samples. The model mostly follows the approach of Schwander et al. (1988, 1993, 1997). In a first step it calculates a depth/density profile for the firn following Herron and Langway (1980) (Fig. 2.2.1). This calculation depends on site-specific parameters such as temperature, accumulation rate and elevation. The ice sampled at Pakitsoq was deposited near the summit of the Greenland ice cap at 70.945 N and 39.824 W (Reeh et al., 2002). This location is about 200 km southwest of the drill sites for the GISP2 and GRIP ice cores (Fig. 2.3.1). Comparison of current conditions at the deposition and drill sites shows that the former is warmer by about 3 °C and has 50 % more ice accumulation (Reeh, personal communication). The conditions during the YD can be constrained using these estimates and by modeling diffusion of air through the firn column. Matching the latter results with $\delta^{15}N$ measurements constrains the accumulation rate, which is the most uncertain parameter. The resulting local temperature was –43 °C and snow accumulation rate was 0.0921 m ice/yr (Severinghaus, personal

communication). Temperature and ice accumulation during the transition and PB were adjusted accordingly using values of Cuffey and Clow (1997; following their ΔL = 200 km scenario). The exact values are listed in Table 2.2.1. Other parameters were calculated as follows:

Density of ice (φ_{ice}) in dependence of local temperature T (in K) is

$$\varphi_{ice} = 916.5 - 0.14438 \times T - 1.5175 \times e^{-04} \times T^2 / 1000 \ \text{g/cm}^3 \qquad (2.5)$$

(Schwander et al. (1997). Also calculated is total porosity s for each depth z (Schwander et al., 1988):

$$s = 1 - \varphi_z / \varphi_{ice} \qquad (2.6)$$

Open porosity s(o) is total porosity minus closed porosity s_c where

$$s_c = s \times \exp(75 \times (\varphi_z / \varphi_{co}) - 1 \qquad (2.7)$$

(Spahni et al., 2003) with φ_{co} as the density at the close off zone. The latter was calculated in dependence of temperature after Martinerie et al. (1994):

$$\varphi_{co} = 1/(1000 \times (1/\varphi_{ice}) + (6.95 \times 10^{-7} \times T) - 4.3 \times 10^{-3}) \ \text{g/cm}^3 \qquad (2.8)$$

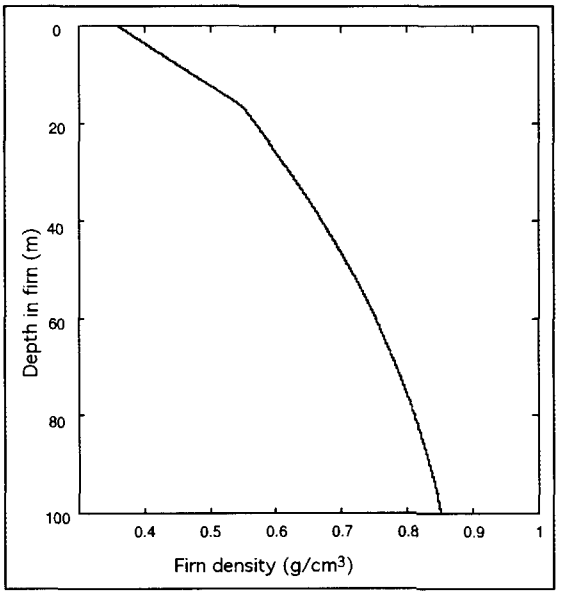

Fig. 2.2.1: Firn density profile for the deposition site of Pakitsoq ice in the YD calculated after Herron and Langway (1980)
The sudden steepening of the curve at around 18 m depth results from the two-step approach of Herron and Langway's model.

However, the tortuosity of firn brings diffusion of gases to a halt above the depth of bubble closure. Schwander et al. (1997) found that diffusion effectively stops several meters above and they defined this depth, which has a density lower than φ_{co}, as the lower boundary of the diffusive column. This was possible because they could match records of atmospheric concentrations to firn measurements. For reconstructions of past conditions this approach is not possible. Instead, this model takes the cut-off as the depth where open porosity reaches a value of 0.12 (Fig. 2.2.2). Below this level, effective diffusion coefficients (D_{eff}) are not defined by the equation in Schwander et al. (1988) (Fig. 2.2.3). Although in this study D_{eff} is calculated after Spahni et al. (2003), a deeper diffusive zone results in unrealistically high firn equilibration times and isotopic fractionation. Diffusive column height (DCH) is a crucial parameter for the model and was examined with sensitivity tests in Chapter 3.

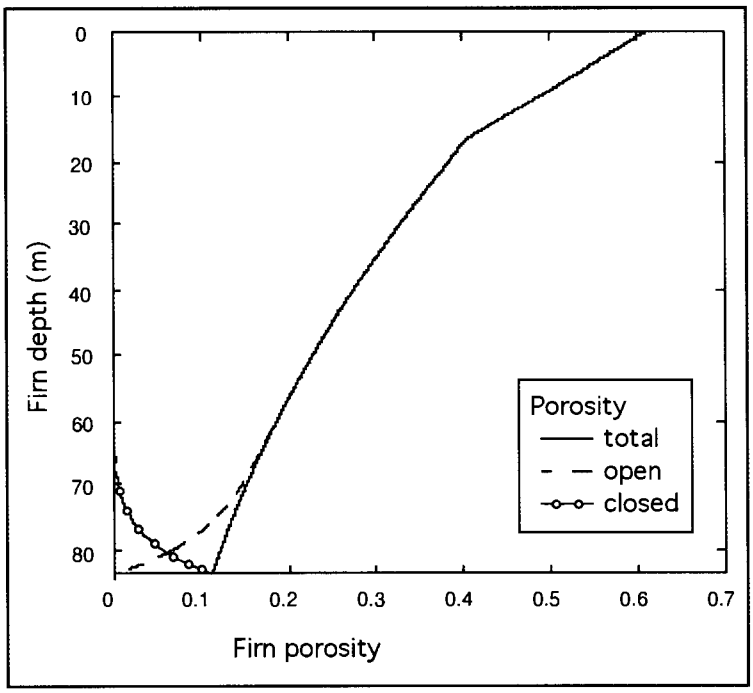

Fig. 2.2.2: Porosity profile for Pakitsoq
Firn profile showing total, open and closed porosity. The curve for closed porosity shows that bubble closure occurs over a depth interval above the calculated close-off depth (according to Martinerie et al., 1994). In the same depth zone a strong decrease in open porosity indicates declining diffusivity. Model parameters are specific for YD.

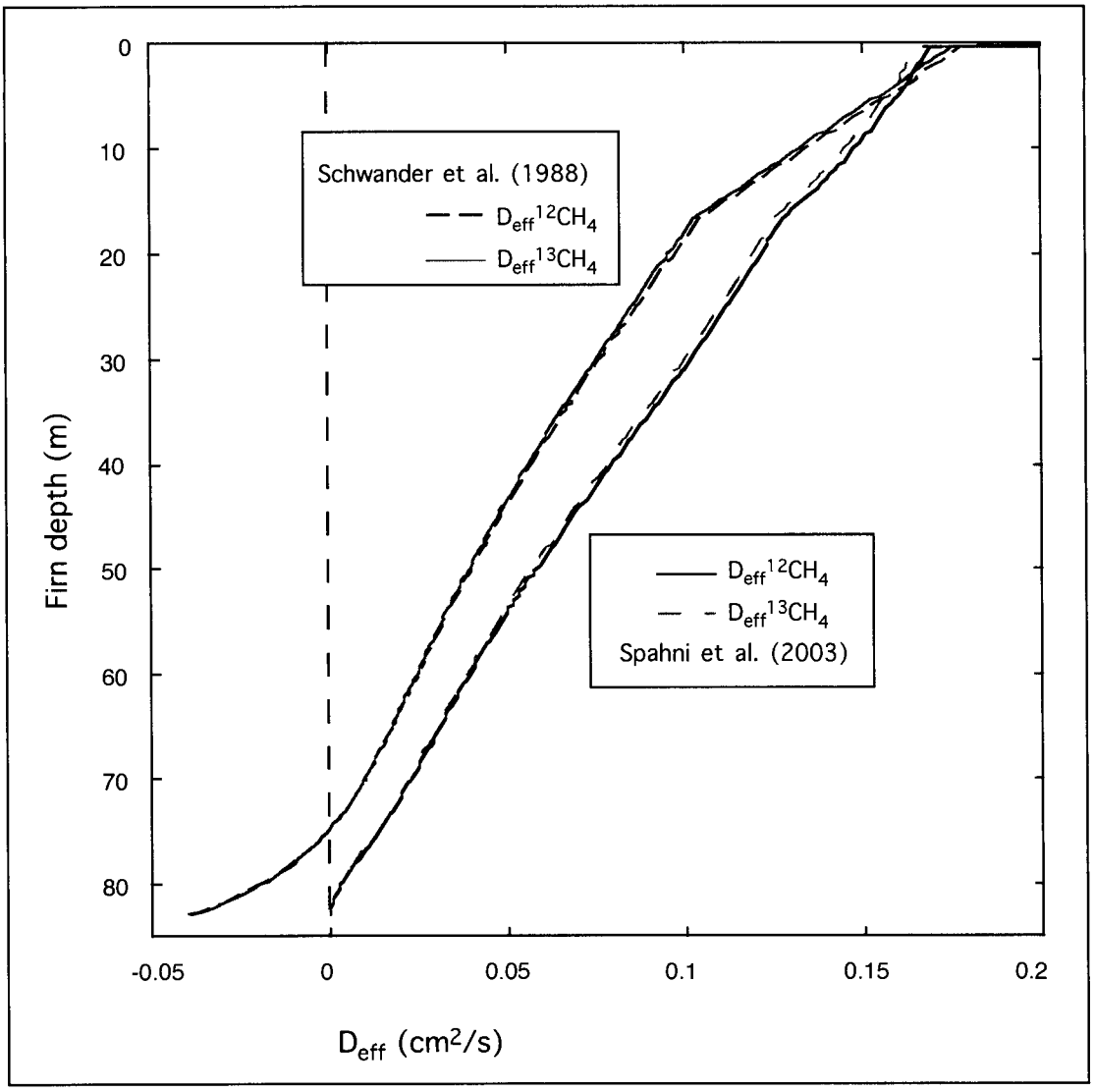

Fig. 2.2.3: Effective diffusion coefficients versus depth
The diagram shows diffusion coefficients (D_{eff}) calculated after Schwander et al. (1988) or Spahni et al. (2003) in a firn profile down to the zone of bubble closure, which is at 85 m. D_{eff} after Schwander et al. (1988) (two curves to the left) are not defined for open porosity lower than 0.12 (negative values for D_{eff}); D_{eff} after Spahni et al. (2003)(two curves to the right) reach zero at 82 m, i.e. above the depth of bubble closure. Model parameters are specific for YD temperature and accumulation rate. Tortuosity parameters for Spahni et al. (2003) specific for present conditions at GRIP drill site at Greenland Summit.

In a second step the diffusive firn layer is subdivided into 200 boxes of equal length. This is a difference to the model of Schwander et al. (1988, 1993, 1997), who use 200 boxes of varying length but equal pore volume. The large degree of subdivision of the firn layer is necessary because the diffusion coefficients vary strongly with depth. For each box center the diffusion coefficients of $^{13}CH_4$ and $^{12}CH_4$ are calculated as a function of density. They are determined through scaling to the free diffusion coefficient D_o of CO_2 in air (0.139 cm^2/sec at –20 °C; Trudinger et al. (1997), which must be corrected for ambient temperature and pressure according to Schwander et al. (1988):

$$D_{Tp} = D_o \times (1013/p) \times (T/253.16)^{1.85} \text{ cm}^2/\text{sec} \qquad (2.9)$$

where p is the ambient pressure in hPa and T is absolute temperature. Free diffusion coefficients for the two methane species are calculated relative to D_{Tp} using scale factors given in Trudinger et al. (1997) as 1.291 and 1.2683 for $^{12}CH_4$ and $^{13}CH_4$, respectively. The effective diffusion coefficients D_{eff} for each depth, which depend on open porosity and tortuosity of the medium are given by:

$$D_{eff} = D_{Tp}/(1 + 0.5 \times (1 - s_o) \times (\alpha_T + (1 - \alpha_T) \times s_o^{-\beta} \text{ cm}^2/\text{sec} \qquad (2.10)$$

where α_T and β are site specific parameters and s_o is open porosity (Spahni et al. (2003). α_T and β are parameters to match an observed diffusion history. For the Pakitsoq deposition site under YD conditions the latter is unknown. According to Spahni et al. (2003), α_T and β depend in first approximation linearly on temperature and accumulation rate, so they can be interpolated from empirical values for Dome C in Antarctica and the GRIP drill site (Greenland ice core project). The uncertainty in these parameters and consequently the magnitude of D_{eff} is of concern and was examined with sensitivity tests (see Chapter 3).

Using the effective diffusion coefficients the model calculates the concentration change $\Delta c(i)$ in a given box i after Schwander et al. (1993) as

$$\Delta c(i) = \Delta t \times D_{eff}(i) \times (c(i-1) - 2 \times c(i) + c(i+1))/\Delta z^2 \qquad (2.11)$$

Here Δt is the time step of the integration and c(i-1) and c(i+1) are the box above and below c(i), respectively. Δz is the depth gradient between the boxes. Note that the gravity component of the original model is neglected, because measurements of $\delta^{15}N$ are used to

account for this effect. The model calculates Δc(i) with a finite difference approach and central difference implementation. All relevant parameters are defined for, and fluxes calculated between, the box centers.

Snow accumulation results in an upward movement of firn relative to the gas in the pore space. Following Schwander et al. (1993), this process is accounted for by moving the gas content of every box down by one box after a defined time step. This step is calculated as the average amount of ice in the boxes divided by the accumulation rate. Due to the increasing ice content in the boxes with depth and the rough discretization of the process this module introduces minute oscillations when modeling the gas fluxes. The latter cancel out when different fluxes are compared, as is done when calculating the correction factors.

The initial condition for all model runs is an equilibrium situation where all firn layers have a methane concentration of 490 ppbV with $\delta^{13}C_{CH4} = -46$ ‰, as was measured for the YD. Driving factor for diffusion is the rise of atmospheric methane at the end of the YD. For the calculations it is taken as a linear increase from 490 ppbV to 725 ppbV over 200 years. Diffusion of $^{13}CH_4$ and $^{12}CH_4$ is calculated separately. The calculations do not use isotope ratios but transform atmospheric methane concentration and isotopic composition into a concentration of $^{13}CH_4$, which drives diffusion of this parameter through the firn layer. $^{12}CH_4$ is modeled as total methane with the appropriate diffusion values. Following Trudinger et al. (1997), a third tracer, $^{13}C_{12}$, is forced with the atmospheric concentration of $^{13}CH_4$ and D_{eff} of $^{12}CH_4$. For the lowermost box, which represents the end of the diffusive zone, the concentrations of $^{12}CH_4$ and $^{13}CH_4$ are transformed back to δ- values according to:

$$\delta^{13}C_{CH4} = (({}^{13}C_{CH4} / {}^{12}C_{CH4(f)} - {}^{13}C_{CH4} / {}^{12}C_{CH4(PDB)}) / ({}^{13}C_{CH4} / {}^{12}C_{CH4(PDB)})) \times 1000 \text{ ‰} \quad (2.12)$$

where f denotes firn values and with $(^{13}C_{CH4} / {}^{12}C_{CH4(PDB)}) = 11237.2 * 10^{-6}$ (Craig, 1957). In the same way, a $\delta^{13}C_{12}$ is calculated from tracer $^{13}C_{12}$ and $^{12}CH_4$. Subtracting $\delta^{13}C_{CH4}$ from $\delta^{13}C_{12}$ removes the effect that is introduced by not driving $^{13}CH_4$ with the concentration gradients of total methane and isolates the fractionation caused by the

different diffusion coefficients for the isotopes. The result is a diffusion correction factor DCF that must be added to ice core data in order to calculate the atmospheric value:

$$DCF = \delta^{13}C_{12} - \delta^{13}C_{CH4} \text{ (‰)} \qquad (2.13)$$

Table 2.2.1: Model input parameters

Parameter		**YD**	**Transition**	**PB**	
Elevation (m.a.s.l.)	3200				a
Temperature (°C)		-43	-36	-28	a/c
Accumulation rate (m/yr)		0.09	0.12	0.20	a/c
α_T		0.85	0.81	0.78	b
β	2.5				b
Methane concentration (ppbV)		490		725	d
$\delta^{13}C_{CH4}$ (‰ PDB)	-46				d

a) Severinghaus (personal communication)
b) after Spahni et al. (2003)
c) Cuffey and Clow (1997)
c) this work

2.2.2. Matching data points with correction factors

The model time scale does not perfectly fit the age record of the ice core data. This is due to the fact that the atmospheric forcing of the model is equal to the observed concentration increase in the ice samples, while the diffusion model creates a time lag between the forcing and the modeled close-off signal (see Fig. 3.4.1 and 3.4.3). As a consequence, ice data have to be matched with the equivalent correction factor. It is assumed that during the time of atmospheric methane increase the correction factor is specific for the modeled methane concentration at the close-off zone. Therefore, modeled and measured methane concentration history are matched to find how model time and real time compare. A scaling factor for model age is established so that correction factors can be calculated for the exact age of a measured data point.

2.2.3. Critique of the model

The model was created specifically to calculate a correction factor for isotopic fractionation by diffusion and not to reconstruct atmospheric records from ice core data. Therefore it is not as sophisticated as others built for similar work (Rommelaere et al., 1997; Trudinger et al., 1997). Specifically, it does not use an iterative approach to match model data and measurements. The following simplifications were made:

- The firn layer is assumed to be isothermal.

- There is no upward movement of air in the firn caused by compaction of snow. Schwander et al. (1993) estimated that this effect is negligible compared to molecular diffusion.

- The lower boundary of the diffusive zone and bubble close-off are assumed to occur at one specific depth instead of a depth interval.

- There is no well-mixed zone at the top of the firn layer. Under certain conditions surface winds will convectively mix gases in the uppermost firn and diffusion starts only below. The height of the diffusive column (DCH) in meters from the surface or well-mixed zone to the close off depth can be calculated using $\delta^{15}N$ data. The atmospheric composition of N-isotopes was unchanged over the time period in question (Mariotti; 1983) and under stable environmental conditions gravitational fractionation is the only agent that influences $\delta^{15}N$ in the firn layer. Its deviation from the atmospheric value (which is 0 ‰) is therefore dependent on DCH and the latter can be calculated following Schwander et al. (1997):

$$DCH = RT/(g \times \Delta m) \times \ln((\delta^{15}N/1000) + 1) \text{ m} \qquad (2.14)$$

Where R is the ideal gas constant (8.314J/mol K), g is gravity acceleration (9.81 m/sec^2) and Δm is the mass difference between the isotopes (0.001 kg/mol). For a $\delta^{15}N = 0.39$ ‰ as measured in Pakitsoq ice (Petrenko et al., in preparation) and temperatures typical for the transition between YD and PB the diffusive column would comprise 74.9 m. This value is very close to our DCH of 74.5 m as determined after Schwander et al. (1988). For the transition period and the PB, DCH cannot be accurately calculated from $\delta^{15}N$, because the data are also affected by thermal fractionation. However, assuming that it will not be shorter than during the YD, the diffusive column comprises the whole firn

profile, which is shallower due to higher accumulation. Therefore no well-mixed zone was included in these model runs.

- Environmental parameters are assumed to be constant over time. While this is plausible for elevation, both temperature and accumulation rate have changed drastically during the time period that is modeled. The changes cannot be easily included. For one, because it is computationally too complex for the framework of this study. For the other, because the changes will affect gas flux through several processes acting on different time scales. There is an immediate impact through higher burial rates and temperature dependence of D_{eff}, while changes in the snow pack, affecting tortuosity, will take years to develop. Three separate model runs with parameters specific for YD, transition period and PB (Severinghaus, personal communication; Cuffey and Clow, 1997; see Table 2.2.1) show the sensitivity of the model to these parameters, which is discussed in Chapter 3.

- The model forcing through the atmospheric concentration of methane is not from actual data but from a simplified linear increase. However, the latter describes the measured records (Brook et al., 1996, 2000; this work) quite well. While it is true that these measured records have undergone the diffusion process (unlike the atmospheric signal that they represent in the model), this only effects the absolute timing of the recorded event (which is meaningless for the model outcome), and smoothing around the inflection point, which does not significantly changes the results, either.

- The isotopic signature of the atmosphere is assumed to be constant at –46 ‰. This matches the record measured in samples from Pakitsoq, but may not be true in other cases. To reproduce such a change in the model would require iterative runs. Note that the three-tracer approach adopted from Trudinger et al. (1997) implies that diffusion of $^{13}CH_4$ and therefore the correction factor DCF is dependent on the concentrations of total methane and not the $^{13}CH_4$ gradient. Therefore the model results from an assumed constant atmospheric $\delta^{13}C_{CH4}$ are appropriate to calculate the correction factor.

The major uncertainty in the model is the unknown dependence of the diffusion coefficients on tortuosity. Fabre et al. (2000) demonstrated the problems associated with the use of uncalibrated models. As seen in the parameterization of D_{eff}, site-specific parameters (α_T and β) are commonly used to match the coefficients to a measured record of firn air. Because such a record obviously does not exist for the Younger Dryas, values for α_T and β were interpolated from results for Dome C in Antarctica and the GRIP drill site (Spahni et al., 2003). The conditions for temperature and snow accumulation, as they presumably existed at the Pakitsoq deposition site at the end of the Younger Dryas, lie between those of the above mentioned sites and can be interpolated linearly as an approximation (Spahni et al., 2003). As D_{eff} is the master parameter of the model, uncertainties in this value will strongly affect the results. Choosing D_{eff} too large means to underestimate the diffusion fractionation. Making it too small results both in high fractionation and unrealistic equilibration times of the concentration gradient in the firn. The latter process provides a constraint because diffusion modeling for $\delta^{15}N$ values at the deposition site with YD conditions shows a mean gas age of around 15 yrs (Severinghaus, personal communication). In addition, Schwander et al. (1993) state that the diffusive equilibrium time is proportional to the square of the firn thickness, which depends on local temperature and snow accumulation. Although these conditions were different during the transition between YD and PB, the mean gas age should be of the same order as today's value, i.e. around 12 yrs (Schwander et al.; 1993). Between runs with different parameterization those with more realistic equilibration times are more likely to result in suitable correction factors. This issue is discussed further in Chapter 3.

2.3. Study sites

Three locations provided samples that were analyzed in this project. Ice from Agassiz ice cap (Ellesmere Island, Canada) and from the Greenland Ice Sheet Project 2 (GISP2) provided a test for accuracy and precision of the analytical method. Measurements to reconstruct the atmospheric history of $\delta^{13}C_{CH4}$ were performed on ice from the western margin of the Greenland ice shield in Pakitsoq.

2.3.1. Agassiz ice cap

A suite of ice cores was drilled on the Agassiz ice cap, Nunavut, Canada (Fisher and Koerner, 1994; Fisher et al., 1995). Of those only ice from a core recovered in 1977 proved useful for testing the gas extraction method. The borehole is located at 80°45' N and 73°10' W at an elevation of 1670 m. The site has today a mean annual temperature of –24.5 °C and an accumulation rate of 0.175 m ice/yr, the firn ice transition is at a depth of 60 m (Fisher and Koerner, 1994).

2.3.2. GISP2

This core was taken near the summit of the Greenland ice sheet at 72.58° N and 38.48° W (Grootes et al., 1993)(see Fig. 2.3.1). Elevation at the site is 3208 m above sea level, mean annual temperature –31 °C, snow accumulation rate 0.24 m ice/yr (Meese et al., 1997) and the firn ice transition occurs at around 80 m depth (Severinghaus et al., 1998). Among many other studies, the core was used to establish a detailed record of atmospheric methane concentrations back to the last ice age (Brook et al., 1996, 2000). In this study core section # 139 was measured, which was originally taken for analysis of cosmogenic particles using ultra-pure drilling techniques. The section comprises a depth interval from 141.0 to 142.2 m, which translates to a gas age between 225 and 229 yr BP. During the sampling procedure the orientation of the section was lost, but for the analysis of the occluded methane this is of no importance, because the recorded time interval is shorter than the smoothing of atmospheric signals in the firn and because methane concentrations were constant during this period.

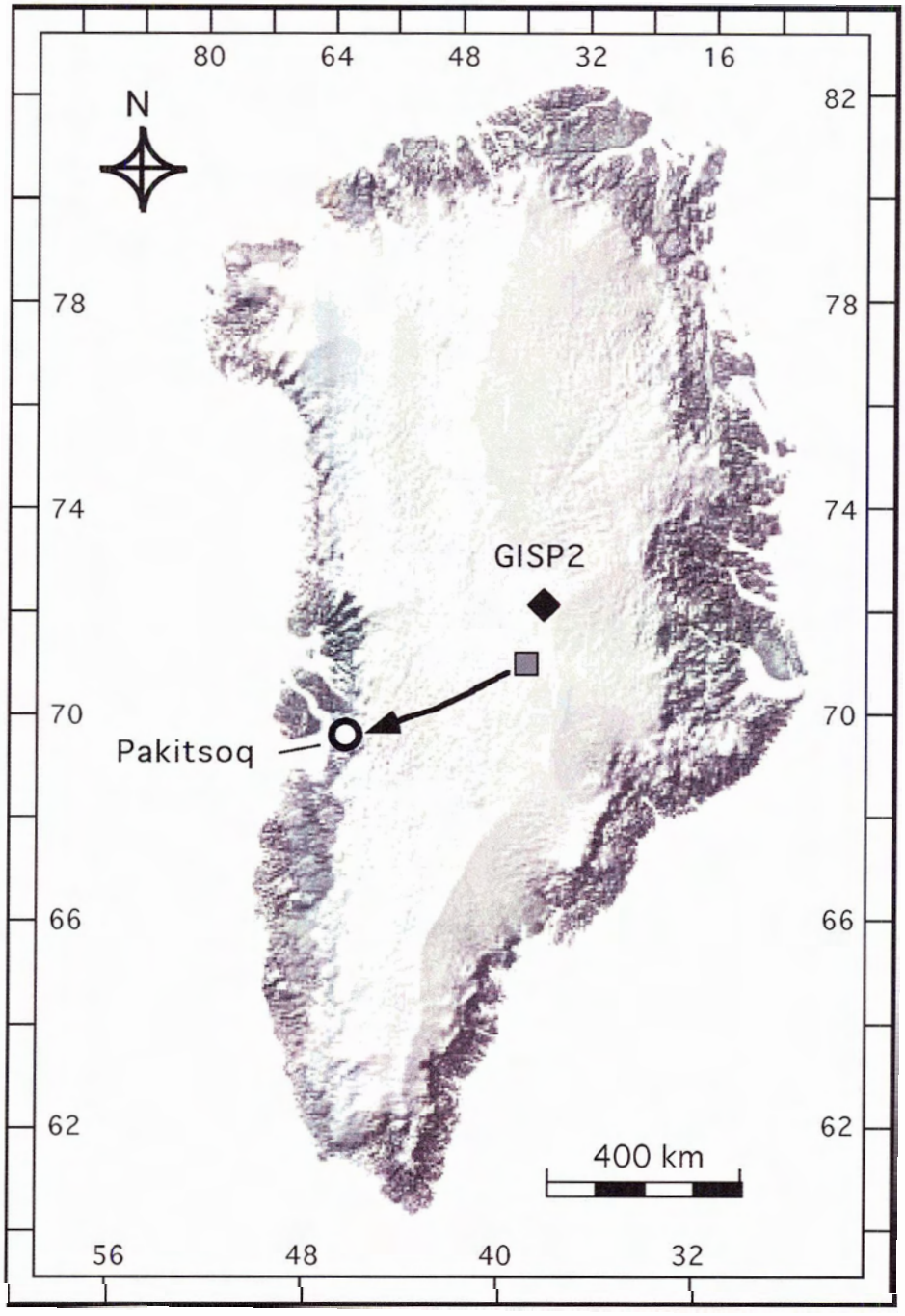

Fig. 2.3.1: Map of the study sites in Greenland
The map shows the location of sampling sites at GISP2 (diamond) and Pakitsoq (circle). The grey square marks the deposition site for YD-ice collected in Pakitsoq, the arrow indicates the ice flow line (after Reeh et al., 2002).

2.3.3. Pakitsoq

In all glaciers and ice sheets, deposited ice becomes progressively buried and at the same time is transported towards the ice margin (Fig. 2.3.2). Theoretically, all deposited layers should be exposed there. Usually this is not the case due to folding, faulting, and, most importantly, basal melting. At the western margin of the Greenland ice sheet near Pakitsoq fjord (69°25.83'N; 50°15.20'W) the normally horizontal ice flow is bent and pushed upwards by bedrock topography (Fig. 2.3.1). Reeh et al. (1987) discovered that this exposes ice from the end of the last glacial at the surface and that oxygen isotope profiles match the records from the Greenland Summit ice cores. With flow models they reconstructed the pathway and the origin of the ice (Reeh et al., 2002). The deposition site varies with ice age, but for the YD was determined as 70.954 °N and 39.824°W, several hundred kilometers SW of the GISP2 drill site. In consequence, temperatures are warmer by ca. 3 °C and accumulation rates higher by about 50 % (0.37 m ice/yr). The conditions during the YD can be derived similarly in relation to results from GISP2 (Grootes et al., 1993, Cuffey and Clow, 1997). An independent check using $\delta^{15}N$ isotope data from Pakitsoq and a firn densification/diffusion model results in a mean annual temperature of –43 °C and an accumulation rate of 0.092 m ice/yr for the YD at this site (Severinghaus, personal communication).

Generally, the pre-Holocene ice at Pakitsoq is exposed in layers of increasing age with growing distance from the margin. Several sections, however, are folded and overturned (Fig. 2.3.3). The profile that provided the samples for this study is situated in the overturned side of a syncline, whose axis plunges at around 20° SW. The strata dip at a 70 ° angle in an easterly direction (Petrenko et al, in preparation). The Pakitsoq margin loses three meters of ice per year through melting (which is roughly balanced through the upward motion of the ice, Reeh et al., in preparation). In consequence, each sampling campaign targets a deeper section of the ice. These can be spatially correlated to previously taken samples by the use of long poles, which are sunk into the ice and serve as markers, but the geology of the ice may slightly shift the relative position of age boundaries relative to the marker and change the thickness of specific sections in deeper horizons.

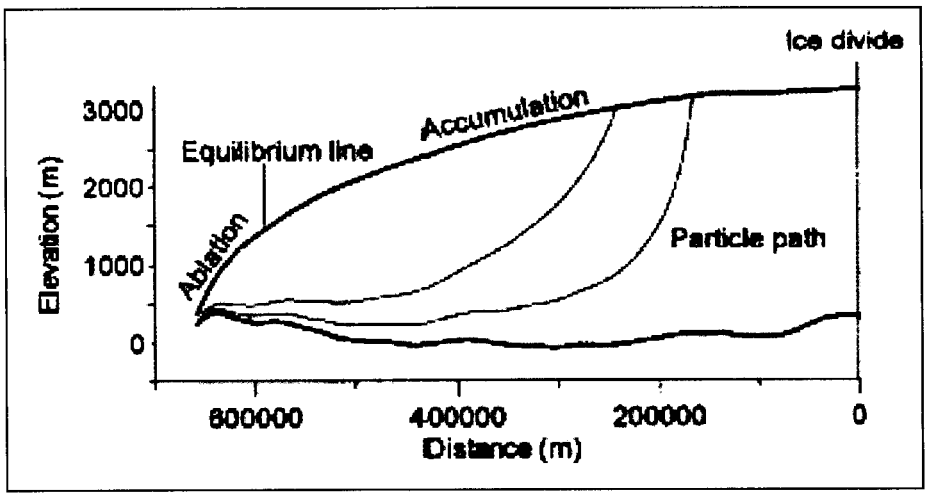

Fig. 2.3.2: Flow patterns in an ice sheet
The curves labeled "Particle path" show how a unit of ice is deposited in the accumulation zone, becomes progressively buried and flows towards the ice margin, where older layers are exposed underneath younger ones (*from* Reeh et al., 2000).

The tectonic stress during transport compromises the integrity of the ice. Visible expressions are bands (strictly speaking layers) of clear or dirty ice. The former are probably refrozen cracks that lack the characteristic bubbles of glacier ice. They can run across the stratigraphy but are often fairly parallel to the ice strata. Dirt bands generally run along the strike of the ice layers, they might represent horizons of ice thinning and therefore age gaps. Both types of bands can be folded, the dirt bands again following the geology of the ice whereas the clear bands often display small scale *en echelon* folds. While the ice of tectonically affected layers is not suitable for methane analysis, rigorous testing established the suitability of undisturbed Pakitsoq ice for gas measurements. In field and laboratory records of methane concentrations (Brook, unpublished data; this study), $\delta^{15}N$ of N_2 and $\delta^{18}O_{atm}$ (Petrenko et al., in preparation) were measured. The results are consistent throughout all three sampling campaigns and in excellent agreement with ice core data from GISP2, proving that atmospheric signals are truthfully recorded in Pakitsoq ice.

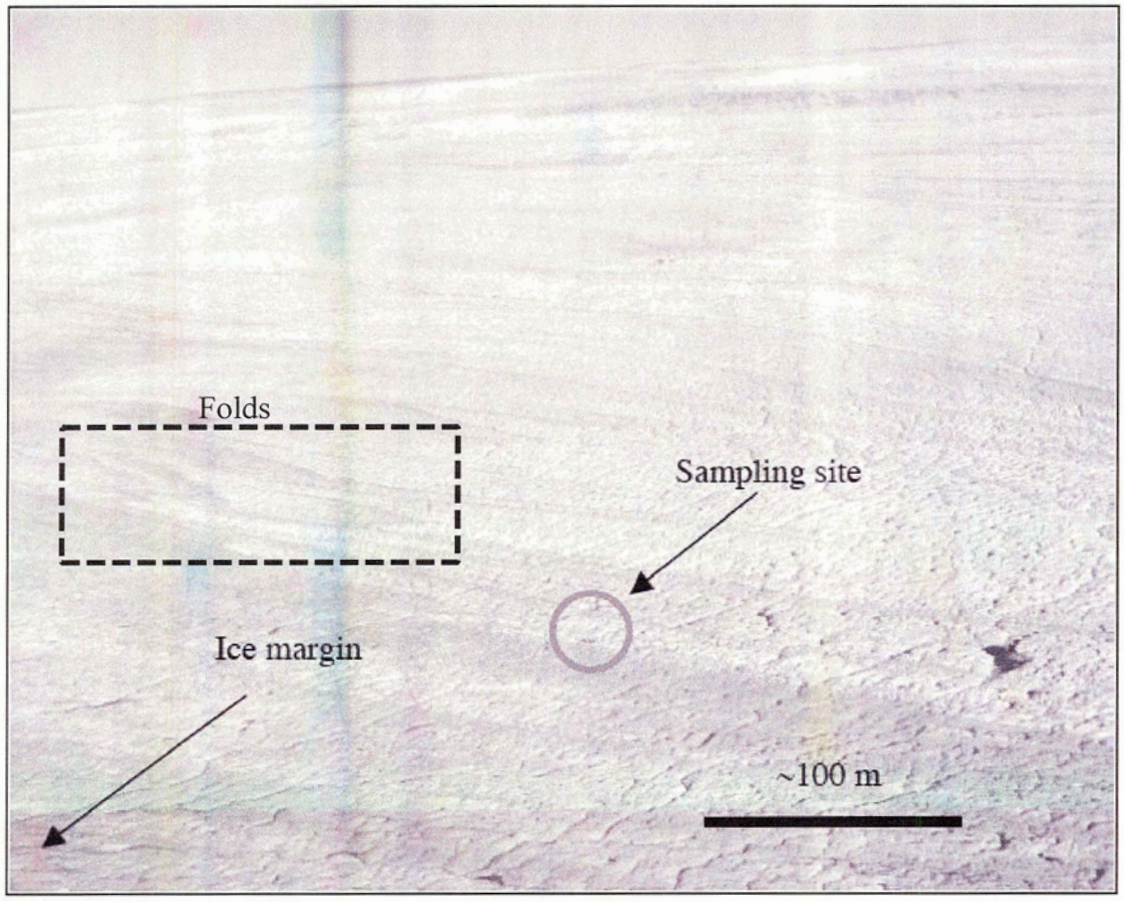

Fig. 2.3.3: Ice margin in Pakitsoq (W-Greenland)
Different shading in the ice indicates layers from warm periods (white) and darker ice with high dust contents from cold periods. Folding is most obvious in, but not restricted to, the dashed square (*from* Petrenko et al., in preparation).

The records have unique combinations of proxy values (e.g. $\delta^{15}N$, methane concentration) that are specific for certain times in climatic history so that they, together with ice matrix isotopes ($\delta^{18}O_{ice}$), provide an age control. Concordance with records from GISP2, which has an established age scale for occluded gases (Severinghaus et al., 1998), allows the dating of the layers of the ice margin (see Chapter 3.3). Field measurements of methane concentrations were used to target specific sections for sampling. We used chain saws to cut samples from the ice at the bottom of a ca. 40 cm deep trench in order to avoid surface contamination.

3. Results

A total of 117 ice samples were analyzed for $\delta^{13}C_{CH4}$ of enclosed methane. These samples came from three different locations, i.e. Agassiz ice cap on Ellesmere Island, Central Greenland (GISP2) and the western margin of the Greenland ice sheet (Pakitsoq) (see Figure 2.3.1). For every sample the methane concentration of the extracted gas was calculated. This parameter in conjunction with visible ice features was used to identify outliers and remove them from the record. In the remaining data the median of replicate measurements was determined to represent $\delta^{13}C$ and concentration of methane in that sample. The age of enclosed gas was calculated for all samples in order to correlate results of different sampling campaigns and literature values. A series of corrections for natural artifacts in $\delta^{13}C$ is applied to obtain the true atmospheric $\delta^{13}C_{CH4}$ from the raw data. This chapter provides details for the different steps outlined above and presents the data derived from them.

3.1. Calculation of methane concentration

Methane concentration was calculated from the height of the m/z 44 peak that represents $^{12}CH_4$ recorded on the mass spectrometer together with sample weight as outlined in Chapter 2.1.5.2. Air content measurements for Pakitsoq ice (Brook, unpublished data) were used in this step. Resulting methane concentrations are shown in Figures 2.1.8, 3.3.1 and 3.5.1.

Table 3.1: IRMS results for Agassiz ice core samples

Sample ID	Age (yr BP)	Methane concentration (ppbV)	$\delta^{13}C$ raw (‰)	Gravitation correction (‰)	$\delta^{13}C_{CH4}$ (‰)	
72a1	322	683	-49.52	-0.28	-49.80	
72a2	320	695	-52.11			36 % melt
72a3	324	590	-49.72	-0.28	-50.00	
72a4	326	581	-49.32	-0.28	-49.60	13 % melt
72a5	328	600	-49.38	-0.28	-49.66	
72a6	330	646	-49.47	-0.28	-49.75	4 % melt
72c1	332	657	-49.25	-0.28	-49.53	
72c3	334	681	-50.08	-0.28	-50.36	
72c4	336	698	-49.38	-0.28	-49.66	
146a1	1867	391	-50.12			fractured
146a2	1871	552	-53.65			fractured
146a3	1876	401	-50.08			fractured
146a4	1880	401	-49.13			fractured
146b1	1885	622	-48.80			fractured
146b2	1889	599	-47.83			fractured
146b3	1893	572	-49.14			fractured
146b4	1898	588	-48.55			fractured
81.1a	12 725	621	-50.40			fractured
81.1b	12 813	551	-51.05			fractured
81.1c	12 901	648	-49.59			fractured
81.2a	13 166	572	-50.15			fractured
81.2b	13 254	501	-49.36			fractured
81.2c	13 342	494	-49.08			fractured
81.2d	13 430	544	-49.19			fractured
81.2e	13 518	444	-49.13			fractured

Table 3.2: IRMS results for GISP 2/139 samples

Sample ID	Age (yr BP)	Methane concentration (ppbV)	$\delta^{13}C$ raw (‰)	Gravitation correction (‰)	$\delta^{13}C_{CH4}$ (‰)
B2	226	805	-50.09	-0.34	-50.43
C2	226	668	-49.69	-0.34	-50.03
D1	227	708	-48.79	-0.34	-49.13
E1	227	716	-49.12	-0.34	-49.46
G1	228	672	-49.36	-0.34	-49.7
G2	229	691	-49.12	-0.34	-49.46
H1	229	683	-48.93	-0.34	-49.27

Table 3.3: IRMS results for Pakitsoq 2001 sample set

Sample ID	Trench location (m)	Age (kyr BP)	Methane concentration (ppbV)	$\delta^{13}C$ raw (‰)	$\delta^{15}N$ correction (‰)	Diffusion correction (‰)	$\delta^{13}C_{CH4}$ (‰)
P4	0.91		571	-52.06		clear band	
P8	1.29	12.552	457	-45.73	-0.38	0.00	-46.11
P10	1.48	12.367	472	-46.50	-0.38	0.00	-46.88
P11A	1.57	12.279	410	-44.86	-0.39	0.00	-45.25
P11B	1.57	12.279	476	-46.23	-0.39	0.00	-46.62
P14	1.83	12.029	483	-44.79	-0.40	0.00	-45.19
P17	2.09	11.778	459	-45.76	-0.40	0.00	-46.16
P23	2.64	11.451	733	-44.98	-0.52	0.00	-45.50
P25	2.79	11.379	677	-46.76	-0.52	0.00	-47.28
P26	2.88	11.337	704	-42.65	-0.51	0.00	-43.16
P29A	3.13	11.219	653	-43.90	-0.50	0.00	-44.40
P29B	3.13	11.219	695	-45.34	-0.50	0.00	-45.84

Table 3.4: IRMS results for Pakitsoq 2002 sample set

Sample ID	Trench location (m)	Age (kyr BP)	Methane concentration (ppbV)	$\delta^{13}C$ raw (‰)	$\delta^{15}N$ correction (‰)	Diffusion correction (‰)	$\delta^{13}C_{CH4}$ (‰)
Aa2	1.64	12.211	473	-45.61	0.37	0	-45.98
Aa3a	1.62	12.233	517	-45.25	0.37	0	-45.62
Aa3b	1.67	12.189	527	-45.42	0.37	0	-45.79
Ab1	1.71	12.150	461	-45.70	0.38	0	-46.08
Ab2	1.74	12.121	533	-45.49	0.38	0	-45.87
Ab3	1.74	12.121	520	-45.49	0.38	0	-45.87
Ba1a	1.83	12.031	692	-45.08	0.39	0	-45.47
Ba1b	1.83	12.031	523	-45.84	0.39	0	-46.23
Ba2	1.83	12.031	535	-45.06	0.39	0	-45.45
Ba3	1.89		679	-42.14	dirt, clear band, intraclast		
Ba4	1.89		595	-43.81	dirt layer		
Ba5	1.94	11.926	527	-44.73	0.42	0	-45.15
C1	2.03		657	-44.37	clear bands		
C2	2.03	11.836	500	-45.39	0.44	0	-45.83
C3	2.09		855	-43.18	clear band (1.5 mm)		
C4	2.09		733	-43.74	clear band (1.5 mm)		
C5	2.14		720	-44.03	clear band		
Dc1	2.24		800	-43.7	clear band (2mm)		
Dc2	2.28		892	-45.85	clear band (2mm)		
Da3	2.28	11.622	582	-46.64	0.52	0.42	-46.73
Da4	2.28	11.622	661	-45.84	0.52	0.42	-45.93
Da5	2.33	11.599	646	-46.55	0.52	0.61	-46.46
E1	2.45		948	-44.39	fracture		
E2	2.45	11.539	756	-46.06	0.53	0.61	-45.98
E3	2.45	11.539	677	-46.20	0.53	0.61	-46.12
E5	2.53	11.503	694	-45.76	0.52	0.57	-45.71
Fa1	2.64	11.451	773	-44.65	0.50	0.08	-45.07
Fa2	2.64	11.451	738	-45.67	0.50	0.08	-46.09
Fa3Fb	2.64	11.447	706	-45.27	0.50	0.07	-45.71
Fc1a	2.70	11.419	798	-45.19	0.51	0.01	-45.68

Table 3.5: IRMS results for Pakitsoq 2003; raw data

Sample ID	Trench location (m)	Methane concentration (ppbV)	$\delta^{13}C_{CH4}$ (‰)
YP1D	2.05	564	-45.87
YP1C	2.05	583	-46.25
YP1A	2.05	575	-46.63
YP1B	2.05	835	-45.56
YP2A2	2.17	612	-45.94
YP2A1	2.17	623	-46.69
YP2A3	2.17	553	-47.92
YP2BC	2.14	560	-46.16
YP2A	2.14	586	-46.56
YP2B2	2.12	561	-46.57
YP2B1	2.12	595	-44.94
YP2B1B3	2.12	538	-46.67
YP3A3	2.26	704	-43.50
YP3A2	2.26	670	-43.67
YP3A1	2.26	715	-46.54
YP3AB	2.24	712	-46.45
YP3B2	2.22	644	-47.47
YP3B1	2.22	672	-46.92
YP4ABC	2.34	746	-47.15
YP4a	2.34	730	-46.37
YP4b	2.34	750	-46.43
YP4c	2.34	693	-46.51
YP5a	2.43	713	-45.32
YP5b	2.43	790	-46.97
YP5AC	2.43	721	-45.52
YP5BD	2.43	741	-46.45
YP6A	2.54	792	-45.59
YP6a	2.54	870	-46.26
YP6D	2.54	829	-45.41
YP6B	2.54	906	-47.07
YP6C	2.54	790	-45.15
YP7BC	2.64	845	-45.30
YP8AC	2.74	747	-46.19
YP8a	2.74	821	-45.97
YP9B	2.83	893	-46.39
YP9A	2.83	819	-45.98
YP9a	2.83	820	-45.26
YP10A	2.93	810	-45.42

Table 3.6: Pakitsoq 2003 median values

Sample ID	Trench location (m)	Age (kyr BP)	Methane concentration (ppbV)	$\delta^{13}C$ raw (‰)	$\delta^{15}N$ correction (‰)	Diffusion correction (‰)	$\delta^{13}C_{CH4}$ (‰)
YP1	2.05	11.746	579	-46.06	-0.40	0.00	-46.46
YP2A	2.12	11.678	561	-46.57	-0.42	0.00	-46.99
YP2B	2.14	11.659	573	-46.36	-0.43	0.00	-46.79
YP2C	2.17	11.641	612	-46.69	-0.45	0.13	-47.00
YP3A	2.22	11.620	658	-47.20	-0.48	0.60	-47.07
YP3B	2.24	11.611	712	-46.45	-0.49	0.69	-46.25
YP3C	2.26	11.603	704	-43.67	-0.51	0.73	-43.45
YP4	2.34	11.570	738	-46.47	-0.54	0.73	-46.29
YP5	2.43	11.532	731	-45.99	-0.54	0.54	-45.99
YP6	2.54	11.486	829	-45.59	-0.53	0.04	-46.08
YP7	2.64	11.445	845	-45.30	-0.52	0.00	-45.82
YP8	2.74	11.403	784	-46.08	-0.51	0.00	-46.59
YP9	2.83	11.365	820	-45.98	-0.52	0.00	-46.50
YP10	2.93	11.324	810	-45.42	-0.52	0.00	-45.94

3.2. Contaminated and compromised samples

As there is only one literature report on measurements of $\delta^{13}C$ of methane in ice samples to date (Craig et al., 1988b), it is largely unknown which processes could lead to contamination of this parameter and how compromised samples can be recognized. In addition, the destructive nature of the analysis makes it impossible to re-examine a sample that produced a questionable result. Craig et al. (1988b) reported that fractured samples gave artificially high $\delta^{13}C_{CH4}$ values. The analysis of samples from the Agassiz core confirms that fractured ice is problematic. We measured multiple samples of three core sections and found that only section Ag77/72 gave consistent results (Fig. 3.2.1). The other two sections were highly fractured and their data sets display a large amount of scatter in $\delta^{13}C_{CH4}$ as well as methane concentration. The contrast between sections Ag77/72 and Ag77/146 is especially striking. Both comprise ice from a short period of time under stable conditions so that the measured values should not deviate significantly within each data set. While Ag77/72 has a standard deviation for $\delta^{13}C_{CH4}$ of 0.27 ‰

(n = 9), that of Ag77/146 is 1.78 ‰ (n = 8). Clearly, fractured ice is not suitable for the analysis of $\delta^{13}C_{CH4}$. The Agassiz records show another feature that can affect isotope measurements: the only outlier in Ag77/72 is from a sample with several visible melt layers, comprising 36 % of sample volume. $\delta^{13}C_{CH4}$ of this sample was 2.5 ‰ more depleted in ^{13}C than the average (Fig. 2.1.8). Although two other samples with smaller amounts of melting (4 and 13 %) gave no suspicious results, the conclusion is that melt layers can adversely affect gas data. The exact reason is unknown, possibly the melt water becomes saturated with methane and traps methane during freezing.

All samples from Pakitsoq were analyzed after recording visible features that may affect the results. I then checked the measured records for outliers. I also specifically examined all data points from samples with certain characteristics as they were noted before the measurement. In this manner it was possible to identify the following visible features that produce erroneous results: dirt layers and dirt inclusions, cracks, in one case an "intraclast" (bubble free inclusion with sharply defined boundaries) and certain types of clear bands. The latter may be refrozen cracks caused by ice tectonics or sampling. All of the features mentioned above resulted in elevated methane concentrations and were anomalously high in ^{13}C. These data were removed from the record and not used further. In contrast, fine (< 1 mm thickness) clear layers and wavy bands with reduced density of bubbles, both more or less parallel to strike, provided normal results. As a matter of caution, samples with these features should nevertheless be avoided in future work. Outliers that were not associated with flaws of the sample are presented with the records.

A special case of contaminated samples in the Pakitsoq 2002 record deserves special discussion. One of the field samples included a conspicuous clear band, possibly a refrozen chainsaw cut. It was analyzed in six sub-samples. In the concentration record, these data points look like the increase associated with the YD termination (Fig. 3.2.1).

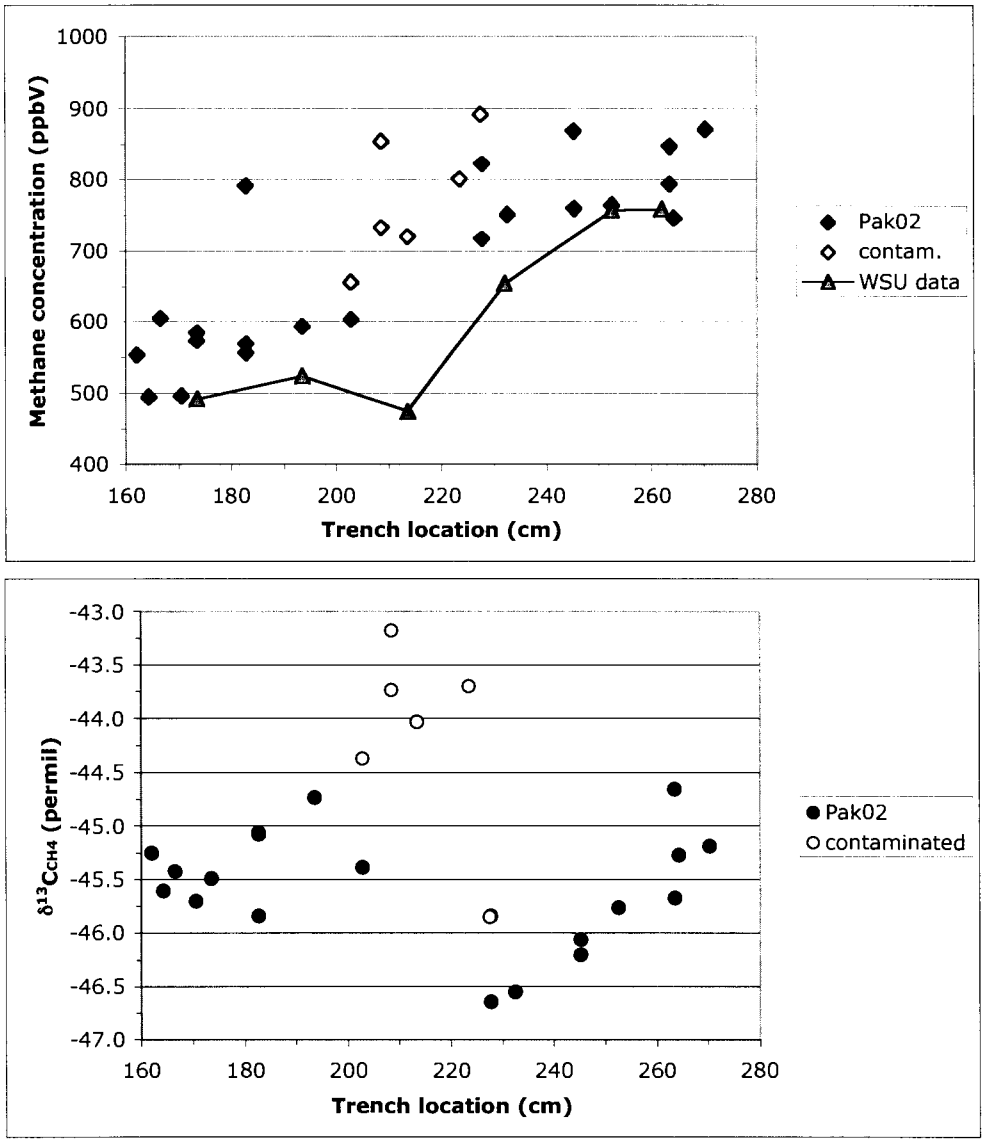

Fig. 3.2.1: Methane concentration and $\delta^{13}C_{CH4}$ from Pakitsoq 2002
Raw data of methane concentration and $\delta^{13}C_{CH4}$ from the 2002 sampling campaign in Pakitsoq are plotted against their position in the profile. Data derived from a contaminated sample with a conspicuous clear band are plotted in open symbols. Elevated methane concentration in this ice masks the true position of the YD termination as seen in data measured at WSU (Brook, unpublished data) (top panel). High $\delta^{13}C$ values are associated with these values (bottom panel). Note the sudden drop without any sign of diffusive smoothing around 2.25 cm. Note that uncontaminated samples give slightly higher methane concentrations than measured at WSU, which is likely a calibration problem. Samples from the Pakitsoq 2003 record, which covered the same time interval, showed no elevated $\delta^{13}C$ values, confirming that the deviation is truly due to contamination of the 2002 sample.

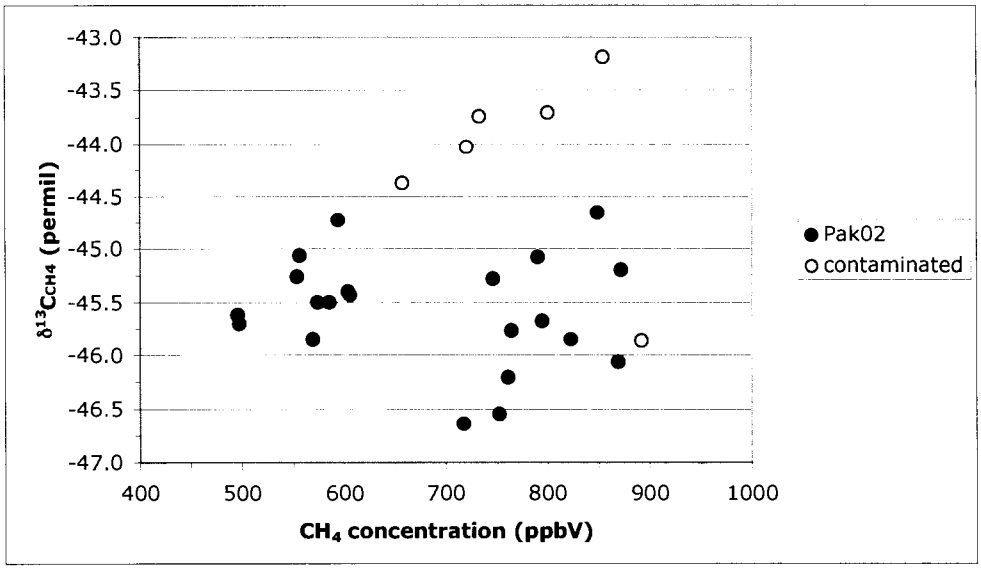

Fig. 3.2.2: Methane concentration vs. $\delta^{13}C_{CH4}$ in normal and contaminated samples Contaminated samples show a clear correlation between methane concentration and $\delta^{13}C_{CH4}$ (with one exception). All $\delta^{13}C_{CH4}$ values higher than –44.5 ‰ are from contaminated samples.

The associated $\delta^{13}C_{CH4}$ values are the only ones in the record above –44.5 ‰ and show a trend of ^{13}C-enrichment followed by a suspicious break relative to the next samples. The elevated methane concentration in these samples starts at a different location of the trench than the actual increase of the termination, which is recorded in ice that is located approximately 15 cm further in the profile. The position of the increase was established with methane concentration measurements in field and laboratory (Brook, personal communication) and recorded in other proxies such as $\delta^{15}N$. The sample must be rejected due to two reasons. For one, because the values are inconsistent with other data sets from the same location; for the other, because they introduce a pattern that is not in agreement with a true environmental signal. Namely the "instantaneous" drop of $\delta^{13}C_{CH4}$ by around 2 ‰ within a time frame of several years would have been smoothed by diffusion if it were an atmospheric signal. One could speculate that the false trend introduced by the compromised sample (Fig. 3.2.2) results from increasing amounts of contaminated ice, as the refrozen crack entered the sample at an angle. In conclusion, the special character of the Pakitsoq sampling site (as opposed to traditional drilling locations) introduces alterations to ice that have to be carefully avoided during sampling.

The final proof that the elevated values are the result of contamination comes from the Pakitsoq 2003 record, which covers the same time period and shows no increase in $\delta^{13}C_{CH4}$ (Figures 3.6.1 and 3.6.2).

3.3. Age correlation

3.3.1. Agassiz ice cores

The core section 72 of ice core Agassiz 1977 comprises the depth interval from 105.6 to 107.1 m, section 146 that from 212.3 to 213.8 m. Section 81/2 from core 1984 is 118 m – 119.5 m deep. The according ages for ice are 580, 2135 and 13,500 yr BP, respectively, where summer of AD 1950 is the reference point (Fisher, personal communication). Occluded gases are younger because air diffuses into the unconsolidated firn layer (Schwander et al., 1988). Gas ages were derived as a rough estimate from the firn ice transition depth, which does not take into account that the average age of air at that depth is older due to diffusion. This introduces an error of about one decade towards younger ages. The respective ages are 330, 1885 and 13166 yr BP.

3.3.2. GISP2 core

Core section #139 of the GISP2 ice core spans the depth from 141.0 to 142.2 m. The according gas age is 225 to 229 yr BP (Brook et al., 1996 and Brook et al., 2000, data available from NSIDC).

3.3.3. Pakitsoq profiles

3.3.3.1. Age scale for Pakitsoq samples

All Pakitsoq samples were collected in a profile perpendicular to the strike of the ice layers, so that the distance from an arbitrary reference point (i.e. "trench location") provides a measure of ice age. Trench location is therefore comparable to the depth of a drilled core. Between sampling campaigns the profiles are correlated using permanent markers. In order to compare the Pakitsoq record to other data, trench locations are converted to an age scale. The age scale adopted here was developed for the GISP2 record and is based on gas-age ice-age differences from a firn densification and diffusion

model (Schwander et al., 1997). It was consequently calibrated and modified using $\delta^{15}N$ of N_2 records (Severinghaus et al., 1998) and is specific for gas occlusions in the GISP2 record. The conversion is done by matching methane concentration data from Pakitsoq (including data measured in the field and at WSU, Brook, unpublished) with those of GISP2 (Brook et al., 1996, 2000, data available from NSIDC) (see Fig. 3.3.1). The latter are converted to the GISP2 gas age scale of Severinghaus et al. (1998). Then the exact time of beginning and end of the methane rise at the YD termination is determined from this record. The corresponding values in the Pakitsoq record are assigned the same dates, i.e. 11.65 and 11.5 kyr BP, respectively. Note that the match is between corresponding inflection points of the two records, and is therefore independent of data scatter and a possible systematic offset between the records. It is assumed that age changes linearly with trench location after the onset of the transition, which is supported by uniform ice accumulation rates in Central Greenland during this period (Cuffey and Clow, 1997). Therefore, age can be calculated from trench location in a linear relationship according to:

$$age_{PB} = -0.477 \times [distance(m)] + 12.71 \text{ (kyr BP)} \qquad (3.1)$$

which is valid in the PB and also the transition period. In the YD, however, accumulation rates were smaller by a factor of two (Cuffey and Clow, 1997), resulting in the relationship:

$$age_{YD} = -0.973 \times [distance(m)] + 13.81 \text{ (kyr BP)} \qquad (3.2)$$

The quoted relationships are specific for the sampling situation in 2002. Due to melting a different part of the folded ice was exposed in 2001 and 2003, so that the ice of the YD-PB transition lies in a slightly different profile location and may also vary in width. For 2001 there are only data outside the transition period, which means that no age control is provided by the data, but also that exact dating is not critical. Therefore the 2002 age scale can be applied to these samples as well.

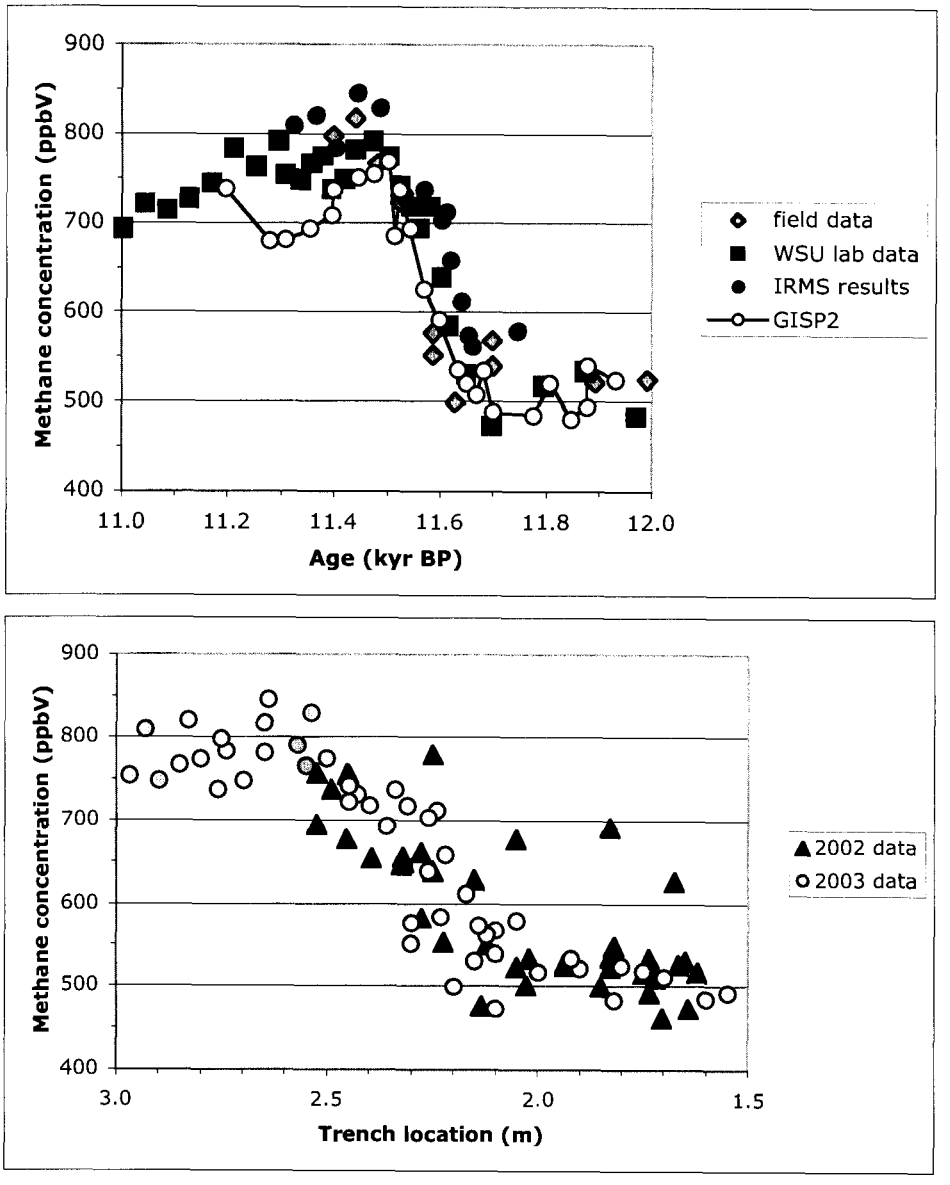

Fig. 3.3.1: Methane concentration data and the Pakitsoq age scale
Top panel shows methane concentration data measured in the field, at WSU and in this study for the 2003 sampling campaign. The different records compare well. GISP2 data (Brook et al., 1996; Brook et al., 2000) are overlaid to provide the age reference. Bottom panel shows the same data set as a composite record and a corresponding one from 2002. Onset of the concentration rise occurs at different trench locations for the two campaigns.

A specific age scale for samples from 2003 differs slightly as:

$$age_{PB} = -0.417 \times [distance(m)] + 12.55 \text{ (kyr BP)} \quad (3.3)$$

$$age_{YD} = -0.973 \times [distance(m)] + 13.74 \text{ (kyr BP)} \quad (3.4)$$

In consequence, age scaling provides a tool to correlate data collected in Pakitsoq during different field campaigns. The age scale is best defined in the transition period between the two fixed dates. The extrapolation into the YD and PB is more uncertain, particularly in the YD where dirt bands in the ice possibly represent sections of tectonically thinned ice. However, in these stable periods accurate ages are less important, assuming that $\delta^{13}C_{CH4}$ will not change independently of methane concentration or climate. The Pakitsoq methane concentrations plotted on the age scales show excellent agreement with GISP2 data in terms of absolute values, which provides a test for the validity of the assumptions and calculations. Also, the relative age between data points is independent of the accuracy of the record, because the samples were collected in one continuous record and is therefore internally consistent. This applies to a lesser degree when records from different sampling campaigns are compared. All data are reported using these gas age scales.

3.3.3.2. Resolution of the Pakitsoq record

Air occlusions in ice record a signal that is integrated over a certain time span, due to diffusional mixing and occlusion that occurs in a depth interval rather than one specific depth (Schwander et al., 1988; Battle et al., 1996). The resulting spread of gas ages in one sample is known as its age distribution. According to Schwander et al. (1993) the age distribution for CO_2 at Summit, Greenland is 12 yrs with a standard deviation of 7.5 yrs. Because methane has a higher diffusion coefficient (D) than CO_2 it is better mixed in the firn and has a smaller age distribution. Dividing results from Schwander et al. (1993) by the ratio of the diffusion coefficients (D_{CH4}/D_{CO2}) = 1.35) gives the age distribution of methane at the close-off depth as 8.9 yrs with a standard deviation of 5.6 yrs. This value was different for the Pakitsoq deposition site under YD conditions. In lower temperatures diffusion is slower and age distribution larger. The exact difference is

hard to determine, but estimates based on our (uncalibrated) diffusion model suggest that 50 % is a conservative estimate. In addition to this inherent age spread of samples, we introduce additional averaging of the signal caused by the time span represented by the thickness of a sample. A calculation of the maximum amount of time recorded in samples shows that the extracted air spans up to 30 yrs, not counting the diffusional age distribution at close off. Taken together, most samples integrate a time interval of 25 to 35 yrs.

Samples from three campaigns result in a composite record from 12,550 to 11,220 yr BP. Within this period average sampling resolution is 36 years, although the largest gap between the irregularly spaced samples is 103 yrs. During the transition period between YD and Preboreal the average resolution is 21 yrs and the largest gap 30 yrs. This constrains possible errors in the time scale significantly. More importantly, both variables of interest for the interpretation, namely atmospheric methane concentration and its $\delta^{13}C$, are recorded in the gas phase of the same sample and measured simultaneously, so that the relative timing of events is directly comparable. Furthermore, $\delta^{15}N$ values measured in the same location (Petrenko et al., in preparation) provide an additional intra-record marker for the exact onset of the termination.

3.4. Corrections for $\delta^{13}C$ values

During the diffusion of air from the atmosphere through the firn layer to the zone of bubble formation gases and isotopic species will fractionate according to their mass and diffusivity. For the interpretation of ice core gas data this means that measurements have to be corrected for the effects of specific diffusion related processes. The most important ones are gravitational separation of gas species and isotopes, fractionation due to thermal diffusion and fractionation of isotopes during times of varying atmospheric concentrations.

3.4.1. Gravitational separation

Gravity will increase the relative abundance of both heavier gas compounds and isotopes in deeper firn layers. Therefore, the concentration of methane in the samples as well as its isotopic composition has to be corrected.

Etheridge et al. (1998) corrected methane concentrations by increasing them by

$$\Delta M \times \delta^{15}N \times [CH_4] \qquad (3.5)$$

where $\Delta M = 13$ is the mass difference between CH_4 and dry air and $\delta^{15}N$ is the measured enrichment of ^{15}N relative to air. For the conditions at which the Pakitsoq samples formed this correction amounts to less than 0.5 % (>4 ppbV) of the measured methane concentration and is negligible; especially so, as the work presented here does not specifically explore or depend on exact values for atmospheric concentrations.

The gravitational fractionation of isotopes can be calculated using a firn densification model (e.g. Schwander et al., 1993) or approximated by the following equation:

$$\Delta = (1.18/T) \times Z \qquad (3.6)$$

in per mille per atomic mass unit (amu). Z is firn depth and T is absolute temperature (Craig et al., 1988a). All samples measured from Agassiz and GISP2 were corrected using this method. For Ag77 we used present day values for local temperature and depth of the diffusive column (Fisher, personal communication). Both might have changed in the last several hundred years but the effects would be negligible. ^{13}C is enriched by 0.28 ‰ relative to the atmosphere. For GISP2 temperature and firn depths are given by Cuffey and Clow (1997) and Alley et al. (1993), respectively. Gravitational fractionation in this case amounts to 0.34 ‰.

For Pakitsoq, Equation (3.6) yields 0.44 ‰ for the Younger Dryas (YD) and 0.41 ‰ for the Preboreal. By comparison to the $\delta^{15}N$ data of the Pakitsoq samples (Petrenko et al., in preparation) the Younger Dryas $\delta^{15}N$ values are somewhat smaller than the theoretical gravitational fractionation. This could indicate either that the diffusive column did not comprise the whole firn depth or that diffusional equilibrium

was not established. In contrast, during the transition $\delta^{15}N$ is considerably larger than gravitational fractionation due to the added effect of thermal fractionation (see 3.4.2). However, the $\delta^{15}N$ data provide a direct quantification of gravitational fractionation for the Pakitsoq samples. Because atmospheric $\delta^{15}N$ was extremely stable over the time period in question (Mariotti; 1983), deviation of ice core $\delta^{15}N$ from the atmospheric value in ice samples is a direct measure of isotopic enrichment due to gravity (as well as thermal fractionation, see below). The assumption of equal fractionation for same mass difference, as is the case for $\delta^{13}C$ and $\delta^{15}N$, holds true only for diffusional equilibrium, i.e. without advection. Trudinger et al. (1997) found for the latter case an offset between $\delta^{13}CH_4$ and $\delta^{15}N$ by a factor of 1.04. Not only is this correction negligible (i.e. far smaller than analytical precision), it is also uncertain whether it has to be applied for our case studies.

3.4.2. Thermal fractionation

The difference in thermal diffusivity between two isotope species, e.g. $^{13}CH_4$ and $^{12}CH_4$, results in an enrichment of the heavier isotope in colder zones. For gas analysis of firn and ice samples this becomes relevant for times of rapid temperature change like the abrupt warming event at the end of the Younger Dryas. At that time a temperature gradient built between overlying air and firn. Consequently, $^{13}CH_4$ becomes enriched in the colder firn layer. As for gravitational fractionation, one can use measurements of $\delta^{15}N$ to quantify this effect and correct for it. In order to examine whether fractionation is the same for methane as for N_2, the change in $\delta^{15}N$ has to be divided into a gravitational and a thermal component. Theoretically, the thermal correction has to be scaled for the different thermal diffusion factors D_T of the isotope pairs of ^{15}N-$^{14}N/N_2$ and $^{13}CH_4/^{12}CH_4$. No data exist on D_T of methane isotopes in air. I used data from Stevens and DeVries (1968), who measured D_T of $^{13}CH_4$ in $^{12}CH_4$, and the approach of Grachev and Severinghaus (2003) to calculate the thermal diffusion sensitivity Ω_T for the temperature range between YD and PB. The same was done for the diffusion of ^{15}N-^{14}N in N_2 with data from Boersma-Klein and DeVries (1966). The sensitivity of methane ranged between $10.35 * 10^{-3}$ and $11.75 * 10^{-3}$ ‰/°C for temperatures between –47 and –30 °C. The equivalent Ω_T values for nitrogen isotopes are $11.76 * 10^{-3}$ and $12.18 * 10^{-3}$ ‰/°C. It

is assumed that these values approximate the thermal diffusion of the respective gases in air fairly well. Note that Ω_T of methane is smaller by 12 % at the most compared to nitrogen. Thermal fractionation observed in $\delta^{15}N$ of Pakitsoq samples is only around 0.15 ‰ (assuming that gravitational fractionation does not change during this time, thermal fractionation is taken as the difference in $\delta^{15}N$ values compared to stable periods). This is already smaller than analytical precision of $\delta^{13}C_{CH4}$ measurements. A scaling of this effect by the calculated factors is unnecessary because the difference would be far from being detectable. Therefore, $\delta^{15}N$ data are simply subtracted from the measured $\delta^{13}C_{CH4}$ values to correct for the combined effect of gravitational and thermal diffusion. Correction factors derived from $\delta^{15}N$ for both thermal and gravitational diffusion are shown in Fig. 3.4.6. The Agassiz and GISP2 records measured in this study all come from times with stable atmospheric temperatures (Grootes et al., 1993), and no correction for thermal fractionation is necessary.

3.4.3. Other isotope effects

Theoretically, additional isotope effects include the enrichment of heavier isotopes in cold horizons within the firn and as a result of effusion from almost sealed cavities, but both are considered to be negligible (Craig et al., 1988a; Schwander et al., 1988).

3.4.4. Diffusion fractionation

Diffusion fractionation occurs in times of changing atmospheric concentrations. Slower diffusion of $^{13}CH_4$ compared to $^{12}CH_4$ means that it takes longer for the former to diffuse from the snow surface to the close off zone. This effective age difference between the isotopic species is irrelevant during times of stable atmospheric concentrations, when equilibrium will be established within decades. Therefore no corrections are necessary for the Agassiz and GISP2 measurements. During times like the end of the YD, however, when atmospheric methane concentrations increased markedly within decades, higher amounts of $^{12}CH_4$ will reach the close-off zone faster than corresponding $^{13}CH_4$. In consequence, the enclosed gas is enriched in ^{12}C compared to atmospheric methane. The effect disappears when atmospheric concentration has stabilized, the diffusion front of

$^{13}CH_4$ reaches the close-off depth, and diffusional equilibrium is re-established. In the meantime, however, the so-called diffusion fractionation can result in a significant isotopic offset between atmosphere and ice core signal.

The magnitude of this effect can be estimated and corrected for using a diffusion model as it is described in Chapter 2.2. The model calculates the offset in isotope ratio between atmospheric and enclosed methane caused by diffusion fractionation at any given time during a transition period. An example of such a deviation is shown in Fig. 3.4.1. The diagram shows the calculated diffusion correction factors (DCF), which are needed to compensate for the diffusion artifact. The deviation caused by diffusion fractionation is therefore identical to the DCF at any given time, but opposite in sign.

The model runs to calculate DCF show three stages in the isotopic response of the firn air to a rise in atmospheric methane concentration (Fig. 3.4.1). At first, strong fractionation occurs when the firn air gets enriched with faster diffusing $^{12}CH_4$. Maximum fractionation is reached within 50 to 100 yrs, depending on the model scenario. Then the model shows a plateau when the diffusive pulse of $^{13}CH_4$ reaches the close-off zone. Consequently, fractionation decreases despite the fact that the atmospheric concentration is still rising. In the third stage, after the atmosphere reached steady state again, diffusion fractionation decreases sharply and approaches zero values. The latter are reached only after the concentration in the occlusion zone has equilibrated with the current atmosphere, i.e. diffusional equilibrium is re-established. Diffusion fractionation is insensitive to variations in atmospheric $\delta^{13}C_{CH4}$ because both isotope species are driven by the same concentration gradient. Diffusion fractionation solely depends on a temporary imbalance of the firn diffusion profile, it returns to zero once a new equilibrium is established. This is independent of the fact that the new equilibrium may have a different concentration level. A different $\delta^{13}C_{CH4}$ in the new state or during the transition would also be canceled out by the model calculations and not affect DCF's, although the value itself would of course be recorded in the ice.

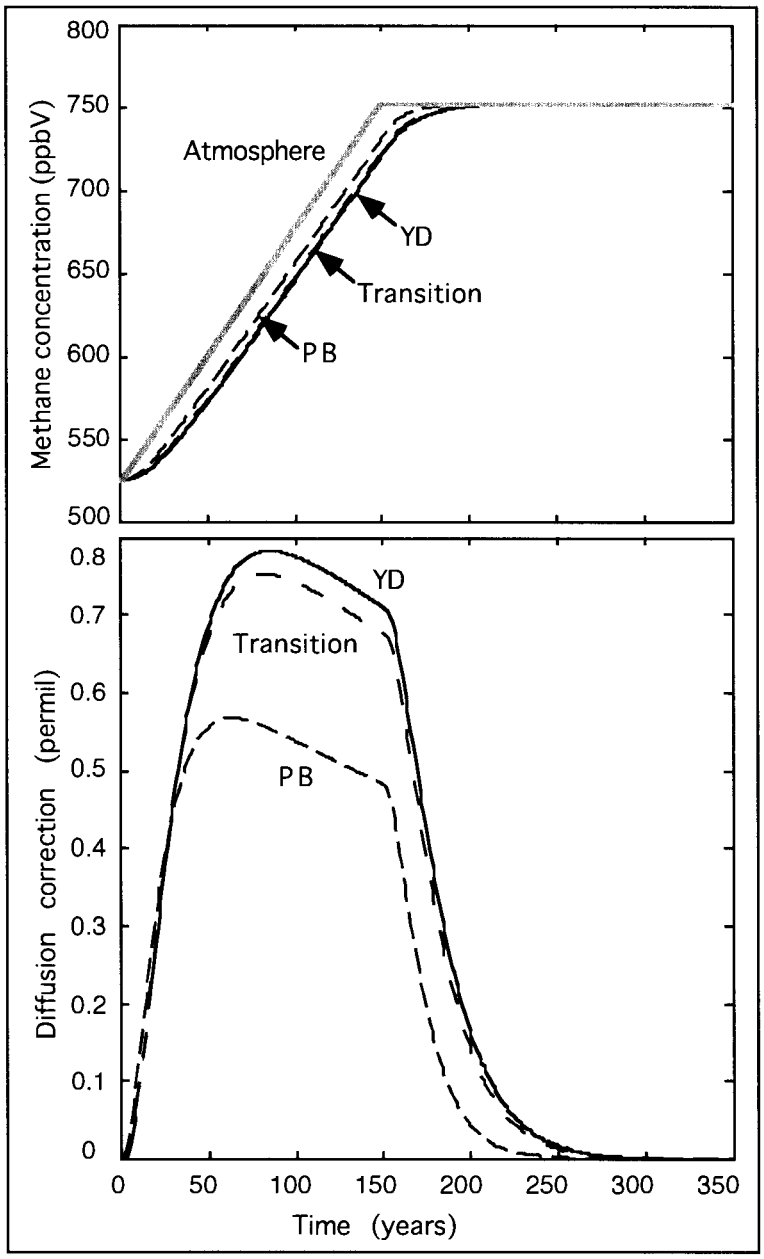

Fig. 3.4.1: Diffusion correction factors for various climatic scenarios
Parameters are specific for YD, transition and PB. The upper panel illustrates the forcing atmospheric increase in methane concentration (thick grey line) and the response at close-off depth for the different parameter sets. The latter is almost identical for YD- and transition models. The lower panel shows the associated diffusion correction factors.

Local temperature and accumulation rate influence DCF. Three different runs show the fractionation associated with values specific to the Younger Dryas, transition period and Preboreal (Fig. 3.4.1). The conditions of the Younger Dryas will determine the nature of the snow pack throughout the transition period. Less than one third of the firn column will have formed in the changing environment by the end of the 150 yr transition. Yet, increasing burial rates and increasing diffusion coefficients due to higher temperatures have an immediate impact. The conditions of the Preboreal are reached only after the main fractionation occurred and even then the snow pack still retains the density profile of the Younger Dryas and transition for decades to centuries. The Preboreal scenario is therefore less likely to accurately reflect the fractionation. The transition scenario works with a temperature and accumulation rate halfway between YD and PB. While this may best average the changing conditions, it does not take into account that most of the firn still dates from the Younger Dryas. Because the diffusion fractionation is most strongly dependent on the firn density profile (calculated after Herron and Langway, 1980), which is determined by Younger Dryas conditions throughout most of the transition, the scenario for YD values with its high fractionation can be taken as an upper limit.

Interestingly, the fractionation curve calculated for the transition is very close to the YD scenario. The difference between DCF calculated for either set of conditions is 0.04 ‰ at the most, a negligible offset. This can be partly explained by the fact that higher temperature and accumulation rate are associated with higher diffusion coefficients and shallower snow pack on one hand, but higher tortuosity on the other hand. We chose the transition scenario to calculate DCF's applied to the Pakitsoq data. In order to determine the exact DCF of any given data point the correlation between DCF and methane concentration at close-off depth (Fig. 3.4.2) was used.

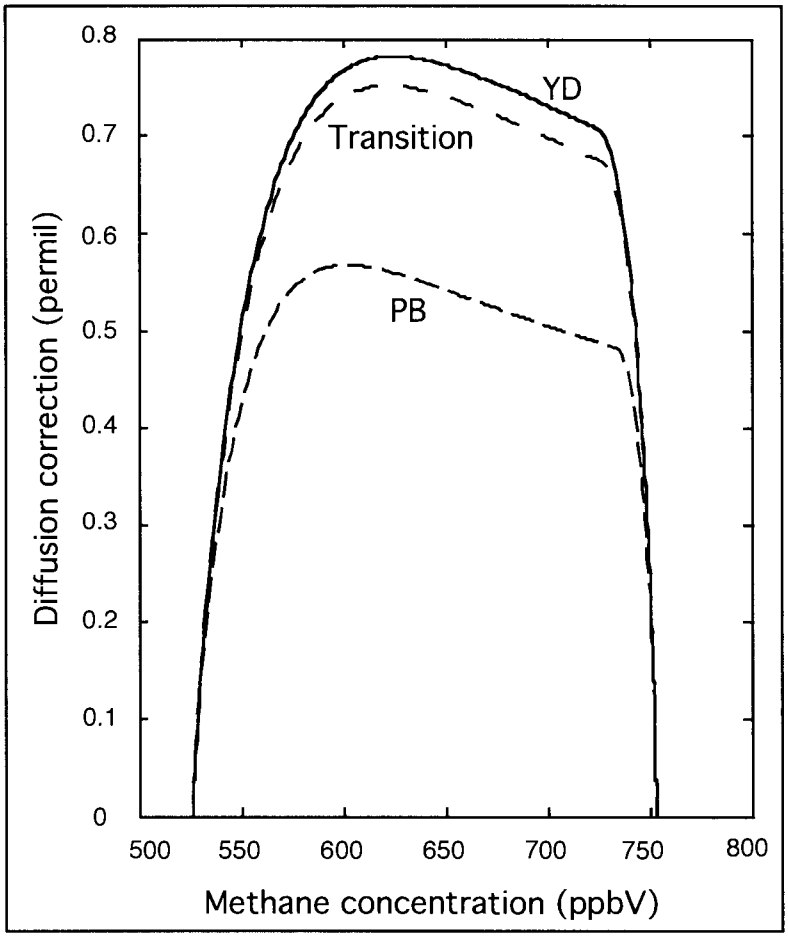

Fig, 3.4.2: Diffusion correction versus methane concentration
Correction depends on the time of the model run, but can be seen as specific for the associated methane concentration at close-off depth. The latter was used to determine specific correction factors for data points.

The possible error associated with the diffusion correction was investigated with sensitivity tests. These were performed with the YD scenario as a base model, but the results are applicable to the conditions of the transition model. At first we examined the sensitivity of the model to the correct choice of diffusive column height (DCH). The choice to calculate diffusion only to the depth where open porosity reaches a value of 0.12, following Schwander et al (1988), is arbitrary. We calculate diffusion coefficients after Spahni et al. (2003) and could run the model closer to the actual close off depth. In fact, calculations with $\delta^{15}N$ data (Schwander et al., 1997; Petrenko et al., in preparation) show that DCH could have been deeper than our scenarios assume. Unfortunately, it is

not possible to use $\delta^{15}N$ as an effective constraint because it is not clear if the correction factors for D_{eff} of Carbon and Nitrogen are the same. One way to test different scenarios is to examine their firn equilibration times. Fig. 3.4.3 shows how concentration in the firn column adjusts after atmospheric concentrations reached the new level. For the transition scenario equilibrium is established within 50 yrs.

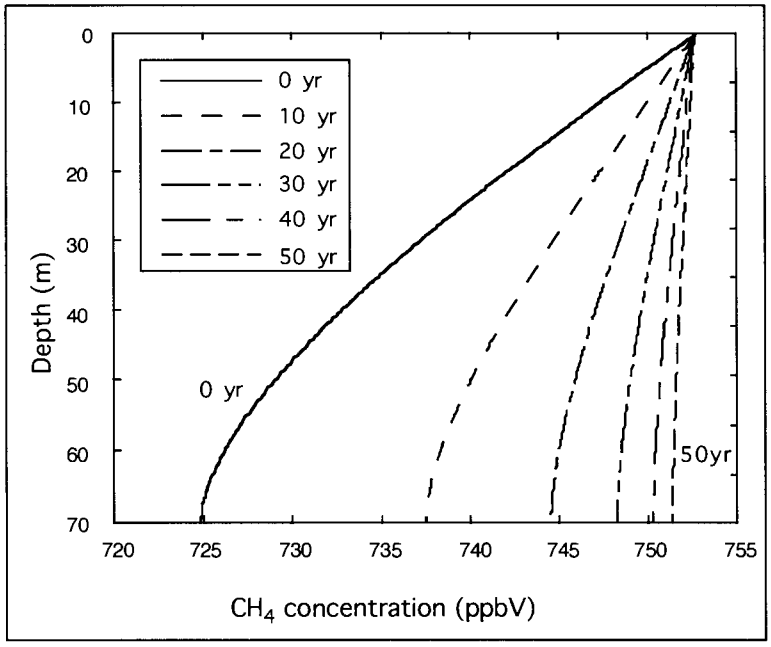

Fig. 3.4.3: Methane concentration gradients in the firn layer
Modeled concentration profiles through the firn layer in 10 yr intervals after the end of the concentration rise (i.e. 0 yr). The concentration gradient disappears within 50 yrs after atmospheric concentration stabilizes. Model parameters are specific for transition.

The transition model was adjusted by first increasing and then lowering DCH by 5 m. Results are shown in Fig. 3.4.4. The shallow firn column had significantly lower correction factors (0.2 ‰), yet there is no reason to assume that diffusion should stop at that depth. Rather, the usual scenario is an upper estimate for the diffusion boundary. Choosing deeper DCH strongly increases diffusion fractionation, but this is associated with longer equilibration times. The standard scenario is likely the most realistic one, but this sensitivity test underlines the uncertainties introduced by using non-calibrated diffusion models.

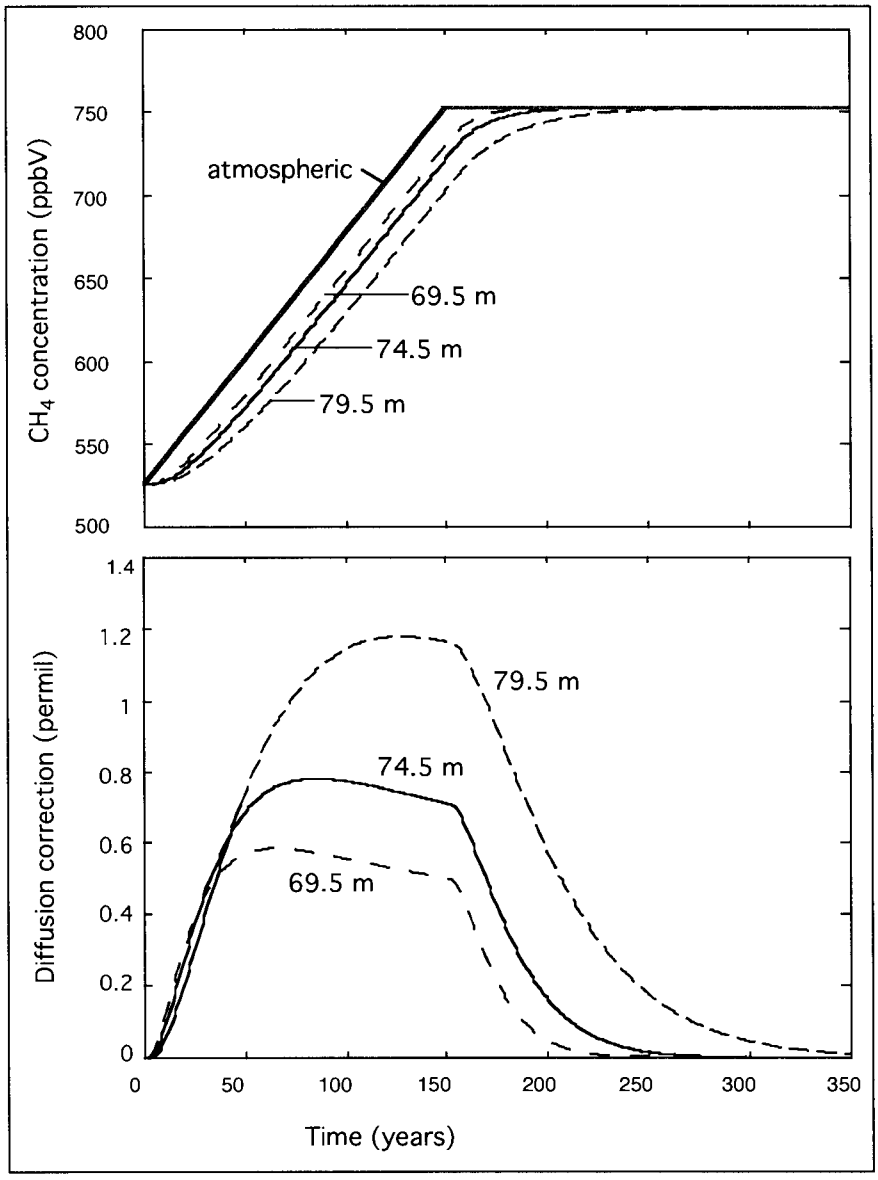

Fig. 3.4.4: Sensitivity tests for diffusive column height (DCH)
Thin black curves show results for DCH determined for open porosity = 0.12 (after Schwander et al. 1988) as used in model runs to calculate diffusion correction factors. Shallower DCH results in lower diffusion fractionation and fast response to changes in atmospheric signal. Deeper DCH gives unrealistically large fractionation and response time. Model parameters are specific for YD.

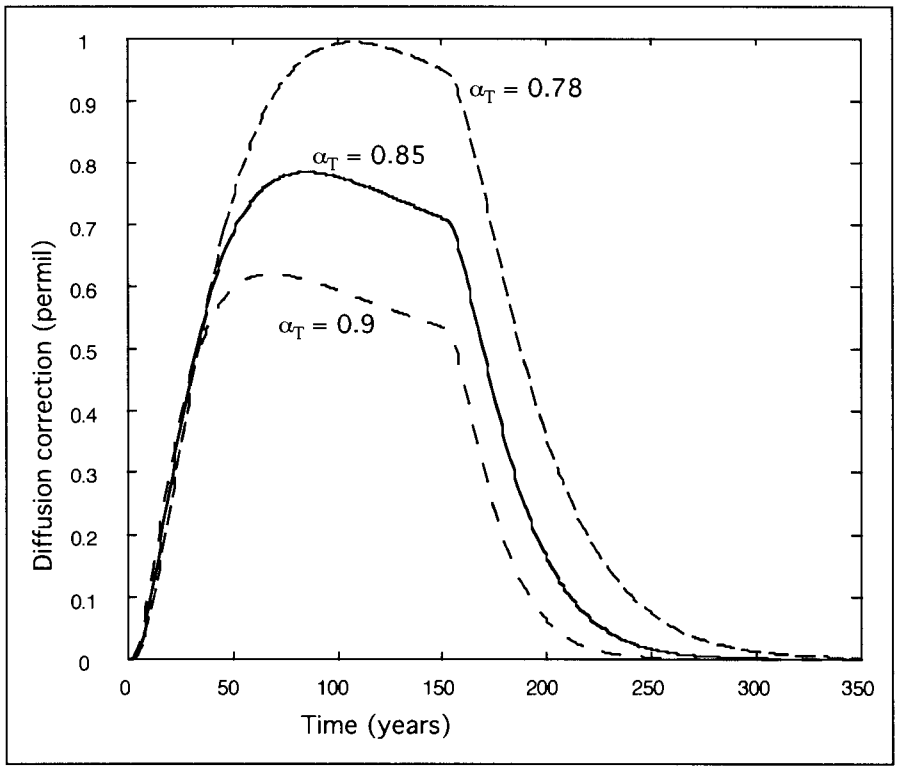

Fig. 3.4.5: Sensitivity tests for tortuosity parameters
Parameter α_T is varied within a range of conditions typical for today's climate in Siple Dome, Antarctica and Greenland Summit. Resulting diffusion fractionation varies by up to 0.4 ‰. Solid curve shows the value interpolated for YD conditions in Central Greenland. Model parameters for T and accumulation rate for YD.

This is also illustrated by sensitivity tests for tortuosity parameters, which are usually used to calibrate a model to firn measurements. Lacking this possibility, we interpolated and extrapolated values from data in Spahni et al. (2003). The test shown in Fig. 3.4.5 shows that varying parameter α_T within conditions typical for either Central Greenland or Siple Dome (Antarctica) can change DCF by up to 0.4 ‰. This, however, is an exaggerated effect because in this test we did not adjust the densification module accordingly, which balances the effect partly. In addition, the estimates for α_T used in the model runs should be quite realistic if the linear dependence on temperature and accumulation rate established by Spahni et al. (2003) is correct.

The scenario we consider most realistic uses environmental parameters that are typical for the transition period. The model shows that significant fractionation starts about 20 yrs after the onset of the termination. Calculated DCF are between 0.6 and 0.75 ‰ throughout the time of rising atmospheric concentrations. Once the latter level out fractionation rapidly declines and equilibrium is re-established within 50 yrs.

3.4.5. Sum of $\delta^{13}C_{CH4}$ corrections

Three different corrections have to be applied to the Pakitsoq samples. One correction factor is equal to the deviation of $\delta^{15}N$ from atmospheric values as measured by Petrenko et al. (in preparation). The only adjustment is an interpolation between data points, to match the value exactly to the position of the $\delta^{13}C_{CH4}$ sample. This correction factor accounts for the combined effect of gravitational and thermal fractionation. Both artificially enrich enclosed methane in ^{13}C, so that measured $\delta^{13}C_{CH4}$ data have to be corrected to lower values. For gravitational fractionation, the correction is around –0.4 ‰ throughout the record, after the onset of warming thermal fractionation requires additional adjustment of 0.1 to 0.15 ‰ (Fig. 3.4.6). Samples that record the YD termination and a short period afterwards also have to be corrected for diffusion fractionation. These values were calculated with a diffusion model, they account for the artificial depletion of methane with ^{13}C and adjust $\delta^{13}C_{CH4}$ to higher values. Maximum DCF are 0.75 ‰.

All correction factors were calculated specifically for every data point and are shown in Fig. 3.4.6. The diagram also displays correction factors for the atmospheric dilution effect for isotopes that is associated with changing concentrations (see Chapter 4.3). The sign of individual correction factors indicates if they lead to higher or lower $\delta^{13}C_{CH4}$ and a total correction factor results from the sum of all individual corrections. The difference between measured and corrected data is illustrated in Figure 3.4.7.

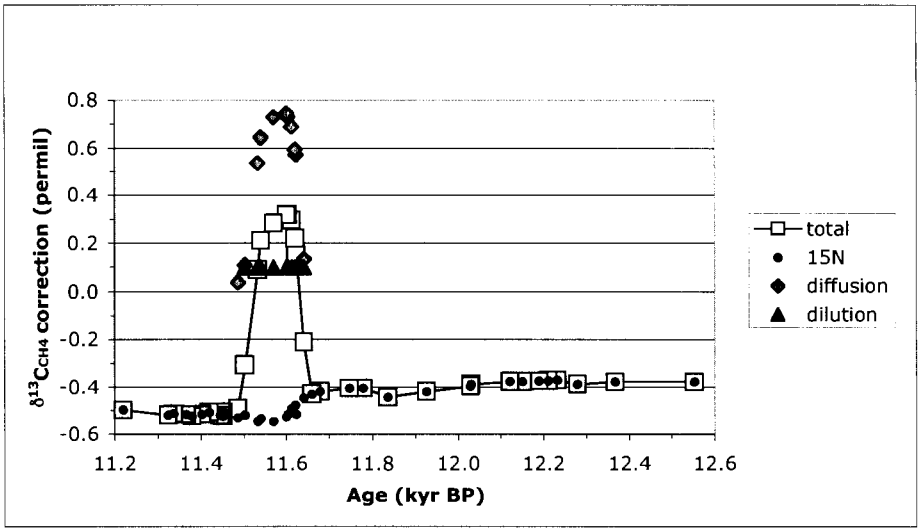

Fig. 3.4.6: Correction factors for $\delta^{13}C_{CH4}$ data
The sign of the factor indicates whether it raises or lowers $\delta^{13}C_{CH4}$. The diagram includes correction factors for $\delta^{15}N$ correction (includes gravitational and thermal fractionation), diffusion fractionation, and the effect of atmospheric dilution. Total correction factors are the sum of individual corrections.

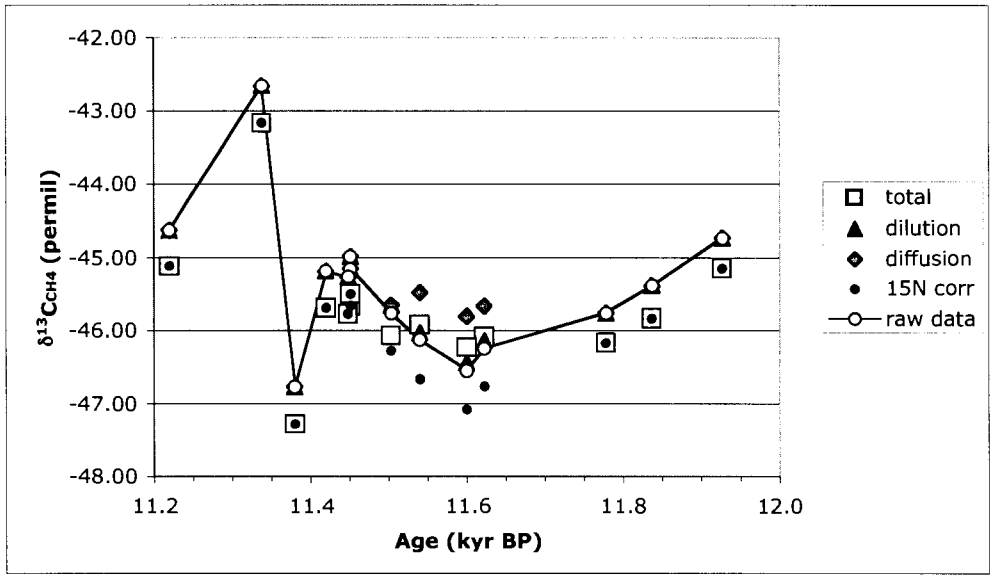

Fig. 3.4.7: Measured and corrected $\delta^{13}C_{CH4}$ values in the Pakitsoq record
For clarity only data from the 2001 and 2002 field campaigns during part of the record are shown (for all data see Tables 3.3 through 3.6). Outside the transition period dilution and diffusion correction are zero and total correction is equal to $\delta^{15}N$ correction. During the termination dilution correction must be applied and diffusion correction becomes predominant, so that total correction switches sign.

3.5. Atmospheric concentrations of methane

Methane concentrations were only corrected for average blanks of the respective measurement period (34 ppbV in 2001; 39 ppbV in 2002; 32 ppbV in 2003). Median values are reported for multiple measurements. Measured values are higher than the average global concentration due to latitudinal gradients (Dlugokencky et al., 1994), which is of no importance in this study. In the Late Holocene atmospheric concentrations are 690 ppbV for 230 yr old ice from GISP2 section 139 and 650 ppbV for 330 yr BP in Ag77/72 (Fig. 2.1.8). This is in fairly good agreement with results from the GISP2 core from Brook et al. (1996, 2000) data available at NSIDC), who found values between 695 and 750 ppbV during the same period.

Concentration data from Pakitsoq measured by GC-IRMS are shown in Fig. 3.5.1. Values from three different sampling campaigns show good agreement in this composite record. The YD is covered in this record from 12,550 to 11,650 yr BP. The median value of data from all data sets during this period is 509 ppbV with a standard deviation of 44 ppbV. The PB part of the record was calculated to span from 11,500 to 11,200 yr BP. During that time median methane concentration is 756 ppbV. Variability is somewhat higher than in the YD, which is reflected in a standard deviation of 60 ppbV. The transition period, when methane concentration rises to Preboreal levels, was determined to last 150 yrs in order to be consistent with findings of the GISP2 project (Brook et al., 2000). Compared to results from Greenland Summit ice cores (Blunier et al., 1995; Brook et al., 1996; Chappellaz et al., 1997; Dällenbach et al., 2000), which are 460-525 ppbV for YD and 718-730 ppbV for PB, the presented concentrations are marginally higher, although they agree within the uncertainty of our measurements. Possible reasons for elevated values include analytical problems and a genuinely different ice signal. As seen in Fig. 3.5.1, GC-IRMS concentration data for 2003 are slightly higher than field and laboratory GC data, pointing to a calibration problem. This would not be critical for the questions addressed in this study. Comparison with Figure 3.3.1 shows that samples measured with a different extraction procedure and GC are somewhat higher than GISP2 values as well, but the disagreement is not significant.

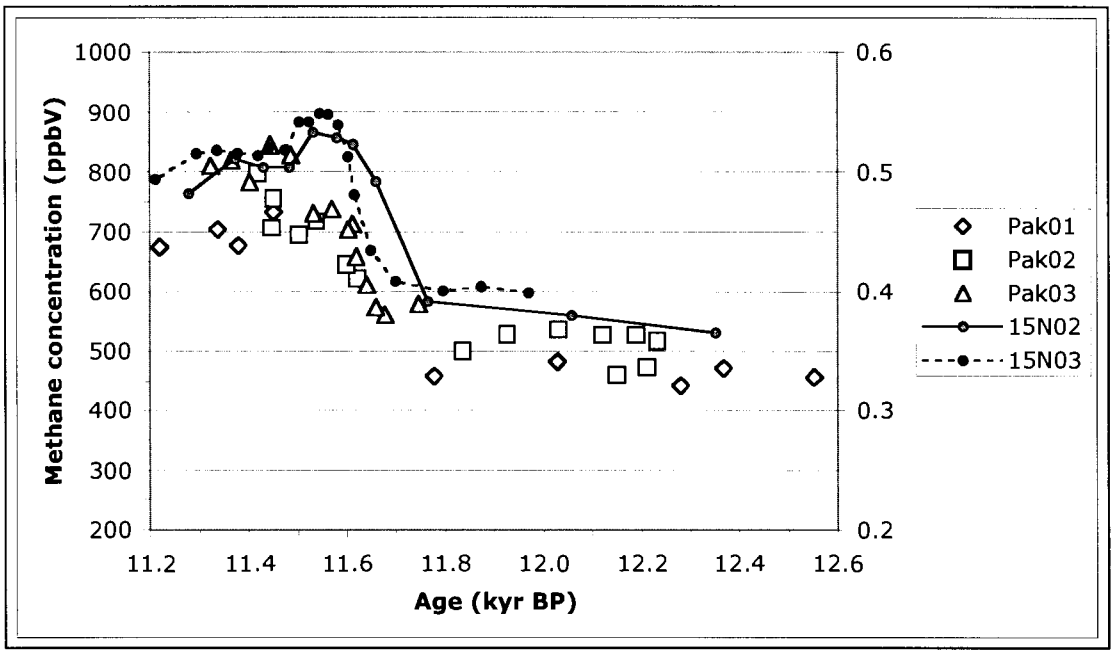

Fig. 3.5.1: Three methane concentration records from Pakitsoq
Methane concentration data from three sampling campaigns plotted on the Pakitsoq age scale. The increase in $\delta^{15}N$ measured at SIO (Petrenko et al., in preparation) indicates the exact onset of atmospheric warming.

Records of $\delta^{15}N$ measured by Petrenko et al. (in preparation) show the exact onset of atmospheric warming at the end of the YD (Fig. 3.5.1). This proxy was measured in the gas phase of collective samples and is immediately comparable with methane data. Slight disagreement between the two $\delta^{15}N$ curves points to a possible offset introduced by different age scales for data sets from 2002 and 2003, but this is a minor inaccuracy (<16 yrs). Comparison of the records for methane concentration and $\delta^{15}N$ as presented in Figure 3.5.1 suggests that concentration started to rise contemporaneously with, or shortly after local temperatures began to increase. This sequence was first discovered by Severinghaus et al. (1998).

In conclusion, GC-IRMS methane concentration data are in reasonable agreement with studies on ice cores. They follow the well known pattern of uniform concentrations during stable climatic periods in YD and PB and rapid concentration rise in between. The latter occurs simultaneously with, or slightly after, the rise of local temperatures. The

concentration data therefore provide an internal reference for changes in climate and methane budget within the measured record.

3.6. Atmospheric $\delta^{13}C$ of methane

$\delta^{13}C_{CH4}$ data for GISP2/139 and Ag77/72 are presented in Chapter 2, Fig. 2.1.8. The plot shows individual measurements, corrected for the effects of gravitational fractionation. The analytical error was estimated from analysis of artificial ice, which served as internal standard. Precision of these measurements was ± 0.26 ‰ for Agassiz and ± 0.44 ‰ (one standard deviation) for GISP2/139. It is interesting that the standard deviation on the GISP2/139 samples is lower than the analytical error (0.32 ‰) at comparable peak heights, suggesting that the internal standards may provide a conservative estimate for the error introduced by the analytical technique. Median values are –49.5 ‰ for GISP2/139 (for 230 yr old ice) and –49.8 ‰ for Ag77/72 (330 yrs BP). The agreement between these values is excellent, as it is with results from Craig et al., (1988b) who measured –49.9 ± 0.3 ‰ and –49.3 ± 0.2 ‰ in two sets of ice of similar age.

The three records collected between 2001 and 2003 in Pakitsoq (Pak01 – Pak03) show good agreement where they overlap (Fig. 3.6.1). No bias to higher or lower values in either sample set is obvious, although they display different degrees of internal consistency (i.e. scattering of data). If there are replicate measurements (n varied between 1 and 5, see Tables 3.3 through 3.6), then $\delta^{13}C_{CH4}$ for that age is reported as the median value. Throughout the record, values fluctuate around a mean of ca. –46.0 ‰, within a range of –45 to –47 ‰. Only three data points scatter outside this envelope and are considered anomalous. As a consequence of the agreement between the individual data sets we combine all measured values in a composite record (Fig. 3.6.2). Precision is specific for the different sampling dates and was determined from internal standard runs (artificial ice). The analytical error indicates changes in the performance of the extraction-GC-IRMS line with standard deviations of 0.44 ‰ (n = 11), 0.37 ‰ (n = 33), and 0.48 ‰ (n = 12) in 2001, 2002 and 2003, respectively. Poor precision in 2003 is

mainly a result of an analytical problem that randomly produced values depleted in ^{13}C- by about 1 ‰ in one out of five or six runs as seen in standard measurements. Multiple analyses were run for every point in the profile to account for this problem.

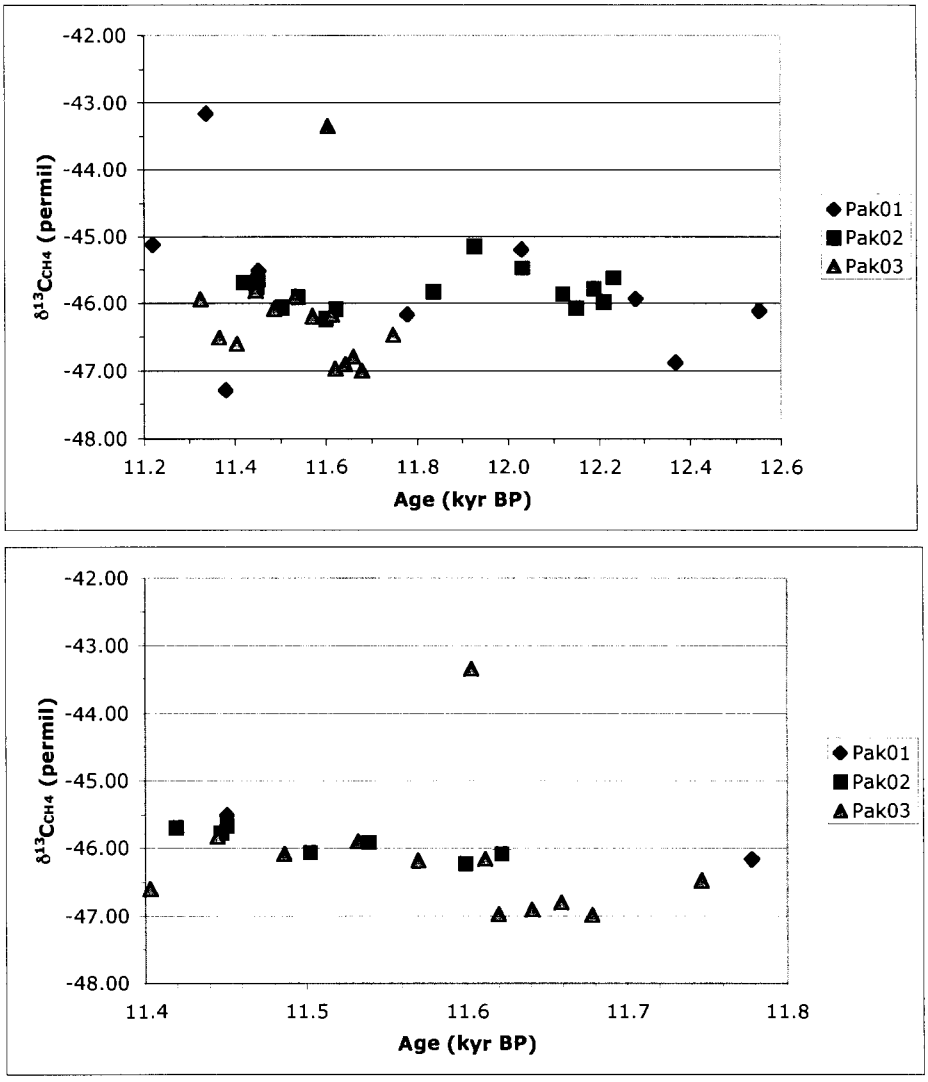

Fig. 3.6.1: Three $\delta^{13}C_{CH4}$ records from Pakitsoq
$\delta^{13}C_{CH4}$ data from three Pakitsoq sampling campaigns in 2001 - 2003. Top panel shows the complete record. General agreement between different sample sets is good. Beginning and end of the record (mainly sample set Pak01) show significant scatter. Values below –47 ‰ and above –45 ‰ seem to be anomalous. The period surrounding the YD termination is enlarged in the bottom panel. A conspicuous group of samples from Pak03 have the lowest values in this period. A single data point with higher $\delta^{13}C$ from Pak02 seems to be coeval, but this is within the uncertainty between the two age scales.

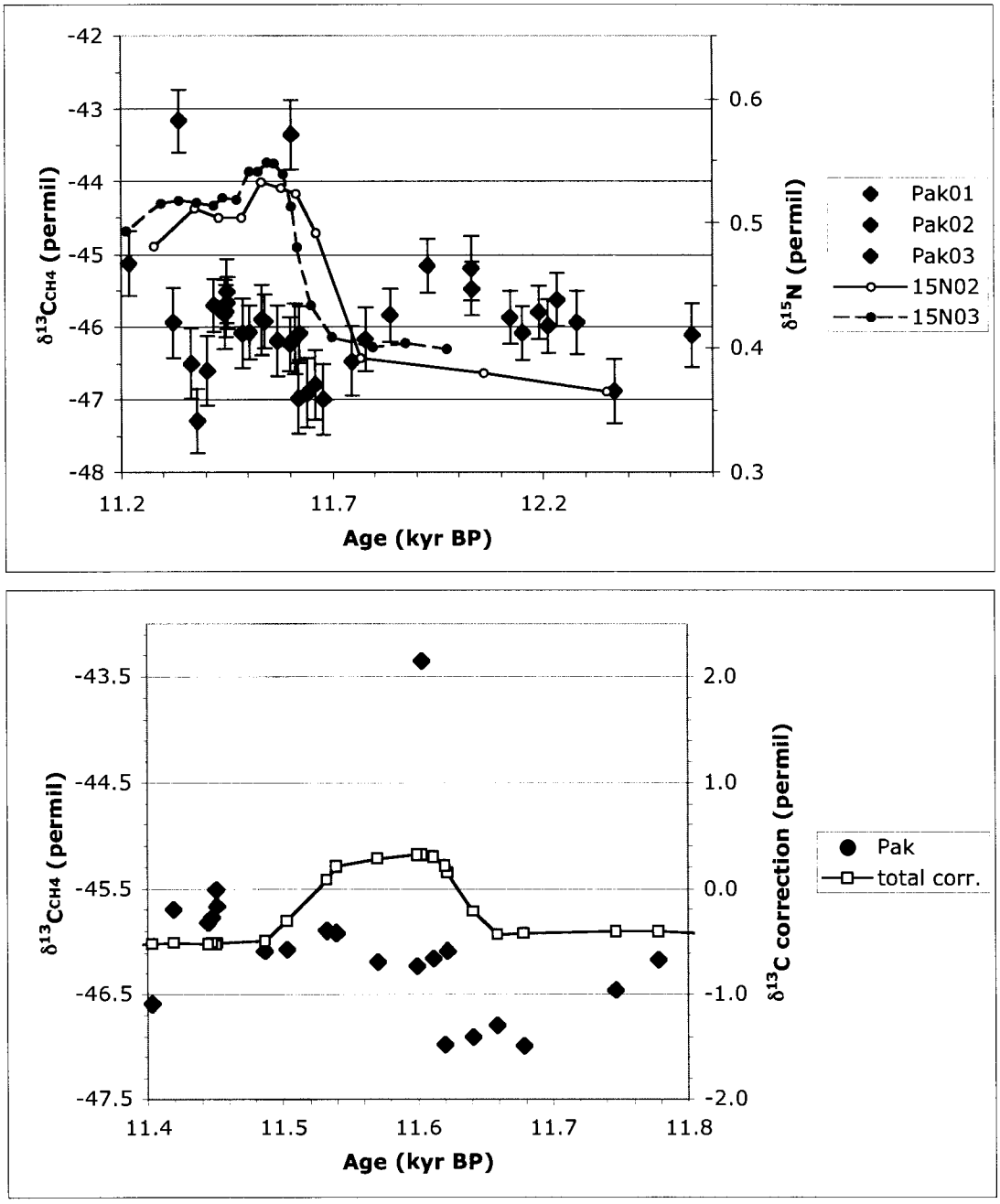

Fig. 3.6.2: Composite $\delta^{13}C_{CH4}$ record from Pakitsoq.
Error bars (± 1 standard deviation) are specific for the original sample sets. Top panel shows the complete record as well as $\delta^{15}N$ data (Petrenko et al., in preparation) from 2002 (open circles) and 2003 (grey circles) that indicate the onset of local warming. Bottom panel shows the YD termination in greater detail. Total correction factors (white boxes) are plotted to scale; they have positive values during the time of rising methane concentrations.

Fluctuations in $\delta^{13}C_{CH4}$ between 12.6 and 11.2 kyr BP stay within the uncertainty of the data. It seems that values around 12.0 kyr BP are slightly elevated, while lower numbers are centered around 11.65 kyr BP, which is right at the beginning of the temperature rise and immediately before methane concentrations start to increase. These small variations are not associated with different methane concentrations (see Fig. 3.6.1), which are all typical for the YD. The total of our $\delta^{13}C_{CH4}$ measurements in this period has a median value of –46.0 ‰ with a standard deviation of 0.55 ‰. Median of all PB samples is –45.8 ‰ with a standard deviation of 1.0 ‰. There is no difference in isotopic composition between the two climatic stages. During the transition period $\delta^{13}C_{CH4}$ also stays stable, except maybe for an insignificant offset compared to the last values in the YD. It is remarkable that the dynamics seen in the concentration data during this stage have no isotopic counterpart. This is also the time when additional corrections for $\delta^{13}C_{CH4}$ apply, as discussed earlier in this chapter (see Figs. 3.4.6 and 3.4.7). Poorly constrained correction factors could potentially introduce artificial trends to the record. In contrast, adjusted values are close to the median of the complete record (Fig. 3.6.2). It appears that fractionation processes during the transition do affect the measured record, but are appropriately corrected for. While it is true that theoretically the correction could mask a fluctuation in the data, it would be very coincidental that they would exactly cancel each other, so that the lack of a trend can be taken as support for the validity of the applied corrections.

The results of the analysis are that $\delta^{13}C$ of atmospheric methane was ^{13}C-depleted by around 2.5 ‰ in the Late Holocene compared to the modern value of –47.3 ‰ as quoted by Quay et al. (1999) and measured by GC-IRMS (see Fig. 2.1.6). The values for 230 and 330 yr BP of –49.5 and –49.8 ‰ agree well with previous measurements by Craig et al. (1988b). In contrast, at the very beginning of the Holocene, during the Preboreal period, $\delta^{13}C_{CH4}$ was higher than in today's atmosphere and had a value of –45.8 ‰. Despite a profoundly different climate and substantially lower atmospheric methane concentrations in the Younger Dryas, $\delta^{13}C_{CH4}$ in this period, with a value of –46.0 ‰, was virtually the same as in the PB. Even the reorganization of the methane budget between the two climatic stages was not associated with a change in $\delta^{13}C_{CH4}$.

4. Controls of isotopic composition of atmospheric methane

In order to interpret the results of $\delta^{13}C_{CH4}$ measurements in ice samples it is necessary to understand which processes determine this value. Atmospheric $\delta^{13}C_{CH4}$ depends mostly on the isotopic composition of methane inputs to the atmosphere (sources) and the fractionation that is associated with methane removal (sinks). Mixing and transport effects are of minor importance. This chapter investigates how these processes and source and sink factors could have varied between industrial and pristine conditions and through climatic stages. Parameters that are crucial for the interpretation of data from ice samples are calculated in these sections. The effects of changing atmospheric methane concentrations and the degree of geographical variability on $\delta^{13}C_{CH4}$ are studied with box models. Methane budgets based on literature data are calculated using isotope mass balance and presented for LGM and PIH, which serve as reference scenarios for the interpretation of our ice data.

4.1. Isotope effects during atmospheric methane oxidation

Methane is removed from the atmosphere through three major processes: oxidation with hydroxyl radicals (OH•) (as well as $O(^1D)$; Saueressig et al., 2001), soil uptake (Fung et al., 1991) and reaction with chlorine radicals, which is concentrated in the stratosphere and the marine boundary layer (McCarthy et al., 2001). All of these processes are associated with isotope effects and consequently a shift in the carbon isotope ratio of atmospheric methane. Knowing the magnitude of these isotope effects is crucial to identify changes in the methane budget because it determines the offset in isotope ratio between the measured atmospheric value and the sum of source components. This offset is hereafter referred to as $\Delta\,\delta$. It is calculated using the proportions of methane removed by each sink (F_R) and their fractionation α_R, which is the ratio of the reaction rates k_1 for $^{12}C_{CH4}$ and k_2 for $^{13}C_{CH4}$. Therefore is

$$\alpha_R = k_1 / k_2 \tag{4.1}$$

and the total sink fractionation $\propto$ is

$$\alpha = F_{R1} \times \alpha_{R1} + \ldots + F_{Rn} \times \alpha_{Rn} \tag{4.2}$$

^{12}C reacts faster and is therefore removed preferentially, leaving atmospheric methane enriched in ^{13}C.

The fractionation coefficient of the hydroxyl reaction α_{OH} has been measured as 1.0054 ± 0.0009 by Cantrell et al. (1990), which is in good agreement with *ab initio* quantum mechanical calculations by Lasaga and Gibbs (1991). Gupta et al. (1997) calculated a value of 1.010 for α_{OH}, which is close to earlier estimates but results in unrealistically high fractionation between source and atmospheric reservoir. Another study, which achieved higher precision, determined $\propto_{OH} = 1.0039 \pm 0.0004$ (Saueressig et al., 2001). This value gave a good fit with results from various other studies and was used consequently in all calculations.

The fractionation factor associated with methane oxidation through soils is experimentally determined in the range of 1.017 (Snover and Quay, 2000), 1.022 (King et al., 1989; Tyler et al., 1994) and 1.025 (Reeburgh et al., 1997). An accepted value for α of stratospheric removal by reaction with Cl is 1.066 (Saueressig et al., 1995, Crowley et al., 1999, Tyler et al., 2000), making this the largest fractionation associated with any sink process.

The fractions (F_R) of methane removed by each sink process are not well constrained. A widely accepted estimate is 0.87, 0.05 and 0.08 for $OH^{\bullet}$-oxidation, soil uptake and stratospheric sink, respectively (Hein et al., 1997; Quay et al., 1999). Using a Raleigh fractionation for steady state and the assumption that source input equals removal from the atmosphere, the fractionation associated with each sink can be calculated as

$$\Delta\delta = F \times (\alpha - 1) \times (1 + 0.001 \times \delta_{atm}) \times 1000 \qquad (4.3)$$

Estimates for $\Delta\,\delta$ derived with this approach range from –5.5 ‰ to –6.8 ‰ (Fung et al., 1991; Quay et al., 1999). Gupta et al. (1996) showed with a three dimensional model of atmospheric methane destruction that $\Delta\,\delta$ is in fact smaller than the value calculated with the above equation due to transport processes and latitudinal distribution of the sinks. The quoted values can be tested through independent estimates of the isotope numbers of atmosphere and source. This has been done through mass balance calculations and

inverse modeling by a number of workers (Quay et al, 1991, 1999; Fung et al., 1991; Whiticar, 1993; Hein et al., 1997). The estimates range from –5.5 to –7.2 ‰ with an average of –6.3 ‰. The latter value will be used for further calculations in this chapter. It includes the effects of all sinks and represents a global average of the fractionation. Lacking a three-dimensional model, Equation (4.3) is used for the following calculations, which determine $\Delta\ \delta$ under different environmental conditions. Because it overestimates $\Delta\ \delta$, all findings are scaled to the –6.3 ‰ value quoted above.

It is not known whether $\Delta\ \delta$ was the same during the Holocene and the ice ages as it is today. From Equation (4.3) follows that each sink will affect $\Delta\ \delta$ if either relative magnitude or fractionation coefficient was different in the past. The following sections investigate possible changes and how large the effect on $\Delta\ \delta$ would be, knowing that all estimates for the past rely on various assumptions, few of which are well constrained. A thorough treatment of the problem would require the use of a model that couples global circulation, atmospheric chemistry and soil interactions. The goal here is to get at least a qualitative estimate of possible changes, which have to be accounted for in the interpretation of $\delta^{13}C_{CH4}$ paleo-records.

4.1.1. Changes between Pre-Industrial Holocene and modern conditions

Anthropogenic activities have an impact on atmospheric chemistry, vegetation, and soil properties, which affects the sink processes of atmospheric methane. The following section studies changes that are due to human influence and occurred since the PIH despite equal climatic conditions.

4.1.1.1. Soil sink

Case studies show that land conversion, agriculture and forestry affect methane consumption of soils (Castro et al., 2000; DelGrosso et al., 2002; Steudler et al., 1996). On a global scale, land use change has decreased soil uptake by around 10 % (Ridgwell et al., 1999, and references therein) since the PIH. This estimate does not take into account the effect of lower atmospheric methane concentration in the PIH. Soil uptake of methane is regulated by diffusion (Striegl, 1993; Tyler et al. 1994). The diffusive flux changes linearly with the concentration gradient across the soil profile. Ojima et al.

(1993) used a methane concentration in soils of 400 ppbV to calculate the air-soil gradient, implying that methane consumption stops below this threshold. Other workers, however, reported depletion of methane to values below the detection limit. Following the second approach, diffusion increased proportionally to atmospheric concentration, i.e. in the PIH it was lower by 60 % (Etheridge et al., 1998). Agricultural changes and diffusion limit together would amount to a 56 % reduction of the PIH soil sink relative to today. This agrees reasonably with the results of Ojima et al. (1993), who calculated an increase from 8 Tg/yr in 1850 AD to 20 Tg/yr today in temperate ecosystems, a 40 % difference. The lower values do not directly translate into a reduction of F_{soil}, because total source and sink rates change as well. In fact, the diffusion effect is dependent on these parameters.

4.1.1.2. Chlorine sink

The concentration of chlorine radicals in the stratosphere increased five-fold in industrial times due to emissions of chlorocarbons as quoted in Gupta et al. (1996). This group modeled $\Delta\,\delta$ for natural levels of Cl-radicals with a 3-D chemical destruction model and found that it was smaller by up to 0.7 ‰, depending on the assumed fractionation coefficient. This is equivalent to a reduction of F_{Cl} by 70 %, according to Equations (4.2) and (4.3).

4.1.1.3. Hydroxyl sink

The loss rate of the OH• sink is calculated as

$$Loss = q \times [OH\bullet] \times [CH_4] \qquad (4.4)$$

where q is a temperature dependent reaction coefficient and [OH•] and [CH_4] represent the atmospheric concentrations of hydroxyl radicals and methane (Fung et al., 1991). Despite the fact that all three parameters were variable in the past, it is unlikely that they affected the relative contribution of the OH• sink. Instead, the atmospheric residence time of methane (τ) changed, which has no effect on $\Delta\,\delta$ under steady state conditions. The reason is that any change in the amount of ^{13}C-enriched atmospheric methane from sink fractionation is balanced by an equal change in source flux of ^{13}C-depleted gas (see also chapter 4.3.2). The current discussion explores how the OH• loss rate changed and

relates it to variations in the other sinks, but F_{OH} is set as the balance of the other removal processes and additional changes are attributed to variations in τ.

Even with atmospheric chemistry models it is difficult to determine OH• concentrations of the past. Some studies find OH• to be lower in the PIH by 6 to 15 % (Martinerie et al., 1995; Crutzen and Brühl, 1993), while others estimate it to be higher by 20 to 30 % (Thompson et al., 1993; Osborn and Wigley, 1994). Staffelbach et al. (1991) measured formaldehyde in ice cores as a proxy for methane oxidation. They concluded that OH• concentration in the PIH was higher than today by 30 %, although this may not have been a global trend (Martinerie et al., 1995). None of the model studies investigated the consequence of resulting changes on the other sink types. Although higher OH• may increase the hydroxyl sink at the expense of other processes, we assume here that it will just balance the lower removal rates in soil and stratosphere. Lower atmospheric methane concentrations decrease the loss rate due to the OH• reaction (see Equation (4.4)), but this should vary in close correlation with emissions and total sink rates and therefore not affect the fraction of methane removed by OH•.

According to the information above, the soil sink in the PIH was 8 Tg/yr (Ojima et al., 1993) of a total sink of 190 Tg/yr (Chappellaz et al., 1993b). The relative contribution of the Cl-sink was 70 % smaller than today (Gupta et al., 1996). If OH• balances these changes, then the fractions of the sink processes are 0.902, 0.042 and 0.056 for OH•, soil and Cl, respectively (Fig. 4.1.1). According to Equation (4.3), $\Delta\,\delta$ was -5.3 ‰ in the PIH (see Figs. 4.1.2 and 4.4.2).

4.1.2. Changes between Last Glacial Maximum and Pre-Industrial Holocene

The relevant differences between LGM and PIH include snow and ice cover, exposure of marine shelf areas, atmospheric chemistry, and climate. Bush and Philander (1999) concluded from a climate model that the LGM was cooler by 4.3°C on the global average. There are conflicting data to the value that applies to the terrestrial tropics, here the number by Bush and Philander (1999) is adopted, which is similar to the global average, whereas landmasses in higher latitudes experienced larger temperature differences, e.g. 10 – 13 °C in central Greenland (Grootes et al., 1993).

4.1.2.1. Soil sink

Tyler et al. (1994) experimentally determined a temperature dependence of α_{soil} of 0.00046/K, where higher temperatures lead to less fractionation. Accordingly, in the glacial environment α_{soil} could have been as high as 1.0259. This is an upper limit, because temperature differences will be dampened in soil layers where methane oxidation occurs. Even so, the new value will not lead to measurable changes due to the small contribution of the soil sink, as can be shown using Equation (4.3). The soil sink would be further decreased at lower temperatures, according to data from Yonemura and Yokozawa (2000) by 15 % for a temperature drop of 7°C, which may be a good approximation of the terrestrial temperature difference between LGM and PIH. Ice cover will decrease the available surface area for methane uptake, although this is partly compensated by exposed continental shelf area. Here it is estimated that ice free land surface was smaller by 2.5 to 7.5 % during the LGM (Gates, 1976; Thompson and Pollard, 1997; shelf area calculated from ETOPO-5 data, National Geophysical Data Center, 1988; Meissner, personal communication). In addition, atmospheric methane concentrations in the LGM are half of those in the PIH, with a proportional decrease in diffusive uptake. The effect of generally drier glacial conditions is hard to quantify, because both extremes in soil moisture will stop methane uptake (either through diffusion limitation in soils or shut down of microbial activity) although Yonemura and Yokozawa (2000) find a general decrease of methane uptake in drier conditions. We neglect this

influence together with changes of vegetation type. Accounting for the effects of land surface change and diffusion, the overall the soil sink may have been as small as 3.2 Tg/yr in the LGM compared to 8 Tg/yr in the PIH.

4.1.2.2. Chlorine sink

There are no available data concerning changes in atmospheric Cl concentration between LGM and PIH. Varying production of the precursor methyl chloride in ocean environments and biomass burning (Wayne, 1991), as well as higher ocean-atmosphere exchange due to different wind patterns could have affected the natural source of Cl. However, not enough information on these processes in the past exists and therefore no effects on F_{Cl} are considered. Tyler et al. (2000) report a temperature dependence of the fractionation coefficient, but the effect, less than 0.4 ‰ for a change of 4 °C, is negligible. For the Cl sink temperatures varied even less, as it occurs mostly in the stratosphere, where temperatures are more stable than in the lower troposphere. Therefore, a reduction in the reaction rate can also be neglected. It would affect only the Cl removal in the marine boundary layer, which amounts to only 12 % of the overall Cl sink (Allan et al., 2001; Prather et al., 2001). In conclusion, the magnitude of the Cl sink was fairly stable. Due to its remote occurrence it is unlikely to increase at the expense of the other sinks, even if those grew weaker. The relative contribution of Cl removal is therefore assumed to be stable between LGM and PIH.

4.1.2.3. Hydroxyl sink

Literature estimates of OH• concentration changes between LGM and PIH are contradictory. They range between +17 and –80 % (Martinerie et al., 1995; Crutzen and Bruehl, 1993; Thompson et al., 1993; Staffelbach et al., 1991) and we cannot estimate an associated change in the hydroxyl sink. The temperature difference had no significant influence on the isotopic fractionation (Cantrell et al., 1990; Lasaga and Gibbs, 1991). The reaction loss rate, however, decreased with temperature, resulting in a lowering of the OH• sink by 10 to 20 % (calculated after Fung et al., 1991; Gierczak et al., 1997; Vaghjiani and Ravishankara, 1991), so that τ was probably longer during the LGM.

In the LGM the total sink was 130 Tg/yr (Chappellaz et al., 1993b). It is assumed here that the soil sink was 2.7 Tg/yr, that the contribution of the Cl-sink remained unchanged and that OH• balanced the changes. The resulting fractions of OH•, soil and Cl sink in the LGM are 0.919, 0.024 and 0.056, respectively (Fig. 4.1.1). The corresponding $\Delta\,\delta$ is –5.1 ‰ (see Figs. 4.1.2 and 4.4.2).

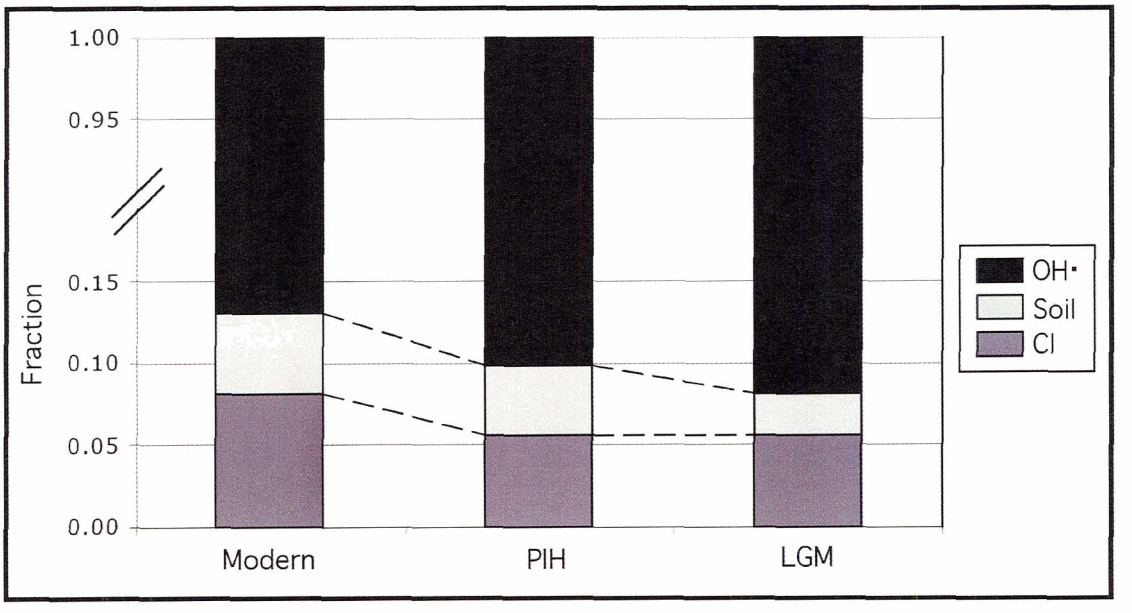

Fig. 4.1.1: Contribution of sink types in LGM, PIH and present
The fractions F_R of hydroxyl- (OH•), soil-, and chlorine (Cl) sink in modern times and how they changed in PIH and LGM, according to calculations based on various literature data. OH• sink balances the other two sources; note scale break.

4.1.3. Conclusions

The isotopic offset Δ δ between methane emissions and atmospheric value, which is caused by preferential removal of ^{12}C by sink processes, changed between modern conditions, PIH and LGM. Lack of anthropogenic emissions and land use, as well as natural variations in climate and atmospheric chemistry, result in a reduction of Δ δ (Figs. 4.1.1 and 4.1.2). Between PIH and today the difference could reach 1 ‰, which is detectable with the measurement techniques used in this study and should therefore be considered in budget calculations. The influence of natural variations on Δ δ is quite small with only 0.2 ‰ between LGM and PIH. This change is less than the analytical precision of ice core data and can be neglected. For mass balance calculations in the PIH Δ δ is established as –5.3 ‰ and for the LGM as –5.1 ‰. The results show that the interpretation of past $\delta^{13}C_{CH4}$ for the development of emission budgets (Craig et al., 1988b, Quay et al., 1988) must account for different environmental conditions. Given the uncertainty of the presented estimates, there is need for a more robust treatment of the problem, including the use of three-dimensional coupled models.

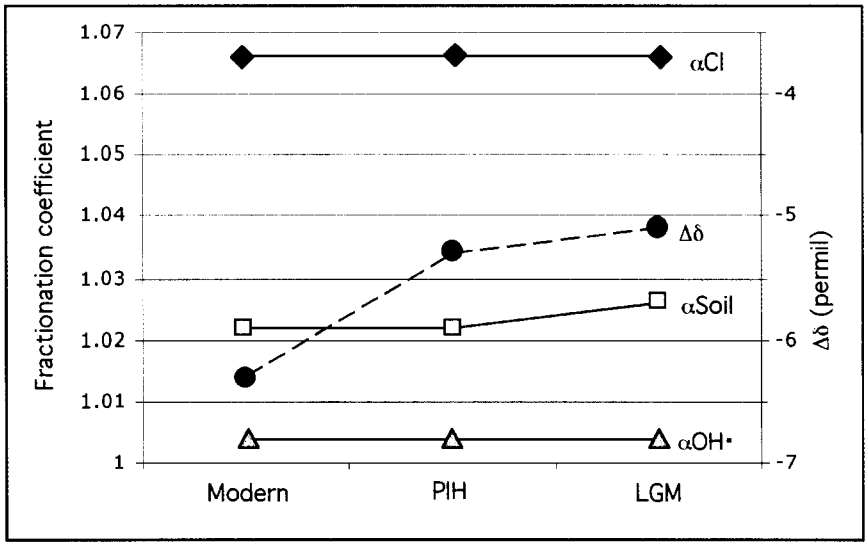

Fig. 4.1.2: Fractionation coefficients and Δδ in LGM, PIH and present
Fractionation coefficients (∝) of the hydroxyl- (OH•), soil-, and chlorine (Cl) methane sink in modern times and how they changed in PIH and LGM, according to calculations based on various literature data. Changes in Δδ result from the depicted differences and those in the relative contributions of the sink types.

4.2. Natural methane sources

Methane is produced during the remineralization of organic matter under anaerobic conditions. This process can be either thermocatalytic, i.e. induced by high pressure and temperature in deeply buried sediment layers, or biogenic, i.e. through microbial activity. Thermogenic methane is usually not considered part of natural emissions, except maybe for small fractions in the oceanic source and in gas hydrates. Thermogenic methane is quite enriched in ^{13}C, because the abiogenic formation discriminates less against the heavier isotope. Therefore the isotopic signature of thermogenic methane is very distinct (Schoell, 1980). Biogenic methane production occurs in shallow freshwater and marine sediments and in anaerobic microenvironments like termite mounds and the intestines of ruminants. $\delta^{13}C$ of the produced methane depends on several factors, most importantly the exact chemical process of the breakdown, e.g. acetate fermentation or CO_2-reduction (Whiticar et al., 1986). Another major influence is the isotopic composition of the precursor material, as well as the fraction of organic material consumed (Games and Hayes, 1976; Whiticar, 1996). If a significant portion of the produced methane is consumed during transport to the atmosphere, the emitted gas will be more ^{13}C-rich (Whiticar and Faber, 1986).

For any given source type these parameters will be somewhat variable, resulting in a typical range of $\delta^{13}C$ for this source rather than one fixed value. Nevertheless, their isotopic signature can distinguish different source types. An overview over methane sources and their isotopic compositions is given in Bréas et al. (2001). This study follows the source classification of Chappellaz et al. (1993b) and calculations are based on their emission rates. Some of the quoted values are controversial (e.g. ocean flux of only 10 Tg/yr, Table 4.2.4) but are adopted in order to be consistent with the vegetation reconstructions of the study. The following overview shortly introduces the source types.

Wetlands are the largest natural methane source. Methane is produced biogenically in anaerobic sediment layers, where acetate fermentation is the major

synthetic pathway (Whiticar et al., 1996). Isotopic composition of emitted methane also depends on transport processes (Popp et al., 1999). Areal extent of wetlands and methane production strongly depend on climatic conditions such as local temperatures and precipitation rates, which resulted in major fluctuations of wetland emissions since the last ice age (Chappellaz et al., 1993b; Kaplan, 2002). There are highly diverse types of wetland ecosystems in different latitudinal belts, which are distinct in their isotopic signature and may respond differently to climatic transitions (see below). Wetlands are most likely to have caused the methane increase during glacial terminations (Petit-Maire et al., 1991; Street-Perrot, 1993; Brook et al., 2000), which will be discussed in detail (Chapter 5).

Ruminants produce methane from symbiotic bacteria in their intestinal tract. Wild animals are a marginal source today (Crutzen et al., 1986, Lerner et al., 1988, Burchard, 1998), but were a significant contributor to the methane budget before large-scale agriculture and industrialization (Chappellaz et al., 1993b). The magnitude of this source depends on the availability of habitat and the character of vegetation, which are climate controlled.

Termite emissions comprise methane produced by endo-symbiotic microbes and from fungus combs in the mounds (Tyler et al., 1988). Estimates of source magnitude are not well constrained (Crutzen et al., 1986, Rasmussen and Khalil, 1983; Zimmermann et al., 1982). The concentration in the tropical belt means that the strongest climatic controls were changes in the monsoon cycle (Petit-Maire et al., 1991; Wang et al., 2001), and desertification must have limited production significantly.

Wildfires emit non-biogenic methane. The amount of gas produced in a burn and its isotopic composition depend largely on the combustion type, i.e. oxygen availability (Stevens and Engelkemair, 1988; Chanton et al. 2000). There is almost no isotopic offset between precursor material and the produced methane, making these emissions the most enriched in ^{13}C (Chanton et al., 2000) and a major factor in methane isotope budgets. Hao and Ward (1993) estimated global emission rates, but prescribed fires and anthropogenic

biomass burning severely changed the natural conditions. Higher fire frequencies when climate was warm and dry are documented in ice cores for the past 1000 yrs (Savarino and Legrand, 1998). Tropical charcoal records reaching back to the last ice age give a more complex picture (Haberle and Ledru, 2001), they show high fire frequencies during times of rapid climate transitions and high climatic variability.

Within the oceanic environment it is mostly shallow coastal seas with high productivity that emit methane (Lambert and Schmidt, 1993; Sansone et al., 1999). The main production pathway in sediments is CO_2-reduction (Whiticar et al., 1986), so that the isotopic composition is different from methane in freshwater environments. Despite high production rates only small amounts of gas reach the atmosphere, because the methane is consumed on its way through aerobic sediment layers and the water column. In the open ocean, methane production in surface waters also leads to slight supersaturation with small flux to the atmosphere (Holmes et al., 2000). All in all, oceans are regarded a minor source (Prather et al, 2001) although several studies show fairly high methane fluxes in specific areas (Hovland et al., 1993, Upstill-Goddard et al., 2000, Sansone et al., 2001). Marine sediments undergo little or no change under different climate conditions and so should their methane emissions. Biological productivity of the ocean was higher in glacial conditions (Sigman and Boyle, 2000), but in total these changes may be negligible for the global methane budget.

Gas hydrates, or clathrates, are a huge reservoir for methane in permafrost regions and marine sediments (Kvenvolden, 1999; Milkov et al, 2003). The gas is mostly of biogenic origin (Kvenvolden, 1993). Clathrates are stable only in a narrow range of environmental conditions governed by pressure and temperature (Xu and Ruppel, 1999). This is the basis for the "clathrate gun" theory, which states that gas hydrates caused large fluctuations in atmospheric methane concentrations and triggered climatic transitions (Kennett et al., 2003; Nisbet, 2002). This theory will be discussed in detail (Chapter 5). Under stable climatic conditions, however, hydrates are in equilibrium and only small amounts decompose. Most of the evading methane is then oxidized before it reaches the atmosphere (Grant and Whiticar, 2002; Kastner et al., 2003), so that gas

hydrates are usually a very small source. Chappellaz et al., (1993b) assumed that the low temperatures of the last ice age stabilized clathrate reservoirs and stopped any emissions.

Reservoirs of natural gas, which is produced thermogenically, are usually not listed as methane sources, at least not before human exploitation began. Yet, several studies show that in tectonically active areas natural gas can seep to the atmosphere (Kvenvolden et al., 1989; Mörner and Etiope, 2002, and references therein). Suggested emission rates are significant, particularly for pre-industrial budgets (Etiope and Milkov, 2004). Due to this potential and the distinct isotopic composition of such a source, we will consider geologic methane emissions in budget scenarios. The magnitude of this source depends on tectonic activity and should not be influenced by climate cycles, although the blocking of seeps through ice cover, as well as tectonic activity due to isostatic loading by ice sheets, may have a minor effect.

Generally, $\delta^{13}C$ of a methane source is determined by unchangeable physical and chemical parameters, such as reaction rates, or by biological characteristics of the ecosystem. Changing environmental conditions should therefore rather affect the geographical distribution of a source type and emission rates, but have very little impact on its isotopic signature. Certain factors, however, could have affected the $\delta^{13}C$ of natural sources under different climatic conditions. Changes in vegetation and temperatures could have had an influence on the $\delta^{13}C$ of the organic precursor material for methane formation and the fractionation associated with this process.

4.2.1. Temperature dependent isotope effects in methane formation

Almost all natural methane emissions are sourced from processes of methanogenesis. These are associated with isotope effects caused by different kinetic behaviour of the isotopes. Methanogenesis in freshwater environments results in a fractionation between precursor and methane of around 50 ‰ (Whiticar et al., 1986). The temperature dependence of the fractionation coefficient $\propto$ associated with CO_2-reduction,

one of two methanogenetic pathways, can be approximated as

$$100 \times \ln\alpha = 2.92 \times (1000/T) - 2.96 \qquad (4.5)$$

where T is absolute temperature.

I am not aware of a study on the temperature dependence of acetate fermentation, the other methanogenetic pathway. Because fractionation is lower for this process than for CO_2-reduction (Whiticar, 1996) one could speculate that the temperature dependence is also lower. The global average of the temperature difference (hereafter referred to as ΔT) between the LGM and the Holocene period is 4.3°C. Warming, however, was not uniform but dependent on latitude. Continental temperature changes ranged from 4 °C in the tropics to 26°C over the ice sheets (Bush and Philander, 1999). For the northernmost regions with methane production an assumed ΔT of 10°C seems a reasonable and maybe conservative estimate (note that even in central Greenland ΔT is at least 10-13 °C; Grootes et al., 1993). All these values are annual averages and ideally the temperature difference of methane producing seasons would be used in these considerations. Unfortunately, these are not available from paleo-reconstructions. Using the average values and Equation (4.5), methane would have been more depleted in ^{13}C by around 1.5 ‰ in the tropics and 4 ‰ in high latitudes during the last ice age. Fractionation as calculated with Equation (4.5) usually exceeds measured isotope effects (Whiticar et al., 1986), so that the calculated values constitute an upper limit.

The process affected only wetland production (maybe also termites, but to a lesser degree), i.e. 40 ‰ of the sources remained unchanged. Furthermore, wetland production in the LGM was concentrated to almost 70 % in the tropics and 30 % in temperate climates (Chappellaz et al., 1993b) where the temperature effect is less pronounced. A mass balance of all sources using the results from Equation (4.5) shows that the total source in the LGM could have been depleted in ^{13}C by up to 1.1 ‰. This value is very likely too high, because the atmospheric temperature change could have been dampened in the anaerobic environments where methanogenesis takes place. Nevertheless, the calculation indicates that there may be a small but measurable difference in the $\delta^{13}C$ of cold and warm periods.

There is no easy answer to the temperature difference between YD and PIH, as this climate event was not of global character (Broecker, 2003). Assuming that the difference was similar to that between LGM and PIH (Dansgaard et al., 1989) for a conservative estimate, then the isotope effect would be comparable. The calculated changes will not be included in mass balance calculations of atmospheric $\delta^{13}C_{CH4}$, but paleo-records should be examined for this effect (see Chapter 5).

An interesting question that was not addressed in this study is the interaction between methane production and consumption in systems like wetlands, where the produced methane has to migrate through an oxidizing environment before reaching the atmosphere. Should either of the two processes be more sensitive to temperature change, then the percentage of methane that is oxidized during transport would change and consequently the isotopic composition of the source. Assuming that higher soil or sediment layers undergo higher temperature fluctuations, then oxidation should be increased relatively to production in warmer periods, leading to higher depletion in ^{13}C. This is opposite to what is observed in the YD record (Chapter 5.2), but a robust treatment of this problem should investigate the temperature sensitivities (Q10 values) of the respective processes.

4.2.2. C_3 and C_4 plants

For the purpose of this discussion, plants can be classified as following one of two major photosynthetic pathways known as C_3 and C_4 type. In C_3 plants carbon dioxide transport is achieved by diffusion, which causes an isotope effect. In contrast, C_4 plants actively transport CO_2 into the cells. In addition, the C_4 photosynthetic reaction discriminates less against ^{13}C than C_3 photosynthesis. This results in a lower isotopic fractionation and C_4 plants with $\delta^{13}C$ of approximately –15 ‰ can be distinguished from C_3 plants with $\delta^{13}C$ around –27 ‰ (Ehleringer et al., 1997). Furthermore, the C_4 pathway is advantageous under certain climatic conditions. While it generally has a lower

quantum yield (or light use efficiency), i.e. less carbon is fixed per unit of light, it outcompetes the C_3 process in warm and dry conditions and under decreased CO_2 levels. Ehleringer et al. (1997) determined a critical temperature at which C_4 photosynthesis becomes more efficient than C_3. This temperature is dependent on ambient CO_2 levels. Collatz et al. (1998) used the approach to model the global distribution of C_3 and C_4 plants for the present, PIH and LGM. C_4 plants are only dominant in grasslands, which comprise around 25 % of the ice free land surface. Collatz et al. (1998) found an increase between the LGM and the PIH from approximately 70 % to 74 % of the grassland area dominated by C_4 plants. In modern times this percentage dropped to 57 %. We would therefore expect all sources that use C_3 and/or C_4 material as the methane precursor to be heavier in the PIH than in the LGM than today. To determine whether this affected the atmospheric isotope mass balance one has to take into account the percentage of grasslands in global vegetation, which also changed over time (Prentice et al., 1993), as well as climate dependent methane production rates in different ecosystems. The influence of vegetation changes between C_3 and C_4 plants on several natural methane sources is studied in more detail in the following sections.

4.2.2.1. Effect on emissions from ruminants

Various studies show that methane produced by ruminants is isotopically dependent on the diet of the animals. Table 4.2.1 presents data from five different studies by Rust (1981), Metges et al. (1990), Levin et al. (1993), Schulze et al. (1998) and Bilek et al. (2001) (data by Metges et al. (1990), in which $\delta^{13}C$ of methane was calculated from $\delta^{13}C$ data of CO_2, were omitted because these values are consistently higher than all other data). The isotopic composition of methane produced by cows is clearly dependent on the ratio of C_3 and C_4 in their diet. An average value for methane from cows feeding on C_3 plants is –68 ‰, whereas cows eating C_4 plants produced methane with –53 %. There seem to be significant interspecific differences in the isotope number of methane produced by cows, sheep, goats and camels (Levin et al., 1993; Schulze et al., 1998), but they are smaller than the intraspecific offset caused by different diets. In addition, the isotopic difference between feed and methane was the same for various diets in all the studies, independent of species. It is therefore assumed for further calculations that $\delta^{13}C$

of methane produced by wild animals is directly and exclusively dependent of that of the diet. Furthermore, $\delta^{13}C$ for pure C_3 and C_4 diets is assumed to be –68 ‰ and –53 ‰, respectively, i.e. the same as observed in cows.

Today the diet of domestic cattle consists of C_3 and C_4 plants at a ratio of 2.5 : 1 at a global level (Stevens and Engelkemeir, 1988), resulting in an expected isotope ratio of methane of –64 ‰. But for wild animals, one would expect the diet to reflect the natural abundance of the two plant types. While preferences of different animal species for plants of a specific metabolic pathway have been reported, there doesn't seem to be evidence for an overall favouring of either type (Ehleringer and Monson, 1993). Using the distribution of grassland types in the past from Collatz et al. (1998) and the isotope numbers quoted above allows to calculate the isotopic composition of methane emitted by wild animals as –59.5 ‰ today, -56.9 ‰ in the PIH and –57.5 ‰ at the LGM (see Appendix). The absolute numbers are not well constrained due to interspecific differences, the effect of the diet on the amount of methane production (Bilek et al, 2001) and the fact that forest living animals are not included. These uncertainties, however, would not affect the isotopic differences between different climatic stages. The difference for modern times between domestic ($\delta^{13}C$ = –64 ‰) and wild animals (-59.5 ‰) is significant. It is also interesting that under unchanged climatic conditions animal emissions in the PIH were 2.5 ‰ more ^{13}C-rich than today, which results from higher atmospheric CO_2 levels and changes in land use. In the LGM $\delta^{13}C$ of methane from animals was 0.6 ‰ more depleted in ^{13}C than in the PIH.

Table 4.2.1: $\delta^{13}C$ of methane produced by ruminants depending on diet

	Author	C_4 in diet	$\delta^{13}C$ diet	$\delta^{13}C$ methane	Offset between diet and methane
		(%)	(‰)	(‰)	(‰)
Cows	L	0	-27	-65.1	38.1
Cows	B	0	-28.9	-72	43.1
Cows	B	0	-28.9	-72.1	43.2
Cows	M	0	-27.1	-70.2	43.1
Cows	R	0	-27	-63.7	36.7
Cows	S	0	-27	-68.2	41.2
Cows	B	3	-27.6	-66	38.4
Cows	B	8	-25.6	-65.2	39.6
Cows	B	8	-25.6	-65.9	40.3
Cows	B	13	-23.6	-62.6	39
Cows	B	13	-23.7	-61.8	38.1
Cows	L	30	-22.8	-63.3	40.5
Cows	L	70	-17.2	-55.6	38.4
Cows	L	100	-13	-54	41
Cows	B	100	-13	-54.5	41.46
Cows	M	100	-12	-56.2	44.2
Cows	R	100	-13	-50.3	37.3
			Average C_3	-68.6	
			Average C_4	-53.7	
Sheep	R	0	-27.9	-68.6	40.7
Sheep	L	0	-27	-70.6	43.6
Sheep	S	0	-27	-74.4	47.4
Camels	S	0	-27	-73.5	46.5
Goats	L	0	-27	-65.2	38.2
				Average	40.9

Sources: R = Rust (1981), M = Metges et al. (199), L = Levin et al. (1993), S = Schulze et al. (1998), B = Bilek et al. (2001).

4.2.2.2. Effect on methane from wildfires

$\delta^{13}C$ of methane produced in biomass burning depends on that of the fuel as stated by Chanton et al. (2000). The study gives a $\delta^{13}C$ for methane from grass fires (C_4) between –17 and –26 ‰ and between –26 and –30 ‰ for forest fires (C_3), depending on combustion efficiency. The changing abundance of C_3 and C_4 plants must therefore affect the isotope number of wild fire methane. Although C_4 plants make up only 18 % of the global biomass by volume (Ehleringer et al., 1997) they are more abundant in tropical and subtropical regions where wild fires are most common. The percentage of C_3 and C_4 plants burnt in wild fires in different ecosystems annually for PIH and LGM was calculated using paleovegetation data from Prentice et al. (1993), natural fire frequencies for different ecosystems (Wright and Bailey, 1982; DeBano et al., 1998) and the distribution of C_3 and C_4 plants from Collatz et al. (1998). Different scenarios comprise the quoted range of both fire frequency and $\delta^{13}CH_4$ in different ecosystems (Table 4.2.2).

The scenarios that use average values result in an overall isotopic shift of methane from biomass burning by 0.1 ‰ between the two stages. Selected scenarios calculated methane to be up to 0.3 ‰ more ^{13}C-depleted in the PIH than during the LGM. Absolute $\delta^{13}C$ values ranged between –24 and –29.5 ‰, but are probably around –26.6 ‰. Using data from Hao and Ward (1993) today's $\delta^{13}C$ is calculated to be –24.6 ‰.

Table 4.2.2: Methane emissions from wild fires and its isotopic composition during LGM and PIH

	Biomass		1/Fire Frequency	Fraction Burned	CH_4/bio-mass	CH_4 emissions			
	LGM	PIH				LGM	LGM average	PIH	PIH average
	(Pg C)	(Pg C)			g/kg	(Tg/yr)	(Tg/yr)	(Tg/yr)	(Tg/yr)
Grassland									
Warm grass- and shrubland	10.27	13	0.1-0.5	0.81	1.5	1.2-6.2	2.1	1.6-7.9	2.6
Cool grass- and shrubland	7.2	5.7	0.04-0.5	0.81	1.5	0.3-4.4	0.6	0.3-3.5	0.5
Wooded tundra	4.2	5.2	0	0.81	1.5	0	0	0	0
Tundra	6.48	5.68	0	0.81	1.5	0	0	0	0
Tropical dry forest and savanna	84.64	79.12	0.1-0.33	0.81	1.5	10.3-33.9	17.1	9.6-31.7	16.0
Tropical forest									
Tropical rain forest	176	164	0	0.45	9.3	0	0	0	0
Tropical seasonal forest	105	102.2	0	0.45	9.3	0	0	0	0
Warm mixed forest	87	62	0.04-0.33	0.45	9.3	14.6-121.4	26.0	10.4-86.5	18.5
Temperate and boreal forest									
Temperate deciduous forest	35	58	0.1-0.14	0.45	6.1	9.6-13.7	11.3	15.9-22.7	18.7
Cool mixed forest	19	49	0-0.17	0.45	6.1	0.1-8.7	0.3	0.4-22.4	0.7
Cool conifer forest	10.08	50.4	0.03-0.33	0.45	6.1	0.9-9.2	1.6	4.3-46.1	7.9
Taiga	22.62	88.74	0	0.45	6.1	0	0	0	0
Northern taiga	6.5	11.5	0	0.45	6.1	0	0	0	0
Cold mixed forest	5	7	0	0.45	6.1	0	0	0	0
Cold deciduous forest	8.7	22.62	0.01	0.45	6.1	0.2	0.2	0.6	0.6
Northern cold deciduous forest	2.61	10.44	0-0.06	0.45	6.1	0-0.4	0.0	0.1-1.7	0.1
Xerophytic wood-, shrublands	55.35	46.33	0.02-0.05	0.65	6.1	5.0-11.0	6.9	4.2-9.2	5.8
				Global C_4		8.3-31.4	13.9	8.5-32.1	14.2
				Global C_3		34.0-178.1	52.3	38.8-200.6	57.3
				$\delta^{13}C$ CH_4 (‰)		-24.1 to -29.4	-26.6	-24.2 to -29.4	-26.7

Biomass estimates from Prentice et al. (1993); fire frequencies after Wright and Bailey (1982) and DeBano et al. (1998); fraction burned and CH_4 produced per burned biomass from Hao and Ward (1993)

4.2.2.3. Effect on wetland emissions

$\delta^{13}C$ of wetland methane is, amongst other factors, dependent on the isotopic signature of the decomposing material. Stevens and Engelkemeir (1988) suggested that measurements in tropical wetlands with C_4-type vegetation, i.e. mainly Africa, are underrepresented in global estimates and that $\delta^{13}C$ of wetlands, especially tropical swamps, might be heavier than widely assumed. Using a compilation of methane emissions from different wetland types in PIH and LGM by Chappellaz et al. (1993b), as well as the modeled C_3 and C_4 distribution in grasslands by Collatz et al. (1998), $\delta^{13}C$ values of the global wetland source were calculated. It is assumed that the produced methane is isotopically directly correlated to the precursor material. Therefore I used $\delta^{13}C = -62$ ‰ for methane derived from C_3 plants and –50 ‰ for methane from C_4 plants. In that case, wetland methane at the LGM was 2.8 ‰ and in the PIH 0.4 ‰ enriched in ^{13}C compared to modern values (see Table 4.2.3).

Table 4.2.3: Methane emissions from different wetlands and their isotopic signature in dependence of C_3 and C_4 vegetation. Emission estimates from Chappellaz et al. (1993b).

	LGM			**PIH**			**Present**		
	emissions in Tg/yr			emissions in Tg/yr			emissions in Tg/yr		
Temperate and boreal	**total**	**C_3**	**C_4**	**total**	**C_3**	**C_4**	**total**	**C_3**	**C_4**
boreal/conifer forest	1	1		17	17		15	15	
tundra	0	0		8	8		8	8	
temperate broad-leaved forest	5	5		20	20		9	9	
open conifer woodlands	2	1.3	0.7	6	3.78	2.22	6	4.38	1.62
total	**8**	**7**	**1**	**51**	**49**	**2**	**38**	**36**	**2**
$\delta^{13}C$ (‰)	**-61.3**			**-61.8**			**-61.8**		
Tropical									
tropical moist forest	16	16		33	33		27	27	
tropical scrub-/woodlands	14	9.1	4.9	27	17.01	9.99	25	18.25	6.75
grassland	33	9.9	23.1	21	5.46	15.54	21	9.66	11.34
semi-desert/steppe	2	0.6	1.4	2	0.52	1.48	2	0.92	1.08
desert	3	0.9	2.1	2	0.52	1.48	2	0.92	1.08
total	**68**	**37**	**32**	**85**	**57**	**28**	**77**	**57**	**20**
$\delta^{13}C$ (‰)	**-56.7**			**-58.3**			**-59.1**		
total	**76**	**44**	**32**	**136**	**105**	**31**	**115**	**93**	**22**
percentage		57.6	42.4		77.4	22.6		81.0	19.0
$\delta^{13}C$ (‰)	**-57.2**			**-59.6**			**-60.0**		

The strong glacial-interglacial difference is explained by the fact that the total contribution of C_4-derived methane in the PIH is only half of that in the LGM (despite the higher percentage of C_4 plants in PIH grasslands). For methane from temperate and boreal wetlands (C_3 dominated), $\delta^{13}C$ is –61.3 ‰ for the LGM and –61.8 ‰ for both PIH and present. For methane from tropical sources (mixed C_3 and C_4), the results are –56.7 ‰ for the LGM and around –58 ‰ and –59 ‰ for PIH and present, respectively. These calculated values lie in the range of isotopic compositions measured in modern wetlands (Bréas et al., 2001). Clearly, wetland ecosystems vary strongly in their isotopic signatures and climatic response.

4.2.2.4. Emissions from termites

Tyler et al. (1988) conducted detailed studies on the isotopic composition of methane produced by termites. They compared different species and various habitats and found no correlation between diet, including C_3 and C_4 plants, and $\delta^{13}C$ of the produced methane, not even within a single species. These results suggest that vegetation changes do not affect the isotopic composition of termite emissions and consequently the modern value should be used throughout.

4.2.2.5. All sources

Table 4.2.4 shows the calculated $\delta^{13}C$ for natural sources of the LGM, PIH and today. Differences are a consequence of assumed shifts in the precursor material due to changes in the dominance of C_3 or C_4 plants as discussed above. $\delta^{13}C$ of the total source is calculated as the mass balance of fluxes and isotopic composition of the single sources as described in Chapter 4.4.

Table 4.2.4: $\delta^{13}C$ of natural methane sources in LGM, PIH, and present

	LGM			PIH			Present		
	Flux (Tg/yr)	C4-derived CH_4 (%)	$\delta^{13}C$ (‰)	Flux (Tg/yr)	C4-derived CH_4 (%)	$\delta^{13}C$ (‰)	Flux (Tg/yr)	C4-derived CH_4 (%)	$\delta^{13}C$ (‰)
Bor. wetland	8	9	-61.3	51	4	-61.8	38	4	-61.8
Trop. wetland	68	46	-56.7	85	34	-58.3	77	26	-59.1
Wild animals	20	70	-57.5	15	74	-56.9	2 – 6	57	-59.5
Termites	20	18	-63.0	20	20	-63.0	20	31	-63.0
Wildfires	5	21	-26.6	5	20	-26.7	5	48	-24.6
Ocean	10		-58.2	10		-58.2	10		-58.2
Gas hydrates	0		-62.5	5		-62.5	5		-62.5
Total	130	39	-57.0	190	25	-58.9	160	21	-59.2

Flux estimates from Chappellaz et al. (1993b). Note that the percentage of today's C_4 methane is relative to natural sources only; when anthropogenic emissions are included the percentage is significantly lower.

The calculated data are a very rough estimate of the potential changes. Uncertainties in the underlying data sets and simplistic assumptions about isotopic compositions and the varying emissions are major restrictions of this approach. Ideally, calculations should be carried out with dynamic, climate driven vegetation models, which is beyond the scope of this study. Recent work by Kaplan et al. (2004) followed that approach and found a 2 ‰ depletion for the LGM methane source. The agreement with the results in Table 4.2.4 supports the calculations presented here. Another argument for the validity of this approach is that errors are likely consistent between LGM, PIH and present, so that the differences between the stages are better constrained. Despite possible

shortcomings of the above calculations, several interesting conclusions can be drawn from this work.

Between PIH and present, when C_3 versus C_4 distribution changed drastically (-17 %), $\delta^{13}C_E$ of total methane emissions stayed almost unchanged at –58.9 % and –59.2 ‰ (Fig. 4.2.1). Between LGM and PIH, however, when the abundance of C_4 plants increased only slightly (+ 4 %), $\delta^{13}C_E$ decreased by 1.9 ‰ to –57.0 % in the LGM. This is not only a significant change, it is also opposite in sign to what would be expected because the Holocene environment hosts more C_4 plants, which have larger $\delta^{13}C$. The trend is reflected in the contributions of C_4-derived methane to the total source: while Collatz et al. (1998) find an increase in abundance of C_4 plants of 4 %, the percentage of methane derived from them drops from 39 % to 25 % between LGM and PIH (Table 4.2.4). Obviously, the atmospheric $\delta^{13}C_{CH4}$ does not reflect the global abundance of C_3 and C_4 plants, but is controlled by emission rates in specific, climate sensitive ecosystems.

The following exercise tries to identify the sources with the biggest influence on the budget. The LGM mass balance was calculated using PIH values of $\delta^{13}C$ for different sources. If this was done for emissions from ruminants, termites or wildfires (Table 4.2.5) the effect was negligible (but opposite in sign to the wetland trend, as is discussed below). Because the emission rates and isotopic compositions of these source types stay fairly stable between LGM and PIH, this is expected. If $\delta^{13}C$ of wetlands (in particular tropical wetlands) was held constant, the difference in isotopic composition of the total source between LGM and PIH (1.9 ‰) decreased by half to 0.9 ‰. The remaining offset must be due to changes in emission rate of specific sources. These tests show that only boreal wetlands (including temperate ecosystems) significantly affect the LGM mass balance if their emissions are set to PIH values (Table 4.2.5). The difference of 1.1 ‰ is large enough to account for the remaining LGM-PIH offset in the basic scenario. In conclusion, half of the isotopic offset between LGM and PIH, i.e. 0.9 ‰, is caused by changes in the relative abundance of C_3 and C_4 plants with the biggest impact on tropical wetlands. The production of C_4-derived methane stays quite stable (Table 4.2.4).

Therefore it is the decrease in C_3 methane at the LGM that drives the change (Fig. 4.2.2). The other half of the offset (ca. 1 ‰) results from the shutdown of boreal wetlands in glacial conditions, so that ultimately changes in total emissions are controlled by variations in C_3-derived wetland methane (Fig. 4.2.2). This study suggests that wetlands with different vegetation types and in different latitudinal belts must be considered separately in isotope budgets in order to avoid significant errors. In addition, the isotopic composition of source types cannot be assumed as constant over climatic transitions.

Table 4.2.5: Influence of sources on the isotopic offset between LGM and PIH

	LGM $\delta^{13}C$ of total source	Difference to PIH
Base scenario	-57.3 ‰	-1.9 ‰
change $\delta^{13}C$ to PIH values		
only wetlands	-57.9	-0.90
only boreal wetlands	-57.0	-0.03
only tropical wetlands	-57.9	-0.86
all others	-56.9	0.09
change emission rates to PIH values		
only wetlands	-58.0	-0.98
only boreal wetlands	-58.1	-1.10
only tropical wetlands	-57.0	0.03
all others	-57.2	-0.24

The discussed effects result from the adjustment of vegetation to different climatic conditions. The time frame over which they are established depends on the rate of climatic change and a response time of the ecosystems, i.e. centuries to millennia in the case of deglaciations. No data sets were available to estimate the $\delta^{13}C$ shift between the YD and the PIH, but the results indicate that they may be significant. As mentioned above, the climatic conditions of the YD are not well constrained. If atmospheric methane concentrations are taken as a proxy for the dominant climate in methane producing regions, then conditions were roughly in between LGM and PIH. Therefore, it seems a reasonable estimate that the YD termination could have led to a $\delta^{13}C$ decrease of about 1 ‰. This change would be detectable in measurements of $\delta^{13}C_{CH4}$ and ice core records should be examined for it.

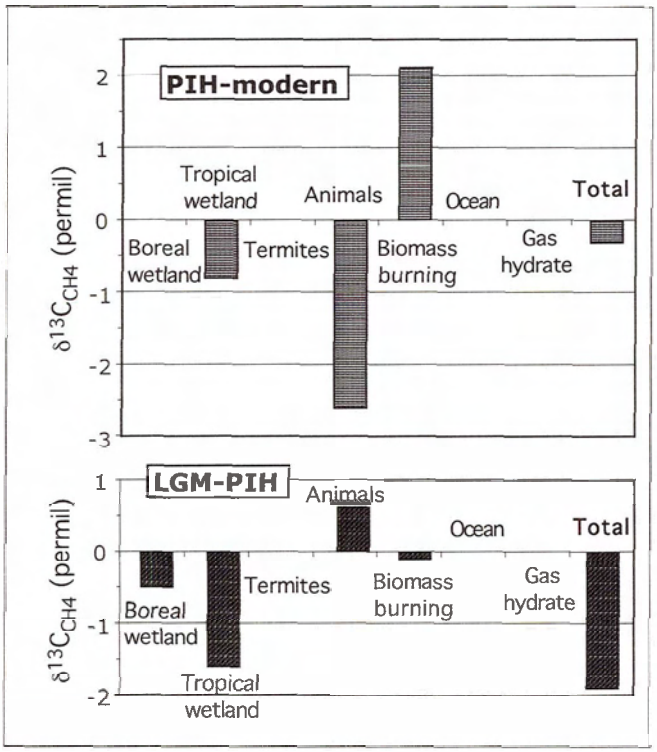

Fig. 4.2.1: Changes in $\delta^{13}C$ of methane sources between LGM, PIH and today
Values are calculated using emission rates from Chappellaz et al. (1993b) and other literature data (see text).

It is very difficult to estimate the uncertainty of the values presented in Table 4.2.4. The calculations are based on two studies (Chappellaz et al., 1993b and Collatz et al., 1998) that do not quantify the errors associated with their reconstructions. In addition, results from several other studies were used, which introduces more (and mostly undetermined) errors. As a consequence, the presented values carry a large degree of uncertainty. The following exercise is an attempt to quantify how relevant this uncertainty is for the overall results. Several values, i.e. those with the biggest potential to affect $\delta^{13}C_E$, are assumed to be false by ±25 % and ±50 %. The associated changes in $\delta^{13}C_E$ show the relevance of the assumed errors. For the two largest sources (boreal and tropical wetlands) and the one with the most extreme $\delta^{13}C$ (biomass burning) the emission rates were varied by ±25 % and ±50 % (Table 4.2.6). Variations by ±25 % affected $\delta^{13}C_E$ by less than analytical precision of ice core measurements in all cases and

are therefore negligible. Significant changes in $\delta^{13}C_E$ are produced by errors of ±50 % in biomass burning for the LGM and boreal wetlands and biomass burning in the PIH. Still, the offset in $\delta^{13}C_E$ is ±0.6 per mille at the most, which is far smaller than the calculated changes in $\delta^{13}C_E$ between the PIH and LGM (Table 4.2.4).

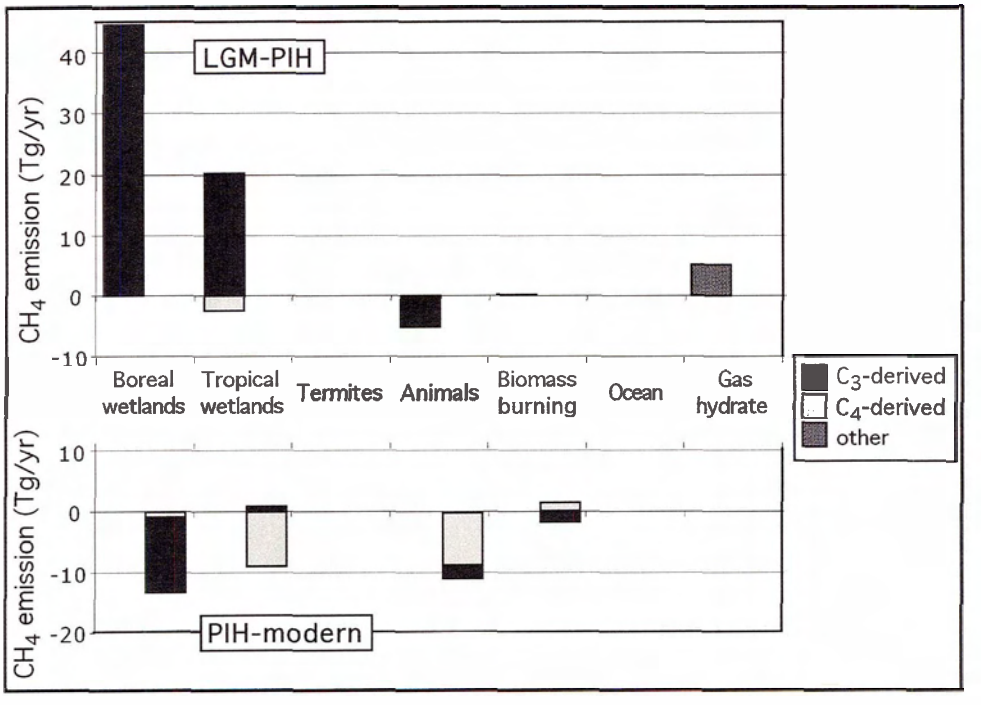

Fig. 4.2.2: Changes in emission rates of methane sources between LGM, PIH and today Emission rates are calculated after Chappellaz et al. (1993b) and other literature data (see text). The diagram illustrates the changes between LGM and PIH (top) and between PIH and modern conditions (bottom). Sources are distinguished between C_3- and C_4-derived, as well as other methane.

To estimate the errors introduced by the calculated isotopic composition of different source types it is assumed that $\delta^{13}C$ of modern natural sources is reasonably well known. Also, the calculated changes in integrated emissions come from deviations from the latter value, caused by changing C_3- and C_4 plant distribution. The largest impact on the budgets comes from tropical wetlands, boreal wetlands and biomass burning. Consequently, errors in the assumptions for these source types will lead to the

highest inaccuracy of the total budgets. In the following experiment, the calculated differences between modern, PIH, and LGM $\delta^{13}C$-values of each of these three sources were assumed to be inaccurate. Revising the respective values of each source first by ±25 % and then by ±50 % quantifies the effect of these errors on total budgets. The assumed errors were insignificant except for tropical wetlands in the LGM, which changed $\delta^{13}C_E$ by ±0.6 per mille. As stated above, a difference of this magnitude does not invalidate the general findings of this chapter. In conclusion, the presented data carry a large degree of uncertainty, but even for possible errors of ±50 % the main conclusions drawn from the calculations remain valid.

Table 4.2.6: Error estimates for source calculations
Calculated are changes in $\delta^{13}C_E$ if the emission rates of a major source types is changed by ±25 % and ±50 % and if the difference in $\delta^{13}C$ of these sources between modern and PIH or LGM values is decreased by ±25 % and ±50 %. For comparison resulting total emission rates of new scenarios and basic scenarios are given, as well as new values for $\delta^{13}C$ of changed sources and their original $\delta^{13}C$.

	Flux				$\delta^{13}C$			
			Total flux				$\delta^{13}C$ of source	
	Change in $\delta^{13}C_E$ (permil)		± 50 %	Basic scenario	Change in $\delta^{13}C_E$ (permil)		±50 %	Basic scenario
	±25 %	±50 %	(Tg/yr)	(Tg/yr)	±25 %	±50 %	(permil)	(permil)
LGM								
Boreal wetland	**±0.1**	**±0.1**	129-133	130	**0.0**	**0.0**	-61.2 to -61.4	-61.3
Tropical wetland	**0.0**	**±0.1**	114-148	130	**±0.3**	**±0.6**	-56.1 to -57.3	-56.7
Biomass burning	**±0.3**	**±0.6**	129-131	130	**0.0**	**0.0**	-26.1 to -27.1	-26.6
PIH								
Boreal wetland	**±0.2**	**±0.4**	166-217	190	**0.0**	**0.0**	-61.8	-61.8
Tropical wetland	**±0.1**	**±0.2**	149-234	190	**±0.1**	**±0.2**	-57.9 to -58.7	-58.3
Biomass burning	**±0.2**	**±0.4**	189-194	190	**0.0**	**0.0**	-25.7 to -27.8	-26.7

4.3. Effects of atmospheric mixing and transport on $\delta^{13}C$ of atmospheric methane

Changes in sink fractionation or in the isotopic composition of the global source are not the only influence on the isotope budget of atmospheric methane. Different processes associated with atmospheric mixing and transport must also be considered. This chapter presents a series of calculations with atmospheric box models that include source, sink, and transport terms between the boxes. All models are based on the two-box model by Tans (1997) and investigate how the following processes affect atmospheric $\delta^{13}C_{CH4}$:

- changing atmospheric residence time of methane (4.3.1)
- rising or falling atmospheric methane concentrations (4.3.2)
- interhemispheric transport and latitudinal gradients (4.3.3)

These three sections address the respective questions in a general way. In contrast, a specific scenario is presented in Section 4.3.4 to quantify isotope effects that may be observed in the ice record of this study. To this end, a three-box model, which comprises the tropics in analogy to Brook et al. (2000), combines previous results with literature data to create a scenario covering the end of the last ice age and investigates how atmospheric mixing and transport affect $\delta^{13}C_{CH4}$ as measured in ice samples.

4.3.1. Changing atmospheric residence time

Lower atmospheric methane concentrations are theoretically associated with higher levels of OH•. Consequently, atmospheric lifetime of methane was probably shorter by up to 30 % in the LGM compared to today (Thompson et al., 1993). This effect would not be evident in the ice core records if an increase in methane emissions balanced the faster removal rate. Atmospheric concentration would be the same but the atmospheric residence time τ would be shorter.

The following section investigates if changes in τ have an effect on the isotopic composition of atmospheric methane. To simplify matters, the atmospheric methane cycle is treated as a Rayleigh distillation with one source and one sink. If the atmospheric concentration of methane is constant over time, then input and removal rate must be the

same. Mook (1983) stated for this steady state scenario that on long time scales the isotopic offset between source and reservoir becomes independent of input and removal rate. $\delta^{13}C$ of atmospheric methane is then only dependent on the isotope number of the source and the fractionation coefficient of the sink.

A one-box model based on Tans (1997) with an input and a removal term illustrates this finding. Atmospheric methane concentration is the sum of initial concentration and emissions, as well as removal, per integration step:

$$[CH_4] = [CH_4]_0 + t \times (E - \lambda \times [CH_4]_0) \tag{4.6}$$

The isotopic composition of atmospheric methane is the sum of the corresponding isotope fluxes:

$$\begin{aligned} \delta^{13}C = (((\delta^{13}C_0 + 1000) \times [CH_4]_0 + t \times ((\delta^{13}C_E + 1000) \times E \\ -\alpha \times \lambda \times (\delta^{13}C_0 + 1000) \times [CH_4]_0)) / [CH_4]) - 1000 \end{aligned} \tag{4.7}$$

where 0 denotes initial conditions, t is time; E is emissions (in Tg/yr); λ is the removal rate (inverse of atmospheric lifetime); $\propto$ is the fractionation coefficient associated with atmospheric removal; $\delta^{13}C_E$ is the isotopic composition of total emissions. For all of the presented calculations in this chapter we used an arbitrary value of –55 ‰ for $\delta^{13}C_E$ (which matches the source composition calculated from the results of Craig et al.; 1988b) and $\propto$ = 1.0054 (Cantrell et al., 1990), the latter to be consistent with Tans (1997). The calculated value for the overall fractionation coefficient of atmospheric removal in PIH and LGM is slightly smaller (1.0053 and 1.0051, respectively, see Chapter 4.1), but the difference is negligible. The importance of this parameter is discussed in Chapter 5. Other values are listed in Table 4.3.1.

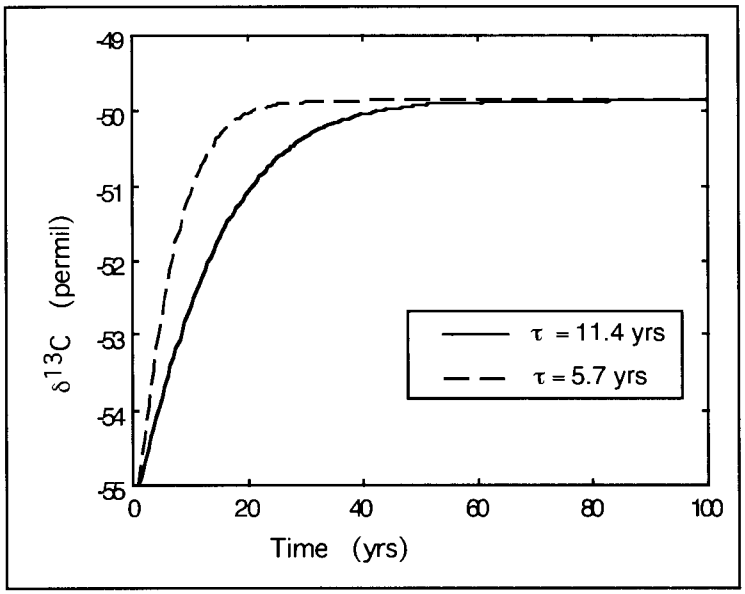

Fig. 4.3.1: $\delta^{13}C_{CH4}$ in dependence of atmospheric residence time
Comparison of $\delta^{13}C_{CH4}$ values for a basic scenario (τ = 11.4 yrs) and one with τ = 5.7 yrs. Model run (1-1) in a one-box model with source and sink terms. At the start of the run, the input atmospheric values are not in equilibrium with the source/sink configuration and adjust within 20 yrs (τ = 5.7 yrs) and 50 yrs (τ = 11.4 yrs), respectively. Both scenarios reach the same equilibrium value, proving that τ has no effect on $\delta^{13}C_{CH4}$.

The following comparison considers two scenarios where one budget has an atmospheric lifetime of 11.4 yrs. The other has both input and removal rates twice as large as the other and τ = 5.7 yrs (model run (1-1), Table 4.3.1). Both scenarios start with an input for atmospheric values that are not in equilibrium with the source/sink configuration of the model. The atmosphere reaches equilibrium within decades (Fig. 4.3.1), although this process is faster for shorter τ. Both scenarios, however, reach the same equilibrium value for $\delta^{13}C_{CH4}$. Once this equilibrium value is attained a change in τ does not affect the atmospheric isotope composition, not even for a limited time as demonstrated with model run (1-2) (Fig. 4.3.2). This model is allowed to run to equilibrium before both source and sink rates are doubled. There is no impact on $\delta^{13}C_{CH4}$. This simplified view does not remain valid once latitudinal gradients in source and/or sink strength and transport processes are taken into account, although the associated effects on atmospheric isotope numbers are minute, as shown in Section 4.3.3. An important conclusion from this finding is that isotope budgets are independent of absolute

emission and loss rates (as long as both are in equilibrium). The latter cannot be constrained through isotope budgets, but do not have to be accounted for either, which reduces the number of unknowns in the system.

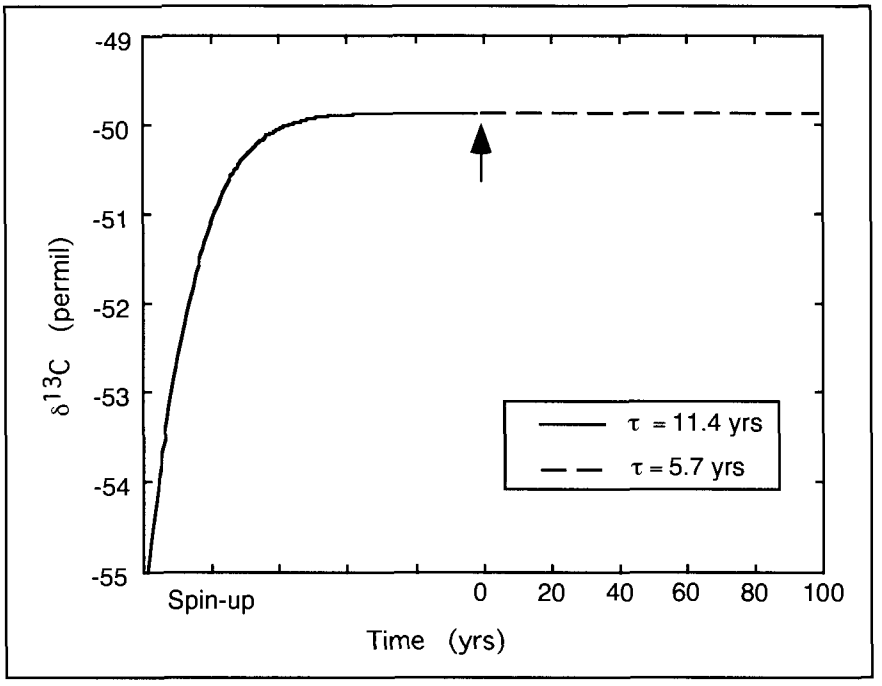

Fig. 4.3.2: Effect of changing residence times in a one-box model
Model runs to equilibrium with τ = 11.4 yrs (solid curve). The arrow indicates when τ is decreased to 5.7 yrs at 0 yrs (dashed line). There is no impact on $\delta^{13}C_{CH4}$.

4.3.2. Changing atmospheric methane concentrations

Rising atmospheric methane concentrations at the end of the last ice age must have affected the atmospheric isotope budget independently of a simultaneous shift in the isotopic composition of the source (Tans, 1997). The reason is that the atmospheric reservoir is enriched in ^{13}C compared to source methane due to the fractionation effect of the sink reactions. Higher input of ^{13}C-depleted methane from stronger sources will be diluted into this reservoir and decrease its $\delta^{13}C_{CH4}$ until a new equilibrium is reached (Fig. 4.3.3). Similarly, falling atmospheric concentration is associated with an increase in $\delta^{13}C_{CH4}$. Hereafter, this isotope effect is referred to as atmospheric dilution or dilution

effect. It is important to understand the nature and magnitude of this effect for the interpretation of isotope budgets, because it will simulate a change in source composition if it is not corrected for. The following calculations constrain the magnitude of the dilution effect. They use the two-box model by Tans (1997), which is equivalent to the one-box model presented in Section 4.3.1 but includes two hemispheric boxes and a transport term between them. The latter specifies which percentage of the interhemispheric difference in methane burden is exchanged. It is controlled by the concentration gradient.

Methane concentration in the North is:

$$[CH_4]_N = [CH_4]_{N_0} + t \times (E_N - \lambda_N \times [CH_4]_{N_0} - \kappa \times ([CH_4]_{N_0} - [CH_4]_{S_0})) \quad (4.8)$$

Methane concentration in the South is:

$$[CH_4]_S = [CH_4]_{S_0} + t \times (E_S - \lambda_S \times [CH_4]_{S_0} + \kappa \times ([CH_4]_{N_0} - [CH_4]_{S_0})) \quad (4.9)$$

Isotopic composition in the North is:

$$\begin{aligned} \delta^{13}C_N = & (((\delta^{13}C_{N_0} + 1000) \times [CH_4]_{N_0} + t \times ((\delta^{13}C_{N_E} + 1000) \times E_N \\ & -\alpha \times \lambda_N \times (\delta^{13}C_{N_0} + 1000) \times [CH_4]_{N_0} \\ & -\kappa \times ((\delta^{13}C_{N_0} + 1000) \times [CH_4]_{N_0} - (\delta^{13}C_{S_0} + 1000) \times [CH_4]_{S_0}))) \\ & /[CH_4]_N) - 1000 \end{aligned} \quad (4.10)$$

Isotopic composition in the South is:

$$\begin{aligned} \delta^{13}C_S = & (((\delta^{13}C_{S_0} + 1000) \times [CH_4]_{S_0} + t \times ((\delta^{13}C_{S_E} + 1000) \times E_S \\ & -\alpha \times \lambda_S \times (\delta^{13}C_{S_0} + 1000) \times [CH_4]_{S_0} \\ & +\kappa \times ((\delta^{13}C_{N_0} + 1000) \times [CH_4]_{N_0} - (\delta^{13}C_{S_0} + 1000) \times [CH_4]_{S_0}))) \\ & /[CH_4]_S) - 1000 \end{aligned} \quad (4.11)$$

where subscripts N and S denote northern and southern box, respectively and κ is the transport coefficient (inverse of mixing time between boxes). Other denominations are as in Equations (4.6) and (4.7).

A strongly simplified scenario investigates the general nature of the processes involved (model run (2-1)). The whole increase in methane emissions between the LGM and the Early Holocene from 110 Tg/yr to 190 Tg/yr (Chappellaz et al., 1993b) is taken

to have occurred in one continuous and uniform rise. It is assumed that the ratio of emissions from both hemispheres stayed the same (the effects of increase in only one box are investigated in Section 4.3.3). Most importantly, the isotopic composition of the source in both hemispheres was kept constant in order to study the isotope changes caused by varying emissions.

In the theoretical case that the new methane budget was established instantaneously, there would be a short-lived (less than 50 yrs) depletion of atmospheric $\delta^{13}C_{CH4}$ by more than 1 ‰. The duration of the excursion depends on the atmospheric lifetime of methane (τ) and may have been shorter in pre-industrial times than today (Thompson, 1992; Martinerie et al., 1995), which is included in the model. Fig. 4.3.4 shows that the effect on the atmospheric isotope ratio strongly depends on the duration of the emission increase. The slower the rate of the emission increase is, the longer the isotope effect persists, but also the less pronounced it is. The duration of the impact lasts for the time of increase and then returns to equilibrium values within a few decades. If the rise is complete within 50 years, the depletion of the atmosphere will be around 0.5 ‰; for 100 and 500 year periods it will be less than 0.3 and less than 0.1 ‰, respectively (model runs (2-0)(2-50), (2-100) and (2-500), Fig. 4.3.4). How fast the values return to equilibrium after the end of a concentration rise depends on τ, but possible changes of this parameter affect the overall picture by a negligible amount. A more realistic scenario is presented in Section 4.3.4, which also illustrates that concentration drops are associated with increases in $\delta^{13}C_{CH4}$.

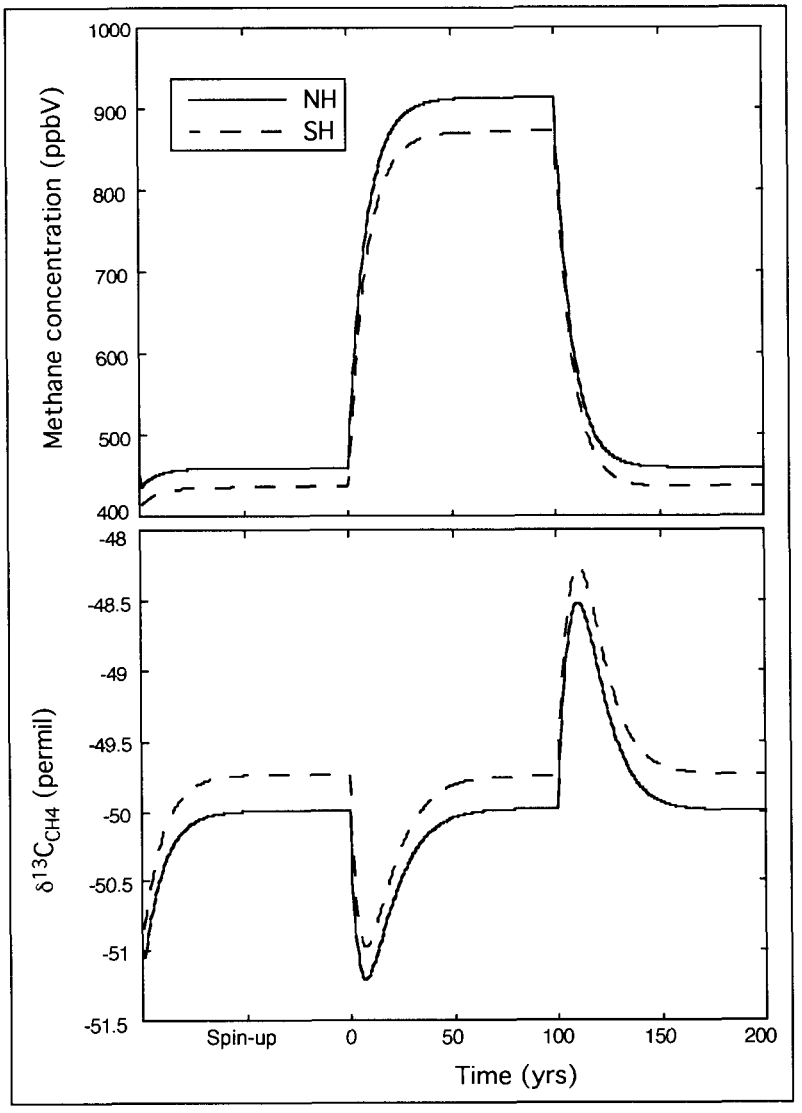

Fig. 4.3.3: Effect of atmospheric dilution on $\delta^{13}C_{CH4}$
2-box model run for an instantaneous increase in source strength from 80 to 140 Tg/yr (NH) and 30 to 50 Tg (SH) and an instantaneous decrease back to initial levels (model run (2-1)). The model first runs to equilibrium (Spin-up). The northern hemisphere has higher methane concentration and lower $\delta^{13}C_{CH4}$ because it includes most sources. The source increase is implemented at 0 yrs and lasts until 100 yrs. Top panel shows atmospheric concentration in northern (solid curve) and southern hemisphere (dashed). Bottom panel shows $\delta^{13}C_{CH4}$ for both hemispheres. The source increase causes a temporary drop in atmospheric $\delta^{13}C_{CH4}$, although the isotopic composition of the source was kept constant. The source decrease at 100 yrs evokes an equivalent response with opposing sign.

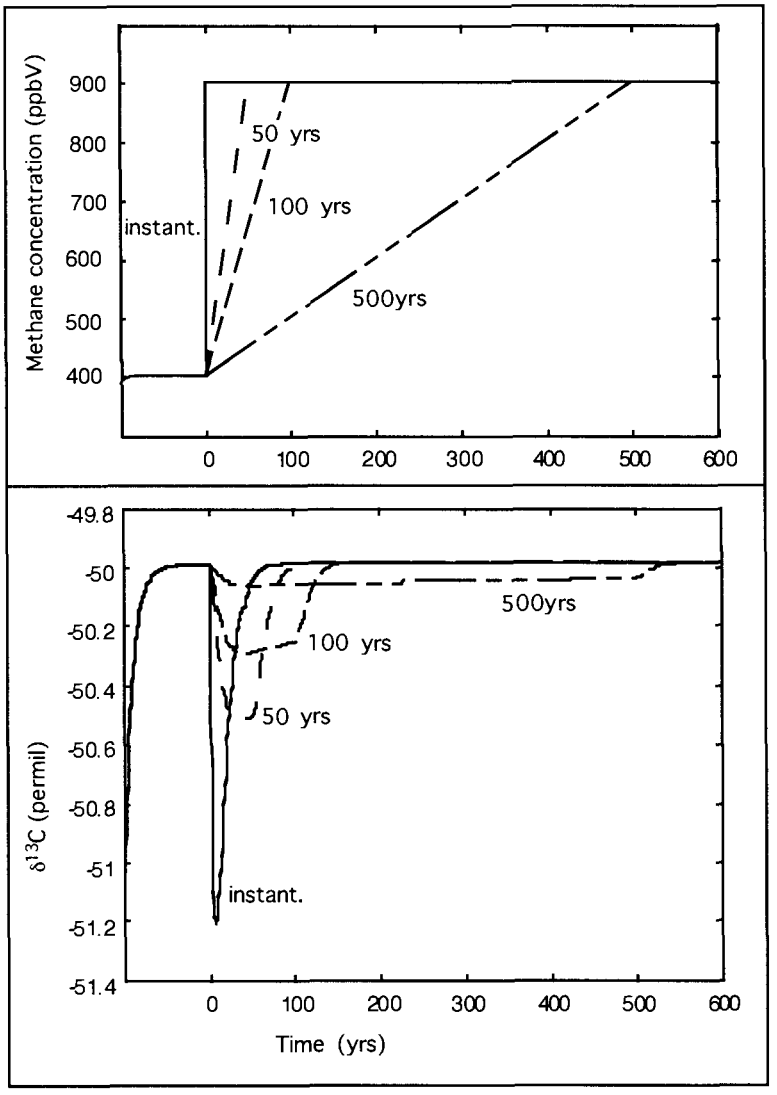

Fig. 4.3.4: Effect of rising methane emissions on atmospheric $\delta^{13}C_{CH4}$
Shown is an increase in source strength from 110 to 190 Tg/yr over the following periods: instantaneous, 50, 100, 500 yrs. Model runs reach equilibrium before the concentration increase starts at 0 yrs. Only NH is shown (2-box model runs (2-0), (2-50), (2-100) and (2-500)). Top panel presents curves for atmospheric concentrations, bottom panel the associated effect on $\delta^{13}C_{CH4}$.

A special case of methane concentration increase is a massive burst, e.g. from dissociating gas hydrate as hypothesized in the clathrate gun theory (see Chapters 1 and 5.3.2). Figure 4.3.5 shows the atmospheric dilution effect for a 4000 Tg (to match Thorpe et al., 1996) burst of methane emitted over 4 yrs (model run (2-B)). The massive increase in methane concentration causes a severe drop in atmospheric $\delta^{13}C_{CH4}$ by almost 3 ‰.

Soon this drop is superimposed by rising $\delta^{13}C_{CH4}$ caused by rapidly decreasing atmospheric concentrations, which eventually results in a 1.5 ‰ total increase in $\delta^{13}C_{CH4}$. The whole perturbation does not last very much longer than typical gas age distributions in ice samples (see Chapter 3.3.3) and would likely be hard to detect in the ice core record. Note that the model does not take into account that the methane burst would strongly affect the methane sink (resulting in a longer duration of the perturbation). In addition, such a strong input from a single source type would certainly change the isotopic composition of the integrated source, which was held constant in the model. Such a shift in $\delta^{13}C_E$ would strongly modulate the observed atmospheric response. The magnitude of the perturbation is limited by the difference between atmospheric $\delta^{13}C_{CH4}$ and $\delta^{13}C_E$.

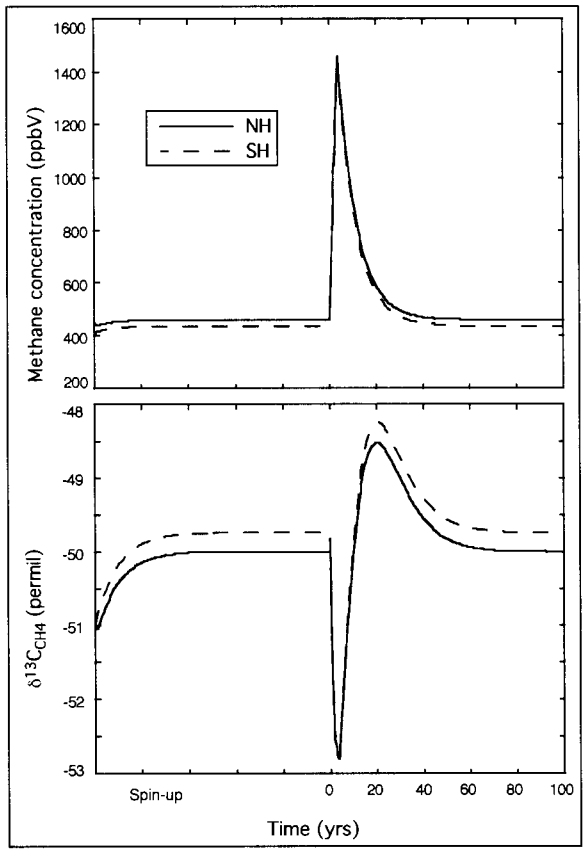

Fig. 4.3.5: Reaction of atmospheric $\delta^{13}C_{CH4}$ to a methane burst
A sudden burst of methane (4000 Tg over 4 yrs) causes a strong (more than ± 2 ‰) but short-lived oscillation in atmospheric $\delta^{13}C_{CH4}$.

Table 4.3.1: Input parameters for model runs

Scenario													
1-box model	E1			E2			k	λ1	λ2		increase at		
1-1	110			220			1	0.123	0.246				
1-2	110			220			1	0.123	0.246		0 yrs		
2-box model	En1		Es1	En2		Es2	k	λ1	λ2	t(rise)	increase		decrease
2-1	80		30	140		50	1	0.123	0.246	0	0 yrs		100 yrs
2-0	80		30	140		50	1	0.123	0.246	0			
2-50	80		30	140		50	1	0.123	0.246	50			
2-100	80		30	140		50	1	0.123	0.246	100			
2-500	80		30	140		50	1	0.123	0.246	500			
2-B	80		30	580		530	1	0.123	0.246	4	0 yrs		4 yrs
3-box model	En1	Et1	Es1	En2	Et2	Es2	k	λ(N)1	λ(N)2	λ(T)1	λ(T)2	λ(S)1	λ(S)2
3-1	65	79	15	97.5	118.5	22.5	1.33	0.064	0.096	0.147	0.221	0.045	0.067
3-N	65	79	15	97.5	79	15	1.33	0.064	0.096	0.147	0.221	0.096	0.147
3-T	65	79	15	65	118.5	15	1.33	0.064	0.096	0.147	0.064	0.045	0.147
3-S	65	79	15	65	79	22.5	1.33	0.064	0.096	0.147	0.064	0.096	0.067
3-Term	En	Et	Es	λ(N)	λ(T)	λ(S)	k				rise (yr)		
LGM	34	65	12	0.064	0.147	0.045	1.33				125		
B-A	43	127	15								310		
YD	39	86	15								175		
PB	64	123	15										
all scenarios :													
α =	0.9946												
$\delta^{13}C_E$ =	-55 ‰												

4.3.3. Transport effects and latitudinal gradients

Both methane emissions and removal from the atmosphere are dependent on latitude (Fung et al., 1991, Dlugokensky et al., 1994). If emissions and sink rate in any latitudinal zone changed, so would the concentration gradient and transport between zones. Brook et al. (2000) used a 3-box model to quantify emission rates in northern and southern latitudes and the tropics. They show that atmospheric concentrations and

gradients between the boxes are not sensitive to the atmospheric lifetime chosen for each box. Here an isotope component is added to their model in order to study possible changes in $\delta^{13}C$ under steady state conditions. In this model, as adapted from Brook et al. (2000), the northern and southern box span 90° to 30° and the tropical box spans 30° N to 30° S. The tropical box has twice the volume of the other boxes. Equations to calculate atmospheric concentration and isotopic composition of methane in each box are equivalent to those presented in Section 4.3.2 except that the tropics exchange methane with both the North and the South. The exact equations are given in the Appendix.

Fig 4.3.5 shows how the isotopic composition in the latitudinal zones changes if τ is decreased by 33 % in all boxes (model run (3-1), Fig. 4.3.6; Table 4.3.1). This scenario assumes that the higher OH• levels of the pre-industrial era (Thompson et al., 1993) had a proportionally lower τ, which is a very conservative estimate. The values in the tropics and the South change only imperceptibly between the two scenarios. The biggest shift occurs in the North. Even this change would be only 0.07 ‰ and not detectable in ice cores. Similar tests were run where source and sink rates where increased in any one of the three boxes (model runs (3-N), (3-T) and (3-S), to test sensitivity of the system to changes in the proportional rates. The differences to the base scenario are less than in run (3-1). In all scenarios the differences for the tropical and southern zone are almost not detectable and in the North they are significantly less than analytical precision of ice measurements.

Quay et al. (1999) reported latitudinal gradients in $\delta^{13}C_{CH4}$, which result from the concentration of terrestrial methane sources in the Northern Hemisphere (Fung et al., 1991) and from latitudinal differences in atmospheric removal (Gupta et al., 1996). Accordingly, the isotopic composition of methane measured in Arctic ice is more depleted in ^{13}C than the global average. The magnitude of the modern latitudinal gradient (i.e. 0.5 ‰, Quay et al., 1999) is less than the precision of our measurements and too small to be considered in isotope budgets. Under glacial conditions the difference between measured and global signal was rather smaller, because high latitude methane production decreased and the sampling locations were more remote from sources.

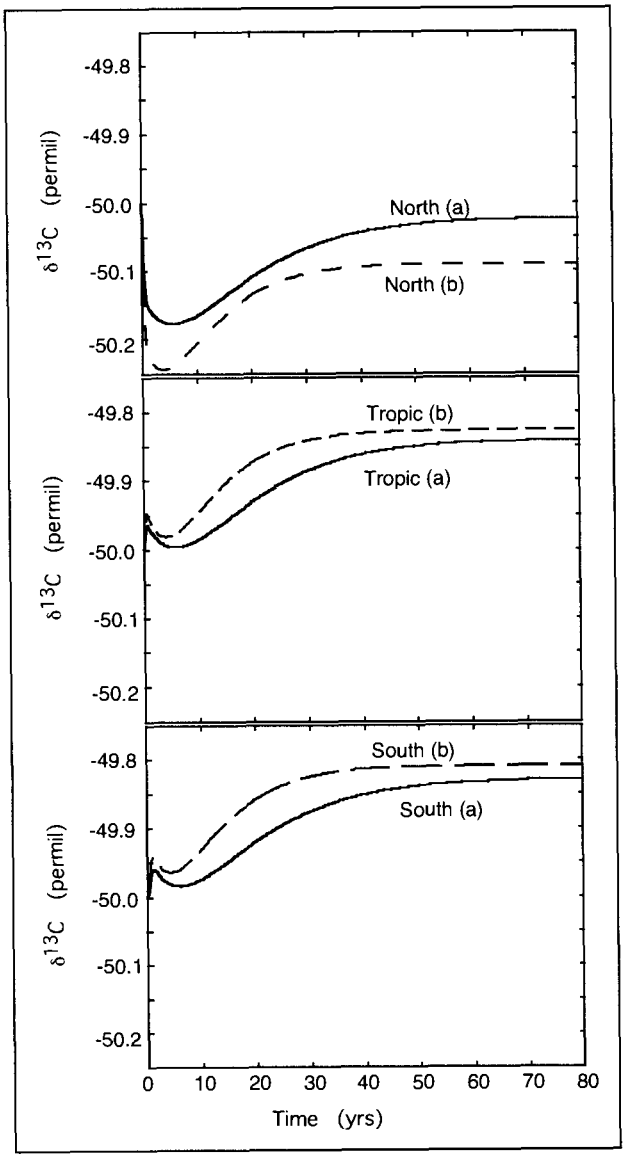

Fig. 4.3.6: Effect of decreasing residence time in a three-box model
Three-box model run to simulate the effect of decreasing τ by 33 % on $\delta^{13}C_{CH4}$ (run (3-1)). Top, center and bottom panels show North, tropics, and South, respectively. Solid curves (a) are the basic scenario. Source and sink rates in all boxes were then increased by 50 % so that τ decreases: dashed curves (b). All curves take ca. 60 yrs to reach equilibrium. With shorter τ equilibrium is achieved faster and equilibrium $\delta^{13}C_{CH4}$ values differ (by a negligible amount) between the two scenarios, which is a result of transport between boxes.

4.3.4. Scenario for the end of the last ice age

The 3-box model can be used to investigate the possible changes of $\delta^{13}C_{CH4}$ at the end of the last ice age. Atmospheric methane concentrations and $\delta^{13}C_{CH4}$ were modeled since the LGM, including the transitions to the Bølling-Allerød (B/A), the YD and into the Preboreal (PB) (model run (3-term)). Data for emission strength and the rates of concentration change during the transitions are taken from Brook et al. (2000). The scenario also adopts their values for mixing times and atmospheric residence times (Table 4.3.1). $\delta^{13}C$ of all sources is kept constant at –55 ‰ in order to study the effect of concentration changes on atmospheric $\delta^{13}C_{CH4}$. The time scale of the model run is not realistic as each of the climatic stages is et to last for 1000 yrs. The duration of the transitions, however, is truthful to the results of Brook et al. (2000) in order to accurately calculate the isotopic excursions.

The modeled atmospheric concentrations match those reported in Brook et al. (2000) (see Fig. 4.3.7). From 360 - 370 ppbV during the LGM they rise to around 640 ppbV in the B/A. In the YD they drop to just below 500 ppbV and rise to around 700 ppbV in the PB. They are highest in the North and lowest in the South, interhemispheric concentration gradients are set to match the findings of Brook et al. (2000). The carbon isotope ratios of methane indicate a latitudinal gradient with the lowest $\delta^{13}C_{CH4}$ values in the North and the highest values in the South (Fig. 4.3.7). This can be explained by high emissions in the North and tropics, enhanced removal and fractionation of methane in the tropics and the fact that the South has the highest percentage of transported methane, which has already been subjected to fractionation in the other boxes. This gradient, however, is 0.15 ‰ at the most. Tropics and southern zone differ more during warm stages than during the cold LGM and YD. Neither of the latitudinal zones shows $\delta^{13}C_{CH4}$ differences by more than 0.05 ‰ between the various climatic stages. The most significant excursions occur during the transition periods when concentrations rise or fall within 100 to 300 years. During the periods of warming and methane rise at the end of the LGM and the YD, $\delta^{13}C_{CH4}$ drops by 0.2 and 0.1 ‰,

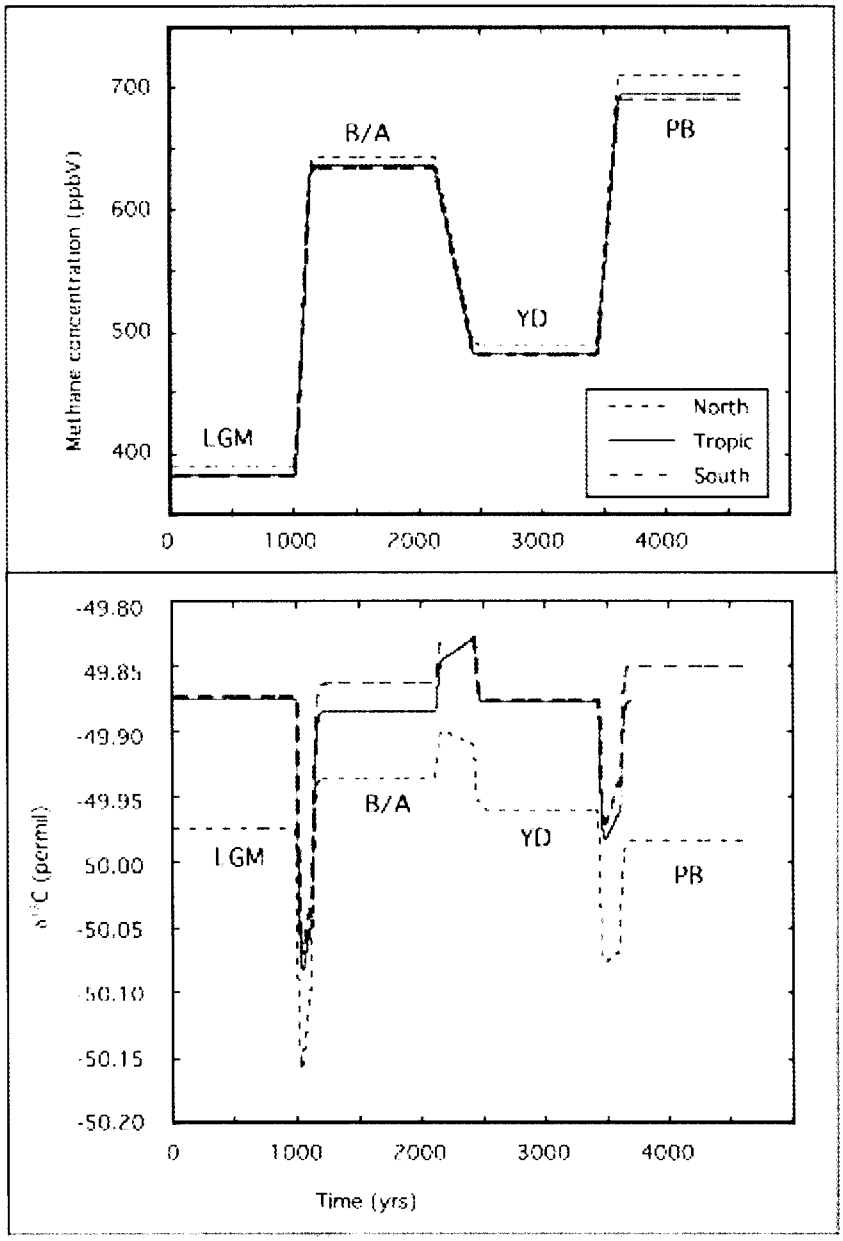

Fig. 4.3.7: Atmospheric isotope effects during termination 1
Three-box-model for the transitions from LGM to B/A to YD to PB (model run (3-term)). Isotopic composition of the source is held constant to investigate the influence of atmospheric concentration changes on $\delta^{13}C_{CH4}$. Top panel shows atmospheric methane concentration modeled to match data in Brook et al. (2000). Duration of climatic stages is set to 1000 yrs, duration of transition periods as determined by Brook et al. (2000). Lower panel shows the effect of atmospheric concentrations changes on $\delta^{13}C_{CH4}$ with negative excursions during times of warming and concentration increase and positive excursions during periods of cooling and decreasing concentration.

respectively. During the start of the YD, a time of cooling and concentration decrease, the isotopic change is less pronounced: $\delta^{13}C_{CH4}$ is rising by 0.05 ‰. All of the calculated gradients and shifts are smaller than the precision of the analytical technique for ice core measurements.

4.3.5. Conclusions

Any changes in methane emissions relative to removal rates affect the atmospheric isotope budget, even if the isotopic composition of the integrated methane source remains the same. This means that changes in atmospheric methane concentration are associated with changes in $\delta^{13}C_{CH4}$. Concentration increases lead to lower $\delta^{13}C_{CH4}$, while concentration drops cause higher $\delta^{13}C_{CH4}$ values. The magnitude of the effect increases with the rate of concentration change. The $\delta^{13}C_{CH4}$ shift persists for the time of increase/decrease and then readjusts to equilibrium values within decades.

The magnitude of source and sink strength under steady state conditions, i.e. the atmospheric lifetime τ of methane, does not affect the isotopic offset between source and atmospheric reservoir. In contrast, latitudinal concentration gradients and transport lead to changing $\delta^{13}C_{CH4}$ if τ is varied, even only in one latitudinal zone, although none of the investigated scenarios produced an isotope effect that would be detectable in measurements of $\delta^{13}C_{CH4}$ in ice samples.

Table 4.3.2: Correction for isotope effects of mixing and transport processes

Process	Box model (run)	Isotope effect	Correction	Section
Changing τ	1-box (1-1; 1-2)	0 ‰	none	4.3.1
Latitudinal gradients / transport effects	3-box (3-term)	> 0.05 ‰	Negligible between YD and PB	4.3.4
Dilution effect	3-box (3-term)	0.1 ‰	+ 0.1 ‰ during YD-termination	4.3.4

A simulation of the events at the end of the last ice age confirms the general findings that changing lifetimes, transport patterns and latitudinal gradients do not affect $\delta^{13}C_{CH4}$ significantly and therefore do not require corrections. There is a negligible difference in isotopic composition between various climatic stages. A correction for the atmospheric dilution effect (i.e. the $\delta^{13}C_{CH4}$ decrease) at the terminations of LGM and YD should be applied when carbon isotope data from ice samples are used for methane budget calculations. Although the calculated deviations are below the detection limit, they occur at critical times when they may add to other processes that affect the recorded $\delta^{13}C_{CH4}$ (which is discussed in chapter 3.4). Based on the findings presented here, ice sample $\delta^{13}C_{CH4}$ data from the YD termination will be corrected for atmospheric dilution by a factor of +0.1 ‰.

4.4. Isotope mass balance and methane budgets

The goal of this study is to interpret variations in $\delta^{13}C$ of atmospheric methane as related to changes in the contributions of different source types. The value measured in ice samples (see Chapters 2.2, 3.4, and 4.3 for necessary corrections due to firn diffusion and atmospheric mixing) represents the atmospheric $\delta^{13}C_{CH4}$. To derive the isotope ratio of methane emissions from this value, one has to account for the enrichment of atmospheric methane associated with removal processes. Correcting the atmospheric number for the associated offset $\Delta\ \delta$ (see Chapter 4.1) gives the isotopic composition of the global source. The latter is a mixture of emissions from different source types, which have distinct isotope ratios (Chapter 4.2). $\delta^{13}C_E$ of the global (or integrated) emissions can be calculated by an isotope mass balance as:

$$\delta^{13}C_E = \sum_1^n (\delta^{13}C_{Ei} \times E_i)/E \qquad (4.12)$$

where E is global emission rate in Tg/yr, and E_1 through E_n individual source types with their respective isotopic compositions $\delta^{13}C_{Ei}$. From Equation (4.12) follows that: (i) $\delta^{13}C_E$ of the source depends on the mixture of source types and that (ii) source types with high emissions or extreme isotope values will have a greater impact on the mass balance. Assuming constant $\Delta\ \delta$, a measured change in atmospheric $\delta^{13}C_{CH4}$ means a change in the mass balance, which in turn indicates that relative contributions of source types or their isotopic compositions have changed. Except for the circumstances discussed in Chapter 4.2, the isotopic composition of source types is assumed to be stable, so that the mass balance can be used to detect changes in emission rates. The system is underdetermined and will not uniquely identify specific changes in the budget, but it provides a constraint to test various possible scenarios and identify source combinations where isotopes and emissions have to add up to the mass balance.

Table 4.4.1: Isotope budgets for atmospheric methane at LGM, PIH, and present. Emission rates (flux) from Chappellaz et al. (1993b), Etiope and Milkov (2004), Whiticar (2000)

	LGM		PIH		Present	
	Flux (Tg/yr)	$\delta^{13}C$ (‰)	Flux (Tg/yr)	$\delta^{13}C$ (‰)	Flux (Tg/yr)	$\delta^{13}C$ (‰)
Source						
Boreal and temperate wetlands	8	-61.3	51	-61.8	38	-61.8
Tropical wetlands	68	-56.7	85	-58.3	77	-59.1
Ruminants	20	-57.5	15	-56.9	80	-63.8
Termites	20	-63.0	20	-63.0	20	-63.0
Biomass burning	5	-26.6	5	-26.7	55	-24.6
Ocean	10	-58.2	10	-58.2	10	-58.2
Gas hydrates	0	-62.5	5	-62.5	5	-62.5
Geologic methane	40	-41.8	40	-41.8	40	-41.8
Rice paddies					110	-63.0
Natural gas exploration					45	-41.8
Coal gas					35	-37.0
Landfills					40	-55.0
Total	171		231		550	
$\delta^{13}C_E$ of total emissions		-53.5		-55.9		-53.0
Sink offset $\Delta\delta$		-5.1		-5.3		-6.3
Atmospheric $\delta^{13}C$		-48.4		-50.6		-47.3

Isotope budgets for methane at LGM, PIH and present are listed in Table 4.4.1 and shown in Figure 4.4.1. Emissions rates for natural sources are from Chappellaz et al., (1993b), for anthropogenic sources from Whiticar (2000). Isotopic compositions for different source types are from a compilation of literature values, including Boehme et al. (1996), Burke and Sackett (1986), Burke et al. (1988), Chanton and Martens (1988), Chanton et al. (1988), Deines (1980), Games and Hayes (1976), Hornibrooke et al. (1997), Lansdown et al. (1992), Levin et al., (1993), Levin (1994), Martens et al. (1986), Oona and Deevey (1960), Ovsyannikov and Lebedev (1976), Popp et al. (1995), Quay et al. (1991), Quay et al. (1988), Rice and Claypool (1981), Rust 1981, Schoell (1980), Stevens and Engelkemeir (1988), Tyler (1986), Tyler et al. (1987), Tyler et al. (1988), Wahlen et al. (1988), Wahlen et al. (1989) and Whiticar et al. (1986). Also, the results from Chapter 4.1 and 4.2 are included in the calculations.

The budgets presented in Table 4.4.1 have one addition compared to Chapter 4.2, which is geologic methane emissions, i.e. the outgassing of thermogenic methane in tectonically active areas. The reason for including this source is the low $\delta^{13}C$ of the global source as calculated in Table 4.2.4. For $\delta^{13}C_E$ = -58.9 and $\Delta\ \delta$ of –5.3 ‰, atmospheric $\delta^{13}C_{CH4}$ in the PIH would be over 4 ‰ more depleted in ^{13}C compared to ice core data from this study and those reported by Craig et al. (1988b) (see Fig. 4.4.2). Including geological methane emissions of 40 Tg/yr (Etiope and Milkov, 2004) balances the isotope budget to better match observations (see Chapter 5.1.3). The addition increases overall emission rates, which means a shorter residence time of methane. The latter has no influence on $\Delta\ \delta$ or atmospheric $\delta^{13}C_{CH4}$ (see Chapter 4.3.1), so that the simplistic approach not to integrate the additional source in the total output is justified. By the same reasoning it is clear that isotope budgets are not suitable to determine atmospheric residence time of methane, absolute values for emission rates or atmospheric loss rates.

Isotope mass balance calculations give $\delta^{13}C_E$ for LGM, PIH, and present. $\Delta\ \delta$ values as determined in Chapter 4.1 are then used to derive the associated atmospheric $\delta^{13}C$ of methane. For the modern scenario the budget is not balanced: the calculated atmospheric $\delta^{13}C_{CH4}$ is too high (i.e. elevated in ^{13}C) by 0.5 ‰ compared to the actual value (which is listed in Table 4.4.1; see Fig. 4.4.2). The reason is that the budget uses emission rates from two different scenarios. For natural sources flux rates are from Chappellaz et al. (1993b) and isotope ratios for these sources were calculated in Chapter 4.2. These results are combined with anthropogenic sources after Whiticar (2000). The two scenarios work with different assumptions (e.g. total emissions) so that single values are weighted in two inconsistent ways.

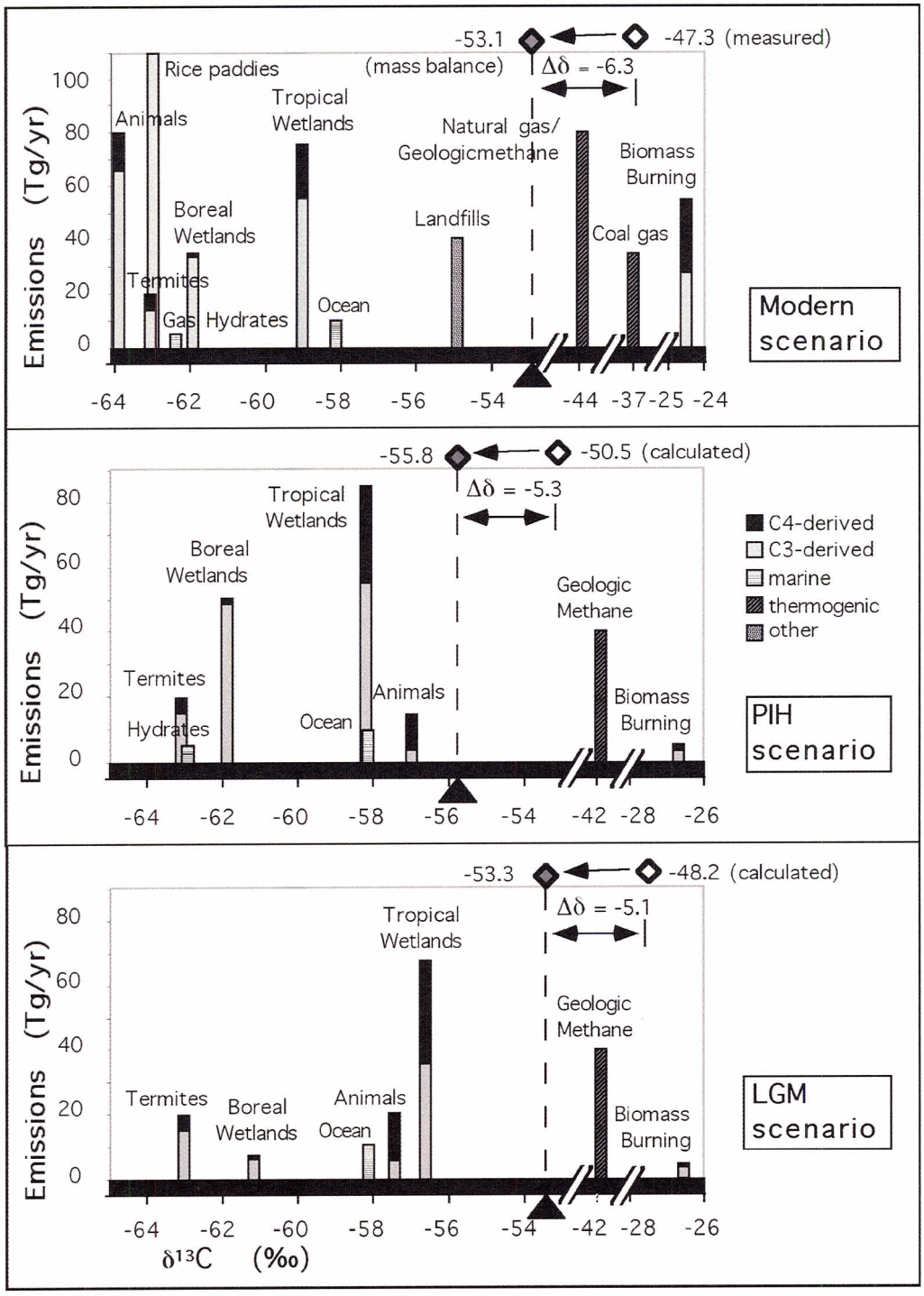

Fig. 4.4.1: Methane budgets for modern conditions, PIH and LGM.
The black triangle indicates the equilibrium point of the source mass balance and $\delta^{13}C_E$ (grey diamonds). Note scale breaks in bottom axes. $\Delta\ \delta$ and atmospheric $\delta^{13}C_{CH4}$ (white diamonds) are not drawn to scale.

For the PIH, the calculated atmospheric $\delta^{13}C_{CH4}$ is lower than ice core data by almost 1 ‰. This is despite the fact that we included higher C_4 contributions (Chapter 4.2) and geologic methane emissions. Both decrease the calculated $\delta^{13}C$ and are not part of commonly accepted budget scenarios. The mass balance indicates a missing factor for ^{13}C enrichment of natural sources, either through higher $\delta^{13}C$ of specific sources or an entirely different source type. This will be discussed in more detail below (Chapter 5). There are no data to calibrate the LGM scenario, and it is intended only to represent *a priori* knowledge and expectations about the methane budget in glacial conditions.

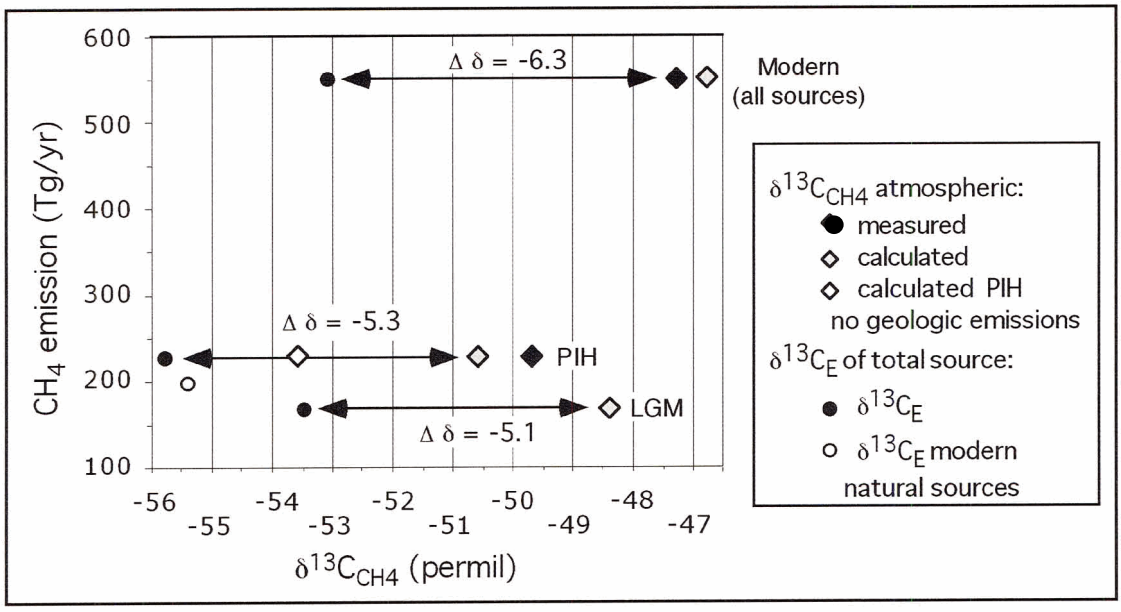

Fig. 4.4.2: Isotope ratios of total emissions and atmospheric CH_4 in LGM, PIH, and today All values used in this diagram are derived from Chapters 4.1 ($\Delta\ \delta$) and 4.2 ($\delta^{13}C_E$). For an estimate of errors involved see Chapter 4.2.2.5.

The budgets presented here are a synthesis of widely accepted knowledge about the natural methane cycle and theoretical observations presented in previous sections of this chapter. They do not take into account several newer studies if those have not been incorporated in other budget scenarios in order to present the consensus of current knowledge. Chapter 5 will discuss studies that present new or controversial results.

The *a priori* budgets provide a test for ice measurements as presented in Chapter 3 and serve to identify possible key players in the budget, where prediction and data disagree.

The budget calculations predict that atmospheric $\delta^{13}C_{CH4}$ in the PIH was more depleted in ^{13}C than it is today. The reason is that ^{13}C-rich anthropogenic sources were absent at that time, which is illustrated by the fact that $\delta^{13}C_E$ of modern natural sources is very similar to the pre-industrial one (Fig. 4.4.2). The isotope shift caused by anthropogenic sources is not as large as previously believed (Craig et al., 1988b; Quay et al., 1988), because there is now better understanding of the isotopic fractionation of sink processes. The main changes in sources that were active both in the PIH and today are that

(i) biomass burning increased by a factor of ten mostly due to slash and burn agriculture;

(ii) methane emissions from wetlands decreased as a result of drainage and land conversion. This process is more relevant in temperate and boreal regions were emissions dropped by 25 %, whereas tropical wetland emissions decreased by 10 % since the PIH;

(iii) wild animals are now a smaller methane source (from 15 Tg/yr to 4 Tg/yr), while emissions from ruminants *per se* increased drastically to now 80 Tg/yr due to cattle farming. Feeding practices in this industry also changed the $\delta^{13}C$ of ruminant methane from around –57 ‰ to ca. –64 ‰ nowadays. All these changes are estimates from bottom-up budgets. The ice core data can confirm the predictions or show that the estimates are not accurate. A first example for the latter case is the necessity to include geologic methane emissions (or another ^{13}C-rich source) in the PIH budget as discussed above and in Chapter 5.

The *a priori* budgets predict that global methane emissions, and consequently atmospheric $\delta^{13}C_{CH4}$, in glacial conditions were significantly more ^{13}C-rich than in the PIH. This is a consequence of an almost complete shut-down of temperate and boreal wetland emissions and a strong decrease in C_3-derived methane in tropical wetlands (see Chapter 4.2). If the $\delta^{13}C_{CH4}$ measurements in ice samples showed this enrichment in ^{13}C it would confirm both the results on the influence of C_3 and C_4 plant material as a methane precursor (Chapter 4.2) and the emission scenarios presented by Chappellaz et al. (1993b) on which the budget calculations are based. These questions are discussed in detail in Chapter 5.

5. Discussion

The underlying question of this study is how climate and natural emissions of greenhouse gases, specifically methane, influence each other. It is well established that the two are closely correlated (Chappellaz et al., 1993a; Brook et al., 1996; Petit et al., 1999), but it is uncertain what the actual controls in this system are. One of the main problems is to identify the methane sources that drive atmospheric concentration changes. As outlined in Chapter 4, the isotopic composition of atmospheric methane can be used to constrain these emissions. The $\delta^{13}C_{CH4}$ measurements in ice samples presented in this study provide information about three periods with stable climatic conditions, namely the Younger Dryas cold period, the Preboreal, which is the very beginning of the current interstadial, and the late pre-industrial Holocene. In top-down budget calculations, the atmospheric $\delta^{13}C_{CH4}$ of these periods can be used to derive the isotopic composition of the total methane emissions $\delta^{13}C_E$. With isotope mass balance calculations one can create possible emission scenarios and identify how methane sources differed between the three stages. With this knowledge, the high resolution record of the YD termination provides the isotopic composition of emissions that cause the concentration increase associated with climate change. The findings provide a test for current theories regarding methane budgets in the past and the causes of the methane increase at the transition to the Holocene.

5.1. Methane budget for the late pre-industrial Holocene

The isotope data from GISP2/139 and Ag77/72 constrain methane sources in the Holocene, before industrial emissions affected the budget. A large part of man-made sources are more enriched in ^{13}C than natural ones. Consequently, we expect atmospheric $\delta^{13}C_{CH4}$ in pre-industrial times to be lower (^{13}C-depleted) than the modern value of –47.3 ‰ (Quay et al., 1999). Indeed, the results for 230 and 330 yr BP are around –49.6 ‰ (Chapter 3.6). With an offset to the atmospheric value ($\Delta\ \delta$) of –5.3 ‰ (see Chapter 4.1), the isotopic composition of the total source at that time had a $\delta^{13}C_E$ of

–54.9 ‰. This value is the isotope mass balance of individual emissions and we can examine what the most likely source composition with an equivalent $\delta^{13}C$ is. Using independent emission estimates, a bottom-up methane budget for the PIH is derived and presented in Chapter 4.2 (Table 4.2.4). The isotopic composition of the global source in that scenario is -58.9 ‰. That is 4 ‰ lower than measured. In order to resolve the discrepancy, emissions of certain source types either have to be larger than assumed or their isotopic composition has to be different from the widely accepted value.

5.1.1. Uncertainties in natural emissions

Biomass burning is a possible candidate for emissions that are misrepresented in the *a priori* budget, because it has the highest $\delta^{13}C$ of all source types. In fact, it generates the only emissions that are more enriched in ^{13}C than the $\delta^{13}C_E$ derived from ice measurements. Mass balance calculations, however, show that wildfires would have to comprise almost 17 % of total emissions, instead of less than 3 %, in order to adjust the budget to the measured $\delta^{13}C_{CH4}$. The emission estimate used in Chapter 4.2 is based on the assumption that natural fire emissions can be estimated as 10 % of today's biomass burning, (Chappellaz et al., 1993b). Although this approach is not well constrained, it seems unlikely that it should underestimate wildfire emissions by a factor of six. In contrary, Hao and Ward (1993) estimate the amount of biomass burned in wildfires as only 5 % of total modern biomass burning. Charcoal records from all continents indicate that fire frequency in the late PIH was not higher than today (Carcaillet et al., 2002). Savarino and Legrand (1998), who used concentrations of ammonium and formate from a Greenland ice core to reconstruct fire history in North America found that during the so-called Little Ice Age fire frequency was low, which is the age of the analyzed $\delta^{13}C_{CH4}$ samples. Although Savarino and Legrand's study (1998) does not quantify global emissions, it suggests that at least temperate zones experienced relative little biomass burning. In conclusion, there is no evidence that biomass burning would have led to higher $\delta^{13}C_{CH4}$ in the late PIH.

Tropical wetlands could change $\delta^{13}C_{CH4}$ significantly, because they are the largest source of methane. There is some uncertainty regarding the actual size of their contribution, because case studies have focused on more accessible temperate and boreal wetlands (Bartlett and Harriss, 1993). In addition, the $\delta^{13}C$ of tropical wetlands as used in most methane budgets is not well constrained either (Stevens and Engelkemair, 1988). This is expressed by the fact that wetlands are commonly not distinguished as C_3- or C_4-dominated. There is a rich literature of case studies on the isotopic composition of wetland methane. Most of this work comes from boreal and temperate locations, and it is challenging to calculate a global mean from the individual measurements. In tropical wetlands, single $\delta^{13}C_{CH4}$ values as high as –43 ‰ (Chanton and Smith, 1993), -41 ‰ (Quay et al., 1988) and –31 ‰ (Tyler et al., 1988) have been reported. However, these numbers are specific for certain plant types or even seasons and represent the extreme in each of the studies.

Only Quay et al. (1988) attempted to quantify $\delta^{13}C$ of the mean flux and estimated it to be –53 ‰, which is close to the average of the ranges reported in the other two studies. This may be an upper limit for $\delta^{13}C_{CH4}$ of tropical wetlands, because the results discussed above do not include lower values from other studies. If the isotopic composition of tropical wetlands in the mass balance is taken as –53 ‰, then total emissions have a $\delta^{13}C$ of -56.5 ‰. This accounts for part of the discrepancy, but is still 1.6 ‰ lower than the observed value. In order for tropical wetlands to account for the whole discrepancy, their $\delta^{13}C$ would have to be –49 ‰, which is within the range of the case study measurements quoted above. However, the published measurements support the lower number of –53 ‰, which will be used for further considerations.

Boreal and temperate wetlands have been studied more intensively than any other methane source so that emission magnitude and $\delta^{13}C_{CH4}$ are likely well constrained in the bottom-up budget. The estimate for the animal source was based on bison populations in North America (Chappellaz et al., 1993b). These animals live in an environment with C_3 contributions above global average, yet in this study the average determines the $\delta^{13}C$ of

the animal source. Consequently, the animal source presented in Table 4.2.4 already is more ^{13}C-rich than appropriate for the flux estimate.

The other sources are small and will not affect the isotope mass balance strongly. For example, oceanic flux from shallow and coastal seas may be underestimated (Lambert and Schmidt, 1993), as are emissions from upwelling areas (Sansone et al., 2001). In addition, $\delta^{13}C_{CH4}$ could be higher than usually assumed due to contributions of thermogenic seeps in shallow seas (Hovland and Judd, 1993) and oxidative enrichment of open water fluxes (Holmes et al., 2000). Increasing the assumed flux by twenty-five percent and using a $\delta^{13}C$ higher by 13 ‰, in order to match the lower range of values reported by Holmes et al. (2000) and Sansone et al. (2001), elevates the calculated global $\delta^{13}C_E$ by 0.9 ‰.

Similarly, methane from marine gas hydrates is partially oxidized in the water column and could be more enriched in ^{13}C by 20 ‰ than the reservoir value of –62.5 ‰ by the time it reaches the atmosphere (Grant and Whiticar, 2002; Kastner et al., 2003). The calculated $\delta^{13}C_E$, however, then increases only by 0.5 ‰. There are no newer findings that would lead to a re-evaluation of emissions from termites.

Chapter 4.1 discussed that the sink fractionation was probably different in the past. If this assumption is false, then $\Delta\ \delta$ would have been larger than the estimated –5.3 ‰ used in the calculation of $\delta^{13}C_E$. However, the use of the well-established modern value of –6.3 ‰ decreases the discrepancy between the measured and the *a priori* value by only 1 ‰. Assuming a pre-industrial $\Delta\ \delta$ that is higher than today is not justified because the highly fractionating Cl-sink was smaller in the pristine atmosphere. The model results of Gupta et al. (1996) for a reduced Cl-sink and those by Ojima et al. (1993) for soil uptake provide fairly good constraints for $\Delta\ \delta$ in the PIH, so that this parameter is not likely to significantly influence the PIH methane budget.

Table 5.1.1. Adjusted PIH methane isotope budget for natural sources

	PIH		Present	
Source type	Flux (Tg/yr)	$\delta^{13}C$ (‰)	Flux (Tg/yr)	$\delta^{13}C$ (‰)
Boreal wetlands	51	-61.8	38	-61.8
Tropical wetlands	85	-53.0	77	-59.1
Wild animals	15	-56.9	80	-63.8
Termites	20	-63.0	20	-63.0
Wildfires	5	-26.7	55	-24.6
Ocean	12.5	-45.0	10	-58.2
Gas hydrates	5	-42.5	5	-62.5
Total	193.5	-55.2	285	-54.4

The above discussion shows that no single source or sink type (with the possible exception of tropical wetlands) can account for the discrepancy between calculations based on *a priori* knowledge and ice core data. Several assumptions of the *a priori* budget, however, may not reflect all of the current knowledge. There is evidence that C_4-dominated wetlands, gas hydrates and the ocean emit methane with a higher $\delta^{13}C$ and that the ocean flux may be larger than commonly estimated. Together, these changes (as discussed above) bring $\delta^{13}C_E$ to –55.2 ‰ (Table 5.1.1), which agrees quite well with the value of –54.9 ‰ derived from ice core measurements. The proposed adjustments of the methane isotope budget may represent an upper limit, but if confirmed they would apply to budgets in other periods as well, including the modern one.

5.1.2. Early anthropogenic methane emissions

It has been suggested that human activities had a measurable impact on methane emissions as early as 5000 yr BP (Ruddiman and Thomson, 2001). By the 16th and 17th century, anthropogenic methane emissions from livestock, domestic sewerage, fuel wood combustion and biomass burning, as well as irrigated agriculture, could have reached a significant contribution to the global methane budget (Kammen and Marino, 1993; Subak, 1994). Table 5.1.2 lists two scenarios for anthropogenic emissions from

Table 5.1.2: Pre-industrial anthropogenic emission scenarios
These emissions would be additional to the ones listed in Table 4.4.1. Total emissions in Subak (1994) are scaled up from human population estimates, whereas Ruddiman and Thompson calculate them as a missing source to explain Late PIH methane concentrations and then attribute them to specific source types.

	Subak (1994)		Ruddiman and Thomson (2001)	
	AD 1600		AD 1700	
Livestock	10 Tg/yr	-60.8 ‰	10.4 Tg/yr	-60.8 ‰
Domestic sewerage			3.1 Tg/yr	-45.0 ‰
Biomass burning and Fuel wood use	30 Tg/yr	-26.7 ‰	4.9 Tg/yr	-26.7 ‰
Agriculture	15 Tg/yr	-63.0 ‰	9.8 – 42 Tg/yr	-63.0 ‰
Total	55 Tg/yr	-42.8 ‰	28 – 60 Tg/yr	-53.9 to –58.8 ‰

Subak (1994) and Ruddiman and Thomson (2001) that are contemporaneous with the measurements from GISP2/139 and Ag77/72. Kammen and Marino (1993) consider only emissions from biomass burning, which they estimate to reach 60 Tg/yr by 1800 AD.

Including the additional emissions into the late PIH mass balance (as presented in Table 4.4.1) has contrary effects for either scenario. Subak (1994) made estimates for the methane production of different early anthropogenic activities and scaled them to population size. An early anthropogenic contribution with a high proportion of biomass burning as proposed in this budget is in good agreement with our isotope data. The resulting total source would be at –55.3 ‰, only 0.4 ‰ lower than the measured value. In contrast, the emissions suggested by Ruddiman and Thomson (2001) hardly affect the scenario. This is a consequence of the high input from agriculture, which is isotopically very similar to C_3-dominated wetland methane. It is, however, worthwhile to discuss how this latter scenario was derived.

Like Subak (1994), the authors scaled current anthropogenic emissions back to the historic population as one part of their approach. They also derived an estimate for how much methane is required to explain the decoupling of atmospheric methane concentration and global temperature since ca. 5000 yr BP (Blunier et al., 1995). Under the hypothesis that the additional methane is anthropogenic, they calculated that by 1700 AD man emitted 60 Tg/yr from various sources. They did not consider a big contribution from biomass burning to these emissions because of stable isotope data, following Quay et al. (1988). Their report used $\delta^{13}C_{CH4}$ results from Craig et al. (1988b) (which agree with data from this study) to rule out a larger PIH source of biomass burning. The conclusion is flawed, because the calculation by Quay et al. (1988) is based on a now outdated determination of $\Delta\ \delta = -11$ ‰ (Davidson et al., 1987). The $\delta^{13}C_E$ valued calculated with this $\Delta\ \delta$ is too depleted in ^{13}C as that ^{13}C-rich wildfire methane could have contributed markedly to the total emissions. In contrast, the $\Delta\ \delta$ value of –5.3 ‰ used in this study and the measured $\delta^{13}C_{CH4}$ values do accommodate a significant contribution of biomass burning to the isotope budget.

Assuming that Ruddiman and Thomson's "missing" anthropogenic source of 32 Tg/yr is biomass burning brings the isotope mass balance to –54.2 ‰ for the global source, even slightly higher than the ice data indicate. Increases in fire frequency during the Holocene are well documented in charcoal records and must be interpreted as human influence on natural fire regimes (Bird and Cali, 1998; Haberle and Ledru, 2001; Carcaillet et al., 2002), which supports this scenario. However, the arguments raised in Ruddiman and Thomson (2001) for a proportionately higher flux from historic rice paddies due to inefficient farming remain valid and point to an anthropogenic flux that is isotopically neutral to the budget or more depleted in ^{13}C. In conclusion, early anthropogenic methane emissions are compatible with $\delta^{13}C_{CH4}$ data from ice cores. Whether the main impact came from biomass burning or irrigated agriculture depends on the assumed natural budget for that time.

5.1.3. Geologic methane emissions

All isotope mass balances examined in this study are underdetermined, because a host of emission rates and isotopic signatures is derived from a single atmospheric value. Consequently, it is not possible to definitely resolve the methane budget. It could be that not only fluxes from different sources have been seriously misrepresented, but also that a source type has been omitted from methane budgets altogether. A ^{13}C-rich natural methane source of medium size would tilt the mass balance to match the ice core data. For example, geologic methane emissions comprise the outgassing from thermogenic reservoirs in tectonically active areas. Associated surface features are mud volcanoes, springs and gas vents, but diffusive flow (microseepage) also contributes significant amounts of gas (Lacroix, 1993; Etiope and Klusman, 2002). In total, geologic methane emissions have been estimated to contribute 35 – 45 Tg/yr to the methane budget (Etiope and Milkov, 2004). This gas is of thermogenic origin and has a $\delta^{13}C$ of ca. –41.5 ‰. The addition of 40 Tg/yr of natural gas to the PIH methane budget is a significant contribution and tips the source balance to –55.8 ‰ (Fig. 4.4.1; Table 4.4.1). That is still depleted in ^{13}C by ca. 1 ‰ compared to the value derived from ice core data, but the discrepancy is significantly smaller, so that geologic methane emissions may be an integral part of the natural methane budget.

5.1.4. Discussion of the PIH methane budget

The discrepancy between calculated and measured $\delta^{13}C_E$ can be explained with any of the following: (i) uncertainties in the common source budget, (ii) early anthropogenic emissions or (iii) geologic methane flux. There are two lines of evidence to assess which of these is the most likely cause for a ^{13}C-rich PIH methane budget. The first approach uses the magnitude of total emissions. As outlined in Chapters 4.3 and 4.4, the isotope mass balance is independent of this value, as long as an equal sink balances it. There are, however, independent estimates of methane flux in the PIH, which provide a test for different scenarios.

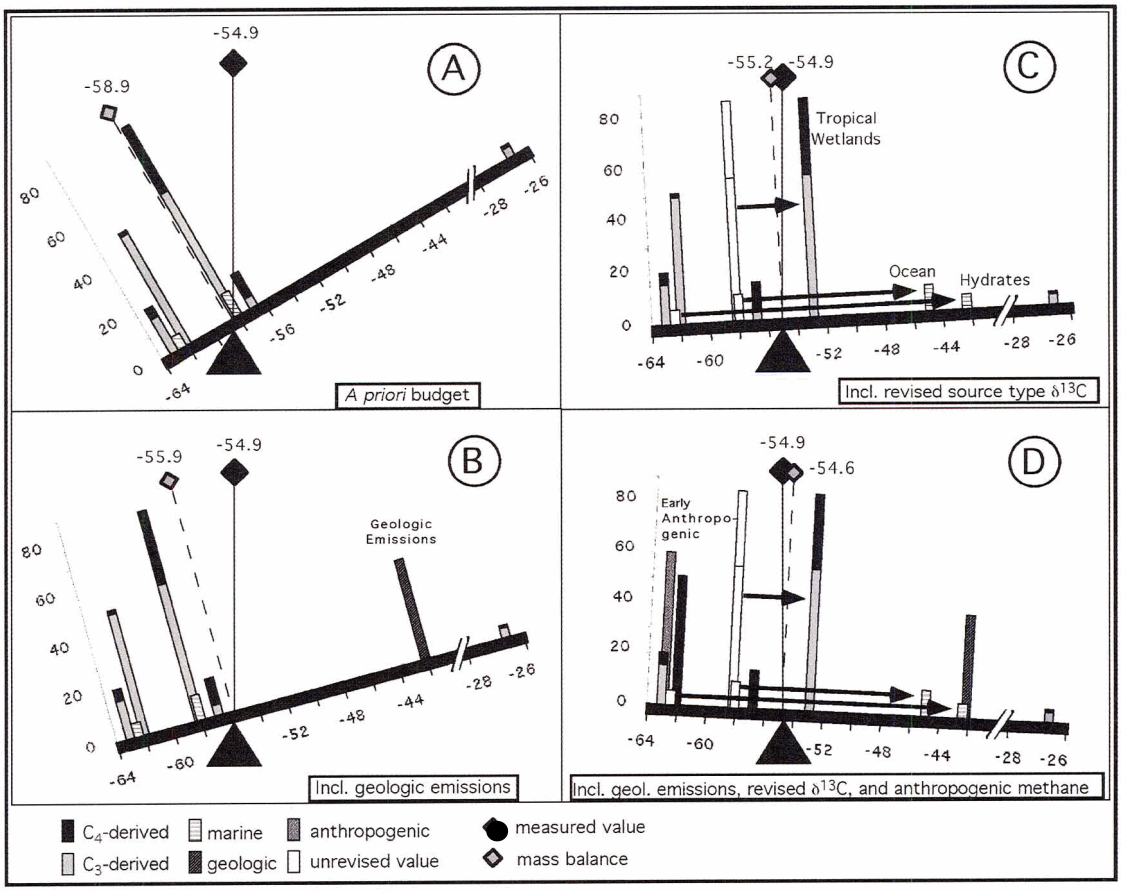

Fig. 5.1.1: Mass balance scenarios for the pre-industrial Holocene
(A) *A priori* budget predicts $\delta^{13}C_E$ to be too ^{13}C depleted;
(B) including geologic methane emissions decreases the discrepancy between measured and calculated $\delta^{13}C_E$;
(C) revised $\delta^{13}C$ for tropical wetlands, gas hydrates, and ocean source balance the budget;
(D) Budget including revised $\delta^{13}C$ and geologic methane emissions, as well as an early anthropogenic source (mostly irrigated agriculture) matches the measured $\delta^{13}C_E$ and is consistent with the atmospheric history of $\delta^{13}C_{CH4}$ measured by Etheridge et al. (2003).

Atmospheric chemistry models suggest that the PIH methane source was between 180 and 210 Tg/yr (Crutzen and Brühl, 1993; Thompson et al., 1993; Martinerie et al., 1995) although a larger estimate is 275 Tg/yr (with a range of 223 – 335 Tg/yr; Osborn and Wigley, 1994). There is better agreement on the lower margin of the range and the estimates are close to the value of 190 Tg/yr, which Chappellaz et al. (1993b) derived by

adding flux estimates from different sources. All presented *a priori* budgets are based on the latter calculations. The additional ^{13}C-rich source should therefore be rather small in order to fit the budget. Consequently, the adjustment of the natural budget presented in Table 5.1.1 is the most likely scenario because it adds only 2.5 Tg/yr to the estimate of Chappellaz et al. (1993b). The second best possibility is geologic methane flux. This is slightly smaller than estimates for anthropogenic input.

However, this conclusion depends on the assumed composition of the latter, because a higher percentage of biomass burning in the anthropogenic source could balance the budget at lower emissions. Given the uncertainties in the various estimates, total methane flux does not provide a strong constraint for the missing source. For the same reason there is no attempt to favour any of the scenarios due to geographic contribution of different sources in order to match interhemispheric methane concentration gradients measured by Chappellaz et al. (1997) and Brook et al. (2000).

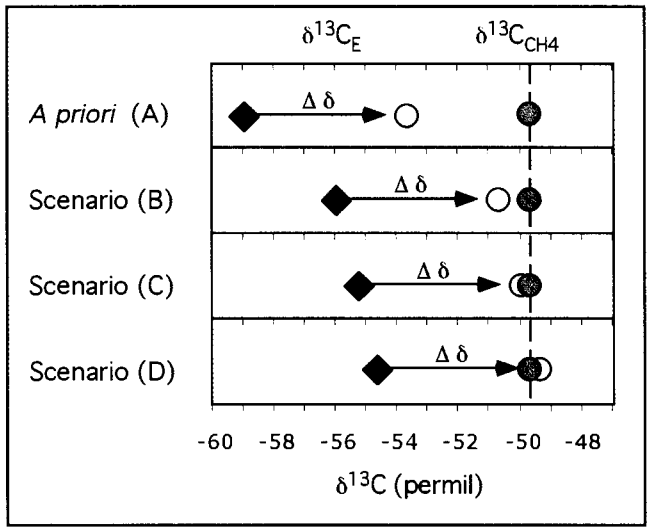

Fig. 5.1.2: Isotopic composition for source and atmosphere in four PIH scenarios
The isotopic composition of total emissions ($\delta^{13}C_E$; black diamonds) and atmospheric methane ($\delta^{13}C_{CH4}$; white circles) are compared to the value measured in ice from GISP2 and Agassiz ice cap (grey circles). The scenarios are the same as in Fig. 5.1.1, i.e. (A) is the a priori PIH budget; (B) includes geologic emissions; (C) uses revised $\delta^{13}C$ for tropical wetlands, gas hydrates, and ocean source; (D) includes geologic emissions, revised estimates for source $\delta^{13}C$ and early anthropogenic emissions following Ruddiman and Thompson (2001).

The second way to test the three possibilities is to regard their historic implications. A revised isotope budget implies unchanged $\delta^{13}C_{CH4}$ during the Holocene, as do geologic methane emissions. In contrast, anthropogenic emissions from biomass burning would have increased with growing human population, so that earlier $\delta^{13}C_{CH4}$ values would have been more depleted in ^{13}C. Preliminary data by Etheridge et al. (2003) show the opposite trend to higher $\delta^{13}C_{CH4}$ values in preceding centuries. This contradicts the scenarios of revised source values and geologic emissions as well as anthropogenic biomass burning. The only case that would fit this pattern of a decrease in $\delta^{13}C_{CH4}$ while human population increases is the input of ^{13}C-depleted anthropogenic emissions from rice cultivation. This scenario, however, is at odds with the absolute $\delta^{13}C_{CH4}$ values for the late PIH in this study. In conclusion, a single scenario can either satisfy the isotope balance of 230 – 330 yrs BP or the observed $\delta^{13}C_{CH4}$ change beforehand. Theoretically, a combination of the different possibilities would match all observations. If the pristine Holocene methane budget included geologic methane emissions and higher $\delta^{13}C$ of natural sources, then $\delta^{13}C_E$ would have been around –53.5 ‰ as measured by Etheridge et al. (2003). Growing input of methane from early agriculture could then have decreased $\delta^{13}C_{CH4}$ by 1600 AD so that it meets the values measured in GISP2/139 and Ag77/72. Such a history of the methane budget is highly speculative. The implied isotope budgets, however, work out reasonably well (Table 5.1.3).

The "pristine" methane budget comprises geologic methane emissions and a more ^{13}C-rich tropical wetland source as well as either partially oxidized gas hydrate methane or an adjusted ocean source. Arbitrarily, the new hydrate value is included because it fits the budget slightly better and arguably involves processes that are better understood. Adding anthropogenic emissions with a high percentage of agricultural flux as described by Ruddiman and Thomson (2000) brings the total source to –54.6 ‰, which is very close to the measured value of –54.9 ‰. At first it seems unlikely that growing anthropogenic emissions strongly changed $\delta^{13}C_{CH4}$ prior to 1600 AD, while the value stays constant over 200 yrs, which is the time covered by our measurements and those of Craig et al. (1988b). This does not refute the case, because $\delta^{13}C_{CH4}$ would have decreased

only from the pristine value to one in equilibrium with the human source. Further increase of this source does not change the isotope mass balance.

The agreement between measured and constructed values is no proof that the outlined history is true. One method to test the scenario would be to match the assumed anthropogenic flux rates against the development of human population. Another way would be to measure the Holocene history of $\delta^{13}C_{CH4}$ and examine it for similar fluctuations when human influence can be ruled out. Without an established data set it is premature to speculate any further. The suggested changes of the natural methane budget, however, should be detectable in pre-Holocene $\delta^{13}C_{CH4}$ measurements from the Younger Dryas as well.

Table 5.1.3: Pristine and agriculturally influenced methane budgets for the Late PIH
The man-made emissions are after Ruddiman and Thomson (2003)

	Pristine Holocene budget		Budget with anthropogenic emissions	
	Flux (Tg/yr)	$\delta^{13}C$ (‰)	Flux (Tg/yr)	$\delta^{13}C$ (‰)
Boreal wetlands	51	-61.8	51	-61.8
Tropical wetlands	85	-53	85	-53
Wild animals	15	-56.9	15	-56.9
Termites	20	-63	20	-63
Wildfires	5	-26.7	5	-26.7
Ocean	10	-58.2	10	-58.2
Geologic	40	-41.5	40	-41.5
Hydrates	5	-42.5	5	-42.5
Livestock			10.5	-60.8
Sewerage			3.1	-45
Biomass burning			4.9	-26.7
Agriculture			42	-63
Total	231	-53.5	291.5	-54.6

5.2. Methane budget of the Younger Dryas

The interpretation of methane isotope data from the YD is complicated by the fact that there are few studies of the methane cycle specific for this period. The vast majority of relevant research has focused on the LGM and PIH. Environmental parameters of the YD lie between the conditions of these stages and a model budget for methane has to be adjusted accordingly. This involves several poorly constrained assumptions, because background data as they were derived for PIH and LGM do not exist. Continental ice cover, global temperature, global precipitation patterns and atmospheric chemistry induce the main changes of the natural methane budget. The situation is further complicated by the fact that the YD is not a uniformly global event. The associated changes are more strongly developed in the Northern Hemisphere and predominant in the Atlantic region (Dansgaard et al., 1989; Blunier et al., 1997). The following assumed changes, however, may be reasonable estimates for a bottom-up methane budget, which is based on those for LGM and PIH.

The extent of ice sheets at the YD is half of the area that deglaciated between LGM and PIH. This estimate is based on sea-level curves (Fairbanks, 1989; Clark and Mix, 2002; Lambeck et al., 2002), which are indicators of global ice volume. Although the latter is not the same as areal ice extent, the correlation between the two should be close enough for this purpose. In addition, one can derive the exposed shelf area from global ice volume, using the ETOPO-5 data set (National Geophysical Data Center, 1988). This gives an estimate of total land surface, which affects the magnitude of the soil sink and of certain source types.

Global climate at the YD is hard to reconstruct, because trends were different at various locations and modeling efforts have concentrated on the LGM. As a rough estimate, global temperature is here assumed to be halfway between LGM and PIH. This may be too warm rather than too cold (Grootes et al. 1993; Maslin and Burns, 2000). Temperature determines the rate of chemical and biological processes as well as

fractionation coefficients. None of these parameters are very sensitive within the range of uncertainty and the approximation should be appropriate.

More difficult is an estimate of the distribution of C_3 and C_4 plants, which depends on temperature, precipitation patterns and atmospheric CO_2 concentration. These changes are treated using the same assumption as for methane emission rates, namely that atmospheric methane concentration reflects the conditions in relevant ecosystems. Differences in $\delta^{13}C$ of vegetation dependent source types are scaled between LGM, YD and PIH by the same factors as observed in the respective atmospheric methane concentrations. The same approach is used for the magnitude of the total source under consideration of each source type's sensitivity to climate. The resulting *a priori* methane budget is presented as Scenario 1 in Table 5.2.1.

Table 5.2.1: *A priori* estimates of the YD methane budget
Scenario 1 uses $\delta^{13}C$ values that are interpolated between the *a priori* LGM and PIH estimates, Scenario 2 uses $\delta^{13}C$ values for gas hydrates and tropical wetlands that are adjusted to findings from the PIH budget as well as the YD C_3 versus C_4 ratio. Scenario 3 is similar to Scenario 2 but uses glacial $\delta^{13}C$ values for all sources.

	YD	Scenario 1	Scenario 2	Scenario 3	Present	
	Flux	$\delta^{13}C$	$\delta^{13}C$	$\delta^{13}C$	Flux	$\delta^{13}C$
	(Tg/yr)	(‰)	(‰)	(‰)	(Tg/yr)	(‰)
Boreal wetlands	26	-61.5	-61.3	-61.3	38	-61.8
Tropical wetlands	75	-57.4	-52.1	-51.4	77	-59.1
Ruminants	18	-57.2	-57.5	-57.5	80	-63.8
Termites	20	-63.0	-63.0	-63.0	20	-63.0
Wildfires	5	-26.6	-26.6	-26.6	55	-24.6
Ocean	10	-58.2	-58.2	-58.2	10	-58.2
Geologic emissions	40	-41.8	-41.8	-41.8		
Gas hydrates	2	-62.5	-42.5	-42.5	5	-62.5
Total source	197	-54.6	-52.4	-52.1	285	-54.4
$\Delta\ \delta$		-5.0	-5.0	-5.0		-6.3
Atmospheric $\delta^{13}C_{CH4}$		-49.6	-47.4	-47.1		-47.3

As expected, source magnitude and $\delta^{13}C_E$ are in between the values estimated for PIH and LGM. While it seems a fairly reliable approach to increase total flux proportional to atmospheric concentration, the $\delta^{13}C$ value of the total source may be a lower limit, which is discussed below. An alternative scenario that can be tested with ice core $\delta^{13}C_{CH4}$ data is included in Table 5.2.1. It uses the same methane fluxes but includes the revised $\delta^{13}C$ of tropical wetlands and gas hydrates as outlined in Section 5.1.1. The isotopic composition of tropical wetlands is further adjusted for the different ratio of C_3 and C_4 plants in the YD compared to the PIH. This is done in a simplistic manner by increasing the calculated YD number relative to the LGM proportionally to the LGM-PIH change. Total sink fractionation during the YD does not fall between the values that were determined for LGM and PIH. The reason is that the magnitude of the soil sink changed only slightly between PIH and YD. In this time interval, continental shelves were flooded at the same rate as ice retreated (unlike during the period between LGM and YD, when ice retreated slower). Consequently, the land surface area available for soil uptake did not change. The impact of this mechanism on $\Delta\ \delta$ is marginal, but it highlights the uncertainties involved with reconstructions.

The methane budget that assumes linear change between LGM and PIH (Scenario 1) predicts an atmospheric $\delta^{13}C_{CH4}$ in the YD of –49.6 ‰. Scenario 2, which includes higher $\delta^{13}C$ values for gas hydrates and tropical wetlands, has a resulting $\delta^{13}C_{CH4}$ of –47.4 ‰, more than 2 ‰ higher than in Scenario 1. The Pakitsoq records do not meet these predictions. The median value of all data for the YD period is –46.0 ‰. This number could theoretically be the result of oxidation processes in the occluded air. Alternatively, it is the true signal resulting from an unexpected composition of the global methane source. First of all, the measured numbers lend support to the hypothesis of geologic methane emissions in the natural budget and revised $\delta^{13}C$ values of certain source types.

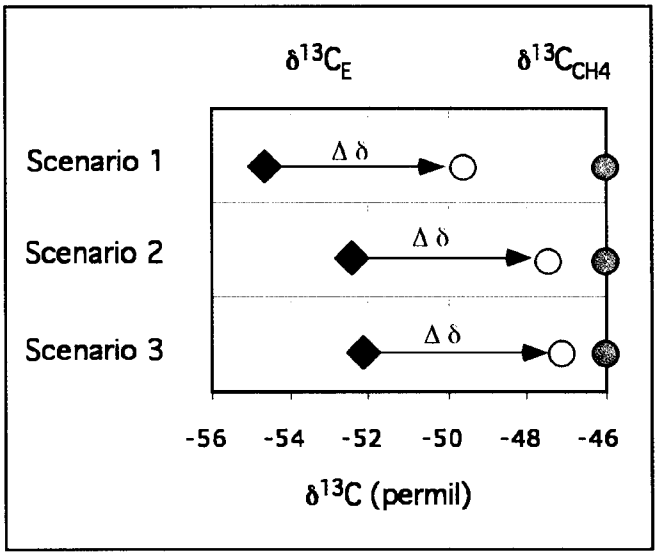

Fig. 5.2.1: Isotopic composition for source and atmosphere in three YD scenarios
The isotopic composition of total emissions ($\delta^{13}C_E$; black diamonds) and atmospheric methane ($\delta^{13}C_{CH4}$; white circles) are compared to the value measured in Pakitsoq ice (grey circles). The scenarios are described in the text and detailed in Table 5.2.1. Scenario 3 matches the measured value best, suggesting that the YD methane budget includes geologic emissions, revised $\delta^{13}C$ for tropical wetlands and gas hydrates and a glacial distribution of vegetation.

5.2.1. Geologic emissions in the YD and $\delta^{13}C$ of other sources

$\delta^{13}C_{CH4}$ data from the Late PIH suggest that outgassing of thermogenic methane could be an integral part of the natural methane budget. These emissions could have varied over time and were likely enhanced in times of higher tectonic activity. Assuming that a gas field of average size contains 200 Tg of methane, then the complete draining of such a reservoir caused e.g. by an earthquake is approximately equivalent to the total annual methane emissions in PIH or YD. This input would be integrated over the time of the draining and therefore be either a short-lived spike or a minor contribution to the budget. Larger fields, reservoir sizes up to 6000 Tg are known today, would have a larger impact, which would undoubtedly be detected in the methane concentration record. At least throughout the Holocene this is not the case (Blunier et al., 1995), therefore geologic emissions can be expected to provide a fairly constant flux to the atmosphere, which must be detectable throughout the record. The results from the YD confirm this possibility. Unlike the situation in the late PIH, including geologic methane emissions

does not balance the isotope budget of the YD. Omitting this source, however, increases the discrepancy between measured and calculated $\delta^{13}C_{CH4}$ by over 3 ‰ (calculated $\delta^{13}C_E$ of total emissions would be –57.6 ‰). Therefore, geologic methane emissions with annual flux rates of 40 Tg could be part of the natural methane budget and are included in the *a priori* estimates presented in Table 5.2.1.

By the same reasoning, the methane isotope budget confirms that the $\delta^{13}C$ value of several natural sources could be higher than assumed in most modern day budgets. If the isotopic compositions for gas hydrates and tropical wetlands (the latter adjusted for YD conditions) as derived for the PIH are used in the mass balance, the discrepancy between measured and calculated $\delta^{13}C_{CH4}$ drops by more than 2 ‰ (Fig. 5.2.1). It is not possible to ascertain whether gas hydrates, the ocean source or a combination of the two is more likely to fit the budget. Tropical wetlands, in contrast, contribute most to the difference and become an integral part of the revised budget. The YD results therefore support a tropical wetland $\delta^{13}C$ of ca. –53 ‰. Finally, the results confirm that it is necessary to account for changing $\delta^{13}C$ values of various source types, which are dependent on C_3 or C_4 plants as a precursor material. The high $\delta^{13}C_{CH4}$ measured in ice samples proves that C_4-derived methane was more abundant in the Younger Dryas, as must be expected in an environment with low atmospheric CO_2 concentration.

5.2.2. Preservation of $\delta^{13}C_{CH4}$ in ice occlusions

So far it has been assumed that atmospheric $\delta^{13}C_{CH4}$ is truthfully preserved once the gas is enclosed in air bubbles. The discrepancy between measured and calculated values in both the PIH and YD could be a sign that this is not the case. The only way to affect the isotopic composition of methane in the occlusions is by adding isotopically different methane or removing gas in a process that involves an isotope effect. Diffusion of gases in glacier ice has been observed for Helium (Raynaud et al., 1993) and for other noble gases if ambient temperatures are not low enough (Severinghaus, personal communication), but not for methane. It is not obvious, however, that this would be true over thousands of years and methane could have diffused through the ice lattice. The strongest argument against this possibility is the existence of steep concentration

gradients in the ice record. For example, in the GISP2 core methane concentration increases from 500 to 700 ppbV over a 7 m interval at the end of the YD, and steeper gradients have been observed in other cores and the Pakitsoq field site. Such strong gradients would have surely been smoothed if methane was mobile in ice. Also, the YD ice contains a local minimum of methane concentration. Any diffusive flux would be directed towards this layer and tend to enrich the gas with faster diffusing $^{12}CH_4$ (see Chapter 2.2). This is the opposite of the observed trend.

Campen et al. (2003) found anomalously high methane concentrations in glacier ice from the Andes and concluded that methane was being produced in the ice. The precursor material must be either organic compounds in dust particles or CO_2 in the air occlusions. Although the study was done in a location with higher average temperatures (-10 °C versus less than -30 °C in Central Greenland; Cuffey and Clow, 1997), which facilitates microbial activity, it must be investigated if Greenland ice could have undergone *in situ* methanogenesis. This process enriches methane in ^{13}C, provided that the precursor material is used near quantitatively in a Rayleigh distillation. A mixing calculation shows that at least 8 % to 26 % (depending on the assumed metabolic pathway) of occluded gas must be generated in situ to account for the potential three per mille isotope shift. These are minimum estimates assuming that all precursors were consumed quantitatively. While this may be reasonable if the latter are organic compounds, it is quite improbable for CO_2-reduction, on which the lower margin of the estimate is based. Campen et al. (2003) pointed out that methanogenesis in ice can occur only in diffusion limited interstices between the ice grains, so that any precursor available to the microbes would be used completely. Nevertheless, it is unlikely that CO_2-reduction should occur without any isotope effect.

Consequently, an isotopic excursion as measured in the Pakitsoq samples would require a substantial input of *in situ* generated methane. The good agreement between Pakitsoq concentration values and those of ice cores from various locations refutes this possibility. In situ methane production and hence concentration should depend on the availability of organic molecules, temperature and maybe crystallography of the ice. Ice

cores from a variety of locations representing a range of physical and environmental conditions show remarkable agreement of methane concentration (Raynaud et al., 1993; Chappellaz et al., 1997; Petit et al., 1999; Brook et al., 2000). A measurable amount of methane production in polar ice cores is therefore ruled out.

Alternatively, occluded methane could have been partly consumed by methanotrophic bacteria. This process leads to enrichment in ^{13}C at a degree that depends on the fraction of methane consumed. A calculation with the Rayleigh distillation equation shows that the loss of methane necessary to account for the observed $\delta^{13}C_{CH4}$ difference is between 15 and 48 % of the initial concentration. This is based on fractionation factors associated with microbial methane oxidation between 1.005 and 1.02, as found in aquatic, sediment and soil environments (Whiticar and Faber, 1986; Tyler et al., 1994). Methane loss of this magnitude is not observed in ice samples, neither in Pakitsoq where concentrations are slightly higher than in GISP2, nor in ice cores in general, which agree closely with each other as discussed above. Therefore in situ microbial activity as well as diffusion cannot explain the observed enrichment in ^{13}C.

5.2.3. Glacial and deglacial methane sources

The $\delta^{13}C_{CH4}$ values measured in the YD show that the global methane budget was fundamentally different from that in the late PIH. The exact time when the shift between the two occurred is not clear. A study by Etheridge et al. (2003) shows that this may have been the case after 400 yr BP, but this is not conclusive because the main history of the Holocene is unknown. The question is important to determine whether the changed budget is a consequence of different climatic conditions during the YD or due to other causes. Until further information is available the isotope record must be examined for the possible influence of climate.

During the transition from the last ice age to the Holocene, the YD is a time when large parts of the Northern Hemisphere and tropical regions experienced cooling to near glacial conditions (Broecker, 2003). Although other areas were not affected and even continued to warm (Blunier et al., 1997; Morgan et al., 2002), regions that are important

for methane production were strongly affected by the temperature reversal. This is documented in the low concentrations recorded between the warm Bølling-Allerød and Preboreal periods (Chappellaz et al., 1993a; Brook et al., 1996). At the same time, ice sheets continued to retreat, although at a reduced pace (Fairbanks, 1989). Ocean circulation reorganized to a glacial pattern during the YD (Broecker, 2003; see references in Marchal et al., 1998, for a different point of view). The permafrost boundary and vegetation patterns adjusted to the changing conditions. Any of these changes could have affected different source types to varying degrees and in different ways, exerting a dominant control on the isotope budget of methane.

A direct effect of temperature alone, e.g. on fractionation coefficients of methanogenesis, cannot have affected the mass balance, because values in the warmer PB are similar. Termite emissions are supposedly independent of climatic conditions in terms of isotopic composition (Tyler et al., 1988) and magnitude (Chappellaz et al., 1993b), although Petit-Maire et al. (1991) cite evidence for higher activity in wetter climates. Any deviation from the assumed values within a reasonable range does not significantly affect the total methane budget. For example, if the emissions were more ^{13}C rich due to more C_4 vegetation (which is not supported by the findings of Tyler et al, 1988) $\delta^{13}C$ of the global source would increase by less than 0.2 ‰. Wild animals were assumed to be more abundant under glacial conditions by Chappellaz et al. (1993b), due to larger grassland ecosystems. Vegetation change certainly lagged the deglaciation process and ruminants probably produced more methane in the YD than assumed in Scenarios 1 and 2, but that would lead to lower $\delta^{13}C_{CH4}$ values, if only by 0.2 ‰.

Charcoal records show that biomass burning varies with climatic conditions. Periods of climate change and with high climatic variability experience more fires (Haberle and Ledru, 2001), especially during global cooling when regions with high biomass transgress into drier regimes (Bird and Cali, 1998). According to the latter findings, the YD should not have a strong methane flux from fires. The YD was a period of exceptionally high biomass burning in Central and South America according to Haberle and Ledru (2001). The study, however, found that at the same time Indonesia

and Papua New Guinea did not have a lot of wildfires, so that there is no global record of increased biomass burning during the YD. Haberle and Ledru (2001) stress the impact of humans on the fire record. The YD coincides with human migration into the Americas, which increases biomass burning through prescribed burns, but no other areas. To test the sensitivity of the methane isotope budget to increased biomass burning in the Americas it is here assumed that the area prone to fires comprises 25 % of global land surface (i.e. the percentage area of the Americas) and that burning increased by an arbitrary factor of five, knowing that both estimates are rather too high. In that case atmospheric $\delta^{13}C_{CH4}$ would increase by 0.5 ‰. This is a significant change, but not enough to account for the discrepancy between measured and calculated isotope values. Also, other studies show that the YD was not a period of high biomass burning in other parts of North America (MaenzaGmelch, 1997).

Theoretically, the ocean environment during the YD was more conducive to methane emissions in some regards but less favourable in others. Total surface area and the percentage of shallow seas decreased with lower sea levels. Together with a smaller concentration gradient between water and atmosphere and higher solubility of gas in colder water this would lead to lower emissions. In contrast, the inundation of terrestrial biomass on newly flooded shelf during the sea level rise and higher open water productivity (Hausman and McElroy, 1999; Sigman and Boyle, 2000) could cause higher methane flux to the atmosphere. The various factors may have partly compensated each other's impact and it is highly speculative what the cumulative effect was. Due to the small methane flux from oceans, it would require substantial changes in the ocean source to affect the methane budget. In the absence of compelling evidence a major influence of the ocean source on the YD methane budget is not considered.

Geologic methane emissions are controlled by tectonic activity and should be largely independent of climate. Cold and dry conditions, however, reduce microbial activity in soils, which consumes methane in micro-seepage areas. Geologic methane emissions could therefore have been higher in the YD (Etiope and Klusman, 2002). Ice cover will block thermogenic methane from reaching the atmosphere and the gas could

be stored as clathrate in bedrock or soil. During the YD, geologic methane emissions were likely somewhat lower due to this blocking effect. The continuously retreating ice, however, could have released the stored clathrates in gas vents, as they are documented in Sweden (Mörner and Etiope, 2002). This could compensate or exceed the blocking effect, but it is impossible to quantify the respective factors. The isostatic disequilibrium caused by retreating ice sheets could have enhanced tectonic activity and with it geologic emissions, again any estimate of this effect remains speculative. Geologic methane emissions may have been higher in the YD but the modern value is the only quantifiable estimate and consequently used in budget scenarios.

Receding permafrost will release methane from terrestrial gas hydrates (Nisbet, 1989, 1992). Although the cooling of the YD would have slowed this process, it could theoretically account for a significant flux. The emitted methane, however, is strongly depleted in ^{13}C and cannot explain why the measured $\delta^{13}C_{CH4}$ is high. Only methane from flooded arctic continental shelf areas would be ^{13}C-rich, if a substantial part was oxidized on its way to the atmosphere. This would also decrease the total flux from a source area that is of limited size, so it is not expected to make a significant contribution. Marine gas hydrate should have been stabilized in the YD by rising sea levels and cold water.

Wetlands, being the largest source and very climate sensitive, have the most potential to influence the isotope balance. While C_4-derived methane emissions stay fairly constant over climatic transitions, it is specifically the flux of C_3-derived methane in tropical wetlands (through the $\delta^{13}C$ of this source) as well as boreal wetlands (through the magnitude of these emissions) that determines the global isotope budget (see Chapter 4.2). For the YD scenarios it was assumed that C_3 wetland emissions increased proportionally to atmospheric concentrations, thereby decreasing atmospheric $\delta^{13}C_{CH4}$. The YD ice core data suggest that wetland emissions rather reverted to a true glacial pattern with a nearly quantitative shut-down of boreal methane production and strong reduction of C_3-derived methane emissions in temperate and tropical areas. The *a priori* LGM scenario, including geologic emissions and revised $\delta^{13}C$ values for tropical

wetlands, matches the measured $\delta^{13}C_S$ almost exactly (-46.1 ‰). This is a strong argument that conditions in the YD were similar to a fully glacial environment.

A method by Dällenbach et al. (2000) and Brook et al. (2000) provides a test for this hypothesis, which states that boreal methane production was low during the YD. Both groups measured the interhemispheric concentration gradient of methane, which is recorded in ice cores from Greenland and Antarctica, during various periods of the last termination. With a three-box atmospheric transport model they reconstructed the amount of methane emitted in the tropics, as well as in northern and southern latitudes. Dällenbach et al. (2000) find that boreal methane flux almost triples its relative contribution between the late glacial period and YD. This closely matches the source reconstructions by Chappellaz et al. (1993b) on which the *a priori* budgets of this study are based. In contrast, Brook et al. (2000) found that the percentage of boreal methane in YD and LGM is the same. The main difference to the results from Dällenbach et al. (2000), however, is not the geographical source distribution of the YD but that of the LGM. Consequently, the results by Brook et al. (2000) do not imply that in the YD northern wetlands were shut down but rather that Chappellaz et al (1993b), and consequently this study, underestimated this source for the LGM.

Due to the conflicting results from transport models and isotope measurements the distribution pattern of wetlands during the YD cannot be resolved with high certainty. The uncertainties of either reconstruction method would allow at least for a partial shut-down of boreal wetlands in the YD, although not as much as calculated for the LGM by Chappellaz et al. (1993b).

The semi-transitional character of the YD could also have affected methane emissions from wetlands in a different way. Continuously retreating ice sheets indicate that the permafrost boundary moved as well. A modern analogy for this situation comes from Eastern Siberia (Nakagawa et al., 2002), where methane production from pre-glacial organic material in newly formed lakes and wetlands is high. The reported $\delta^{13}C$ of this gas, however, is close to –60 ‰. Even though there may be some variation in this value,

the reported measurements indicate that the methane is far more ^{13}C-depleted than the necessary value of –49 ‰ and cannot balance the YD methane budget to the observed $\delta^{13}C_{CH4}$.

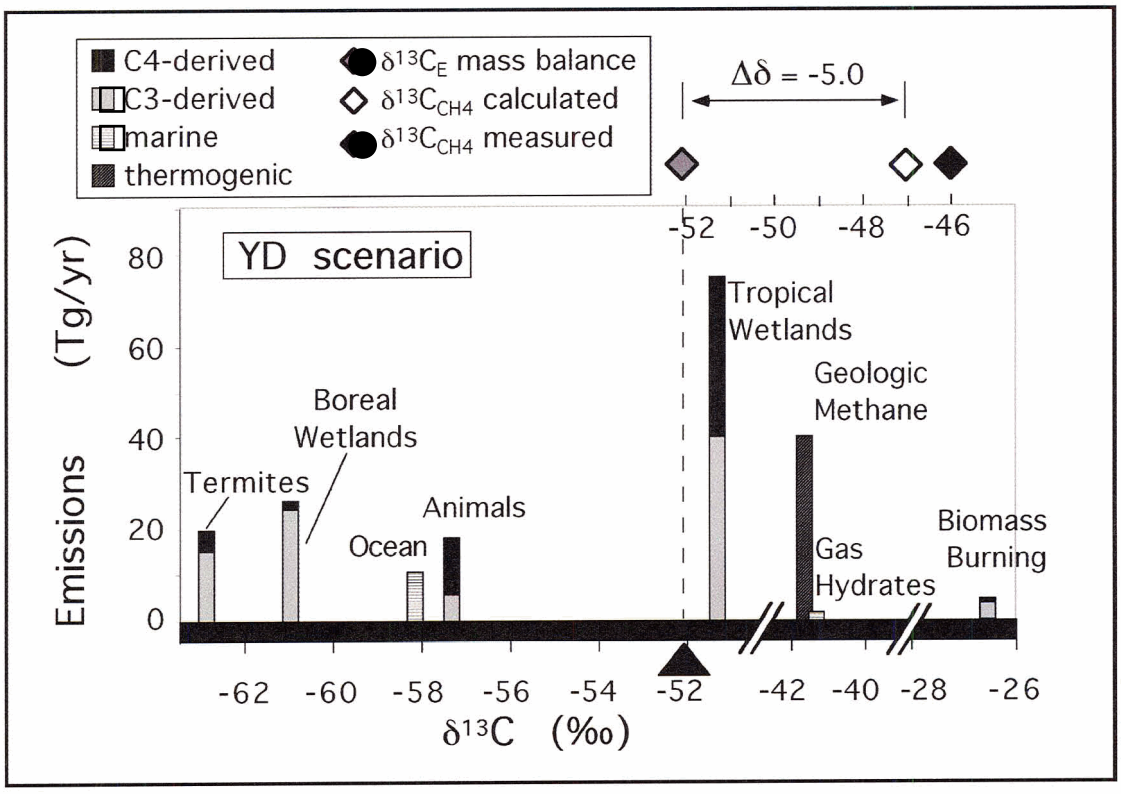

Fig. 5.2.2: Methane budget for the Younger Dryas
The diagram shows a methane budget as calculated in Scenario 3 for the YD. Emission rates are interpolated between the PIH and LGM values of Chappellaz et al. (1993b). Geologic emissions are included and $\delta^{13}C$ of tropical wetlands and gas hydrates are adjusted to higher values. The vegetation pattern of C_3 and C_4 plants is assumed to be glacial. The calculated total source is more depleted in ^{13}C than ice measurements suggest. Possibly the ocean source has a higher $\delta^{13}C$ than shown. Also, boreal wetland emissions could have been smaller, which would account for the difference.

5.2.4. Discussion of the YD methane isotope budget

There are no signs of post-occlusion alteration of methane in polar ice. Yet, the measured $\delta^{13}C_{CH4}$ value is higher than *a priori* estimates (Table 5.2.1 and Figs. 5.2.1 and 5.2.2). The offset would be even bigger if the isotopic composition of the sources had not been adjusted to the appropriate C_3/C_4-distribution. The discrepancy supports the hypothesis that geologic methane emissions are an integral part of the natural methane cycle and that methane emitted from tropical wetlands, gas hydrates and the ocean may be more ^{13}C-rich than is commonly estimated. A revised budget including these changes is closer to the measured value, although a difference of 1.4 ‰ remains. This offset is substantial. It means that the proposed methane budget either overestimates ^{13}C-depleted methane emissions (boreal wetlands, ruminants, termites, ocean, gas hydrates) by 40 % or a ^{13}C-rich source (ca. -40 ‰) that comprises more than 13 % of total emissions is missing.

Various environmental proxies suggest that the YD had a climate that was similar to the LGM (Grootes et al, 1989; Maslin and Burns, 2000). The corresponding contribution of wetland emissions would balance the isotope budget, but is in conflict with the findings of Dällenbach et al. (2000) and Brook et al. (2000). If the climatic conditions were closer to the LGM, so would be the pattern of C_3 and C_4 vegetation. Adjusting the $\delta^{13}C$ of sources that depend on this parameter results in a slightly higher $\delta^{13}C_E$, namely by 0.3 ‰. Together with a decrease of C_3-dominated wetlands (within the uncertainty of the studies by Dällenbach et al., 2000 and Brook et al., 2000), this could account for a fair amount of the remaining discrepancy. A methane budget that includes all outlined adjustments is presented as Scenario 3 in Table 5.2.1. With the currently available evidence, this is a best guess that is in reasonable agreement with the measured $\delta^{13}C_{CH4}$ value of –46 ‰.

5.3. Methane isotope budget of the YD termination

The interpretation of $\delta^{13}C_{CH4}$ values during the YD termination suffers from the uncertainties of the YD isotope budget, which is the baseline for variations. Nevertheless, the observed deviations (or lack thereof) from YD values can be used to examine the changing methane cycle. The latter is of interest because it provides information about environmental conditions in widespread areas, and elucidates the role of methane in climatic reorganizations. The transition period comprises ca. 150 yrs when atmospheric methane concentrations rise from about 500 to 700 ppbV. Obviously, methane emissions from one or several source types increase strongly to drive the increase. Calculations with a one-box model as used by Tans (1997) (see Chapter 4.3.1) allow estimates of magnitude and isotopic composition of this source. A two- or three-box model does not provide more information, because there are no constraints on isotope numbers other than in the Northern Hemisphere.

The difference between $\delta^{13}C_{CH4}$ in the YD and the PB is within the error margin of the measurements and should not receive much focus in the interpretation. Nevertheless, the presented model scenario (Table 5.3.1, Fig. 5.3.1) assumes that there is a transition source with slightly higher $\delta^{13}C$ that gets progressively added to the budget until it equals the observed and estimated values for the PB. The transition source as modeled reaches a maximum of 33 Tg/yr. It is over 1 ‰ more ^{13}C-rich than the total YD source, which depends on the model assumption and is an upper limit for this value. Its most likely range is –51 to –49.5 ‰.

Table 5.3.1: One-box model of YD termination parameters and output

	YD	Transition source	PB
CH_4 concentration	509 ppbV		756 ppbV
Total source	157 Tg/yr	33 Tg/yr	190 Tg/yr
$\delta^{13}C$ source	-50.8 ‰	-49.6 ‰	-50.6 ‰
Atmospheric $\delta^{13}C_{CH4}$	-46.0 ‰		-45.8 ‰

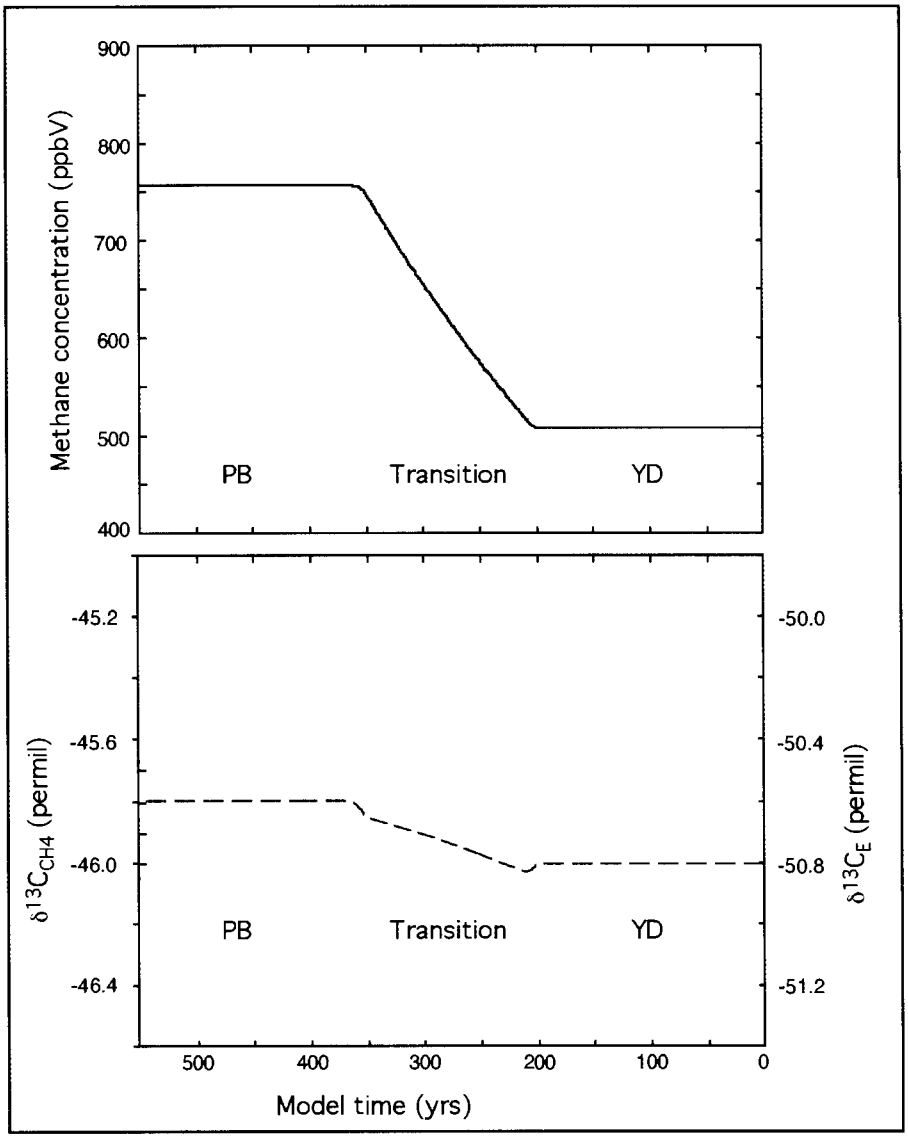

Fig. 5.3.1: One-box model for the YD termination
Top panel shows atmospheric methane concentration, bottom panel atmospheric $\delta^{13}C_{CH4}$. Model parameters were chosen to fit the Pakitsoq record. Source strength after Chappellaz et al. (1993b). The modeled curves are the signal recorded in Greenland, which differs from the global average (Chappellaz et al., 1997; Quay et al., 1999) by a negligible amount. The transition starts at 200 yrs model time and lasts for 150 yrs. The curve in the lower panel can be read as either atmospheric isotope composition (left scale) or $\delta^{13}C_E$ (right scale). The model run determines the transition source at $\delta^{13}C$ = -49.6 ‰. The small dip in $\delta^{13}C_{CH4}$ at its beginning and the jump at its end result from the dilution effect (see Chapter 4.3), which has been corrected for in the data. Note that the scale exaggerates the differences in $\delta^{13}C_{CH4}$, which are within the analytical uncertainty.

What has been termed the transition source so far is not necessarily emissions from only one source type. The fact that $\delta^{13}C_{CH4}$ basically does not change throughout the transition means that theoretically all sources could have increased in step. Alternatively, a few sources, whose isotope balance happened to equal the total source, could have caused the concentration rise. The last case seems to be too coincidental to present a serious possibility. A uniform increase of all source types is also unlikely, because the various emissions are controlled by such different parameters. For example, there is no reason why methane flux from wetlands, termites and the ocean should have increased in synchronicity. The sudden additional flux from a single source alone is challenging to explain and will be the focus of the following discussion.

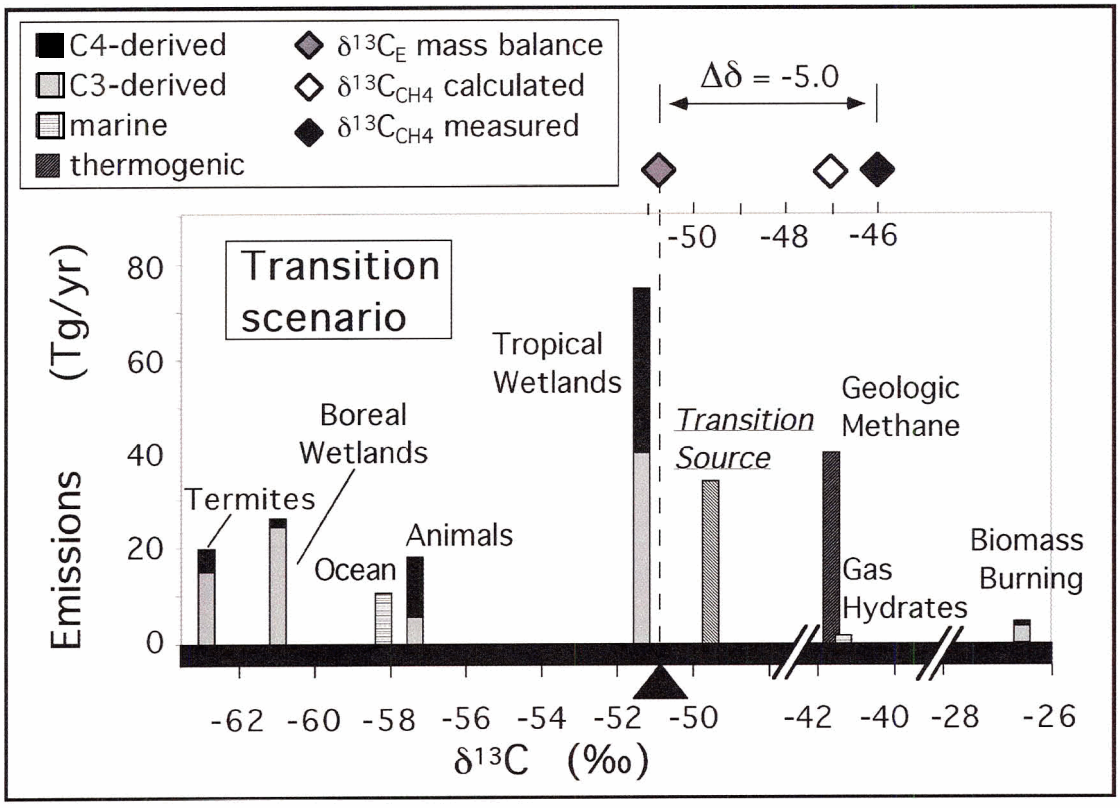

Fig. 5.3.2: Methane budget for the YD to PB transition
This budget is based on the YD Scenario 3. The additional source that drives the increase in atmospheric concentration is included. Of the known natural methane sources tropical wetlands show by far the best match in isotopic composition to the transition source.

5.3.1. Wetlands as drivers of the concentration increase

There is no source type in the YD methane budget that exactly matches the modeled $\delta^{13}C_{CH4}$ of the transition source (-49.6 ‰), but tropical wetlands are conspicuously close in isotopic composition. The next closest ones are geologic methane and wild animals. Ruminant emissions are easily ruled out as they could not have doubled their methane output over just a few generations. Geologic methane emissions have the potential to supply enough methane for the increase, but it would require twelve gas fields of average size to completely and simultaneously be drained, or a single one that would be half as big as the largest presently known reservoir. Two arguments speak against geologic emissions. For one, they have a higher $\delta^{13}C$ than the observed source. While methane emissions can become enriched in ^{13}C, e.g. by oxidation processes, there is no mechanism to deplete them. For the other, while it is conceivable that there are bursts of geologic methane, they are not linked to climatic changes. It seems too much of a coincidence that such a burst should have occurred right at the end of the YD but has not been observed ever since (Blunier et al., 1995). The methane increase cannot have caused the warming either, because the latter starts first (Severinghaus et al. 1998) and the associated radiative forcing is too weak (Raynaud et al., 1993).

The close correlation between atmospheric methane concentration and the monsoon cycle, i.e. tropical climate (Chappellaz et al., 1990, Petit et al., 1999), suggests a causal link. Wang et al. (2001) provide further proof of the strong connection between East Asian monsoon cycles and the climate records of Central Greenland (and consequently methane history) from the study of speleothems in China. Petit-Maire et al. (1991) demonstrated that increased methane levels occur during wet periods in the tropics. A strong and rapid increase of precipitation at the YD termination has been demonstrated for Greenland (Alley et al., 1993), the African tropics (DeMenocal et al., 2000; Gasse, 2000) and the Amazon basin (Maslin and Burns, 2000). This could have caused the concentration increase by turning large areas into wetlands that produced excess methane. Criticism of the so-called wetland hypothesis focuses on the short response time to climatic change, which would have been only several decades according to Severinghaus et al. (1998). Extensive mature wetlands are thought to have developed

only after atmospheric methane had reached Holocene values (Nisbet, 1992; Kennett et al., 2003), but these are no precondition for methanogenesis (see also Smith et al., 2004, for new findings to wetland growth in Siberia through the earliest Holocene). If the environmental conditions necessary for methane production could have developed within less than half a century is still a matter of debate.

This study, however, shows that C_4-dominated wetland emissions not only have the potential to drive the methane increase of the YD termination, but also show the best agreement with the required isotopic composition. The isotope budget indicates that a wetland transition source is not necessarily restricted to the tropics, but could also include C_4-dominated regions in the temperate zone. The agreement of $\delta^{13}C$ values between C_4-dominated wetlands and the modeled transition source is poor for traditional estimates of wetland methane, but excellent for the revised value. This is a reasonable assumption because the number is an integral part of the YD and PIH budgets. The $\delta^{13}C$ of tropical wetlands of YD Scenario 3 (-51.4 ‰) is in excellent agreement with that of the modeled transition source (-49.5 to –51 ‰). The methane isotope record from Pakitsoq therefore supports the hypothesis that tropical or C_4-dominated wetlands caused the methane increase at the YD termination.

5.3.2. The gas hydrate theory

A widely discussed alternative to the wetland hypothesis considers emissions from destabilized gas hydrates as the cause of rising methane concentrations (MacDonald, 1990; Nisbet, 1990 and 2002; Paull et al., 1991; Kennett et al., 2003). Thorpe et al. (1996), Chappellaz et al. (1993a, 1997) and Brook et al. (2000) discussed the implications of this theory for the ice core record. All studies concluded that a gradual contribution to the methane budget could not be ruled out. The isotope budget of the YD termination seems to refute such a possibility. With typical $\delta^{13}C$ values of –60 ‰ to -65 ‰ gas hydrates are by far more depleted in ^{13}C than the transition source.

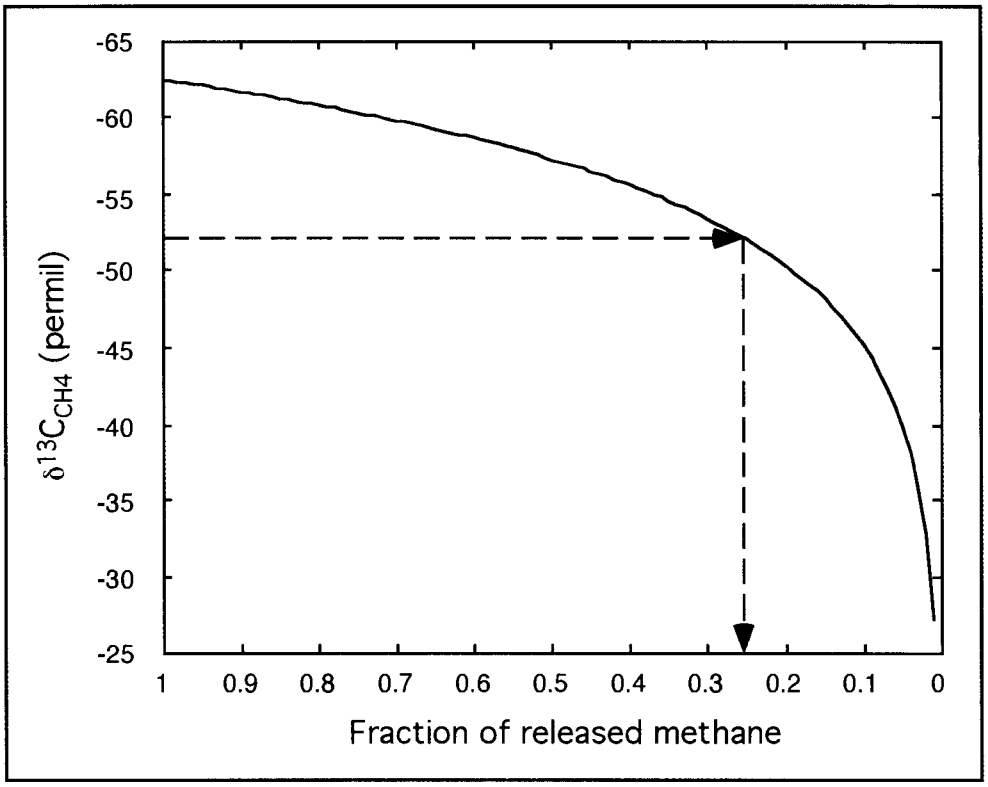

Fig. 5.3.3: Rayleigh fractionation on methane released from gas hydrates
The curve illustrates how the remaining fraction of a methane volume (initial $\delta^{13}C$ = -62.5 ‰) becomes enriched in ^{13}C as increasing amounts are oxidized on the way through sediment and water column. Arrows indicate the remaining fraction (0.26) when methane reaches the $\delta^{13}C$ of the transition source.

The argument is more complicated, however, because the quoted $\delta^{13}C$ values were measured in hydrate reservoirs, not in gas emitted from this source. Newer studies have shown that methane from marine hydrates gets severely enriched in ^{13}C while it is being partially consumed on the way through sediment and water column (Grant and Whiticar, 2002; Kastner et al., 2003). Partial oxidation provides a mechanism to explain the discrepancy in isotope numbers, but it also constrains the amount of methane that reaches the atmosphere. The necessary isotope shift of ca. 9 ‰ requires that only 26 % of the released methane is emitted to the atmosphere. This can be shown (Fig. 5.3.3) with a Rayleigh distillation calculation using a fractionation coefficient $\propto$ = 1.008 (Grant and Whiticar, 2002). Over the 150 yr transition period a total of almost 960 Tg CH_4 causes the concentration increase. Consequently, a minimum of 2,600 Tg must have been

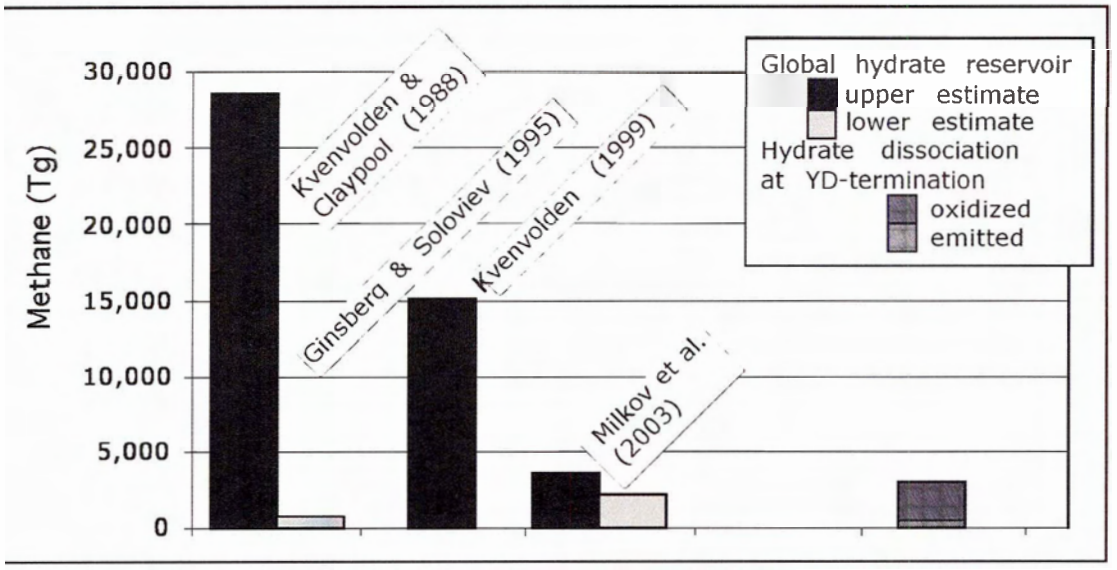

Fig. 5.3.4: Gas hydrate reservoir estimates
Upper and lower estimates for the size of the present day global gas hydrate reservoir as quoted in Kvenvolden (1999) and Milkov et al. (2003). For comparison the amount of methane that would have been mobilized during the YD-termination is shown, divided into emissions that reached the atmosphere and methane that was oxidized in sediment and water column. The total is as high as estimates by Milkov et al. (2003) and equivalent to a substantial part (>17 %) of the number given by Kvenvolden (1999).

released from destabilized methane hydrate. This amount is comparable to the most recent estimates for the global hydrate reservoir of 2,100 – 3,600 Tg (Milkov et al., 2003). Some older estimates (see Kvenvolden, 1999, and references therein) are high enough to accommodate the necessary amount of hydrate dissociation, but even the "consensus value" of 15,000 Tg in that study is regarded the upper limit of the most likely range. The global volume of methane stored in hydrates might have been different in the YD, but seen that this period followed a time of low sea levels (which destabilize hydrates) the total was likely smaller rather than larger. As seen in Fig. 5.3.4, the isotope calculation means that all or at least a large part of the marine hydrate pool would have dissociated within less than two centuries in order to account for the well documented increase in atmospheric methane. This contradicts the main argument of the clathrate gun theory, namely that the dissociation of only a small fraction of the huge reservoir would suffice to cause drastic changes in atmospheric methane concentration.

In contrast, hydrates in geographically diverse areas would have to dissociate simultaneously, which is unlikely in the light of different local topographies and oceanography. Thorpe et al. (1996) even suggested that the ice core concentration record be a lower limit of the true rise (due to diffusional smoothing and possibly resolution problems), an assumption that is necessary for the climate feedback implied by the theory. A gas hydrate source as the cause for the observed, or an even higher, concentration increase is at odds with atmospheric isotope values presented here. A catastrophic burst of methane from hydrates to the atmosphere would have been too depleted in ^{13}C, whereas a gradual release would have consumed the majority of the global reservoir.

5.4. Methane isotope budget of the Preboreal

Even more so than other time periods, the conditions for methane production in the PB are hard to estimate. After a major atmospheric reorganization climate stabilized with higher temperatures and precipitation rates, but vegetation and ice sheet configuration continued to adjust to the new conditions on different time scales. The PB has therefore both a stable and a transitional character. There are not enough independent constraints to develop a detailed methane budget for the PB. The isotope mass balance indicates that the PB methane budget was not substantially different from that of the YD, except for a higher total of emissions. If the wetland hypothesis is correct, then the higher flux comes from C_4-dominated wetlands. As ice sheets retreat and interstadial conditions develop other climate sensitive methane sources may catch up, which should be studied with an extended record of $\delta^{13}C_{CH4}$. Certain physical parameters must have been affected by the higher temperature of the PB, first of all fractionation coefficients during methane formation and methane oxidation. Calculations presented in Chapter 4.2.1 suggest that the glacial methane could therefore be ^{13}C-depleted by around 1 ‰. This difference is not evident in values measured in the PB and YD, which indicates that the temperature dependence of fractionation processes during methane production and removal is not important for the isotope budget.

6. Conclusions

The work presented in this study is based on the development of a novel technique to extract gas from ice samples and measure the stable carbon isotope ratio in the liberated methane. These measurements require small amounts of sample (150 g to 200 g), which makes it possible to study changes in the methane cycle thousands of years ago with a temporal resolution on the order of decades. First results agree with other methods and are precise enough to detect past changes in methane isotope composition. The method was applied to samples from three different locations covering four distinct periods since the end of the Pleistocene.

Theoretical considerations and calculations based on independent studies, as well as model results, provide a framework for the interpretation of the measured data. In a pristine environment atmospheric methane removal by chlorine was lower. The soil sink changed because there was no restriction of methane uptake due to agriculture on one hand, but diffusional flux was lower as the result of a different concentration gradient on the other. The cumulative effects decrease the offset between $\delta^{13}C$ of the total source and atmospheric methane from –6.3 ‰ today, to –5.3 ‰ in the PIH, -5.0 ‰ in the YD and –5.1 ‰ in the LGM. The offset was quite insensitive to the climatic and environmental changes at the end of the last ice age.

Anthropogenic changes also affect isotopic composition of natural source types. Together with environmental parameters they determine the distribution of plants that use the C_3 or C_4 photosynthetic pathway and with it the isotopic composition of methane precursors. Emissions from wild animals, biomass burning and wetlands were therefore different in the past. The effect on the total source composition is small in the pre-industrial Holocene, but results in a ca. 2 ‰ enrichment of ^{13}C in glacial times. The main factor is the abundance of C_3-dominated wetlands in all latitudes. These results carry a large degree of uncertainty, they require further study with sophisticated models. Despite of this, they are confirmed qualitatively through the ice core data from the YD.

The influence of atmospheric transport and mixing processes, e.g. in the form of latitudinal gradients, is mostly negligible for the interpretation of ice core data. An exception is the so-called atmospheric dilution effect that lowers atmospheric $\delta^{13}C$ when methane concentrations rise. The impact can be modeled and corrected for. The same is true for isotopic fractionation during diffusion of air in the unconsolidated snow layer, with additional correction factors derived from measurements of nitrogen isotopes.

The measured isotope record, which covers the late pre-industrial Holocene and documents the transition from the Younger Dryas to the Preboreal, does not seem to be affected by alterations after occlusion of the gas. The values represent the true atmospheric signal. For the Late PIH, the data show that the natural methane budget is more enriched in ^{13}C (by 4 ‰) than previously assumed (measured value of $\delta^{13}C_{CH4}$ = -49.6 ‰). Emissions of thermogenic methane from tectonically active areas can account for part of the difference, as do revised $\delta^{13}C$ values for the ocean and gas hydrate source. The results suggest that methane from tropical wetlands must be substantially enriched in ^{13}C ($\delta^{13}C$ = -53 ‰) compared to common estimates ($\delta^{13}C$ = -58 ‰), in accordance with several reported field measurements. An anthropogenic influence on the methane cycle before the industrial period may be detectable in the presented record, although this result is speculative and partly based on preliminary data from a different study. If confirmed, the data would indicate that irrigated agriculture, i.e. rice farming, and not biomass burning caused the major man-made impact before industrialization. A scenario that combines a revised isotopic composition for tropical wetlands, a geologic methane source, as well as early anthropogenic emissions from irrigated agriculture is the only one to explain both the measured atmospheric isotope signatures reported in this study and a recently discovered depletion in ^{13}C in the last centuries before the industrial revolution.

The data for the Younger Dryas ($\delta^{13}C_{CH4}$ = -46.0 ‰) support that the distribution of C_3 and C_4 vegetation under different climatic regimes affects the methane budget and that a distinction between different wetland types has to be made. Suitable classifications are either by latitude or by vegetation type (using the C_3 or C_4 photosynthetic pathway),

although the two parameters are correlated. According to the isotope data the methane cycle of the Younger Dryas was closer to a glacial than an intermediate mode, although this is in conflict with atmospheric concentration data and independent studies. During the YD termination C_4-dominated wetlands are the most likely cause of the well-documented concentration increase to Holocene values, because their isotopic signature (-53 ‰) matches the reconstructed source of the concentration rise (-51 ‰). Marine gas hydrates cannot be the driver of the increase. A rapid release of methane from this source would be more depleted in ^{13}C than the measurements in this study require. A slow release of methane from clathrates would lead to ^{13}C-enricment of this source because substantial amounts would be oxidized during transport to the atmosphere. Due to this mechanism gas hydrates could produce methane with the observed $\delta^{13}C$, but then the required total flux (i.e. four times of the amount reaching the atmosphere) would equal or exceed the global hydrate reservoir. This supports the hypothesis that in the natural system increased methane concentrations are a result of climate change and not its driver.

The Preboreal methane cycle ($\delta^{13}C_{CH4}$ = -45.8 ‰) is still governed by environmental conditions as they were established in the Younger Dryas and during the transition period. This shows that physical parameters, like the temperature dependence of fractionation coefficients, are of minor influence while environmental factors control the methane cycle.

If the results of this study are confirmed it would affect modern methane budgets and the role of anthropogenic emissions should be re-examined. At this point, however, it may be premature to take such a step. Some of the results presented here are preliminary or uncertain to some degree. To extend the record back to the last glacial maximum and over the complete Holocene would address many of these issues. As expected, a record of the isotopic composition of methane does not supply definite answers for methane budgets of the past. Nevertheless, it provides useful and important constraints for the methane cycle and its role in climate change.

Appendix

A.1. Calculating $\delta^{13}C$ of source types (Chapter 4.2)

A.1.1. Calculation of $\delta^{13}C$ from animals

The isotopic composition of methane produced by ruminants is calculated as:

$$\delta^{13}C = F_3 \times \delta^{13}C_3 + F_4 \times \delta^{13}C_4 \qquad \text{(A.1)}$$

where F_3 and F_4 are the proportions of C_3 and C_4 plants in grasslands at the time according to Collatz et al. (1998) and $\delta^{13}C_3$ and $\delta^{13}C_4$ are the average isotopic compositions of methane produced by cows on a pure C_3 and C_4 diet respectively. Note that this approach neglects all forest dwelling animals.

A.1.2. Calculation of $\delta^{13}C$ from wild fires

To calculate the methane emissions (E) produced in a certain ecosystem annually the following equation applies:

$$E = B \times f \times a \times b \qquad \text{(A.2)}$$

where B is the above ground biomass of the ecosystem (data from Adams et al., 1990 and Prentice et al., 1993);

f is 1/natural fire frequency (data from Wright and Bailey, 1982 and DeBano et al., 1998);

a is the fraction of biomass burnt (Hao and Ward, 1993);

b is the amount of methane produced per unit of burned biomass (Hao and Ward, 1993). The methane produced from C_3 and C_4 plants in grasslands was taken to be proportional to the distribution stated in Collatz et al. (1998).

The isotope ratio of methane from biomass burning is then:

$$\delta^{13}C = \sum_1^n (E_i \times \delta_i) / \sum_1^n E_i \qquad \text{(A.3)}$$

where δ_i ranges between –17 ‰ and –30 ‰ (Chanton et al., 2000) for ecosystems i = 1,…,n in dependence of C_4 and C_3 plants (data from Collatz et al., 1998). Many of these parameters are not well known or have been measured only for certain conditions. The results of these calculations overestimate the annual amount of burned biomass and consequently the release of methane from wild fires by a factor of 100. The major source

for errors is presumably data on fire frequency. One can argue that the calculated relative shift is still realistic as it is quite insensitive to fire frequencies within the quoted range.

A.1.3. Calculation of $\delta^{13}C$ from wetlands

First the $\delta^{13}C$ of wetland methane emissions (E_3 and E_4) from C_3 and C_4 environments is calculated, assuming that total wetland methane emissions E_{To} today have an isotopic composition ($\delta^{13}C_{To}$) of –60 ‰ and $\delta^{13}C_3$ is lower than $\delta^{13}C_4$ by 12 ‰. Then

$$\delta^{13}C_{To} \times E_{To} = \delta^{13}C_3 \times E_3 + (\delta^{13}C_3 - 12) \times E_4 \quad \text{(A.4)}$$

Using data from Chappellaz et al. (1993b) results in $\delta^{13}C_3$ = -62.3 ‰ and $\delta^{13}C_4$ = -50.3 ‰. These values in a mass balance with additional data from Chappellaz et al. (1993b) give $\delta^{13}C_{To}$ for LGM and PIH. The underlying assumptions are as follows: all boreal and temperate wetlands produce only C_3 derived methane. Tropical wood and shrub-lands are assumed to produce 50 % CH_4 from woody plants (all C_3) and 50 % from grasses (both C_3 and C_4). For the latter as well as the grassland sources the percentages of C_3 to C_4 plants are given in Collatz et al. (1998).

A.2. Three-box atmospheric methane model (Chapter 4.3)

Methane concentrations in the North, tropics and South are:

$$[CH_4]_N = [CH_4]_{N_0} + t \times (E_N - \lambda_N \times [CH_4]_{N_0} - \kappa \times (2 \times [CH_4]_{N_0} - [CH_4]_{T_0})) \quad \text{(A.5)}$$

$$[CH_4]_T = [CH_4]_{T_0} + t \times (E_T - \lambda_T \times [CH_4]_{T_0} + \kappa \times (2 \times [CH_4]_{N_0} - [CH_4]_{T_0}) - \kappa \times ([CH_4]_{T_0} - 2 \times [CH_4]_{S_0})) \quad \text{(A.6)}$$

$$[CH_4]_S = [CH_4]_{S_0} + t \times (E_S - \lambda_S \times [CH_4]_{S_0} + \kappa \times ([CH_4]_{T_0} - 2 \times [CH_4]_{S_0})) \quad \text{(A.7)}$$

Isotopic compositions in the respective boxes are:

$$\delta^{13}C_N = (((\delta^{13}C_{N_0} + 1000) \times [CH_4]_{N_0} + t \times ((\delta^{13}C_{N_E} + 1000) \times E_N - \alpha \times \lambda_N \times (\delta^{13}C_{N_0} + 1000) \times [CH_4]_{N_0} - \kappa \times ((\delta^{13}C_{N_0} + 1000) \times 2 \times [CH_4]_{N_0} - (\delta^{13}C_{T_0} + 1000) \times [CH_4]_{T_0}))) / [CH_4]_N) - 1000 \quad \text{(A.8)}$$

$$\delta^{13}C_T = (((\delta^{13}C_{T_0} + 1000) \times [CH_4]_{T_0} + t \times ((\delta^{13}C_{T_E} + 1000) \times E_T - \alpha \times \lambda_T \times (\delta^{13}C_{T_0} + 1000) \times [CH_4]_{T_0} + \kappa \times ((\delta^{13}C_{N_0} + 1000) \times 2 \times [CH_4]_{N_0} - (\delta^{13}C_{T_0} + 1000) \times [CH_4]_{T_0}) - \kappa \times ((\delta^{13}C_{T_0} + 1000) \times [CH_4]_{T_0} - (\delta^{13}C_{S_0} + 1000) \times 2 \times [CH_4]_{S_0}))) / [CH_4]_T) - 1000 \quad \text{(A.9)}$$

$$\delta^{13}C_S = (((\delta^{13}C_{S_0} + 1000) \times [CH_4]_{S_0} + t \times ((\delta^{13}C_{S_E} + 1000) \times E_S - \alpha \times \lambda_S \times (\delta^{13}C_{S_0} + 1000) \times [CH_4]_{S_0} + \kappa \times ((\delta^{13}C_{T_0} + 1000) \times [CH_4]_{T_0} - (\delta^{13}C_{S_0} + 1000) \times 2 \times [CH_4]_{S_0}))) / [CH_4]_S) - 1000 \quad \text{(A.10)}$$

where T stands for the tropical box; other parameters as listed for equations (4.6) through (4.11) in Chapter 4.3. κ is assumed to be the same for transport between the North and the tropics and between the tropics and the South.

References

Adams, J. M., H. Faure, et al. (1990). "Increases in terrestrial carbon storage from the Last Glacial Maximum to the present." Nature **348**(711-714).

Allan, W., D. C. Lowe, et al. (2001). "Active chlorine in the remote marine boundary layer: Modeling anomalous measurements of $\delta^{13}C$ in methane." Geophysical Research Letters **28**(17): 3239-3242.

Alley, R. B., D. A. Meese, et al. (1993). "Abrupt increase in Greenland snow accumulation at the end of the Younger Dryas event." Nature **362**: 527-529.

Bartlett, K. B., and R. C. Harriss, (1993). "Review and assessment of methane emissions from wetlands." Chemosphere **26** (1-4): 261-320.

Battle, M., M. Bender, et al. (1996). "Atmospheric gas concentrations over the past century measured in air from firn at the South Pole." Nature **383**: 231-235.

Bilek, R. S., S. C. Tyler, et al. (2001). "Investigation of cattle methane production and emission over a 24-hour period using measurements of $\delta^{13}C$ and δD of emitted CH_4 and rumen water." Journal of Geophysical Research **106**(D14): 15,405-15,413.

Bird, M. I. and J. A. Cali (1998). "A million-year record of fire in Sub-Saharan Africa." Nature **394**: 767-769.

Blunier, T., J. A. Chappellaz, et al. (1995). "Variations in atmospheric methane concentration during the Holocene epoch." Nature **374**: 46-49.

Blunier, T., J. Schwander, et al. (1997). "Timing of the Antarctic Cold Reversal and the atmospheric CO_2 increase with respect to the Younger Dryas." Geophysical Research Letters **24**(21): 2683-2686.

Boehme, S.E., N. E. Blair, et al. (1996). "A mass balance of C-13 and C-12 in an organic-rich methane-producing marine sediment." Geochimica et Cosmochimica Acta 60(20): 3835-3848.

Boersma-Klein, V. and A. E. De Vries (1966). "The influence of the distribution of atomic masses within the molecule on thermal diffusion." Physica **32**: 717-733.

Bréas, O., C. Guillou, et al. (2001). "The global methane cycle: isotopes and mixing ratios, sources and sinks." Isotopes in Environmental and Health Studies **37**: 257-379.

Broecker, W. S. (2003). "Does the trigger for abrupt climate change reside in the ocean or in the atmosphere?" Science **300**:1519-1522.

Brook, E. J., T. Sowers, et al. (1996). "Rapid variations in atmospheric methane concentration during the past 110,000 years." Science **273**: 1087-1091. Data archived by the World Data Center for Paleoclimatology, Boulder, Colorado, USA.

Brook, E. J., S. Harder, et al. (2000). "On the origin and timing of rapid changes in atmospheric methane during the last glacial period." Global Biogeochemical Cycles **14**(2): 559-572. Data archived by the World Data Center for Paleoclimatology, Boulder, Colorado, USA.

Burchard, I. (1998). "Anthropogenic impact on the climate since man began to hunt." Paleogeography, Paleoclimatology, Paleoecology **139**: 1-14.

Burke, Jr., R. A., and W. M. Sackett (1986). "Stable hydrogen and carbon isotopic composition of biogenic methane from several shallow aquatic environments." In: Sohn, M. L. (Ed.), Organic Marine Geochemistry (Washington, D.C., USA): 297-313.

Burke, Jr., R. A., T. R. Barber, et al. (1988). "Methane flux and stable hydrogen and carbon isotope compositions of sedimentary methane from the Florida Everglades." Global Biogeochemical Cycles **2**(4): 329-340.

Bush, A. B. G. and S. G. H. Philander (1999). "The climate of the last glacial maximum: results from a coupled atmosphere-ocean circulation model." Journal of Geophysical Research **104**(D20): 24,509-24,525.

Campen, R. K., T. Sowers, et al. (2003). "Evidence of microbial consortia metabolizing within a low-latitude mountain glacier." Geology **31**(3): 231-234.

Cantrell, C. A., R. E. Shetter, et al. (1990). "Carbon kinetic isotope effect in the oxidation of methane by the hydroxyl radical." Journal of Geophysical Research **95**: 22,455-22,462.

Carcaillet, C., H. Almquist, et al. (2002). "Holocene biomass burning and global dynamics of the carbon cycle." Chemosphere **49**: 845-863.

Castro, M. S., H. L. Gholz, et al. (2000). "Effects of forest harvesting on soil methane fluxes in Florida slash pine plantations." Canadian Journal of Forest Research **30**(10): 1534-1542

Chanton, J. P., and C. S. Martens (1988). "Seasonal variations in ebullative flux and carbon isotopic composition of methane in a tidal freshwater estuary." Global Biogeochemical Cycles **2**(3): 289-298.

Chanton, J. P., G. G. Pauly, et al. (1988). "Carbon isotopic composition of methane in Florida Everglades soils and fractionation during its transport to the troposphere." Global Biogeochemical Cycles **2**(3): 245-252.

Chanton, J. P. and L. K. Smith (1993). "Seasonal variations in the isotopic composition of methane associated with aquatic emergent macrophytes of the central Amazon basin." In: The Biogeochemistry of global change: Radiative trace gases. R. S. Oremland. New York, Chapman & Hall: 619-633.

Chanton, J. P., C. M. Rutkowski, et al. (2000). "Factors influencing the stable carbon isotopic signature of methane from combustion and biomass burning." Journal of Geophysical Research **105**(D2): 1867-1877.

Chappellaz, J. A., J.-M. Barnola, et al. (1990). "Ice-core record of atmospheric methane over the past 160,000 years." Nature **345**: 127-131.

Chappellaz, J. A., T. Blunier, et al. (1993a). "Synchronous changes in atmospheric CH_4 and Greenland climate between 40 and 80 kyr BP." Nature **366**: 443-445.

Chappellaz, J. A., I. Y. Fung, et al. (1993b). "The atmospheric CH_4 increase since the Last Glacial Maximum (1). Source estimates." Tellus **45B**: 228-241.

Chappellaz, J. A., T. Blunier, et al. (1997). "Changes in the atmospheric CH4 gradient between Greenland and Antarctica during the Holocene." Journal of Geophysical Research **102**(D13): 15,987-15,997.

Cicerone, R. J. and R. S. Oremland (1988). "Biogeochemical aspects of atmospheric methane." Global Biogeochemical Cycles 2(4): 299-327.

Clark, P. U. and A. C. Mix (2002). "Ice sheets and sea level of the Last Glacial Maximum." Quaternary Science Reviews **21**: 1-7

Collatz, G. J., J. A. Berry, et al. (1998). "Effects of climate and atmospheric CO_2 partial pressure on the global distribution of C_4 grasses: present, past, and future." Oecologia **114**: 441-454.

Craig H. (1957). "Isotopic standards for carbon and oxygen and correction factors for mass spectrometric analysis of carbon dioxide." Geochimica et Cosmochimica Acta **12**: 133-149.

Craig, H., Y. Horibe, et al. (1988a). "Gravitational separation of gases and isotopes in polar ice caps." Science **242**: 1675-1678.

Craig, H., C. C. Chou, et al. (1988b). "The isotopic composition of methane in polar ice cores." Science **242**: 1535-1539.

Crowley, T. J. (1991). "Ice age methane variations" Nature **353**: 122-123.

Crowley, J. N., G. Saueressig, et al. (1999). "Carbon kinetic isotope effects in the reaction CH_4 + Cl: a relative rate study using FTIR spectroscopy." Chemical Physics Letters **303**: 268-274.

Crutzen, P. J., I. Asselmann, et al. (1986). "Methane production by domestic animals, wild ruminants, other herbivorous fauna, and humans." Tellus **38B**: 271-284.

Crutzen, P. J. and C. Bruehl (1993). "A model study of atmospheric temperatures and the concentrations of ozone, hydroxyl, and some other photochemically active gases during the glacial, the pre-industrial Holocene and the present." Geophysical Research Letters **20**(11): 1047-1050.

Cuffey, K. M. and G. D. Clow (1997). "Temperature, accumulation, and ice sheet elevation in central Greenland through the last deglacial transition." Journal of Geophysical Research **102**(C12): 26,383-26,396.). Data archived by the World Data Center for Paleoclimatology, Boulder, Colorado, USA.

Dällenbach, A., T. Blunier, et al. (2000). "Changes in the atmospheric CH_4 gradient between Greenland and Antarctica during the Last Glacial and the transition to the Holocene." Geophysical Research Letters **27**(7): 1005-1008.

Dansgaard, W., J. W. C. White, et al. (1989). "The abrupt termination of the Younger Dryas climate event." Nature **339**: 532-534.

Davidson J. A., C. A. Cantrell et al. (1987). "Carbon kinetic isotope effect in the reaction of CH_4 with OH." Journal of Geophysical Research **92**: 2195-2199.

DeBano, L. F., D. G. Neary, et al. (1998). "Fire's effects on ecosystems." J. Wiley, New York: 333 p.

Deines, P. (1980). "The isotopic composition of reduced organic carbon." In: Fritz, P. and J.-C. Fontes (Eds.), Handbook of Environmental Isotope Geochemistry **2B** (Elsevier, Amsterdam, The Netherlands): 329-393.

Del Grosso S., D. Ojima, et al. (2002). "Simulated effects of dryland cropping intensification on soil organic matter and greenhouse gas exchanges using the DAYCENT ecosystem model." Environmental Pollution **116**: S75_S83

DeMenocal, P., J. Ortiz, et al. (2000). "Abrupt onset and termination of the African Humid Period: Rapid climate responses to gradual insolation forcing." Quaternary Science Reviews **19**: 347-361

Dlugokencky, E. J., L. P. Steele, et al. (1994). "The growth rate and distribution of atmospheric methane." Journal of Geophysical Research **99**(D8): 17,021-17,043.

Dlugokencky, E. J., S. Houweling et al. (2003). "Atmospheric methane levels off: Temporary pause or a new steady state?." Geophysical Research Letters **30** (19): doi:10.1029/2003GL01812

Dlugokencky, E. J., P. Lang et al. (2004). "Influences on the growth rate of atmospheric methane." National Ocean and Atmospheric Administration: www.cmdl.noaa.gov/gallery/annual_meetin_2004_dlugokencky

Donner, L. and V. Ramanathan (1980). "Methane and nitrous oxide: Their effects on terrestrial climate." Journal of Atmospheric Sciences **37**: 119-124.

Ehleringer, J. R. and R. K. Monson (1993). "Evolutionary and ecological aspects of photosynthetic pathway variation." Annual Review of Ecology and Systematics **24**: 411-439.

Ehleringer, J. R., T. E. Cerling, et al. (1997). "C_4 photosynthesis, atmospheric CO_2, and climate." Oecologia **112**: 285-299.

Etheridge, D. M., L. P. Steele, et al. (1998). "Atmospheric methane between 1000 A.D. and present: evidence of anthropogenic emissions and climatic variability." Journal of Geophysical Research **103**(D13): 15,979-15,993.

Etheridge, D., D. Ferretti, et al. (2003). "Carbon-13 evidence of the causes of the atmospheric methane concentration increase since 1700 AD and of a varying methane budget beforehand." Eos Transactions, AGU, Fall Meeting Supplement **84**(46): **Abstract** A42D-07.

Etiope, G. and R. W. Klusman (2002). "Geologic emissions of methane to the atmosphere." Chemosphere **49**: 777-789.

Etiope, G. and A. V. Milkov (2004). "A new estimate of global methane flux from onshore and shallow submarine mud volcanoes to the atmosphere." Environmental Geology in press.

Fabre, A., J.-M. Barnola, et al. (2000). "Determination of diffusivity in polar firn: comparison between experimental measurements and inverse modeling." Geophysical Research Letters **27**(4): 557-560.

Fairbanks, R. G. (1989). "A 17,000-year glacio-eustatic sea level record: influence of glacial melting rates on the Younger Dryas event and deep-ocean circulation." Nature **342**: 637-642.

Fisher, D. A., R. M. Koerner (1994). "Signal and noise in four ice-core records from Agassiz Ice Cap, Ellesmere Island, Canada: details of the last millennium for stable isotopes, melt and solid conductivity." Holocene **4**(2): 113-120.

Fisher, D. A., R. M. Koerner, et al. (1995). "Holocene climatic records from Agassiz Ice Cap, Ellesmere Island, NWT, Canada." Holocene **5**(1): 19-24.

Fuchs, A., J. Schwander, et al. (1993). "A new ice mill allows precise concentration determination of methane and most probably also other trace gases in the bubble air of very small ice samples." Journal of Glaciology **39**(131): 199-203.

Fung, I. Y., J. John, et al. (1991). "Three-dimensional model synthesis of the global methane cycle." Journal of Geophysical Research 96(D7): 13,033-13,065.

Games, L. M. and J. M. Hayes (1976). "On the mechanisms of CO_2 and CH_4 production in natural anaerobic environments." In: Environmental Biogeochemistry Vol. 1: Carbon, nitrogen, phosphorus, sulphur and selenium cycles. J. O. Nriagu (Ed.)Ann Arbor, Michigan, Ann Arbor Science Pub. Inc.: 51-73.

Gasse, F. (2000). "Hydrological changes in the African tropics since the Last Glacial Maximum." Quaternary Science Reviews **19**: 189-211.

Gates, W. L. (1976). "Modeling the ice-age climate." Science **198**: 1138-1144.

Gierczak, T., R. K. Talukdar, et al. (1997). "Rate coefficients for the reactions of hydroxyl radicals with methane and deuterated methanes." Journal of Physical Chemistry **101**: 3125-3134.

Grachev, A. M. and J. P. Severinghaus (2003). "Laboratory determination of thermal diffusion constants for $^{29}N_2/^{28}N_2$ in air at temperatures from -60 to 0°C for reconstruction of magnitudes of past climate changes using the ice core fossil-air paleothermometer." Geochimica Cosmochimica Acta **67**(3): 345-360.

Grant, N. J. and M. J. Whiticar (2002). "Stable carbon isotope evidence for methane oxidation in plumes above Hydrate Ridge, Cascadia Oregon Margin." Global Biogeochemical Cycles **16**(4): 71-1 to 71-13.

Grootes, P. M., M. Stuiver, et al. (1993). "Comparison of oxygen isotope records from the GISP2 and GRIP Greenland ice cores." Nature **366**: 553-554.

Gupta, M. L., S. Tyler, et al. (1996). "Modeling atmospheric $\delta^{13}CH_4$ and the causes of recent changes in atmospheric CH_4 amounts." Journal of Geophysical Research **101**(D17): 22,923-22,932.

Gupta, M. L., M. P. McGrath, et al. (1997). "$^{12}C/^{13}C$ kinetic isotope effects in the reactions of CH_4 with OH and Cl." Geophysical Research Letters **24**(22): 2761-2764.

Haberle, S. G. and M.-P. Ledru (2001). "Correlations of char coal records of fires from the past 16,000 years in Indonesia, Papua New Guinea, and Central and South America." Quaternary Research **55**: 97-104.

Hao, W. M. and D. E. Ward (1993). "Methane production from global biomass burning." Journal of Geophysical Research **98**(D11): 20,657-20,661.

Hausman, E. D. and M. B. McElroy (1999). "Role of sea-surface temperature and ocean circulation changes in the reorganization of the global carbon cycle at the last glacial termination." Global Biogeochemical Cycles **13**(2): 371-381.

Hein, R., P. J. Crutzen, et al. (1997). "An inverse modeling approach to investigate the global atmospheric methane cycle." Global Biogeochemical Cycles **11**(1): 43-76.

Herron, M. M. and C. C. J. Langway (1980). "Firn densification: an empirical model." Journal of Glaciology **25**(93): 373-3385.

Holmes, M. E., F. S. Sansone, et al. (2000). "Methane production, consumption, and air-sea exchange in the open ocean: An evaluation based on carbon isotopic ratios." Global Biogeochemical Cycles **14**(1): 1-10.

Hornibrooke, E. R., F. J. Longstaffe, et al. (1997). "Spatial distribution of microbial CH_4 production pathways in temperate zone wetland soils: Stable carbon and hydrogen isotope evidence." Geochimica et Cosmochimica Acta **61**: 745-753.

Hovland, M., A. G. Judd, et al. (1993). "The global flux of methane from shallow submarine sediments." Chemosphere **26**(1-4): 559-578.

Intergovernemental Panel on Climate Change (2001). "Climate change 2001: the scientifique basis. Third Assessment Report." J. T. Houghton et al. (Eds.) Cambridge University Press, published for IPCC.

Kammen, D. M. and B. D. Marino (1993). "On the origin and magnitude of pre-industrial anthropogenic CO_2 and CH_4 emissions." Chemosphere **26**(1-4): 69-86.

Kaplan, J. O. (2002). "Wetlands at the Last Glacial Maximum: distribution and methane emissions." Geophysical Research Letters **6**: 3-1 to 3-4.

Kaplan, J. O., G. Folberth, et al. (2004). "Ice Age Methane Revisited: Oceans, Lightning, and the Steady Wetland Source." EOS Transactions, American Geophysical Union Joint Assembly Supplement **85**(17): **Abstract** GC21A-18

Kastner, M., C. Solem, et al. (2003). "The Extent of CH_4 Emission and Oxidation in Thermogenic and Biogenic Gas Hydrate Environments."
EOS Transactions American Geophysical Union Fall Meeting Supplement **84**(46): **Abstract** OS42B-07

Kennett, J. P., K. G. Cannariato, et al. (2000). "Carbon isotopic evidence for methane hydrate instability during Quaternary interstadials." Science **288**: 128-133.

Kennett, J. P., K. G. Cannariato, et al. (2003). Methane hydrates in Quaternary climate change. Washington, DC, American Geophysical Union.

King, S. L., P. D. Quay, et al. (1989). "The $^{13}C/^{12}C$ kinetic isotope effect for soil oxidation of methane at ambient atmospheric concentrations." Journal of Geophysical Research **94**: 18,273-18,277

Knox, M., P. D. Quay, et al. (1992). "Kinetic isotope fractionation during air-water gas transfer of O_2, N_2, CH_4 and H_2." Journal of Geophysical Research **97**(C12): 20.335-20,343.

Kvenvolden, K. A., B. R. T. Simoneit, et al. (1989): "Chemical and isotopic compositions of natural gas from seeps in Yellowstone and Grand Teton national parks, Wyoming." In: Forthieth Field Conference, Wyoming Geological Association Guidebook: 241-246.

Kvenvolden, K. A. (1993). "Gas hydrates - geological perspective and global change." Reviews of Geophysics **31**(2): 173-187.

Kvenvolden, K. A. (1999). "Potential effects of gas hydrates on human welfare." Proceedings of the National Academy of Sciences of the United States of America **96**(7): 3420-3426.

Kvenvolden, K. A. and T. D. Lorenson (2001). "The global occurrence of gas hydrates." In: Natural gas hydrates: occurrence, distribution and detection. C. K. Paull and W. P. Dillon (Eds.) Washington, DC., American Geophysical Union. 124: 3-18.

Lacroix, A. V. (1993). "Unaccounted-for sources of fossil and isotopically-enriched methane and their contribution to the emissions inventory: a review and synthesis." Chemosphere **26**(1-4): 507-557.

Lambeck, K., T. M. Esat, et al. (2002). "Links between climate and sea levels for the past three million years." Nature **419**: 199-206.

Lambert, G., and S. Schmidt (1993). "Reevaluation of the oceanic flux of methane: uncertainties and long term variations." Chemosphere **26**(1-4): 579-589.

Lansdown, J. M., P. D. Quay, et al. (1992). "CH_4 production via CO_2 reduction in a temperate bog: A source of ^{13}C-depleted CH_4." Geochimica et Cosmochimica Acta **56**: 3493-3503.

Lasaga, A. C. and G. V. Gibbs (1991). "Ab initio studies of the kinetic isotope effect of the $CH_4 + OH^{\cdot}$ atmospheric reaction." Geophysical Research Letters **18**(7): 1217-1220.

Lelieveld, J., P. J. Crutzen, et al. (1998). "Changing concentration, lifetime and climate forcing of atmospheric methane." Tellus 50B: 128-150.

Levin, I., P. Bergamaschi, et al. (1993). "Stable isotopic signature of methane from major sources in Germany." Chemosphere **26**: 161-177.

Levin, I. (1994). "The recent state of carbon cycling through the atmosphere." In: Carbon cycling in the glacial ocean: constraints on the ocean's role in climate change. R. Zahn. New York, Springer.

Lerner, J., E. Matthews, et al. (1988). "Methane emission from animals; a global high-resolution data base." Global Biogeochemical Cycles **2**(2): 139-156.

MacDonald, G. J. (1990). "Role of methane clathrates in past and future climates." Climate Change **16**: 247-281.

MaenzaGmelch, T.E. (1997). "Late-glacial early Holocene vegetation, climate, and fire at Sutherland Pond, Hudson Highlands, Southeastern New York, USA." Canadian Journal of Botany **75**(3): 431-439

Mann M. E., P. D. Jones (2003). "Global surface temperatures over the past two millennia." Geophysical Research Letters **30** (15) doi:10.1029/2003GL017814

Marchal, O., T. F. Stocker, et al. (1998). "Impact of oceanic reorganizations on the ocean carbon cycle and atmospheric carbon dioxide content." Paleoceanography **13**(3): 225-244.

Mariotti, A. (1983). " Atmospheric nitrogen is a reliable standard for natural ^{15}N abundance measurements." Nature **303**: 685-687

Martens, C. S., N. E. Blair, et al. (1986). "Seasonal variations in the stable carbon isotopic signature of biogenic methane in a coastal sediment." Science **233**: 1300-1303.

Martinerie, P., V. Y. Lipenkov, et al. (1994). "Air content paleo record in the Vostok ice core (Antarctica): A mixed record of climatic and glaciological parameters." Journal of Geophysical Research **99**: 10,565-10,576.

Martinerie, P., G. P. Brasseur, et al. (1995). "The chemical composition of ancient atmospheres: a model study constrained by ice core data." Journal of Geophysical Research **100**(D7): 14,291-14,304.

Maslin, M. A. and S. J. Burns (2000). "Reconstruction of the Amazon basin effective moisture availability over the past 14,000 years." Science **290**: 2285-2287.

Maslin, M. A. and E. Thomas (2003). "Balancing the deglacial global carbon budget: the hydrate factor." Quaternary Science Reviews **22**: 1729-1736.

Maslin, M. A., M. Owen, et al. (2004): "Linking continental-slope failures and climate change: Testing the clathrate gun hypothesis" Geology **32**(1): 53–56.

McCarthy, M. C., P. Connell, et al. (2001). "Isotopic fractionation of methane in the stratosphere and its effect on free tropospheric isotopic compositions." Geophysical Research Letters **28**(19): 3657-3660.

Meese D. A., A. J. Gow, et al. (1997). "The Greenland Ice Sheet Project 2 depth-age scale: Methods and results." Journal of Geophysical Research **102**(C12): 26,411-26,423.

Metges, C., K. Kempe, et al. (1990): "Dependence of the carbon-isotope contents of breath carbon dioxide, milk, serum, and rumen fermentation products on the δ13C value of food in dairy cows." British Journal of Nutrition 63: 187-196.

Milkov A. V., G. E. Claypool et al. (2003)"In situ methane concentrations at Hydrate Ridge, offshore Oregon: New constraints on the global gas hydrate inventory from an active margin" Geology **31**(10): 833-836.

Mörner, N.-A. and G. Etiope (2002). "Carbon degassing from the lithosphere." Global and Planetary Change **33**: 185-203.

Mook, W. G. (1983). "Principles of Isotope Hydrology." Introductory course on isotope Hydrology, Bundesanstalt für Geowissenschaften und Rohstoffe, Hannover.

Morgan, V., M. Delmotte, et al. (2002). "Relative timing of deglacial climate events in Antarctica and Greenland." Science **297**: 1862-1864

Nakagawa, F., N. Yoshida, et al. (2002). "Production of methane from alasses in eastern Siberia: Implications from its ^{14}C and stable isotopic compositions." Global Biogeochemical Cycles **16**(3): 14-1 to 14-5.

National Geophysical Data Center (1988). "ETOPO-5, bathymetry/topography data." Data Announcement 88-MGG-02, National Ocean and Atmosphere Administration, U.S. Department of Commerce, Washington, D.C.

Nisbet, E. G. (1990). "The end of the ice age." Canadian Journal of Earth Sciences **27**: 148-157.

Nisbet, E. G. (1992). "Sources of atmospheric CH_4 in early postglacial time." Journal of Geophysical Research **97**(D12): 12849-12867.

Nisbet, E. G. (2002). "Have sudden large releases of methane from geological reservoirs occurred since the Last Glacial Maximum, and could such releases occur again?" Philosophical Transactions of the Royal Society of London **360**: 581-607.

Ojima, D. S., D. W. Valentine, et al. (1993). "Effect of land use on methane oxidation in temperate forest and grassland soils." Chemosphere **26** (1-4): 675-685.

Oona, S. and E. S. Deevey (1960). "Carbon-13 in lake waters and its possible bearing on paleoclimatology." American Journal of Science **258**(A): 253-272.

Osborn, T. J. and T. M. L. Wigley (1994). "A simple model for estimating methane concentration and lifetime variations." Climate Dynamics **9**: 181-193.

Ovsyannikov, V. M. and V. S. Lebedev (1976). "Isotopic composition of carbon in gases of biogenic origin." Geochemistry International **4**: 453-458.

Paull, C. K., W. Ussler, et al. (1991). "Is the extent of glaciation limited by marine gas hydrates?" Geophysical Research Letters **18**(3): 432-434.

Petit, J. R., J. Jouzel, et al. (1999). "Climate and atmospheric history of the past 420,000 years from the Vostok ice core, Antarctica." Nature **399**: 429-436.

Petit-Maire, N., M. Fontugne, et al. (1991). "Atmospheric methane ratio and environmental changes in the Sahara and Sahel during the last 130,000 years." Paleoceanography, Paleoclimatology, Paleoecology **86**: 197-206.

Popp, B. N., F. J. Sansone, et al. (1995). "Determination of concentration and carbon isotopic composition of dissolved methane in sediments and near shore waters." Analytical Chemistry **67**: 405-411.

Popp, T. J., J. P. Chanton, et al. (1999). "Methane stable isotope distribution at a *Carex* dominated fen in North Central Alberta." Global Biogeochemical Cycles **13**(4): 1063-1077.

Prather, M. (1994). "Lifetimes and eigenstates in atmospheric chemistry." Geophysical Research Letters **21**(9): 801-804.

Prather, M., D. Ehhalt, et al. (2001). "Atmospheric chemistry and greenhouse gases." In: Climate change 2001: the scientifique basis. J. T. Houghton et al., Cambridge University Press, published for IPCC.

Prentice, I. C., M. T. Sykes, et al. (1993). "Modelling global vegetation patterns and terrestrial carbon storage at the last glacial maximum." Global Ecology and Biogeography Letters **3**: 67-76.

Prinn, R. G., R. F. Weiss, et al. (1995). "Atmospheric trends and lifetime of CH_3CCl_3 and global OH concentrations." Science 269: 187-192.

Quay, P. D., S. L. King, et al. (1988). "Isotopic composition of methane released from wetlands: implications for the increase in atmospheric methane." Global Biogeochemical Cycles **2**(4): 385-397.

Quay, P. D., S. L. King, et al. (1991). "Carbon isotopic composition of atmospheric CH_4: fossil and biomass burning source strengths." Global Biogeochemical Cycles **5**(1): 25-47.

Quay, P. D., J. Stutsman, et al. (1999). "The isotopic composition of atmospheric methane." Global Biogeochemical Cycles **13**(2): 445-461.

Rasmussen, R. A. and M. A. K. Khalil (1983). "Global production of methane by termites." Nature **301**(5902): 700-702.

Raynaud, D., J. Jouzel, et al. (1993). "The ice record of greenhouse gases." Nature **259**: 926-934.

Raynaud, D., J. A. Chappellaz, et al. (1997). "Air content along the Greenland Ice Core Project core: A record of surface climate parameters and elevation in central Greenland." Journal of Geophysical Research **102**(C12): 26,607-26,613.

Reeburgh, W. S., A. I. Hirsch, et al. (1997). "Carbon kinetic isotope effect accompanying microbial oxidation of methane in boreal forest soils." Geochimica Cosmochimica Acta **61**(22): 4761-4767.

Reeh, N., H. H. Thomsen, et al. (1987). "The Greenland ice-sheet margin - a mine of ice for paleo-environmental studies." Paleogeography, Paleoclimatology, Paleoecology **58**: 229-234.

Reeh, N., H. Oerter, et al. (2002). "Comparison between Greenland ice-margin and ice core oxygen-18 records." Annals of Glaciology **35**: 136-144.

Rice, D. D. and G. Claypool (1981). "Generation, accumulation and resource potential of biogenic gas." Bulletin of the American Association of Petroleum Geologists **65**: 5-25.

Ridgwell, A. J., S. J. Marshall, et al. (1999). "Consumption of atmospheric methane by soils: A process-based model." Global Biogeochemical Cycles **13**(1): 59-70.

Rommelaere, V., L. Arnaud, et al. (1997). "Reconstructing recent atmospheric trace gas concentrations from polar firn and bubbly ice data by inverse methods." Journal of Geophysical Research **102**(D25): 30,069-30,083.

Ruddiman, W. F. and J. S. Thomson (2001). "The case for human causes of increased atmospheric CH_4 over the last 5000 years." Quaternary Science Reviews **20**: 1769-1777.

Rust, F. E. (1981). "$\delta(^{13}C/^{12}C)$ of ruminant methane and its relationship to atmospheric methane." Science **211**: 1044-1046.

Sansone, F. J., E. M. Holmes, et al. (1999). "Methane stable isotopic ratios and concentrations as indicators of methane dynamics in estuaries." Global Biogeochemical Cycles **13**(2): 463-474.

Sansone, F. J., B. N. Popp, et al. (2001). "Highly elevated methane in the eastern tropical North Pacific and associated isotopically enriched fluxes to the atmosphere." Geophysical Research Letters **28**(24): 4567-4570.

Saueressig, G., P. Bergamaschi, et al. (1995). "Carbon kinetic isotope effect in the reaction of CH_4 with Cl atoms." Geophysical Research Letters **22**(10): 1225-1228.

Saueressig, G., J. N. Crowley, et al. (2001). "Carbon 13 and D kinetic isotope effects in the reactions of CH_4 with $O(^1D)$ and OH: New laboratory measurements and their implications for the isotopic composition of stratospheric methane." Journal of Geophysical Research **106**(D19): 23,127-23,138.

Savarino, J. and M. Legrand (1998). "High northern latitude forest fires and vegetation emissions over the last millennium inferred from the chemistry of a central Greenland ice core." Journal of Geophysical Research **103**(D7): 8267-8279.

Schoell, M. (1980). "The hydrogen and carbon isotopic composition of methane from natural gases of various origins." Geochimica et Cosmochimica Acta **44**: 649-661.

Schulze, E, S. Lohmeyer, et al. (1998). "Determination of $^{13}C/^{12}C$-ratios in rumen produced methane and CO_2 of cows, sheep and camels." Isotopes in Environmental and Health Studies **34**: 75-79.

Schwander, J., B. Stauffer, et al. (1988). "Air mixing in firn and the age of the air at pore close-off." Annals of Glaciology **10**: 141-145.

Schwander, J., J.-M. Barnola, et al. (1993). "The age of the air in the firn and the ice at Summit, Greenland." Journal of Geophysical Research **98**(D2): 2831-2838.

Schwander, J., T. Sowers, et al. (1997). "Age scale of the air in the summit ice: implication for glacial-interglacial temperature change." Journal of Geophysical Research **102**(D16): 19,483-19,493.

Severinghaus, J. P., T. Sowers, et al. (1998). "Timing of abrupt climate change at the end of the Younger Dryas interval from thermally fractionated gases in polar ice." Nature **391**: 141-146.

Severinghaus, J. P. and E. J. Brook (1999). "Abrupt climate change at the end of the Last Glacial Period inferred from trapped air in polar ice." Science **286**: 930-933.

Severinghaus, J. P. and E. J. Brook (2000). "An overview of the precise timing of atmospheric methane change relative to abrupt Greenland climate events in the past 60 ky." EOS Transactions American Geophysical Union Fall Meeting Supplement **81**(48): **Abstract** A61F-02

Sigman, D. M. and E. A. Boyle (2000). "Glacial/interglacial variations in atmospheric carbon dioxide." Nature **407**: 859-869.

Simpson, I.J., D. R. Blake et al. (2002). "Implications of the recent fluctuations in the growth rate of tropospheric methane." Geophysical Research Letters **29** (18): 117-1 to 117-4.

Smith, L. M., J. P. Sachs, et al. (2001). "Light $\delta^{13}C$ events during deglaciation of the East Greenland continental shelf attributed to methane release from gas hydrates." Geophysical Research Letters **28**(11): 2217-2220.

Smith, L. C., G. M. MacDonald, et al. (2004). "Siberian peatlands a net Carbon sink and global methane source since the Early Holocene." Science 303: 353-356.

Snover, A. K. and P. D. Quay (2000). "Hydrogen and carbon kinetic isotope effects during soil uptake of atmospheric methane." Global Biogeochemical Cycles **14**(1): 25-39.

Spahni, R., J. Schwander, et al. (2003). "The attenuation of fast atmospheric CH_4 variations recorded in polar ice cores." Geophysical Research Letters **30**(11): 25-1, 25-4.

Staffelbach, T., A. Neftel, et al. (1991). "A record of the atmospheric methane sink from formaldehyde in polar ice cores." Nature **349**: 603-605.

Steudler P. A., J. M. Melillo, et al. (1996). "Consequence of forest-to-pasture conversion on CH_4 fluxes in the Brazilian Amazon Basin." Journal of Geophysical Research **101**(D13): 18,547-18,554

Stevens, C. M. and A. Engelkemeir (1988). "Stable carbon isotopic composition of methane from natural and anthropogenic sources." Journal of Geophysical Research **93**(D1): 725-733.

Stevens, G. A. and A. E. De Vries (1968). "The influence of the distribution of atomic masses within the molecule on thermal diffusion. II. Isotopic methane and methane/Argon mixtures." Physica **39**, 346-360.

Stocker, T. F., U. Siegenthaler et al. (2004). "Pre-Vostok Greenhouse Gas Concentrations Reconstructed From the EPICA Dome C Ice Core." EOS Transactions American Geophysical Union Fall Meeting Supplement **85**(47): **Abstract** U23A-08

Street-Perrott, F. A. (1993). "Ancient tropical methane." Nature **366**: 411-412.

Striegl, R. G. (1993). "Diffusional limits to the consumption of atmospheric methane by soils." Chemosphere **26**(1-4): 715-720.

Subak, S. (1994). "Methane from the house of Tudor and the Ming dynasty: anthropogenic emissions in the sixteenth century." Chemosphere **29**(5): 843-854.

Tans, P. P. (1997). "A note on isotopic ratios and the global atmospheric methane budget." Global Biogeochemical Cycles **11**(1): 77-81.

Thompson, A. M. (1992). "The oxidizing capacity of the Earth's atmosphere: Probable past and future changes." Science **256**: 1157-1165.

Thompson, A. M., J. A. Chappellaz, et al. (1993). "The atmospheric CH_4 increase since the Last Glacial Maximum (2). Interactions with oxidants." Tellus **45B**: 242-257.

Thompson, S. L. and D. Pollard (1997). "Ice-sheet mass balance at the Last Glacial Maximum from the GENESIS version 2 global climate model." Annals of Glaciology **25**: 250-258.

Thorpe, R. B., K. S. Law, et al. (1996). "Is methane driven deglaciation consistent with the ice-core record?" Journal of Geophysical Research **101**(D22): 28,627-28,635.

Tohjima, Y., T. Tominaga, et al. (1991). "Determination of methane concentration in air extracted from Antarctic ice core samples." Bulletin of the Chemical Society of Japan **64**: 3457-3459.

Trudinger, C. M., I. G. Enting, et al. (1997). "Modeling air movement and bubble trapping in firn." Journal of Geophysical Research **102**(D6): 6747-6763.

Tyler, S.C. (1986). "Stable carbon isotope ratios in atmospheric methane and some of its sources." Journal of Geophysical Research **91**(D12): 13,232-13,238.

Tyler, S. C., D. R. Blake, et al. (1987). "$^{13}C/^{12}C$ ratio in methane from the flooded Amazon forest." Journal of Geophysical Research **92**: 1044-1048.

Tyler, S. C., P. R. Zimmerman, et al. (1988). "Measurements and interpretation of $\delta^{13}C$ of methane from termites, rice paddies, and wetlands in Kenya." Global Biogeochemical Cycles **2**(4): 341-355.

Tyler, S. C., P. M. Crill, et al. (1994). "$^{13}C/^{12}C$ fractionation of methane during oxidation in a temperate forested soil." Geochimica et Cosmochimica Acta **58**(6): 1625-1633.

Tyler, S. C., O. Henry, et al. (2000). "Experimentally determined kinetic isotope effects in the reaction of CH4 with Cl: Implications for atmospheric CH4." Geophysical Research Letters **27**(12): 1715-1718.

Upstill-Goddard, R. C., J. Barnes, et al. (2000). "Methane in the southern North sea: Low-salinity inputs, estuarine removal, and atmospheric flux." Global Biogeochemical Cycles **14**(4). 1205-1217.

Vaghjiani, G. L. and A. R. Ravishankara (1991). "New measurement of the rate coefficient for the reaction of OH with methane." Nature **350**: 406-409.

Wahlen, M., N. Tanaka, et al. (1988). "^{13}C, D and ^{14}C in methane." In: Report to Congress and Environmental Protection Agency on NASA Upper Atmospheric Research Program (NASA, Washington, D.C., USA): 315-316.

Wahlen, M., B. Deck, et al. (1989). "Profiles of $\delta^{13}C$ and δD in methane from the lower stratosphere." EOS Transactions American Geophysical Union: **70**(43): 1017.

Wang, Y. J., H. Cheng, et al. (2001). "A high-resolution absolute-dated Late Pleistocene monsoon record from Hulu Cave, China." Science **294**: 2345-2348.

Wayne, R. P. (1991). "Chemistry of atmospheres." Calendon Press, Oxford: 447 p.

Whiticar, M. J. and E. Faber (1986). "Methane oxidation in sediment and water column environments - isotopic evidence." Organic Geochemistry **10**(4-6): 759-768.

Whiticar, M. J., E. Faber, et al. (1986). "Biogenic methane formation in marine and freshwater environments: CO_2 reduction vs. acetate fermentation-isotopic evidence." Geochimica et Cosmochimica Acta **50**: 693-709.

Whiticar, M. J. (1993). "Stable Isotopes and global budgets." In: Atmospheric methane: sources, sinks and role in global change. M. A. K. Khalil (Ed.) Berlin Heidelberg, NATO ASI Series. **113**: 138-167.

Whiticar, M. J. (1996). "Isotope tracking of microbial methane formation and oxidation." Mitteilungen der Internationalen Vereinigung für Limnologie **25**: 39-54.

Whiticar, M. J. (2000). "Can stable isotopes and global budgets be used to constrain atmospheric methane budgets?" in: Atmospheric methane, its role in the global environment. M. A. K. Khalil. Berlin-Heidelberg, Springer: 63-85.

Whiting, G.J. and J. P. Chanton (1993). "Primary production control of methane emission from wetlands." Nature **364**: 794-795.

Wright, H. A., and A. W. Bailey (1982). "Fire ecology, United States and southern Canada." Wiley and Sons, New York: 501 p.

Xu, W. and C. Ruppel (1999). "Predicting the occurrence, distribution and evolution of methane gas hydrate in porous marine sediments." Journal of Geophysical Research **104**(B3): 5081-5095.

Yonemura, S. and M. Yokozawa (2000). "A process-based model for the global estimation of CH_4- and CO-uptake strengths by soils." World Resource Review **12**(1): 149-170.

Zimmerman, P. R., J. P. Greenberg, et al. (1982). "Termites, a potentially large source of atmospheric methane, carbon dioxide, and molecular hydrogen." Science **218**: 563-565.